A novel role for 14-3-3ζ in coordinating interneuron development through regulation of Rac1 and non-canonical Shh signalling.

A thesis submitted in fulfilment of requirements for Doctor of Philosophy.

In

The School of Pharmacy and Medical sciences

University of South Australia

By

Zarina Isis Greenberg

B. Medical and Pharmaceutical sciences (Honours)

2017

Table of Contents

Table of Contents ..... **ii**

Index of Figures ..... **vi**

Index of Tables ..... **ix**

Abbreviations ..... **x**

Summary ..... **xiv**

Declaration ..... **xv**

Acknowledgments ..... **xvi**

Publications ..... **xvii**

Chapter 1: Introduction **1**

1.1 THE MAMMALIAN BRAIN 1

1.1.1 General brain development 1

1.1.2 Neuronal development in mammals 2

1.1.3 Regions within the brain 2

1.2 THE STRUCTURE OF THE ADULT CEREBRAL CORTEX 5

1.2.1 Laminar layers 5

1.2.2 Cell types 6

1.3 CORTICAL INTERNEURONS 6

1.3.1 Introduction to cortical interneurons 6

1.3.2 Classification of cortical interneurons 8

1.3.3 Interneurons in other regions of the brain 11

1.4 DEVELOPMENT OF CORTICAL INTERNEURONS 11

1.4.1 Ventral telencephalon 11

1.4.2 Ganglionic eminences 12

1.5 SIGNALLING PATHWAYS INVOLVED IN PATTERNING THE VENTRAL TELENCEPHALON 14

1.5.1 Sonic hedgehog signalling induces cortical interneuron formation 16

1.5.2 BMP signalling 19

1.5.3 Fgf signalling 21

1.5.4 Wnt signalling 21

1.6 CELL PROLIFERATION AND CELL CYCLE IN CORTICAL INTERNEURON DEVELOPMENT 22
1.7 MIGRATION OF CORTICAL INTERNEURONS DURING DEVELOPMENT 26
1.7.1 Tangential migration of cortical interneurons 26
1.7.2 Radial migration and laminar distribution of interneurons in the cortex 30
1.8 INTERNEURONS IN SCHIZOPHRENIA AND NEURODEVELOPMENTAL DISORDERS 31
1.8.1 Hippocampal interneurons in schizophrenia 32
1.9 SCHIZOPHRENIA 33
1.9.1 Impact of schizophrenia 33
1.9.2 Proposed aetiologies of schizophrenia 34
1.9.3 Mouse models of schizophrenia 37
1.10 14-3-3ζ 38
1.10.1 The 14-3-3 family proteins 38
1.10.2 The known intracellular functions of 14-3-3ζ 40
1.10.3 The molecular structure of 14-3-3ζ 41
1.10.4 The role of 14-3-3s in schizophrenia and neurodevelopmental disorders 44
1.10.5 The *14-3-3ζ* KO mouse model 46
1.11 PROJECT AIMS AND OBJECTIVES 48
Chapter 2: Materials and methods 51
2.1 Materials 51
2.1.1 Chemicals 51
2.1.2 Animals 51
2.1.3 Culture media 52
2.1.4 Bacteria 52
2.1.5 Primers 52
2.1.6 RNA probes 55
2.1.7 Antibodies 56
2.2 Methods 57
2.2.1 Genotyping 57
2.2.2 Behavioural assays 58
2.2.3 Collection of brains and embryos 58
2.2.4 DNA and RNA techniques 59
2.2.5 Histological techniques 63

2.2.6 Western blotting 70
2.2.7 *In vitro* cell culture experiments 72
2.2.8 Statistics 73
2.2.9 Figure preparation 74
Chapter 3: Characterization of interneuron deficiency in *14-3-3ζ* KO mice 75
3.1 Background 75
3.2 Results 76
3.2.1 *14-3-3ζ* is expressed in interneurons 76
3.2.2 Loss of GABAergic interneurons in the cortex of *14-3-3ζ* KO mice 77
3.2.3 *14-3-3ζ* KO mice display a subtype specific reduction in PV+ interneurons. 80
3.2.4 Ablation of *14-3-3ζ* leads to minor defects in laminar distribution of PV+ interneurons. 86
3.2.5 Loss of PV+ interneurons does not arise from increased cell death in the hippocampus or cortex. 89
3.2.6 Loss of PV+ interneurons does not arise from neurodegeneration but from defects in neurodevelopment. 89
3.3 Discussion 93
Chapter 4: Ablation of *14-3-3ζ* impedes formation of MGE derived interneurons 96
4.1 Background 96
4.2 Results 97
4.2.1 Ablation of *14-3-3ζ* results in interneuron migration defects during development. 97
4.2.2 Loss of *14-3-3ζ* leads to morphological changes in cortical interneurons. .. 102
4.2.3 Altered transcriptional profile and formation defects observed in MGE-derived interneurons in *14-3-3ζ* KO mice. 102
4.2.4 Ablation of *14-3-3ζ* does not affect the proliferation of MGE-derived progenitors. 105
4.2.5 Loss of *14-3-3ζ* results in dysregulation of cell cycle exit. 108
4.2.6 14-3-3ζ plays an important role in interneuron development prior to cell cycle exit. 111
4.2.7 Microarray analysis reveals changes in the Shh signalling pathway in *14-3-3ζ* KO mice. 114
4.2.8 Structural disorganization and impaired formation of the MGE in *14-3-3ζ* KO mice. 118
4.3 Discussion 125
Chapter 5: A novel role for 14-3-3ζ in augmenting non-canonical Shh signalling within the ventral telencephalon. 130

5.1 Background 130
5.2 Results 133
5.2.1 Non-canonical Shh signalling is disrupted in *14-3-3ζ* KO mice. 133
5.2.2 Addition of exogenous Shh normalizes interneuron formation defects in *14-3-3ζ* KO mice *in vitro*. 136
5.2.3 Small GTPase Rac1 regulates *Nkx2.1* to control interneuron development. 138
5.2.4 Shh acts upstream of Rac1 signalling. 138
5.2.5 Non-canonical Shh signalling pathway is augmented by 14-3-3ζ and Rac1 to control interneuron development. 141
5.3 Discussion 145
Chapter 6: Discussion 150
6.1 Final discussion 150
6.2 Future Directions 156
Chapter 7: References 159
Appendix 185
A.1. Microarray analysis: raw data 185
A.1.1 Genes upregulated in *14-3-3ζ* KO mice 185
A.1.2 Genes down regulated in *14-3-3ζ* KO mice 191

Index of Figures

Figure 1.1: Stages of brain development after neural tube formation. 3

Figure 1.2: Regions of the adult mouse brain. 4

Figure 1.3: Laminal layers of the neocortex. 7

Figure 1.4: Schematic illustration of the complex identity of interneurons. 9

Figure 1.5: Schematic illustration of the ventral telencephalon region in the developing mouse brain. 13

Figure 1.6: Canonical Shh signalling pathway. 15

Figure 1.7: Specification of cortical interneurons. 18

Figure 1.8: Potential interactions of Shh, Wnt, Fgf and BMP signalling in the MGE. .. 20

Figure 1.9: Overview of the cell cycle. 24

Figure 1.10: Migration of cortical interneurons. 27

Figure 1.11: Schematic diagram of the nine 14-3-3ζ alpha helices. 42

Figure 1.12: Dimeric 14-3-3ζ interacting with ligand. 43

Figure 1.13: 14-3-3ζ knockout gene trap. 47

Figure 3.1: 14-3-3ζ is expressed in PV+ interneurons. 78

Figure 3.2: GAD67 is reduced in the brains of adult 14-3-3ζ KO mice. 79

Figure 3.3: Loss of GAD67+ cells during embryonic development. 81

Figure 3.4: No change in the number of CR+ cells in 14-3-3ζ KO mice. 83

Figure 3.5: Subtype specific loss of PV+ interneurons in absence of 14-3-3ζ. 84

Figure 3.6: Loss of PV+ cells in the hippocampus of 14-3-3ζ KO mice. 85

Figure 3.7: PV+ cells decreased over entire cortex of 14-3-3ζ KO mice. 87

Figure 3.8: Aberrant laminar distribution of PV+ interneurons in the absence of 14-3-3ζ. 88
Figure 3.9: Loss of interneurons does not result from an increase in cell death in adult 14-3-3ζ KO mice. 90
Figure 3.10: Loss of interneurons does not result from an increase in cell death in adolescent 14-3-3ζ KO mice. 91
Figure 3.11: Loss of PV+ interneurons does not result from neurodegeneration. 92

Figure 4.1: Ablation of 14-3-3ζ leads to aberrant migration of GABAergic interneurons into the developing neocortex. 99
Figure 4.2: 14-3-3ζ is not required for expression of common factors involved in tangential migration. 100
Figure 4.3: MGE-derived cell migration defects observed in the absence of 14-3-3ζ. 101
Figure 4.4: Analysis of migration dynamics in 14-3-3ζ KO interneurons. 103
Figure 4.5: 14-3-3ζ KO MGE derived cells display morphological changes. 104
Figure 4.6: Loss of MGE identity in *14-3-3ζ* KO mice. 106
Figure 4.7: EdU incorporation shows no change in proliferation of interneurons in 14-3-3ζ KO mice. 107
Figure 4.8: No significant change in cell cycle exit at E12.5 in 14-3-3ζ KO mice. 109
Figure 4.9: Interneurons display delayed cell cycle exit at E13.5 in 14-3-3ζ KO mice. 110
Figure 4.10: 14-3-3ζ is not required for interneuron development in post mitotic MGE-derived cells. 112
Figure 4.11: Dlx5/6-Cre; 14-3-3$\zeta^{fl/fl}$ mice do not display locomotive defects or hyperactivity. 113

Figure 4.12: Ablation of 14-3-3ζ in mitotic cells leads to a reduction in PV+ interneurons. 115
Figure 4.13: Sex differences potentially account for microarray variability. 116
Figure 4.14: Validation of Wnt signalling genes identified by microarray. 120
Figure 4.15: Loss of β-catenin in GE of 14-3-3ζ KO mice. 121
Figure 4.16: Defects in the organization of the MGE in 14-3-3ζ KO mice..... 123
Figure 4.17: N-cadherin staining confirms abnormal architecture of the MGE in 14-3-3ζ KO mice. 124

Figure 5.1: Canonical and non-canonical Shh signalling pathways. 132
Figure 5.2: Ablation of 14-3-3ζ leads to aberrant non-canonical Shh signalling. 134
Figure 5.3: Gli3 processing is unaffected in 14-3-3ζ KO mice. 135
Figure 5.4: Exogenous Shh rescues Nkx2.1 expression in the GE of 14-3-3ζ KO mice ex vivo. 137
Figure 5.5: Exogenous Shh rescues Nkx2.1 expression in MGE cells in vitro. 139
Figure 5.6: Inhibition of Rac1 activity reduces the expression of Nkx2.1 in GE derived cells. 140
Figure 5.7: Exogenous Shh leads to increased activation of Pak1. 142
Figure 5.8: Ablation of 14-3-3ζ leads to reduced Rac1 signalling in vivo. 143
Figure 5.9: Working model of how 14-3-3ζ augments the Shh signalling pathway. ... 144

Index of Tables

Table 1.1: Summary of aims 50

Table 2. 1: Primers for quantitative real time polymerase chain reaction (qPCR) 53

Table 2. 2: Primers for genotyping 55

Table 2. 3: RNA probes for in situ hybridization 55

Table 2. 4: Primary antibodies 56

Table 2. 5: Secondary antibodies 57

Table 4. 1: Gene ontology analysis of molecular pathways 119

Abbreviations

°C	Degrees celsius
nM, μM, mM, M	nano molar, micro molar, milli molar, molar
β, ε, γ, η, σ, τ, ζ	Beta, epsilon, gamma, eta, sigma, tau, zeta
5HT3aR	Serotonin 5-hydroxytryptamine 3A receptor
14-3-3	Tyrosine 3-monooxygenase/tryptophan5- monooxygenase activation protein
BMP	Bone morphogenetic protein
BrdU	5-bromo 2'-deoxyuridine
CA	Cornu Ammonis
CDK	Cyclin-dependent kinase
CGE	Caudal ganglionic eminence
CNS	Central nervous system
CR	Calretinin
CXCR	CXC chemokine receptors
DAPI	4’,6-diamidino-2-phenylindole
DG	Dentate gyrus
DIG	Digoxigenin
DISC1	Disrupted in schizophrenia 1
DIV	days *in vitro*
Dlx	Distal-less family homeobox transcription factor
DMEM	Dulbecco’s Modified Eagle’s medium
DMSO	Dimethyl sulfoxide
DNA	Deoxyribonucleic acid
DNase	Deoxyribonuclease

E	Embryonic day
E. coli	Escherichia coli
EdU	5–ethynyl–2′–deoxyuridine
ES	Embryonic stem cells
ErbB	Erythroblastic leukemia viral oncogene homolog
FCS	Foetal calf serum
Fgf	Fibroblast growth factor
Flp	Flippase
FRT	Flippase recognition target
GABA	Gamma-aminobutyric acid
GAD67	Glutamic acid decarboxylase isoform 67kDa
GE	Ganglionic eminence
GFP	Green fluorescent protein
Het	Heterozygous
IF	Immunofluorescence
IPTG	Isopropyl β-D-1- thiogalactopyranoside
IZ	Intermediate zone
kDa	Kilo dalton
KO	Knock-out
LB	Luria Bertani
LGE	Lateral ganglionic eminence
Lhx	LIM homeobox protein
Mash1	Mammalian achaete scute homolog-1
MGE	Medial ganglionic eminence
MZ	Mantle zone

NBT	Nitro blue tetrazolium chloride
NCx	Neocortex
Nrg	Neuregulin
Nkx2	NK2 homeobox
NPY	Neuropeptide Y
Olig2	Oligodendrocyte transcription factor-2
P	Postnatal day
Pak	P21 activated kinase
PBS	Phosphate buffered saline
PCR	Polymerase chain reaction
Ptch1	Patched
PV	Parvalbumin
PFA	Paraformaldehyde
POa	Preoptic area
qPCR	Quantitative real time polymerase chain reaction
RNase	Ribonuclease
Rac1	Ras-related C3 botulinum toxin substrate 1
SDS	Sodium dodecyl sulfate
Sema3	Semaphorin class 3 protein
Shh	Sonic hedgehog
Smo	Smoothened
Sox	SRY (sex determining region Y)-box
SST	Somatostatin
SVZ	Subventricular zone
TAE	Tris-acetic-EDTA

TBS	Tris-buffered saline
VIP	Vasoactive intestinal peptide
VZ	Ventricular zone
VT	Ventral telencephalon
Wnt	Wingless-INT
WT	Wild-type
X-gal	5-bromo-4-chloro-3-indolyl- beta-D-galactopyranoside

Summary

Schizophrenia is a devastating neurodevelopmental disorder widely believed to arise from defects during brain development. Indeed, dysfunction in the formation and function of GABAergic cortical interneurons has been implicated as a central pathogenic mechanism in this, and other, neurodevelopmental disorders. 14-3-3ζ is part of a family of highly conserved intracellular proteins, that bind to the phosphoserine/theronine sites on target proteins and is highly expressed in the brain. Interestingly, several findings in recent years implicate 14-3-3ζ as a candidate risk factor for schizophrenia including: 1) *14-3-3ζ* is downregulated in post-mortem schizophrenic brain samples at the mRNA level; 2) 14-3-3ζ is downregulated across multiple neuroproteomic studies on schizophrenia patient samples; 3) linkage studies have implicated 14-3-3 family proteins in numerous neurodevelopmental disorders, and 4) genetic mutations in the gene encoding 14-3-3ζ (*YWHAZ*) have been found in schizophrenia patients. Previous studies have shown that *14-3-3ζ* KO mice exhibit anatomical and behavioural traits akin to those seen in schizophrenia and other neurodevelopmental disorders. Here we expand on previous findings by identifying a novel role for 14-3-3ζ in interneuron development. A key observation of this study was a subtype specific reduction in parvalbumin expressing interneurons throughout the cortex of *14-3-3ζ* KO mice. Through a series of molecular, biochemical and morphological studies and analyses of unique mouse mutants I identified defects in the specification and formation of interneurons during early brain development. Furthermore, my data fits with the notion that 14-3-3ζ regulates the non-canonical Shh signalling pathway via Rac1 to control interneuron development. Taken together, this work provides novel insight into the role of 14-3-3ζ in controlling interneuron development and hence identifies a novel role of 14-3-3ζ in the pathogenesis of schizophrenia.

Declaration

I declare that this thesis presents work carried out by myself and does not incorporate without acknowledgement any material previously submitted for a degree or diploma in any university; to the best of my knowledge it does not contain any materials previously published or written by another person except where due reference is made in the text; and all substantive contributions by others to the work presented, including jointly authored publications, is clearly acknowledged.

Zarina Isis Greenberg

Acknowledgments

My PhD journey has been such a wonderful experience; from the science that has fascinated me every day, to the people who have helped and supported me throughout. The people I have met have been amazing and this would have been a very different experience without them.

First, I would like to thank my supervisors, Quenten Schwarz and Hayley Ramshaw who gave me the opportunity to undertake this work. Your support, guidance and contagious enthusiasm has always kept me going.

To the members of the Schwarz lab, both past and present, thank you for always taking the time to teach and help me. To Sophie and Rachael, thank you for teaching me so much and for always making it such a fun environment. To Jun, who I owe a special debt of gratitude, for doing so much for me throughout my PhD. To Eiman, for being my 14-3-3ζ buddy, friend and guiding the way for what this entailed.

To all the others who in various ways helped me navigate my PhD, offered encouragement or helped with my work. Especially, to Mel for always helping me with my genotyping.

Of course, I must also thank my parents, whose belief and support in me is unwavering, for which I couldn't be more grateful.

Publications

H Ramshaw*, X Xu*, E J Jaehne, P McCarthy**, Z Greenberg**, E Saleh, B McClure, J Woodcock, S Kabbara, S Wiszniak, Ting-Yi Wang, C Parish, M van den Buuse, B T Baune, A Lopez and Q Schwarz, Locomotor hyperactivity in 14-3-3ζ KO mice is associated with dopamine transporter dysfunction, **Translational Psychiatry** (2013) 3, e327.

Xiangjun Xu, Emily J. Jaehne, **Zarina Greenberg**, Peter McCarthy, Eiman Saleh, Clare Parish, Julian Heng, Matilda Haas, Bernhard T. Baune, Maarten van den Buuse, Angel Lopez1, Hayley Ramshaw* & Quenten Schwarz*, 14-3-3ζ deficient mice in the BalBC background display behavioural and anatomical defects associated with neurodevelopmental disorders**, Scientific Reports** (2015) 5, 12434.

Greenberg Z, Ramshaw H & Schwarz Q, Time Windows of Interneuron Development: Implications to our Understanding of Schizophrenia, **AIMS neuroscience** (2015) 2(4), 294-321.

Greenberg Z, Ramshaw H, Xu X, Schwarz Q, 14-3-3ζ augments non-canonical SHH signalling to control interneuron development through regulation of Rac1**, In preparation.**

The introduction of this thesis contains sections which have been derived from

Greenberg et al., 2015

Chapter 1: Introduction

1.1 THE MAMMALIAN BRAIN

The mammalian brain is said to be the most improbable of all cellular aggregates with neural tissue and cells forming complex connections still not completely understood today. Evolving over millions of years to control everything from sensory and motor control to consciousness and non-conscious functioning, the brain communicates both chemically and electrically with neurotransmitters and action potentials, respectively. Typically, the brain uses different forms of communication to gain the widest range of diverse function, including the use of neural oscillations, rhythmic patterns of action potentials, and slower acting neurotransmitters. The long, complex and unique development of the brain is essential in order for normal functioning and specialized activity in higher vertebrates.

1.1.1 General brain development

The brain is a complex structure and hence undergoes a complex development which begins embryonically and continues prominently through to adulthood. Brain development is initiated by a process called neurulation, in which neural stems cells from the ectoderm rapidly proliferate to eventually form the neural plate and then the neural tube (Rath et al., 1995; Brown et al., 2001). The neural tube is an embryonic structure which will eventually give rise to the central nervous system. Following formation of the neural tube, three primary brain vesicles begin to form at the anterior region of the embryo which become the forebrain, midbrain and hindbrain (Figure 1.1). As development continues these structures subdivide giving rise to secondary structures, with the forebrain giving rise to the telencephalon and diencephalon, the midbrain to the mesencephalon and

the hindbrain to the metencephalon and myelencephalon (Brown et al., 2001). Following on from this, neural stems cells migrate into different regions and undergo different developmental programs depending on the region of their birth. This development eventually gives rises to a complex brain structure with specialized regions that control a variety of specialized functions.

1.1.2 Neuronal development in mammals

Mammalian brain development is highly conserved between species undergoing similar neuronal formation with neurogenesis, neuronal patterning and proliferation leading to similar structures and connectivity of mouse and human brain (Finlay & Darlington, 1995). Indeed, comparative brain studies demonstrate similarities in gene expression between species (Chan et al., 2009; Yue et al., 2014). Though this is not to say that there are not significant difference between the human and mouse brain, besides the mouse brain being relatively smaller than the human brain, one of the major differences is that the mouse brain has a smooth surface whereas the human brain is covered in folds. Evolutionary, these folds have developed in order to increase the surface area of the human brain and increase its connectivity. Despite these differences, the mouse brain is often used as a model system to investigate neuronal development.

1.1.3 Regions within the brain

The primitive structures which divide the brain into segmental regions will ultimately develop into much more complex regions (Figure 1.2). The telencephalon will give rise to the cerebrum, which is made up of several structures including the cerebral cortex, hippocampus and olfactory bulb. The cerebrum is the largest and most developed region of the brain and is critical in conscious functions. The diencephalon gives rise to thalamus and hypothalamus, while the mesencephalon or midbrain does not subdivide.

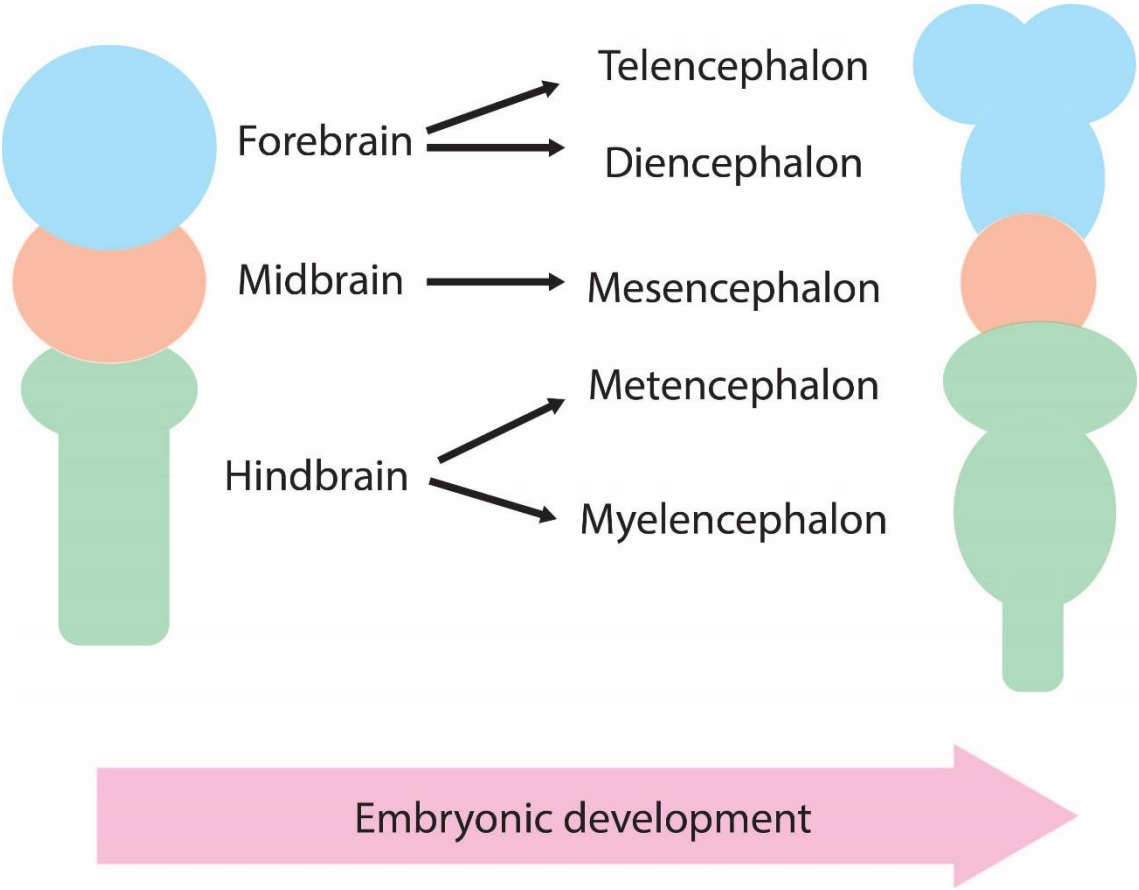


Figure 1.1: Stages of brain development after neural tube formation.

In early neural tube development, the primary vesicles will develop into the forebrain, midbrain and hindbrain. As development continues these vesicles give rise to secondary structures including the telencephalon, diencephalon, mesencephalon, metencephalon and myelencephalon.

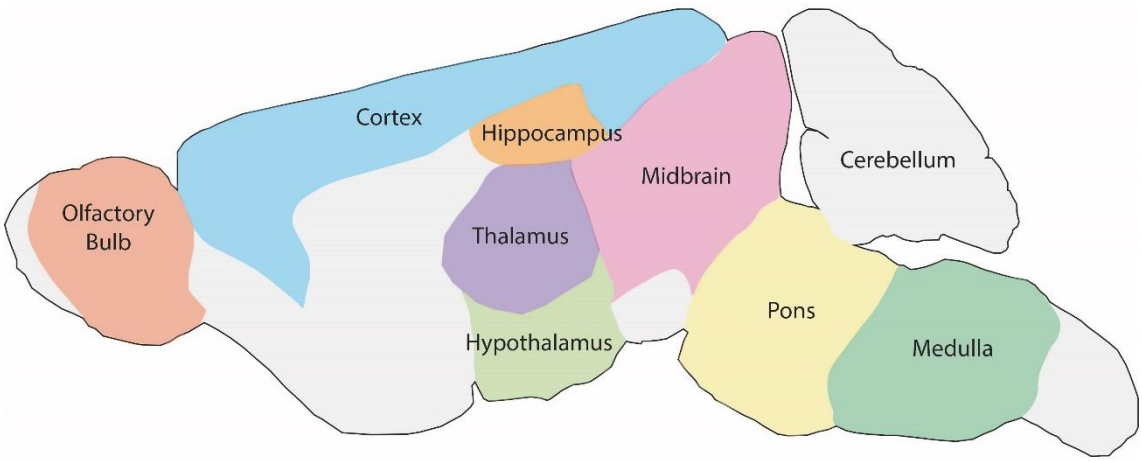


Figure 1.2: Regions of the adult mouse brain.

Schematic overview of the adult mouse brain. A sagittal view of different regions in the mouse brain depicted in different colours.

(Adapted from Boaru et al., 2014)

The metencephalon gives rise to the pons and cerebellum while the myelencephalon gives rise to the medulla oblongata (Watson et al., 2010). Of these structures the cerebrum and in particular the cerebral cortex has been of particular interest when studying the brain given its role in higher level brain functioning such as, consciousness, memory and learning and it has been implicated in many brain pathologies.

1.2 THE STRUCTURE OF THE ADULT CEREBRAL CORTEX

1.2.1 Laminar layers

The cerebral cortex is formed from an outer layer of neural tissue of the forebrain and is essential for higher brain functioning (Mountcastle, 1997, 1998; Karlen and Krubitzer, 2006; Medina and Abellan, 2009). Within the cerebral cortex, cytoarchitectonically distinct regions were first identified in 1908 by Brodmann and found to have significant functional differences (Brodmann, 1908). The neocortex is the largest part of the cerebral cortex and the most recent region to develop evolutionarily. It is comprised of six distinct horizontal layers known as laminae (Figure 1.3). These six layers that make up the neocortex are numbered layers I to VI from the pial surface to the white matter (Mountcastle, 1997, 1998). Located directly below the pia mater, layer I (molecular layer) contains mostly axons and apical dendrites from pyramidal neurons. Layer II (external granular layer) consists of small pyramidal neurons and numerous stellate neurons. Layer III (external pyramidal layer) contains small and medium sized pyramidal neurons. Layer IV (internal granular layer) is composed of different types of stellate neurons and relatively few medium size pyramidal neurons. Layer V (internal pyramidal layer) contains large pyramidal cells. The final layer, layer VI (multiform layer) is made up of small spindle-like pyramidal cells and multiform neurons

(Mountcastle, 1997, 1998). The laminae are identified by the distinct distribution and density of the cells (Mountcastle, 1998; Medina and Abellan, 2009) (Figure 1.3).

1.2.2 Cell types

As in the rest of the nervous system, the cellular component of the cerebral cortex includes neuronal and non-neuronal cells (i.e. microglia and astrocytes). The cerebral cortex is principally comprised of two distinct neuronal populations, excitatory pyramidal neurons which constitute approximately 80% of neurons in the cerebral cortex, and GABAergic inhibitory interneurons which constitute the remaining 20% (Hendry et al., 1987; Meinecke & Peters, 1987). A fine balance between these two neuronal types is crucial for proper functioning of the complex brain networks. Interestingly, there is also a small population of short axon excitatory neurons which use L-Glutamate as their main neurotransmitter (DeFelipe, 1993). These are generally considered interneurons since their axons remain within the neocortex, however are often omitted when discussing interneurons. For simplicity, this small group of cells was excluded from my analysis and only short axon GABAergic cells were identified as interneurons in this thesis.

1.3 CORTICAL INTERNEURONS

1.3.1 Introduction to cortical interneurons

After initially being described over 100 years ago by Santiago Ramon y Cajal, interneurons were distinguished based on their morphology due to their short axons compared to excitatory neurons with little regard for their physiological properties (DeFelipe et al., 2013). However, Ramon y Cajal realized the functional importance of interneurons with an early description stating; “My investigations showed that the functional superiority of the human brain is intimately bound up with the prodigious

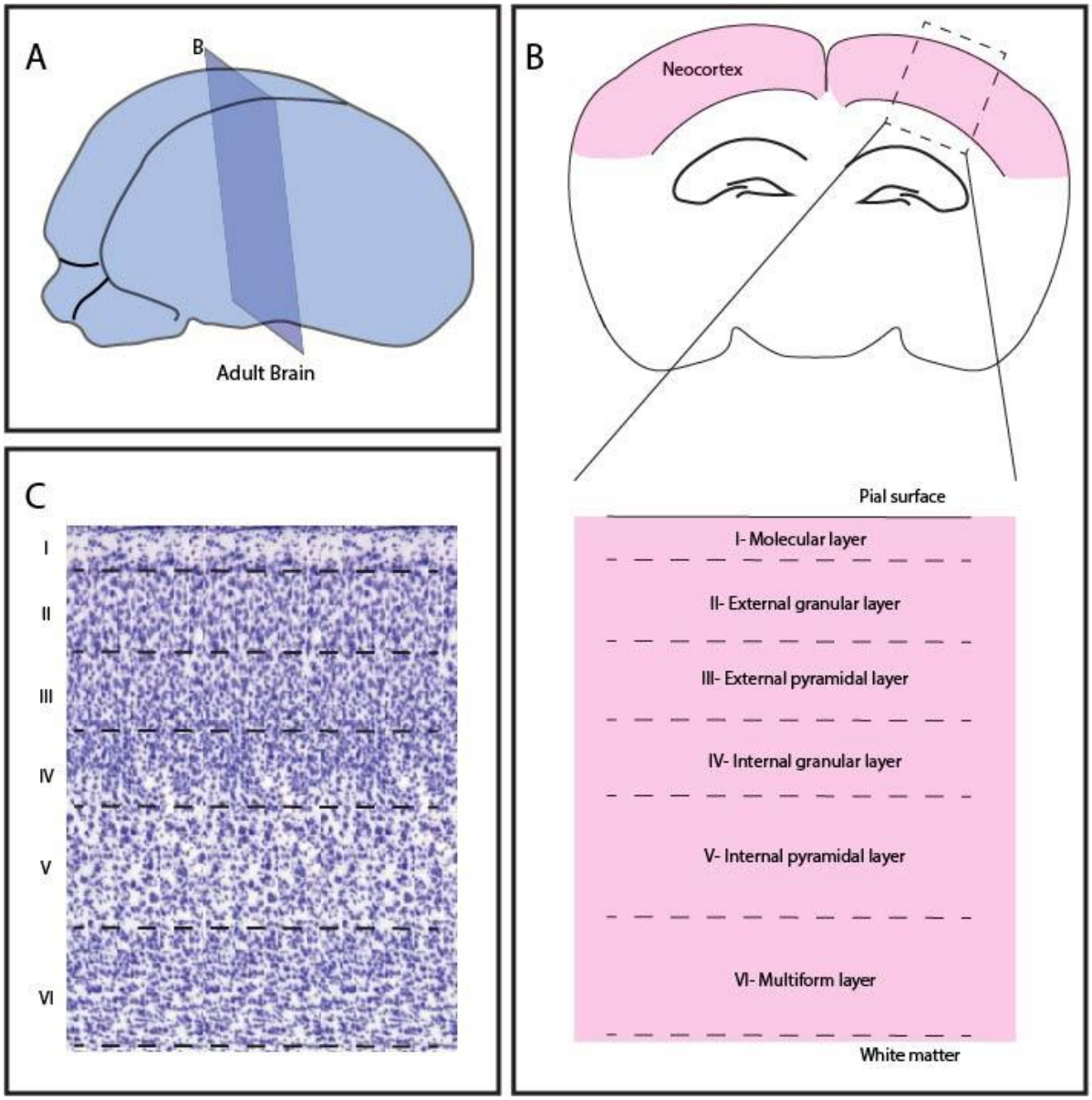


Figure 1.3: Laminal layers of the neocortex.

(A,B) Schematic illustration of the six laminae comprising the cerebral neocortex. The layers vary in thickness and neuronal composition. (C) The six layers of the neocortex visualized through Nissel staining (Belgrand et al., 2011).

abundance and unusual wealth of forms of the so-called neurons with the short axons" (Ramon y Cajal, 1908; Translation by DeFelipe).

The main distinction between cortical interneurons and excitatory neurons is that the former use the GABA(γ-Aminobutyric acid)ergic signalling pathway. GABA is an inhibitory neurotransmitter which causes hyperpolizsation of target neurons reducing neuronal excitablity. Indeed, glutamate decarboxylase (GAD), which catalyzes the decarboxylation of glutamate to GABA, is often used as a marker of interneurons. Interneurons arborize within the cerebral cortex and project axonal terminals vertically or laterally. Though they predominantly innervate local pyramidal cells, they can receive inhibitory or excitatory synapses onto their somata and are capable of acting on several cell populations, including other interneurons. Different interneuron populations can have dramatically different roles, though the primary function of cortical interneurons is to control brain activity and synchronize brain function (Somogyi et al., 1998; DeFelipe et al., 1997).

1.3.2 Classification of cortical interneurons

Different interneuron subpopulations show extraordinary diversity with distinct morphological, physiological and transcriptional profiles (Figure 1.4) (Gonchar & Burkhalter, 1997; Kawaguchi & Kubota, 1997; DeFelipe, 2002). The remarkable diversity of interneurons accounts for the complexity of inhibition required for proper brain function, however this complexity also makes the study of interneurons difficult. There is still a great amount of inconsistency in classifying interneurons with some researchers referring to interneuron subclass based on morphology and cell type whilst others refer to their expression of marker proteins. Though their classification has been far from consistent over the last few decades, interneurons were traditionally sub-divided

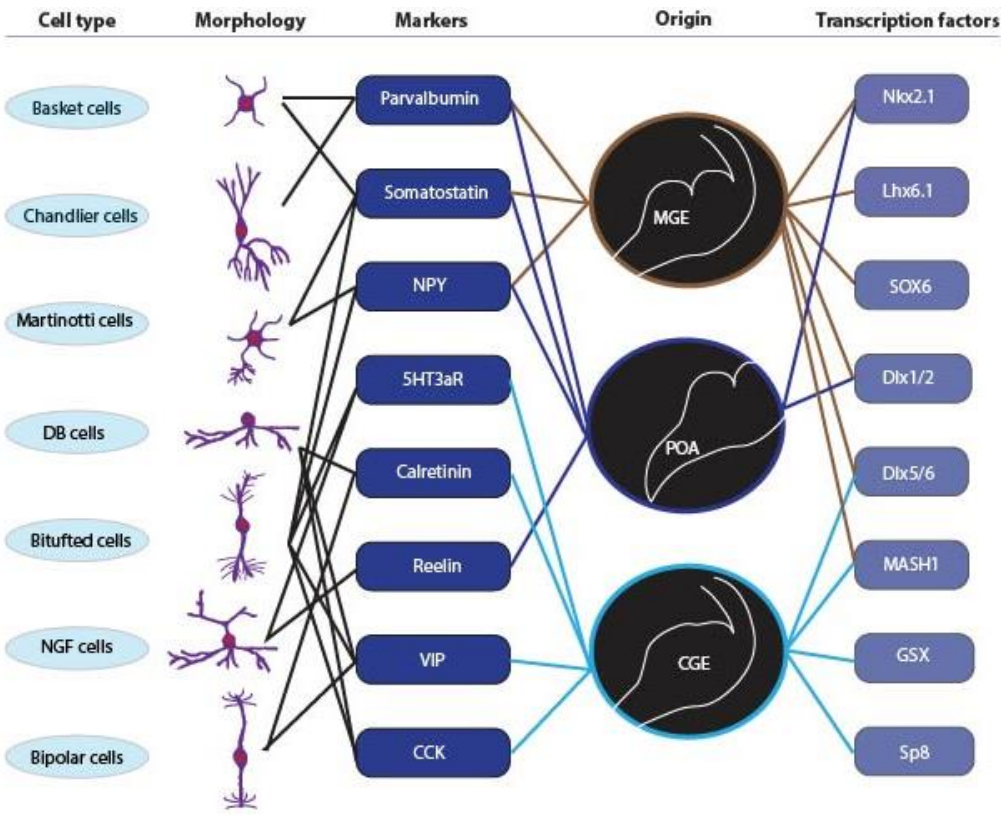


Figure 1.4: Schematic illustration of the complex identity of interneurons.

Cortical interneuron function can be classified based on their cell type, morphology, marker expression, origin and transcriptional profile. DB, double bouquet; NGF, neurogliaform; NPY, neuropeptide Y; VIP, vasointestinal peptide; CCK, cholecystokinin; 5HT3aR, 5-hydroxytryptamine 3a receptor.

(Taken from Greenberg et al., 2015)

into three largely non-overlapping groups based on their expression of calcium binding proteins parvalbumin (PV), calretinin (CR) and the neuropeptide somatostatin (SST) (Gonchar & Burkhalter 1997; DeFelipe et al., 2013; Ascoli et al., 2008). Recently, this classification standard has changed with Lee and colleagues (2010) reporting that serotonin 5-hydroxytryptamine 3A receptor (5HT3aR) is expressed in the vast majority of interneurons that do not express PV or SST (Lee et al., 2010). Each interneuron subtype has a unique function in controlling inhibition and excitation which is dependent on the position of the interneuron within the cortical circuit and its chemical profile. To control both inhibition and excitation of cortical networks, interneurons regulate projection neurons in addition to other interneurons. Interneurons expressing similar markers will often have similar functions, origins and positions in the brain, however it is important to consider that interneurons in each group have different morphology and intrinsic properties (Rudy et al., 2011). PV expressing interneurons are mostly characterized as fast-spiking neurons essential for gamma oscillations, while SST+ interneurons have been established as low-threshold interneurons with SST+ Martinotti cells reported to fire at theta frequency (Fanselow et al., 2008), and capable of sending low-threshold calcium spikes. Fast spiking interneurons have a unique function in feed forward inhibition in the brain due to their early response which allows them to expand the dynamic range of interneuron activity (Hu et al., 2014). SST expressing interneurons in the fourth layer of the cortex act specifically in a disinhibiting context (Xu et al., 2013), this is contrasted by SST+ interneurons in layers 2/3 of the cortex whose primary function is to inhibit pyramidal neurons. Takada et al. reported that alterations to the distribution and/or subtype of interneurons leads to disorganized oscillation and lack of control of brain activity (Takada et al., 2014).

1.3.3 Interneurons in other regions of the brain

Interneuron populations are very diverse with populations found in all areas throughout the central nervous system, including the cortex, striatum, hippocampus, thalamus, cerebellum, hypothalamus, olfactory bulb and spinal cord. Interneurons in different areas have vastly different characteristics reflective of their area of location due to the neurochemical environment of each area of the brain as well as the function of the interneuron within the region. When studying the role of interneurons, it is important to consider that within the different regions of the brain interneurons will arise from different proliferative zones and ultimately develop through varying signalling and transcriptional mechanisms. Interneurons often express different genes between regions of the brain, supporting the notion that local signals may direct interneuron specification, for example, *Dlx1, Zfhx1b and Elmo1* are known to be expressed by interneurons within the cortex but not the striatum (McKinsey et al., 2011; De Marco Garcia et al., 2011; van den Berghe et al., 2013; Kepecs & Fishell, 2014). Furthermore, the interneuron marker expressed by certain cell types is also dependent on the area of the brain. For example, in the hippocampus SST is expressed in Oriens Lacunosum-Moleculare cells, however in cortical interneurons SST is predominately expressed in Martinotti cells (Ma et al., 2006; Forro et al., 2015).

1.4 DEVELOPMENT OF CORTICAL INTERNEURONS

1.4.1 Ventral telencephalon

During the early stages of development, the forebrain separates into the diencephalon and the telencephalon, which in turn becomes the cerebrum. In mice, by embryonic day (E) 12.5 the telencephalon has developed into a series of proliferative zones, including the cortical and hippocampal regions, known as the dorsal telencephalon

(pallium), and the the basal ganglia and ganglionic eminences (GE), known as the ventral telencephalon (VT) (Fishell, 1997; Wilson and Rubenstein, 2000; Jimenez et al., 2002; Nery et al., 2002).

1.4.2 Ganglionic eminences

Cortical interneurons are born in the ganglionic eminences and the preoptic area (PoA) in the ventral telencephalon of the developing rodent brain. These ganglionic eminences can be subdivided into various regions depending on their physical location, including the lateral ganglionic eminence (LGE), medial ganglionic eminence (MGE) and caudal ganglionic eminence (CGE) (Figure 1.5). Anatomically, the ganglionic eminences are transient embryonic telencephalon structures which become evident as they protrude into the walls of the ventricles. The MGE is distinguished from the other areas based on the expression of several transcription factors which are exclusive to the region: *Nkx2.1*, *Nkx6.2*, *Lhx6* and *Lhx8* (Bulfone et al., 1993; Sussel et al., 1999; Marin et al., 2000, Toresson and Campbell, 2001; Asbreuk et al., 2002; Zhao et al., 2003; Alifragis et al., 2004; Liodis et al., 2007; Du et al., 2008; Zhao et al., 2008, Fragkouli et al., 2009). Cytoarchitectonically, the GE is comprised of three regions, ventricular zone (VZ), subventricular zone (SVZ) and mantle zone (MZ), with the ventricular layer located closest to the ventricle. The different layers of the GE have different transcriptional profiles. For example, *Nkx2.1* and *Mash1* are expressed in the VZ. *Dlx1* and *Dlx2* are expressed in the VZ and SVZ whereas *Dlx5* is expressed in the SVZ and MZ and *Dlx6* primarily in the MZ (Price et al., 1991; Bulfone et al., 1993; Liu et al., 1997; Eisenstat et al., 1999; Puelles et al., 2000). The area in which an interneuron is born dictates its fate and function. For example, an interneuron born in the MGE will incur an MGE-like fate and likely give rise to a PV or SST phenotype. Interneurons born in the CGE will likely express 5HT3aR and have a different transcriptional profile than MGE derived

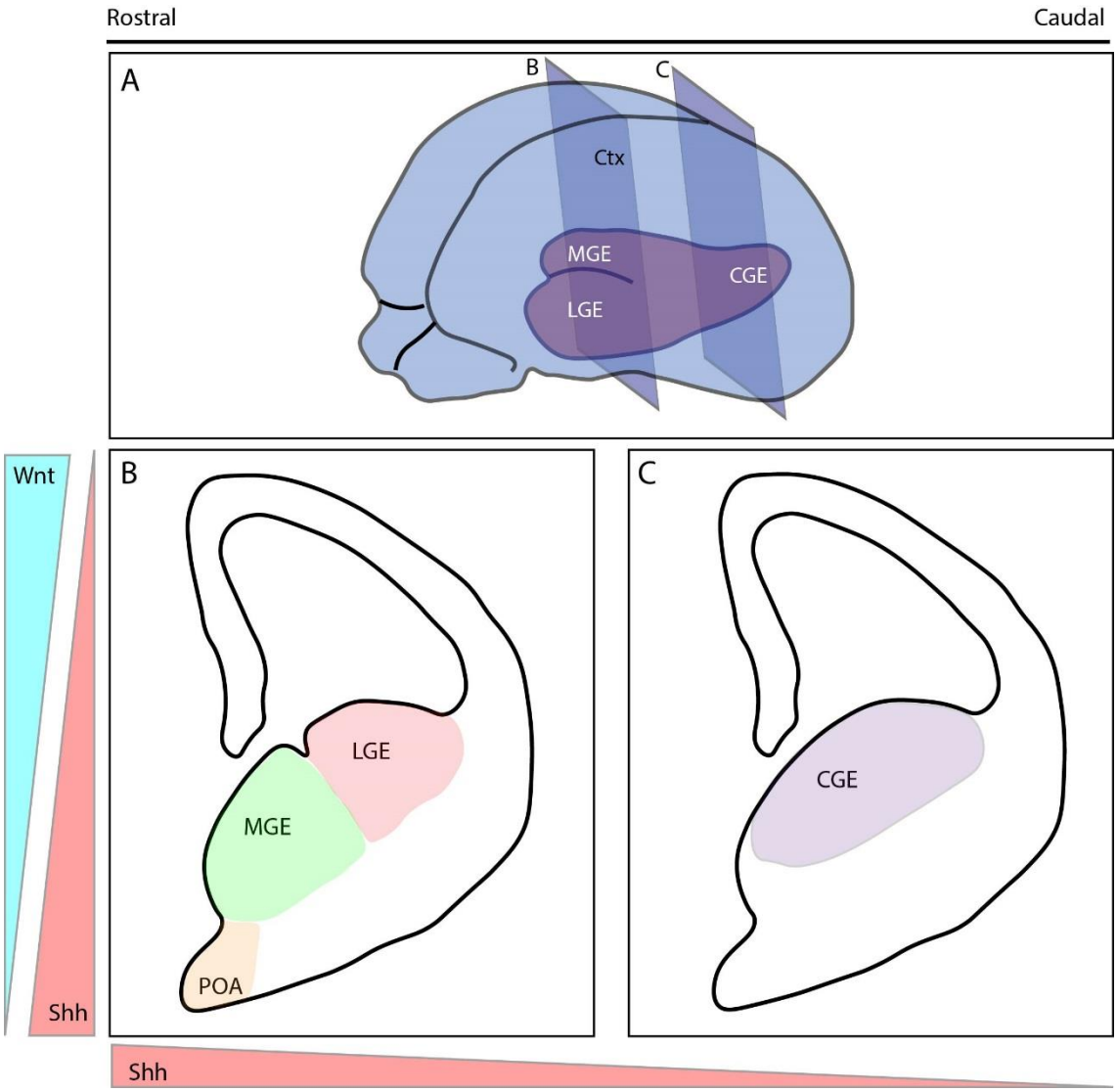


Figure 1.5: Schematic illustration of the ventral telencephalon region in the developing mouse brain.

Interneurons are born in the ventral telencephalon of the developing rodent brain, specifically the medial (MGE), lateral (LGE) and caudal (CGE) ganglionic eminences, and to a lesser extent the preoptic area (PoA). Shh and Wnt signalling are important pathways in the development of interneurons and are expressed in high to low gradients throughout the developing brain. This gradient is important in establishing different classes of interneurons from different ganglionic regions.

(Taken from Greenberg et al., 2015)

interneurons (Lee et al., 2010). Though the LGE has been associated with some interneuron populations (i.e. olfactory bulb and striatal interneurons), it has not been found to produce any cortical interneuron populations in mice. Indeed, most fate mapping studies in mice suggest that the vast majority (approximately 70%) of cortical interneurons derive from the MGE (Peyre et al., 2015).

1.5 SIGNALLING PATHWAYS INVOLVED IN PATTERNING THE VENTRAL TELENCEPHALON

The sonic hedgehog (Shh) signalling pathway has been identified as a key factor in interneuron specification and development. In the rodent brain, the morphogen Shh is secreted from the floor plate of the neural tube along the entire rostral/caudal axis between E8.5 - E9.0. This initial expression later induces *Shh* expression in the PoA region and mantle zone of the MGE, where post mitotic MGE neurons are located (Ericson et al., 1995; Shimamura et al., 1995; Flandin et al., 2011). Though reduced, *Shh* expression continues throughout development and in certain cell types even into adulthood (Flandin et al., 2011). The most well characterized Shh signalling pathway is mediated via a Gli dependent pathway. Shh binds to patched (Ptch1), an inhibitory cell surface receptor containing the Shh binding domain which will then undergo a conformational change releasing cell surface protein receptor smoothened from a state of inhibition. Disinhibition of smoothened then leads to activation of the Gli transcription factors that relocate to the nucleus (Figure 1.6). In the contexts of the MGE, activation of Gli family proteins leads to the up regulation and maintenance of the early NK homeobox transcription factor *Nkx2.1*, as well as providing positive feedback to maintain expression of *Shh* itself (Flandin et al., 2011; Sussel et al., 1999).

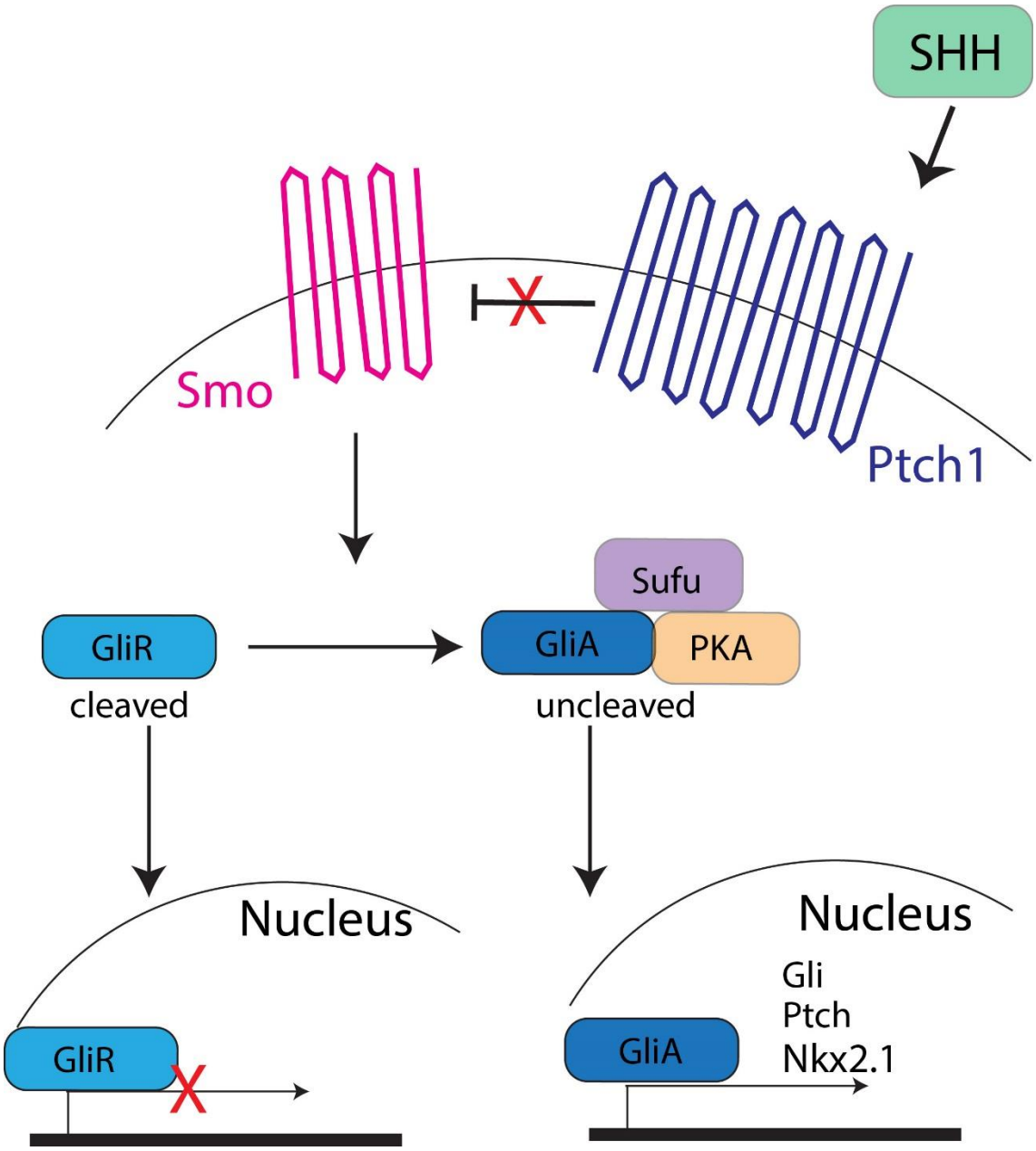


Figure 1.6: Canonical Shh signalling pathway.

Schematic summary of the canonical Shh signalling pathway in the MGE. When Shh is present it activates Ptch1 which disinhibits smoothened to promote Gli. When Gli is activated (GliA) it relocates to the nucleus where it initiates transcription. Alternatively, when Shh is absent Gli is cleaved and acts as a repressor. GliA, Gli activator; GliR, Gli repressor.

1.5.1 Sonic hedgehog signalling induces cortical interneuron formation

Despite Shh signalling being generally well characterized, its expression and function within the ganglionic eminences is complicated and to date, incompletely understood. Shh signalling has a critical role in the formation of the ganglionic eminences, as highlighted in the *FoxG1-Cre:Smoothened*$^{fl/fl}$ line where smoothened is deficient in the telencephalic neural precursor population from E9.5 (Fuccillo et al., 2004). In these mice, the ganglionic eminences fail to undergo initial expansion and patterning, emphasizing a critical role of Shh in the development of all cortical interneurons. A reduction in *Shh* after the formation of the ganglionic eminences at E12.5 has also been documented to lead to a reduction in the SST+ and PV+ expressing interneurons (Wonders et al., 2008; Xu et al., 2005; Xu et al., 2004). However, in this case the altered interneuron landscape occurs without affecting the total number of interneurons in the cell cycle (S-phase), and with only minimal effect on CGE derived interneurons (Xu et al., 2005). These findings correspond well with the expression gradient of *Shh* along the rostral/caudal axis and within the PoA and MGE. Interestingly, Xu et al. 2010 showed that overexpression of *Shh* in the MGE resulted in low-threshold SST subtype interneurons being favoured at the expense of fast spiking PV+ cells (Xu et al., 2010). This is fitting since the SST population of interneurons predominantly arise from cells located more rostrally than those giving rise to PV+ interneurons. Hence, although some cell types are favoured by alteration in *Shh* expression, Shh signalling is crucial for all interneuron subtypes and a delicate balance of Shh activity is essential for proper interneuron development and cell identity. Based on these observations there are three core roles for Shh in interneuron development: contribution to initial patterning and specification in early development (E9-E12.5), expansion of progenitors in the ventral

telencephalon (E12.5), and maintaining expression of *Nkx2.1* within the MGE (E12.5 onwards) (Xu et al., 2010).

At the earliest stages of interneuron specification, Shh initiates a signalling cascade that leads to the up regulation of *Gli1* and *Gli3* transcripts, which results in expression of the transcription factor *Nkx2.1* within the MGE and PoA. The expression of *Nkx2.1* is crucial at an early time point to generate a downstream transcriptional response which leads to the specification of different interneuron subclasses (Figure 1.7). As the loss of *Nkx2.1* results in no changes to CGE derived interneurons, this further suggests that *Nkx2.1* is preferentially required by the MGE and the PoA (Xu et al., 2005). *Sox6* and *Lhx6* act downstream of *Nkx2.1* and have a key role in the differentiation and migration of MGE derived interneurons. In *Sox6* knockout mice MGE derived neurons are mispositioned and fail to express PV and SST correctly (Batista-Brito et al., 2009). Interestingly, while this altered expression profile and mispositioning phenotype is also observed in *Lhx6* knockout mice, in these mice the MGE derived cells are pushed toward a CGE like cell fate. Given the dual defects of interneuron positioning and specification, this raises the question of whether the role of specification has downstream effects on migration or whether *Lhx6* acts upon multiple developmental processes independently. After initially deriving from the floor plate and the PoA, *Shh* expression is later driven in the MGE by *Nkx2.1* and the *Lhx* transcription factor family via a positive feedback loop. While *Lhx6* and its homolog *Lhx8* have largely redundant functions in regulating interneuron development, when removed together *Lhx6;Lhx8* double knockout mice lack *Shh* expression in early MGE derived neurons (E11.5) (Flandin et al., 2011).

Despite its initial role acting under the Gli-dependent pathway, Shh has also been found to have Gli-independent actions in maintaining *Nkx2.1* expression at later developmental stages (i.e. after E12.5). Gulacsi and Anderson (2006) found that removal

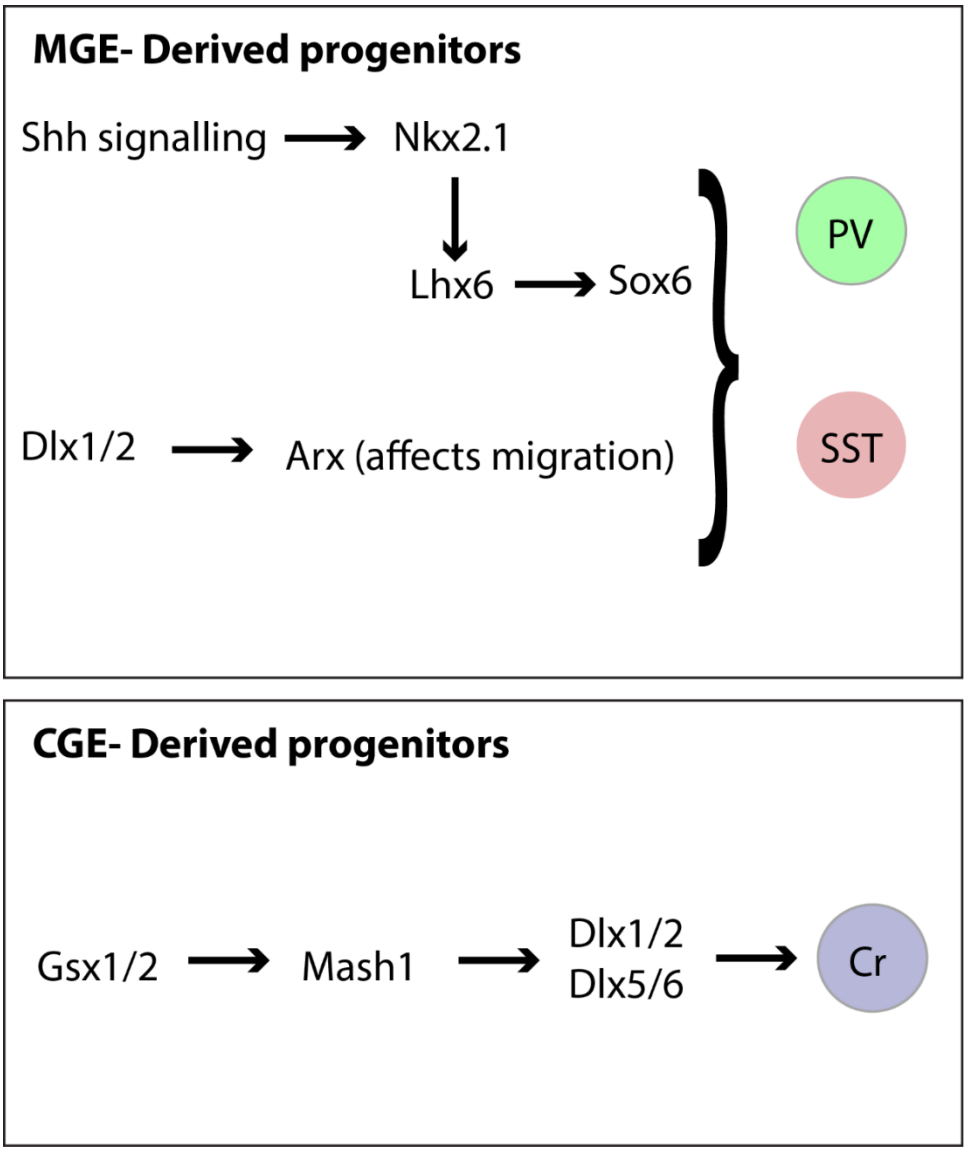


Figure 1.7: Specification of cortical interneurons.

Summary of text describing specification of interneurons. Shh signalling activates Nkx2.1 leading to a downstream cascade to specify PV+ and SST+ interneurons. Gsx1/2 and Mash1 have a key role in specification of CGE-derived progenitors. Dlx1/2 has key roles in specification of both MGE and CGE derived interneurons.

(Adapted from Kelsom & Lu, 2013)

of *Shh* in a *Gli3* null background was necessary to inhibit *Nkx2.1* expression. While the initial patterning of the MGE relies on the Gli dependent pathway, progenitor expansion and patterning maintenance also requires a Gli independent pathway (Gulacsi & Anderson, 2006). Furthermore, Shh's role in maintaining *Nkx2.1* expression in the absence of Gli may be indirect. Gulacsi & Anderson (2006) put forward the hypothesis that Shh may regulate *Nkx2.1* in the absence of *Gli* by repressing the inhibitory effect of Wnt or bone morphogenic protein (BMP). To date there has been few reports looking into the mechanism of Shh maintenance of *Nkx.2.1* in a Gli independent manner. In this thesis, I examine this pathway and identify 14-3-3ζ and Rac1 as playing a critical role in regulating non-canonical Shh signalling, as well suggest several other potential candidate proteins to be involved within the pathway.

1.5.2 BMP signalling

Although Shh signalling arguably plays the most important role in patterning the ganglionic eminences, the Wnt, Fgf and BMP signalling pathways have also been implicated in coordinating cortical interneuron development. In many cases these signalling pathways interact in a reciprocal manner, with the activation of one pathway inhibiting the activity of the other (Figure 1.8) (Lei et al., 2006).

BMPs signal through phosphorylation of molecules like SMADs, which regulate gene transcription, by binding to receptors (BMPR1a, BMPR1b and BMPR2). The BMP family is known to repress the expression of Shh via a negative feedback loop in tissues outside the brain (Aoto et al., 2002) and represses Shh induced interneuron production in cortical explants (Gulacsi & Lillien, 2003). BMPs are essential for refinement of the expression patterns of *Shh* within the ventral midline prior to induction of *Nkx2.1* in the ganglionic eminences (Anderson et al., 2002). After initial specification within the MGE

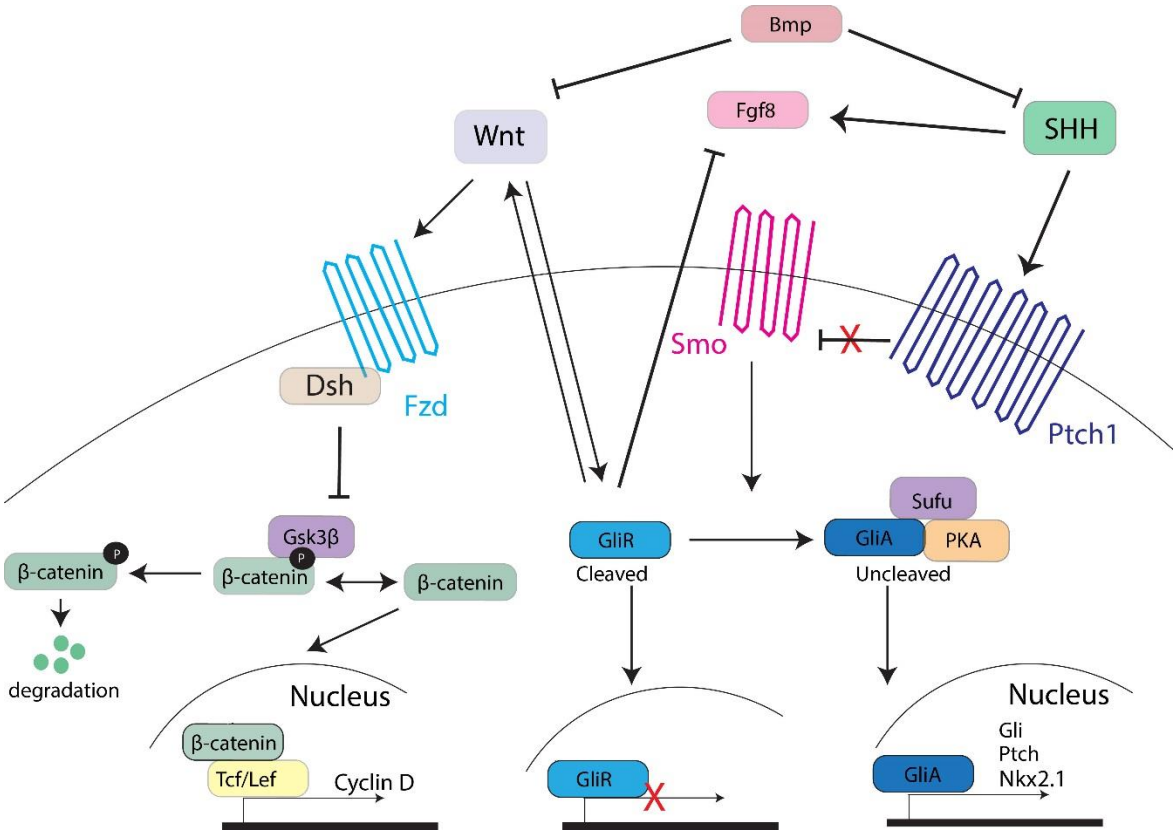


Figure 1.8: Potential interactions of Shh, Wnt, Fgf and BMP signalling in the MGE.

Schematic summary of the interactions between the different signalling pathways important in specification of the MGE. Shh acts via interactions with Ptch1 and Smo to promote GliA to initiate target gene expression. In the absence of Shh, Gli is cleaved to its repressor form, GliR, which does not initiate gene transcription and can activate Wnt signalling and inhibit Fgf8 expression. Shh also signals to activate Fgf8 expression. Wnt signalling acts via Fzd and β-catenin to upregulate target genes and in addition to this, Wnt can activate GliR to inhibit Shh signalling. Gsk3β phosphorylates β-catenin rendering it inactive, in the presence of Wnt dishevelled (Dsh/Dvl) inhibits Gsk3β allowing β-catenin to accumulate in the cytoplasm and travel to the nucleus. BMP inhibits both Shh and Wnt signalling pathways.

interneurons migrate into the cortical layers. Upon reaching the cortex BMPs play important roles in interneuron subtype specification (Mukhopadhyay et al., 2009; Samanta et al., 2007; Wine-Lee et al., 2004). Indeed, while mice lacking the BMP receptors *BMPR1a* and *BMPR1b* have a similar degree of GABAergic neurons overall, they have reduced PV+ expressing interneurons compared to controls.

1.5.3 Fgf signalling

Fibroblast growth factor (Fgf) signalling is also essential for expansion and patterning of the MGE, with most evidence suggesting that Fgfs act as effectors of Shh signalling. In the absence of Fgf receptors (i.e. *Fgfr1; Fgfr2* double knockout mice) the MGE fails to express *Nkx2.1* though *Shh* and *Gli1* expression is normal (Gutin et al., 2006). This morphogenic cascade is further supported by the finding that *Fgf8* expression is dysregulated in both *Gli3* and *Shh* knockout mice (Aoto et al., 2002; Ohkubo et al., 2002).

1.5.4 Wnt signalling

Wnt signalling pathways are conventionally categorized as either canonical or non-canonical depending on whether β-catenin is the primary target of the cascade. In canonical Wnt signalling, activation of Wnt ligands stabilizes cytoplasmic β-catenin which would otherwise be degraded by GSK3β. This stabilization leads to a build-up of β-catenin in the cytoplasm and initiates its transportation to the nucleus where it interacts with transcriptional co-regulators to promote target gene expression. Wnt signalling has well defined roles in promoting neuronal identity, proliferation and migration (Machon et al., 2003; Woodhead et al., 2006; Zhou et al., 2006; Zhou et al., 2004) and has been shown to negatively regulate cell fate and neuronal identity in the subpallium (Backman et al., 2005). More recently, canonical Wnt signalling has been shown to directly mediate

interneuron cell cycle progression. Using *Nkx2.1Cre;* β-*cat*$^{fl/fl}$ mice and a range of *ex vivo* assays in which the Wnt signalling pathway had been modulated, Gulacsi & Anderson (2008) found that loss of canonical Wnt signalling led to proliferation defects within the MGE (Gulacsi & Anderson, 2008). The Wnt/β-catenin pathway has also been shown to promote expression of the transcription factor *Sox5* to control interneuron proliferation within the spinal cord (Martinez-Morales et al., 2010). However, whether this molecular pathway is also at play in the subpallium remains to be explored. Recent findings in the olfactory bulb have also shown that non-canonical Wnt signalling is important for interneuron development in other regions of the brain. Pino et al. (2011) identified a role for Wnt5a (associated with non-canonical Wnt signalling) but not Wnt3a (associated with canonical Wnt signalling) in neurite formation and morphology of olfactory bulb interneurons *in vitro* (Pino et al., 2011). Indeed, modulation of receptors specific to the canonical pathway would assist in determining which defects arising from β-catenin deficiency are specific to Wnt signalling.

1.6 CELL PROLIFERATION AND CELL CYCLE IN CORTICAL INTERNEURON DEVELOPMENT

Neurogenesis and cell proliferation within ganglionic eminences is tightly regulated and dependent on the ability of cells to progress through the cell cycle and divide. For any cell to successfully proliferate, it must first undergo DNA replication/synthesis and then mitosis. Between these stages there are gap phases in which cells are able to prepare for the transition to the next stage by synthesising gap specific proteins. Hence, the cell cycle is typically divided into 4 main stages; gap 1 (G1) phase, synthesis (S) phase, gap 2 (G2) phase and mitosis (M) phase (Figure 1.9). At each stage, there are check points to ensure the integrity of the cell, cyclins and cyclin dependent kinases (CDKs) are necessary at these points to allow cell cycle progression. Though all

phases of the cell cycle are important, the regulation of G1 phase has been a focal point in neurodevelopmental research, given the recent hypothesis that lengthening of G1 phase increases the likelihood that daughter cells will exit the cell cycle upon completion of a division (Calegari and Huttner, 2003; Calegari et al., 2005; Lange et al., 2009; Pilaz et al., 2009).

G1 phase is the initial stage of the cell cycle and the point at which a cell commits to a round of division. This phase contains two checkpoints which the cell must pass prior to DNA synthesis. Studies have found that at the first of these checkpoints, cyclin D (D1, D2 or D3) forms a complex with CDK4 or CDK6 (Sherr, 1995). For a cell to progress through G1 phase, the cyclin D/ CDK4/6 complex phosphorylates retinoblastoma protein (Rb), inactivating it and releasing transcription factors required for synthesis of E type cyclins and thereby allowing progression from G1 to S phase. Cyclin E molecules couple with CDK2 to drive G1 to S phase progression through phosphorylation of cyclin dependent kinase inhibitor, $P27^{Kip1}$ (Sheaff et al., 1997). G1 phase is the main point of the cell cycle where cells respond to mitogenic factors in the cellular environment. The G2 to M phase transition has also been of interest since it is the last opportunity to repair damaged DNA before undergoing mitosis. The G2-M checkpoint is tightly regulated by Cdc25 which activates the formation of the cyclin B/CDK1 complex which in turn drives the transition from G2 to M (Ross et al., 2011). Once a cell completes the cell cycle, the daughter cells must either exit the cycle or prepare to advance through G1 (Figure 1.9).

Interestingly, there have been several molecules that have been found to act as mitogens in cell cycling. The Shh signalling pathway is important for interneuron progenitors to enter S phase by upregulating and maintaining the interactions of cyclins and retinoblastoma (Kenney & Rowitch, 2000). Thus, Shh leads to an increase in the

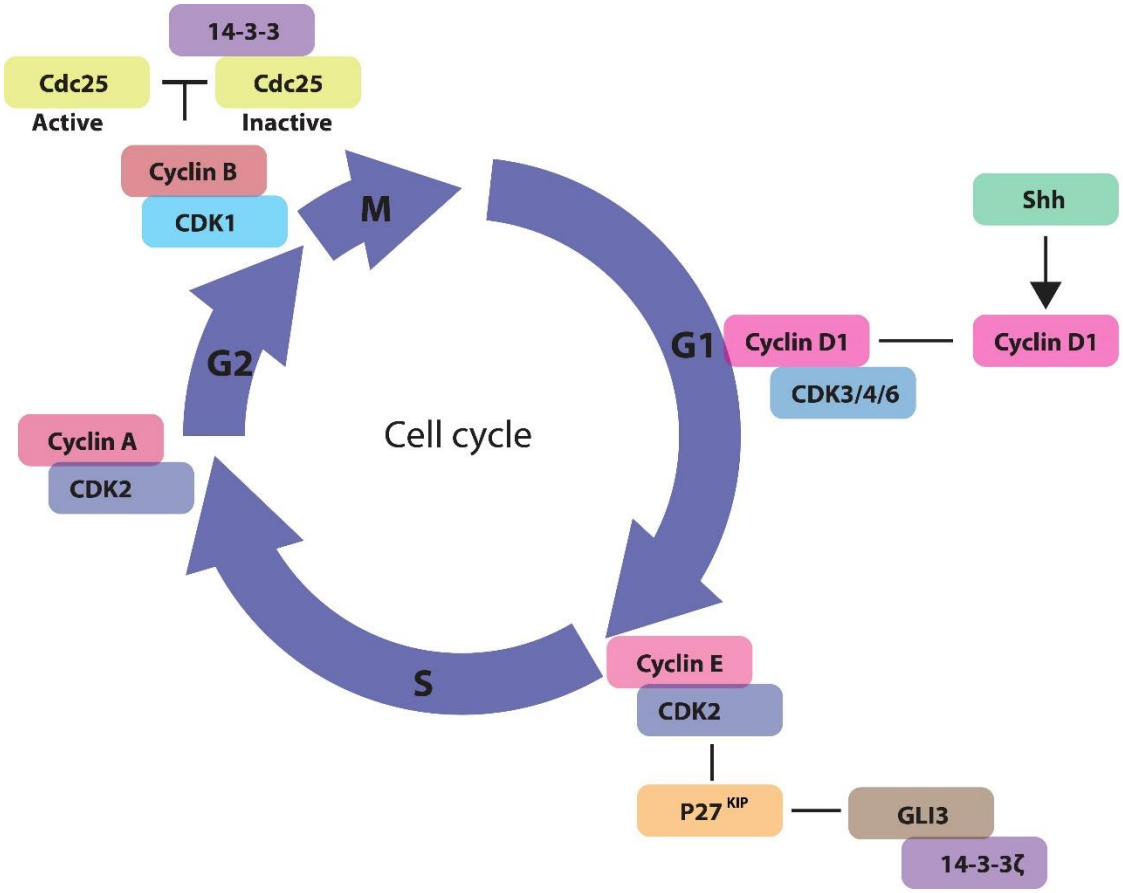


Figure 1.9: Overview of the cell cycle.

Cells enter the cell cycle at G1 which is controlled by two restriction points governed by interactions of Cyclins D/E and CDKs. After passing the second restriction point cells are committed to entering S phase. Following completion of DNA synthesis, cells enter G2 phase. Entry into mitosis phase is controlled by interactions of cyclin B and CDK1. After mitosis is complete cells can exit the cell cycle or commit to another round. 14-3-3ζ has been implicated in regulating transition from G1-S phase and G2-M phase, through interactions with $p27^{Kip}$ and Cdc25 respectively.

expression of *cyclin D1* to allow cells to pass through G1 phase. Furthermore, several studies have also implicated small GTPases in cell cycle progression, including Rho family proteins (Olson et al., 1995; Joyce et al., 1999; Mettouchi et al., 2001; Vidaki et al., 2012). Vidaki et al. showed Rac1 is necessary for MGE precursors to transition from G1 to S phase, by regulating *cyclin D* levels and retinoblastoma protein phosphorylation (Vidaki et al., 2012). Furthermore, pre-mitotic but not post-mitotic MGE cells where Rac1 was abolished show defects not only in cell cycle progression but also in specification and migration (Vidaki et al., 2012).

Dysfunction in cell cycle progression is found to have several downstream effects, with aberrant regulation of the cell cycle resulting in premature terminal differentiation and reduced proliferation and neurogenesis. This is seen in both *cyclin D1* and *D2* deficient mice, which display consistently smaller forebrains (microcephaly) than their littermates (Sicinski et a., 1995; Ciemerych et al., 2002; Glickstein et al., 2007). Furthermore, *Cyclin D1* KO mice show thinning of the cortical layers (Glickstein et al., 2007b). In contrast, *Cyclin D2* KO mice show a disproportionate reduction in PV+ cortical interneurons suggesting an MGE-specific requirement of cyclin D2 (Glickstein et al., 2007b). Interestingly, analysis of these mice has revealed unique and separate functions of cyclin D molecules within the MGE. The alternative roles of cyclin D molecules is supported by the findings that *cyclin D1* and *D2* are differentially expressed in different regions of the MGE. Thus, *Cyclin D1* is expressed in cells in the VZ and *cyclin D2* is induced in cells entering the SVZ (Glickstein et al., 2007a; Glickstein et al., 2007b; Glickstein et al., 2009).

1.7 MIGRATION OF CORTICAL INTERNEURONS DURING DEVELOPMENT

1.7.1 Tangential migration of cortical interneurons

Interneurons initiate migration from the ganglionic eminences at approximately E11.5 in response to chemoattractant and chemorepellent cues from the cortex and striatum. This migration will continue throughout embryonic development until the formation of new neurons within the ganglionic eminences has ceased. Unlike other neuronal cell types, interneurons exit the cell cycle before migration, with *Lhx6* being expressed after undergoing cell cycle exit. Failure to exit the cell cycle before migration results in aberrant migration and ectopic positioning of postnatal interneurons within the cortex. For example, Vidaki and colleagues (2012) showed that a reduction of *Rac1* in progenitor interneurons perturbed G1 cell-cycle progression thus resulting in a subsequent loss of MGE derived interneurons in the cortex (Vidaki et al., 2012); however, reduction of *Rac1* after the onset of interneuron migration had no effect on the cell cycle and showed little to no effect on the interneuron landscape in older mice.

To reach their appropriate position within the cortex interneurons must first navigate away from the ganglionic eminences and into the dorsal pallium. Invasion of the cortex is highly ordered and occurs through two major tangential migration pathways. The first neurons to exit the ganglionic eminences are primarily biased toward PV+ fate and migrate around the striatum and into the marginal zone (MZ). In contrast, the neurons born at later time points consist of a mixed population of interneurons that migrate through the subventricular zone (SVZ) (Figure 1.10). The first stage of migration out of the ganglionic eminences is primarily controlled by chemorepulsion signals that were originally described as axonal guidance cues. The class 3-semaphorins (Sema3A and Sema3F) are expressed by the striatum and interact with the cell surface neuropilin

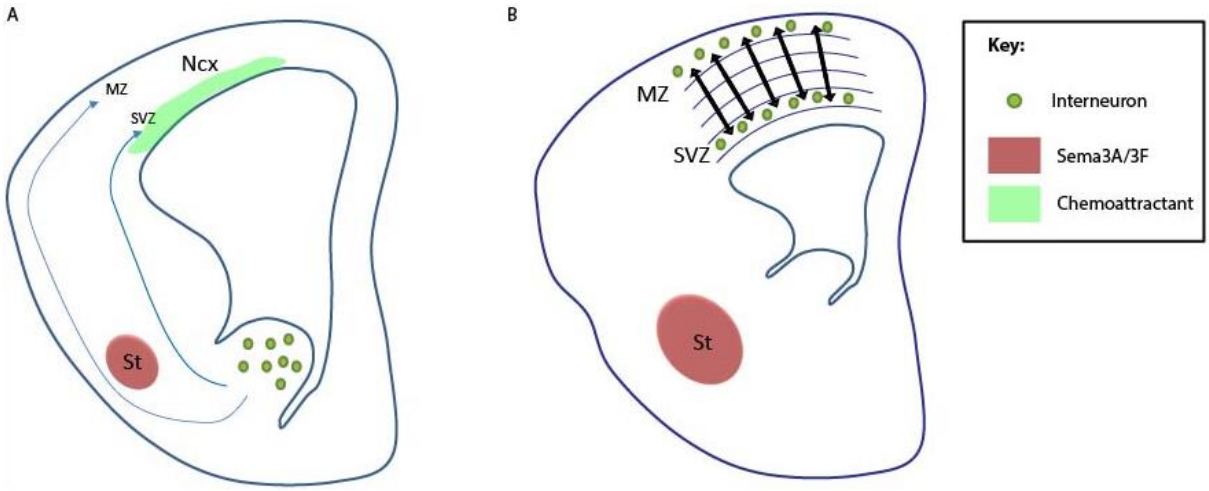


Figure 1.10: Migration of cortical interneurons.

(A) Cortical interneurons born in the ganglionic eminences will migrate via two spatially distinct pathways to the neocortex. Early migrating cells will migrate from the MGE and into the marginal zone (MZ) and later migrating cells will migrate via the subventricular zone (SVZ). Repulsive cues, specifically Sema3A and Sema3F, are expressed in the striatum to aid in directing cortical migration away from the striatum and towards the neocortex. Nrg-1 also acts as a morphogenic factor to direct migration to the neocortex. (B) Interneurons switch from tangential migration to radial migration once they reach the neocortex. Radial migration will allow interneurons to distribute throughout the cortex into their ultimate laminar position. Early migrating interneurons will occupy the deeper layers of the cortex whereas later migrating interneurons will occupy the more superficial layers.

(Taken from Greenberg et al., 2015)

receptors Nrp1 and Nrp2 which are expressed on migrating interneurons. Due to the presence of chemorepulsive signals in this environment, interneurons expressing the neuropilin receptors migrate around the striatum in a distinctive path. Indeed, deficiency of the neuropilin receptors leads to aberrant interneuron migration with an increased number of interneurons localising to the striatum (Marín et al., 2001). Notably, the interneurons that target the striatum during normal developmental contexts lack expression of the neuropilin receptors (Marin et al., 2000). This semaphorin / neuropilin axis therefore represents part of the mechanism for sorting different classes of interneurons to their appropriate locations, similar to their roles in other neuronal types (Lumb et al., 2014; Schwarz et al., 2009; Schwarz & Ruhrberg, 2010). Hernández-Miranda et al. (2011) showed that the roundabout guidance receptor 1 (Robo1) is also important for guiding newly formed interneurons out of the ganglionic eminences and along the tangential migration paths (Hernández-Miranda et al., 2011). Robo1 is a transmembrane receptor that recognises secreted chemorepulsive ligands from the Slit family. *Robo1* is expressed by migrating interneurons within the ganglionic eminences and the *Slit* ligands are expressed in a complementary pattern within the ventricular zone of the cortex (Marín et al., 2002). However, rather than controlling migration along the tangential paths in the cortex, the Slit/Robo signalling pathway also helps to keep interneurons away from the striatum (Marín et al., 2001; Hernández-Miranda et al., 2011). The overlap in phenotypes of the *Slit/Robo* and *semaphorin/neuropilin* knockout mice may be partly explained by the finding that Robo1 can physically interact with neuropilin (Hernández-Miranda et al., 2011), perhaps suggesting that the two pathways functionally interact. The Eph/Ephrin signalling pathway also plays important roles in promoting the initial phases of interneuron migration away from the ganglionic eminences. *EphrinB3* and *EphA4* are reciprocally expressed in MGE and POA derived interneurons and through

forward/reverse signalling are involved in sorting these different classes toward different cortical migratory streams (Zimmer et al., 2011). *EphrinA5* is also expressed in the ventricular zone of the MGE and interactions between EphrinA5 and EphA4R are required to push interneurons away from the ventricular zone (Zimmer et al., 2008). The aristaless related homeobox transcription factor Arx has also been suggested to have an important role in promoting early interneuron migration. *Arx* knockout mice display an aberrant accumulation of interneurons in the proliferative zones of both the MGE and the CGE which results in the loss of cortical interneurons at later stages (Friocourt & Parnavelas, 2010). However, as interneuron progenitors fail to exit the cell cycle in Arx deficient mice, its role in migration as opposed to specification is unclear.

Cortical interneurons that navigate around the striatum to enter the pallium then migrate further dorsally under control of chemoattractive cues. The epidermal growth factor family member neuregulin-1 *(Nrg-1)* is expressed in the cortex and has been proposed to act as an attraction signal for interneurons expressing the tyrosine kinase family receptor *ErbB4* (Flames et al., 2004). However, the exact role of neuregulins in interneuron development is still open to debate. Contrary to the notion that neuregulin's act as chemoattractive cues, data recently reported by Li et al. (2012) suggest that neuregulin may instead act to inhibit the tangential migration of interneurons (Li et al., 2012). In the latter example the authors found minimal overlap between interneurons and neuregulin expression domains in wild-type mice but found significant colocalisation of interneurons in these expression domains in *ErbB4* knockout mice. The chemokine receptors CXCR4 and CXCR7, which interact with the secreted ligand SDF-1, have also been found to have a role in tangential migration within the cortex (Balabanian et al., 2005). Interestingly, in *CXCR4* and *CXCR7* knockout mice there is a 25% reduction in *Lhx6* expressing interneurons in the lateral regions of the neocortex (Wang et al., 2011).

1.7.2 Radial migration and laminar distribution of interneurons in the cortex

Once interneurons reach the developing neocortex they change from long distance tangential migration to radial migration, before settling in their final resting place in which they integrate into local cortical circuits. Interneurons sort into deep and superficial layers in an inside out fashion with the first-born MGE derived interneurons occupying the deeper layers and later CGE derived interneurons occupying more superficial layers (Figure 1.10). The final position of interneurons is dictated at their time of birth and these interneurons will ultimately localise to the same cortical layer as projection neurons born at the same time. While the mechanisms controlling this colocalization remain unknown, it has been suggested that interneuron radial migration may be arrested in response to interactions with projection neurons born on the same day in neurogenesis (Hevner et al., 2004).

Correct distribution of interneurons throughout the cortical layers is essential for their ultimate function and the formation of cortical microcircuits. In comparison to the well described migration route of pyramidal neurons along radial glial scaffolds, interneurons have been found to migrate independently of glia and in response to different molecular cues (Nadarajah & Parnavelas, 2002; Nadarajah et al., 2003; Polleux et al., 2002). While SDF-1 is a positive regulator of tangential migration within the cortex, its down regulation may also play an important role in promoting the switch to radial interneuron migration at later stages of development. Indeed, the inhibition of SDF-1/ CXCR signalling in slice cultures after interneurons had already navigated into the cortex was shown to promote a rapid switch from tangential to radial migration (Lysko et al., 2011). Furthermore, p35/CDK5 interactions were found to be crucial in both pyramidal and interneuron radial migration. Defects in radial migration have also been shown in *Lhx6* deficient mice. In these mice interneurons failed to occupy the middle neocortex,

and instead occupy the very deep or superficial layers (Miyoshi & Fishell, 2011; Vogt et al., 2014). Interestingly, this deficiency was somewhat reversed by the addition of downstream proteins CXCR7 and Arx at E13.5, identifying this as a critical period for interneuron radial migration.

1.8 INTERNEURONS IN SCHIZOPHRENIA AND NEURODEVELOPMENTAL DISORDERS

The link between interneuron deficiency and schizophrenia was first identified in the 1970s by Perry and colleagues (Perry et al., 1979) who reported a loss of the inhibitory neurotransmitter GABA in post-mortem brain samples. In the 40 years since this first description, interneuron defects have been consistently found in post-mortem tissue samples of schizophrenia patients (Farzan et al., 2010; Yoon et al., 2010), however this is not a global reduction as CR+ interneurons remain unaffected (Hashimoto et al., 2003; Fung et al., 2010). Indeed, many studies have now shown a reduction of PV+ interneurons in schizophrenia patients compared to controls (Beasley & Reynolds, 1997; Zhang & Reynolds, 2002; Wang et al., 2011), though some studies have also reported a reduction in SST+ interneurons (Fung et al., 2010; Wang et al., 2011; Joshi et al., 2015). Interestingly, one of the most consistent findings in schizophrenia has been a reduction in *GAD67* expression in PV interneurons (Volk et al., 2000; Guidotti et al., 2000; Hashimoto et al., 2003; Lewis et al., 2005). Furthermore, patients with schizophrenia have been found to have decreased coordination of brain activity (Kikuchi et al., 2011) and reduced gamma oscillatory activity during cognitive tasks due to the loss of PV+ interneurons, whereas there is no change in the gamma oscillations at rest (reviewed in Uhlhaas & Singer, 2010). Recent genetic analyses including whole exome sequencing and Genome Wide Association Studies (GWAS) on large schizophrenia cohorts further strengthen the link between interneuron deficiency and disease pathogenesis. For

example, from the analysis of 623 schizophrenia trios Fromer et al. (2014) revealed missense mutations in several genes known to play critical roles in interneuron development, including *LHX6, GLI2, GLI3 and ERBB2* (Fromer et al., 2014). Moreover, GWAS studies have also found links to genes and molecular pathways involved in interneuron development, including *NRG-1*, *ERBB4* and genes within the WNT signalling pathway (Hosak, 2013; Silberberg et al., 2006). Expression studies on patient samples also provide correlations between interneuron deficiency and clinical symptoms. Notably, from the list of genes introduced in this introduction, the expression of both *CXCR4* and *CXCR7* have recently been found to be altered in post-mortem schizophrenia patient samples (Volk et al., 2015).

1.8.1 Hippocampal interneurons in schizophrenia

Due to aberrant hippocampal formation being associated with schizophrenia, many studies have focused on the hippocampus when investigating interneuron deficiencies in post-mortem brains of patients with schizophrenia. Early studies examining aberrant GABAergic activity in schizophrenia found a region-specific upregulation in GABA(A) receptor in the hippocampus of schizophrenic patients, suggesting a decrease in GABA activity in the hippocampus (Benes et al., 1996). Subsequently, a follow up study found reduced *GAD67* expression specific to the same area of the hippocampus (Benes et al., 2007). Since then several studies have identified a loss of PV and SST interneurons in the hippocampus as well as a reduced mRNA expression of *PV*, *SST* and *GAD67* in post-mortem brains of schizophrenic patients (Konradi et al., 2011).

1.9 SCHIZOPHRENIA

1.9.1 Impact of schizophrenia

Schizophrenia is the most persistent and disabling of the major mental illnesses and affects 1% of the world's population (Saha et al., 2005). It is a complex psychiatric disorder with a largely unknown pathophysiology and aetiology. Characterized by poor emotional interactions and a breakdown in thought processes, the main features of schizophrenia are its debilitating psychosis and cognitive dysfunction. Patients present with both positive symptoms including hallucination, paranoia and delusions and negative symptoms such as social withdrawal and disorganized thought. Cognitive symptoms, including deficits in attention, learning and memory, have also been found in people with schizophrenia. Family and twin studies have shown that schizophrenia is transmitted in a polygenic, non-mendelian fashion, leading to the proposal that its pathogenesis arises from a complex network of interactions between susceptibility genes and environmental risk factors occurring in early neurodevelopment (Harrison & Weinberger, 2005). Schizophrenia generally presents in late adolescence and young adulthood, often with warning signs occurring at a younger age, with the environmental factors associated with schizophrenia generally occurring in the prenatal period of life (Lewis and Levitt, 2002). Schizophrenia is commonly associated with severe disability in personal functioning and often results in a reduced quality of life. There is an extremely high rate of suicide among those affected with schizophrenia, with 40% of people diagnosed attempting suicide, 12 times higher than that of the general population. There is a significant financial and social impact for both the individual and the community. Due to its chronic nature, schizophrenia has a severe financial burden on the economy, in 2001 the direct expenditure on schizophrenia in Australia, which spends at the low end

of the spectrum for developed countries, was 661 million Australian dollars (WHO, 2001).

1.9.2 Proposed aetiologies of schizophrenia

Though the aetiology of schizophrenia is not well understood, there is general consensus within the field that disrupted connectivity is a central component in its pathology (English et al., 2009). Furthermore, neuroimaging studies have shown that structural brain abnormalities are characteristic in schizophrenia patients and have implicated that a loss of grey matter and general architecture of the brain are involved in its pathogenesis (Clapcote et al., 2007). Recent studies have shown that neuronal migration, neurite formation and disruption of synapses are key influences in the formation of clinical symptoms (Insel, 2010; Walsh et al., 2008). These findings provide strong support to the notion that the pathophysiology may be due to underlying disturbances in brain formation. Indeed, further support of a neurodevelopmental origin has come from the absence of neurodegenerative defects in post-mortem schizophrenia brain samples (Lewis & Levitt, 2002).

There are several hypotheses regarding the aetiology of schizophrenia, with one of the major hypotheses put forward being the hippocampal hypothesis. Disturbances in hippocampal formation and plasticity have been implicated in numerous brain disorders from both degenerative and developmental origins (Preston et al., 2005; Olincy et al., 2006; Koolschijn et al., 2010; Heckers & Konradi, 2015), with hippocampal formation being one of the most studied neuronal systems in the brain (Andersen et al., 2007). The hippocampus is central to the neuropathology and pathophysiology of schizophrenia (Harrison et al., 2004). Over the past few decades there have been numerous studies to support non-degenerative hippocampal formation as a key defect in schizophrenia

(Heckers et al., 1991; Walker et al., 2002; Schmitt et al., 2009; Konradi et al., 2011; Allen et al., 2016). Neuroimaging data (reviewed in Heckers et al., 2001) show a decreased volume in the hippocampus of patients with schizophrenia compared with healthy individuals (Lawrie and Abukmeil, 1998; Nelson et al., 1998; Wright et al., 2000). However, it should also be noted that other studies claim that hippocampal cell loss is not associated with schizophrenia (Heckers et al., 1991). Regardless of these inconsistencies, the finding of structural changes in the brain in some patients adds strength to the hypothesis that schizophrenia is a developmental disorder. Another consistent finding in schizophrenia patients is the molecular disorganization observed in the cornu ammonis region of the hippocampus, where mislocalized neurons alter the formation of the hippocampal tri-synaptic circuit (Jakob and Beckmann, 1986; Falkai et al., 2000; Tamminga et al., 2010).

Alternatively, many studies have implicated aberrant neurotransmitter systems, including dopamine, glutamate and GABA, in the pathology of schizophrenia (Matthysse, 1973; Perry et al., 1979; Bogerts et al., 1983; Benes et al., 1992; Kegeles et al., 2000; Iversen & Iversen, 2007; Inan et al., 2013). The neurotransmitter hypotheses have been complicated by the fact that each system is dependent on the functioning of the other, hence dysfunction in any particular system can lead to abnormal functioning in other systems.

The dopamine hypothesis has been formulated for over 50 years and though there have been several reformulations, the theory suggests that hyperactivity of the dopamine pathway causes the symptoms associated with schizophrenia. There are two main observations that give support to this, 1) most current antipsychotic drugs target the dopamine signalling pathway (Carlsson & Lindqvist, 1963; Horn & Snyder, 1971; Seeman & Lee, 1975), and 2) psychosis can be induced by activation of dopamine

signalling (Lieberman et al., 1987; Curran et al., 2004). Indeed, neuropharmacological studies with antipsychotic drugs suggest that many of the positive symptoms associated with schizophrenia arise from hyperactive dopamine signalling. This has been closely tied to the glutamate (glutaminergic) hypothesis, suggesting that schizophrenia arises as a result of hypoformation in N-methyl-D-aspartate NMDA receptor signalling in glutamatergic neurons (Cioffi, 2013). This hypothesis is further supported by the manifestation of schizophrenia like symptoms with the administration of NMDA antagonists (Voineskos et al., 2013). Studies using NMDA antagonists have also found downstream effects on inhibitory neurons suggesting a delicate interplay between excitatory and inhibitory neurotransmission mediated through NMDA receptors.

The GABAergic/interneuron hypothesis has gained significant attention in recent years since it integrates defects in both dopaminergic and glutamatergic hypotheses. Direct interplay between the GABAergic and hypoglutamatergic hypotheses has been shown in mice by the specific removal of *NMDAR* in GABAergic interneurons (Belforte et al., 2010). In strong support of interneuron deficiencies aligning with the glutamatergic dysfunction these mice presented with molecular, behavioural and physiological defects akin to those seen in the human condition (Belforte et al., 2010). Direct interactions between aberrant cortical inhibition and dopamine signalling have also been proposed, however how this link is functionally established is highly debated. One possible link is cortical disinhibition leading to increased dopamine in the nucleus accumbens, as found when NMDAR antagonists were infused into the prefrontal cortex of mice (Del Arco et al., 2008). Considering the role of interneurons in modulating many neuronal networks it is likely that deficiency of interneurons during development may also contribute to the decreased glutamatergic and increased dopaminergic basis of disease progression.

1.9.3 Mouse models of schizophrenia

In order to understand the neurobiological basis and disease pathogenesis of schizophrenia several mouse models of schizophrenia risk factors have been developed. Despite the genetic heterogeneity of the disorder, many of these mouse models have demonstrated interneuropathies (reviewed in Inan et al., 2013) and behavioural phenotypes akin to those seen in the human condition. One of the most replicated risk factors for schizophrenia is Disrupted in Schizophrenia 1 (*DISC1*) that was first identified in a large Scottish family who had a breakpoint in this gene that occurred through a balanced chromosomal translocation (Millar et al., 2000). To recapitulate this mutation several mouse models have been generated to either remove or knock down the *DISC1* gene in a cell type specific manner. Notably, removal of *DISC1* from MGE at E13.5 has been shown to lead to a loss of cortical interneurons in adult mice that arises from aberrant tangential migration. How DISC1 modulates interneuron migration and whether this defect replicates the schizophrenia-like behavioural defects of *DISC1* knockout mice remains to be explored (Steinecke et al., 2012).

Another well-accepted mouse model of schizophrenia is the gestational MAM model. MAM is an anti-mitotic and anti-proliferative agent that methylates DNA (Matsumoto & Higa, 1966) and recapitulates many of the anatomical, behavioural and processing defects observed in schizophrenia. The MAM model has been used to demonstrate that a loss in PV+ interneurons in the cortex results in a loss of function in oscillation activation (Lodge et al., 2009). In subsequent reports, interneuron transplantation was able to rescue the observed interneuron deficiency in MAM mice. Interneuron transplantation was initially described by Wichterle and colleagues (1999), where interneurons derived from embryonic MGE where injected into adult mice (Wichterle et al., 1999). Remarkably, interneurons were able to migrate through the adult

cortex and disperse into the appropriate layers. This technique has since been performed on several mouse models of psychosis and other neurodevelopmental disorders (reviewed in Tyson & Anderson, 2014) and provides hope of a cellular based therapy for neuropsychiatric disorders.

There are several mouse models that provide insight to the molecular mechanisms controlling interneuron development, which also model schizophrenia. For example, *Nrg-1* and its receptor *ErbB4* are known susceptibility genes for schizophrenia (Silberberg et al., 2006; Agim et al., 2013; Lu et al., 2010; Shi et al., 2009) and mouse models removing these genes have been explored widely. Notably, many of these studies not only highlight the critical roles of these genes in interneuron development but also in interneuron function. Deficiency of *Shh* and *Nkx2.1* in the MGE clearly lead to interneuron defects. However, given the lethality of mice lacking these genes their roles in behaviours associated with the human condition have been harder to address (Kimura et al., 1996; Chiang et al., 1996).

In Summary, schizophrenia is a highly heterogeneous disorder with a largely unknown origin. While mouse models have begun to provide insight into its potential aetiology, there is still much to learn. In the following sections I discuss 14-3-3ζ and its potential role as a risk factor for schizophrenia, in which I discuss the 14-3-3ζ mouse model as model for schizophrenia.

1.10 14-3-3ζ

1.10.1 The 14-3-3 family proteins

14-3-3 proteins are a family of acidic intracellular proteins (27-33kDa) that are highly conserved and believed to be ubiquitously expressed in all eukaryotic organisms. They are regarded as the most widely expressed proteins in the brain, accounting for 1%

of soluble brain protein (Boston et al., 1982; Pawson & Scott, 1997; Baxter et al. 2002). The term 14-3-3 was originally derived from the elution position on a two-dimensional DEAE-cellulose chromatography and migration pattern on starch gel electrophoresis, in the 14th fraction and in the latter step, the 3.3 fraction (Moore & Perez, 1967). 14-3-3 was the first family of proteins identified as phosphoserine/phosphothreonine binding molecules, though others have subsequently been reported (Yaffe and Elia, 2001). Interactions with a range of structurally and functionally diverse ligands regulate and mediate a variety of cellular processes including signal transduction, cell migration, cell cycle, cell division and cytoskeleton rearrangement (Berg et al., 2003). 14-3-3 proteins are found abundantly in all mammalian tissues (Messaritou et al., 2010) with seven known highly homologous mammalian isoforms (β, σ, ε, η, γ, τ, and ζ) each having a diverse range of interactions and functions. Despite their functional diversity, all isoforms share some of the same biochemical properties for activation and regulation, including interactions with similar enzymes (Fu et al., 2000). The similar structural and functional nature of 14-3-3 proteins can allow for compensation between isoforms, as observed in *14-3-3γ* knockout mice where no phenotype is observed (Steinacker et al. 2005). However, although there are a number of compensatory and redundant roles, studies continue to identify unique functions between the isoforms.

14-3-3s are adaptor proteins, primarily interacting with kinase family molecules, receptor proteins and enzymes (Fu et al., 2000). Though 14-3-3 is predominantly found in the cytoplasm of the cell, it can be localized to a number of different locations including mitochondria, plasma membrane and cytoskeleton (Zhang et al., 1999; Muslin & Xing, 2000). The versatile and flexible nature of 14-3-3 allows interaction with a diverse range of binding partners, where 14-3-3 optimally binds via phosphorylated serine/threonine motifs corresponding to mode-1 RSXpSXP and mode-2 RXF/YXpSXP sequences where

p denotes phosphorylated residue (Yang et al., 2006). Though 14-3-3 has been characterized as a phosphorylated serine/threonine binding protein, there are several interactions which are not phospho-dependent. Not all 14-3-3 interactions conform to the known binding consensus site or even phosphorylation, possibly suggesting that 14-3-3 binding has evolved differently between proteins (Aitken, 2006). 14-3-3s interactions are tightly controlled in normal cells, and hence de-regulation has been implicated in several disorders and diseases.

1.10.2 The known intracellular functions of 14-3-3ζ

14-3-3ζ is a robust protein and is not easily degraded, which may be significant to its diverse range of essential functions within cells (Sluchanko et al., 2011). The involvement of 14-3-3ζ in mediating a wide variety of biological responses was originally characterized based on functional studies aimed at identifying regulatory proteins (Fu et al., 2000). The function of 14-3-3ζ can generally be classified in 4 ways: (1) changes conformation of binding partner, often to increase affinity or stabilization, (2) physically occludes sequence specific or structural features of binding partner, (3) mediates cellular localization and (4) functions as a scaffold protein, stimulating protein-protein interactions (Obsilová et al., 2008). 14-3-3ζ's interaction with its ligand can drive a cascade of reactions leading to the regulation of cell cycle, apoptosis, cell migration, signal transduction and cytoskeleton coordination (Gardino et al., 2006). The role 14-3-3ζ plays within a biological pathway is largely dependent on its binding partners, for example, interactions with Cdc25 can regulate the cell cycle and interactions with Raf-1 kinase and BAD control the regulation of apoptotic and cell death pathways (Yang et al., 2006).

1.10.3 The molecular structure of 14-3-3ζ

The structure of 14-3-3 proteins is unique with the only significant homology to other proteins being the tetraricopeptide repeat (TPR), which forms repeats that mediate protein-protein interactions (Aitken, 2006). 14-3-3ζ's crystal structure was first determined by Liu et al. 1995 and consists of nine antiparallel alpha helices (αA-I) which interact between both monomers in order to maintain a dimeric state. The first four helices (αA-D) form the dimer interface as well as the floor of the channel in the amphipathic groove, the other helices αE-H (5-8) form the roof of the channel and the side walls of the protein (Figure 1.11A) (Liu et al., 1995; Yaffe and Ya, 2002). Helices A and B from one monomer interact with C and D from another to maintain the dimeric structure (Figure 1.11B). 14-3-3ζ is generally a negatively charged molecule with the exception of a strongly charged basic section that consists of Lys49, Arg56, and Arg127 residues which engage in ligand binding and make up the amphipathic groove (Yang et al., 2006). The amphipathic groove, which contains the phosphoserine and phosphothreonine binding motifs, is characterized by both polar and non-polar chains, consisting of a hydrophobic surface which is highly conserved between isoforms. Disruption to the amphipathic groove can inhibit 14-3-3ζ's ability to bind ligands and hence may render it non-functional.

The dimerization of 14-3-3ζ is important to its function within a cell. 14-3-3ζ is able to form either a homodimer, or a heterodimer, which is essential for its ability to bind potential ligands. When dimerized, 14-3-3ζ contains two binding grooves, which enable simultaneous binding of two phosphorylated ligands, a property permitted by 14-3-3ζ's flexible nature (Figure 1.12) (Reinhardt & Yaffe, 2013). This has been found to increase the efficiency of 14-3-3ζ binding (Fu et al., 2000). Furthermore, the phosphorylation of 14-3-3ζ itself has an important regulatory role with phosphorylation on specific residues

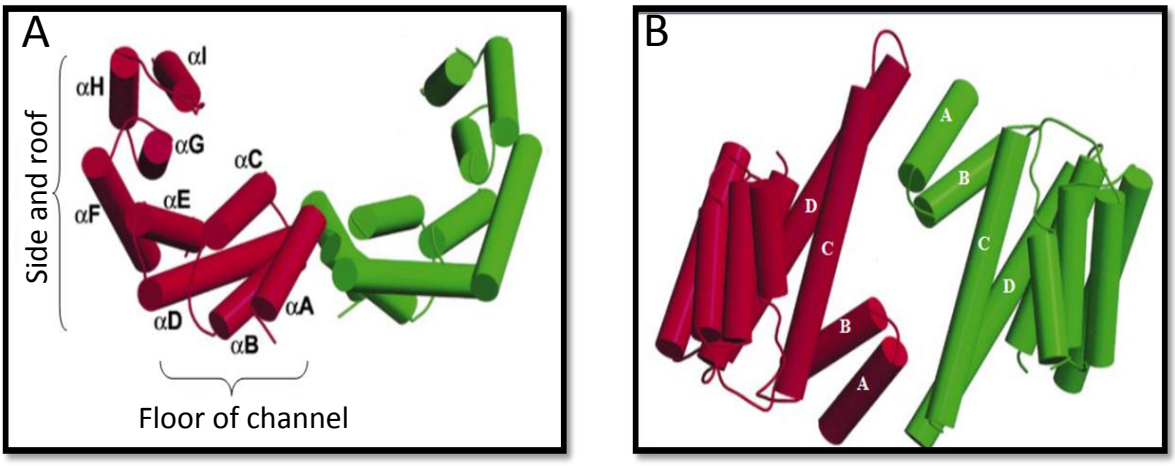


Figure 1.11: Schematic diagram of the nine 14-3-3ζ alpha helices.

(A) The crystal structure of 14-3-3ζ indicating the 9 antiparallel helices (αA-I). Helices A-D make up the floor of the 14-3-3ζ amphipathic groove and helices E-I make up the side and roof. (B) A bottom view of the interaction between each monomer of 14-3-3ζ (represented in red and green). Helices A and B from one monomer (red) interact with helices C and D from the other (green) to maintain the dimeric structure.

(Adapted from Yaffe and Ya, 2002).

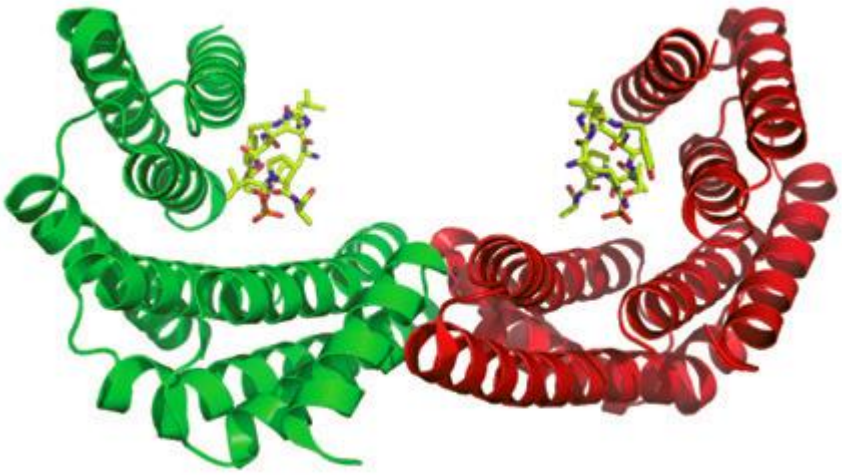


Figure 1.12: Dimeric 14-3-3ζ interacting with ligand.

The crystal structure of 14-3-3ζ in its dimeric form, which consists of 2 monomers (green and red). Two binding partners (yellow) interact at the amphipathic groove of 14-3-3ζ simultaneously.

(Adapted from Reinhardt & Yaffe, 2013).

preventing dimerization (Woodcock et al., 2003). In order to maintain the dimeric structure of the protein, salt bridges form between the monomeric units. 14-3-3 molecules elect to homo or hetero dimerize depending on which will provide the most stable structure. For example, 14-3-3σ will only homo dimerize since it forms a unique salt bridge not present on any other isoform. In contrast, 14-3-3ζ is able to either homo or hetero dimerize, as both will provide similar stability (Yang et al., 2006).

The highly acidic C-terminus of 14-3-3ζ is extremely flexible and is believed to be involved in ligand binding, however due to its instability it is often naturally cleaved (Gardino et al., 2006). The C-terminal region does not display in electron microscope density in crystal structures and hence has required other methods to identify its structure. Several studies suggest that the C-terminus folds back into the binding pocket until displaced by tight binding of the ligand, acting as a molecular switch (Gardino et al., 2006). Truong et al. 2002 showed using C-terminally truncated 14-3-3ζ, that mutant 14-3-3ζ increased binding to ligands BAD and Raf-1 compared to the wild type. This suggests an autoinhibitory role for the C-terminal tail in order to protect against non-specific interactions of inappropriate ligands.

1.10.4 The role of 14-3-3s in schizophrenia and neurodevelopmental disorders

The high expression of 14-3-3 proteins in the brain suggest an important role in neuronal functions. Several of the 14-3-3 family proteins, most notably 14-3-3ε, 14-3-3ζ, 14-3-3η and 14-3-3σ, to a lesser extent, have been reported to have roles in neuropsychiatric and neurodevelopmental disorders (Muratake et al., 1996; Toyo-oka et al., 2003; Wong et al., 2005; Middleton et al., 2005; Cheah et al., 2012; Foote et al., 2012). A single nucleotide polymorphism (SNP) in the 14-3-3η gene has been identified in studies using human samples from patients with schizophrenia (Toyo-oka et al., 1999;

Bell et al., 2000; Wong et al., 2003). Furthermore, genetic analyses have suggested a link between chromosomal region 22q12-13, where the *14-3-3η* gene is located, and schizophrenia (Muratake et al., 1996).

Several studies have focused on 14-3-3s role in neuronal migration, in particular investigating the relationship between 14-3-3 and lissencephaly, a neural migration disorder resulting in 'smooth brain'. Proper neuronal function is dependent on the Ndel1/LIS1/14-3-3 protein complex which promotes the recruitment, organization, and movement of microtubules. In this pathway, both 14-3-3ε and 14-3-3ζ interact with phosphorylated Ndel1, protecting it from dephosphorylation, which in turn allows for the recruitment of LIS1 to this protein complex (reviewed in Kato & Dobyns, 2003). 14-3-3ε KO mice have altered brain structures, including cortical thinning and hippocampal defects (Toyo-oka et al., 2003). Furthermore, these mice show altered cellular dynamics such as aberrant neuronal migration and increased neuronal cell death. Interestingly, mice with mutations in both 14-3-3ε and LIS1 have more severe neuronal migration defects compared to mice with a single mutation (Toyo-oka et al., 2003).

Of this family of proteins *14-3-3ζ* has gained more attention in recent years, being implicated in several neurodevelopmental disorders. *14-3-3ζ* has recently been proposed as a risk factor for neurodevelopmental disorders based on the identification of genetic mutations in both schizophrenia and autism (Toma et al., 2013; Fromer et al., 2014) and the finding that it is consistently down-regulated in post-mortem schizophrenia brain samples (Wong et al., 2005; Middleton et al., 2005; Sivagnanasundaram et al., 2007; English et al., 2009, English et al., 2011). Whole-exome sequencing analyses identified a non-synonymous heterozygous point mutation in *14-3-3ζ* (*14-3-3ζ*-K115R) in a schizophrenia patient which leads to an alteration of a lysine residue required for proper protein function (Fromer et al., 2014). Similarly, a mutation in *14-3-3ζ* (*14-3-3ζ*-fs220)

was identified in an autism patient, which resulted in a non-synonymous frame-shift mutation leading to a premature truncation of the protein (Toma et al., 2013). Using DNA microarray analysis, Middleton and colleagues reported reduced expression of *14-3-3ζ* in the prefrontal cortex of patients with schizophrenia. This was supported by proteomics studies which identified reduced protein expression of 14-3-3ζ in patients with schizophrenia. Interestingly, 14-3-3ζ also interacts with several proteins thought to be involved in schizophrenia, including DISC1 (Angrand et al., 2006; Cheah et al., 2012). Taken together, these findings identify 14-3-3ζ as a candidate risk factor for schizophrenia and associated disorders.

1.10.5 The *14-3-3ζ* KO mouse model

Due to the similarities in structure and function, interactions of the 14-3-3 family proteins are often compensated for by other 14-3-3 members, potentially masking a distinctive phenotype in knockout models. This, however, is not the case with *14-3-3ζ* KO mice, which show a distinct developmental phenotype akin to defects seen in neurodevelopmental disorders.

14-3-3ζ KO mice were generated at the Centre for Cancer Biology, University of South Australia as described by Cheah and colleagues (Cheah., et al., 2012). Briefly, using a gene trap vector inserted into the first intron of *14-3-3ζ* (Figure 1.13), this mouse line was generated in SV129 background and then backcrossed into BALB/c and C57BL/6 backgrounds. The gene cassette contains two long terminal repeats (LTR) and *βGeo* gene encoding β galactosidase/neomycin phosphotransferase fusion gene expressed under the endogenous *14-3-3ζ* promoter. Our group has published studies in SV129 and BALB/c background mice primarily focused on behavioural and cognitive defects. Notably, *14-3-3ζ* KO mice have defects in spatial learning and memory, locomotor

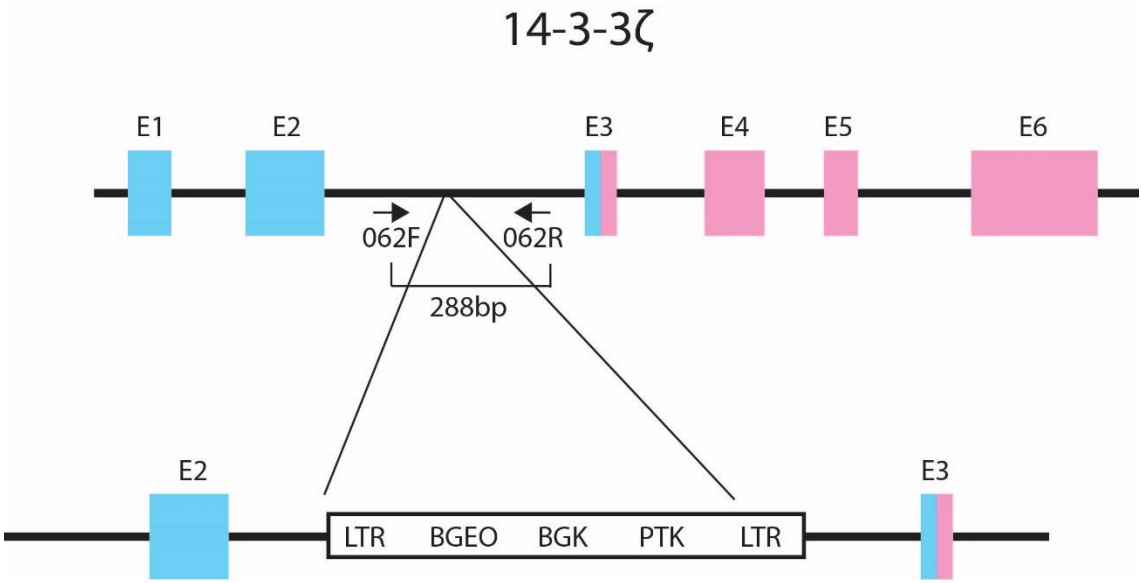


Figure 1.13: *14-3-3ζ* knockout gene trap.

Schematic representation of the *14-3-3ζ* gene showing the insertion point for the gene trap to create the 14-3-3ζ KO mice. The gene trap vector contains two long terminal repeats (LTR), as well as *βGeo* for β galactosidase/neomycin phosphotransferase fusion gene expressed under the endogenous *14-3-3ζ* promoter. The vectors also contain a *PGK* promoter followed by Bruton's Tyrosine Kinase gene (*BTK*), which contains termination codons in all reading frames to prevent translation of downstream fusion transcripts. Blue boxes indicate non-coding untranslated sequence and pink boxes denote coding sequence. Arrows represent primers used for genotyping.

(Adapted from Cheah et al., 2012)

hyperactivity and sensorimotor gating (Cheah et al., 2012, Ramshaw et al., 2013; Xu et al., 2015). In addition, these *14-3-3ζ* KO mice demonstrate structural defects in the hippocampus, abnormal neuronal positioning and disrupted organization of glutamatergic synapses (Cheah et al., 2012). Using calbindin immunostaining abnormal mossy fibre pathways were also demonstrated in *14-3-3ζ* deficient mice. *14-3-3ζ* KO mice were additionally found to have aberrant dopamine signalling leading to the locomotive hyperactivity (Ramshaw et al., 2013). Notably, hyperactivity of *14-3-3ζ* KO mice is rescued by treatment with the antipsychotic drug clozapine. Taken together, these findings highlight that *14-3-3ζ* KO mice are an ideal model of schizophrenia with high construct, predictive and face validity. Interestingly, defects in both dopaminergic and glutamatergic function have been previously linked to reduced inhibition and hence it would be of interest to examine interneuron function in these mice.

1.11 PROJECT AIMS AND OBJECTIVES

Dysfunction in the formation and function of GABAergic cortical interneurons has been implicated as a central pathogenic mechanism in schizophrenia and other neurodevelopmental disorders. Given that *14-3-3ζ* knockout mice show an anatomical and behavioural phenotype akin to that seen in patients with schizophrenia, we hypothesized that these mice would have a deficiency in the formation and/or function of interneurons.

The first aim of this thesis was to investigate and characterize interneuron formation in *14-3-3ζ* KO mice. My analysis presented in chapter 3 showed a subtype specific reduction in MGE derived interneurons. The second aim was to investigate the origin of the interneuron deficiency in *14-3-3ζ* KO mice. In chapter 4, I identified aberrant progression through the cell cycle as an underlying defect of interneuron development.

The final aim of this thesis was to explore the molecular mechanism(s) giving rise to interneuron deficiency and to understand which signalling pathways 14-3-3ζ may regulate. My analysis in chapter 5 identified a key role for 14-3-3ζ and Rac1 in non-canonical Shh signalling pathway.

Taken together this thesis identifies a novel role for 14-3-3ζ in the formation of interneurons and further provides critical insight to the key signalling pathways controlling interneuron development. Furthermore, this thesis strongly supports a role of 14-3-3ζ in the aetiology of schizophrenia and neurodevelopmental disorders and identifies new tools in understanding interneuron formation.

Table 1.1: Summary of aims

Overall hypothesis: *14-3-3ζ* KO mice have a deficiency in the formation and/or function of interneurons.
Aim 1: Characterization of interneurons in *14-3-3ζ* KO mice Hypothesis: *14-3-3ζ* KO mice will have a reduced number of interneurons. Objectives: • To determine if interneurons are reduced in the *14-3-3ζ* KO mice. • To determine which interneuron subtypes are altered in the *14-3-3ζ* KO mice. • To establish whether interneuron deficiencies arise from a neurodevelopmental origin.
Aim 2: To investigate the origin of the interneuron deficiency in *14-3-3ζ* KO mice Hypothesis: Loss of interneurons arises from defects in specification, migration and/or differentiation. Objectives: • To investigate whether loss of PV+ interneurons arises from specification, migration and/or differentiation. • To determine if 14-3-3ζ has a cell autonomous role in interneurons. • To explore the formation of the MGE in the *14-3-3ζ* KO mice.
Aim 3: To explore the molecular mechanism(s) giving rise to interneuron deficiency in the *14-3-3ζ* KO mice. Hypothesis: Aberrant Shh signalling underlies the interneuron deficiency in the *14-3-3ζ* KO mice. Objectives: • To determine if Shh signalling is aberrant in the *14-3-3ζ* KO mice. • To determine if the aberrant Shh signalling in the *14-3-3ζ* KO mice is acting via the canonical or the non-canonical pathway. • To identify additional molecules regulating the non-canonical Shh signalling. • To determine where 14-3-3ζ may be acting within the non-canonical Shh signalling pathway.

Chapter 2: Materials and methods

2.1 Materials

2.1.1 Chemicals

All chemicals were obtained from Sigma, BD Biosciences, Chem-Supply, Merck, Life Technologies, Promega, MP Biomedicals, RCI Labscan, Neurotechnologies and Thermo Fisher Scientific, unless otherwise stated. Dissection equipment was obtained from Fine Science Tools, BD Biosciences, Swann-Morton and Cutisoft. Sectioning and immunostaining materials were obtained from ProSciTech, Molecular Probes, EMS, Tissue-Tek, Ibidi, Sigma, Vector Laboratories and Invitrogen, unless otherwise stated. All DNA/RNA techniques were performed using New England Biolab (NEB), Qiagen or Promega reagents.

2.1.2 Animals

Experimental procedures were performed in accordance with the Animal Ethics Committee of SA Pathology and the University of South Australia. *14-3-3ζ* KO mice were generated as described previously (Cheah et al., 2012). *Dlx5/6-Cre* mice were kindly provided by Joanne Britto (Wang et al., 2010). Olig2-Cre mice were kindly supplied by Jinhua Xiao (University of Melbourne).

To generate a conditional *14-3-3ζ* mouse line, the EUCOMM gene trap mouse embryonic stem (ES) cell line EUCE0076e02 was microinjected into blastocysts of C57BL/6 mice at the Australian Phenomics Network (APN 272) (Monash University). The resulting chimeras were bred with wildtype C57BL/6 mice to generate *14-3-3ζ*$^{gt/+}$ mice. By inter-crossing *14-3-3ζ*$^{gt/+}$ mice to a line expressing FlpE in the germline the *14-3-3ζ*$^{fl/+}$ mice were generated. EUCE0076e02 cells contain a gene trap cassette in which the splice acceptor *βGeo* is surrounded by inverted heterotypic loxP and Frt sites to promote gene trap inversion in the presence of Cre and FlpE recombinases. The gene trap is inserted between exon 3 and 4 of the

14-3-3ζ gene. In the "forward" orientation (*14-3-3ζ*$^{gt/gt}$) the splice acceptor site integrates into the upstream exons of *14-3-3ζ* to interrupt mRNA transcription. In the "reverse" orientation the splice acceptor is restricted to the non-coding strand and *14-3-3ζ* is expressed normally to create a conditional allele referred to as *14-3-3ζ*$^{fl/fl}$.

All mouse strains were maintained in a SV129, CD1, C57BL/6 or BALB/c background, however due to increased litter sizes only BALB/c mice were used in this study unless otherwise stated, these mice have previously been shown to exhibit anatomical and behavioural deficits (Xu et al., 2015). The day the vaginal plug was found was considered as embryonic day (E) 0.5, and day of birth was considered as postnatal day (P) 0.

2.1.3 Culture media

Cell culture media including Dulbecco's Modified Eagle's medium (DMEM) and Neurobasal media were obtained from Gibco, Invitrogen (Mount Waverly,Victoria). Supplements including B27 and foetal calf serum were from Gibco, Invitrogen. All other cell culture media or supplements were obtained from Sigma, Life Technologies, Worthington Biochemicals, Peprotech and Roche Applied Science unless otherwise stated. Sterile tissue culture plasticware was obtained from BD Biosciences and Millipore.

2.1.4 Bacteria

DH5α chemically competent strains of Escherichia coli (*E. Coli*) bacteria were used for the standard propagation of DNA plasmids.

2.1.5 Primers

Primers were obtained from GeneWorks or Sigma unless otherwise stated.

Table 2. 1: Primers for quantitative real time polymerase chain reaction (qPCR)

Primer	Sequence	AT (°C)
Gapdh	F- 5'-ACCCAGAAGACTGTGGATGG-3' R- 5'-CAGTGAGCTTCCCGTTCA-3'	60 60
B-actin	F- 5'-GATCATTGCTCCTCCTGAGC-3' R-5'-GTCATAGTCCGCCTAGAAGCAT-3'	60 60
14-3-3ζ	F- 5'-CAAGAAAGGAATTGTGGACCAG-3' R- 5'-TTCTCTGGGGAGTTCAGGAT-3'	60 60
Sema3A	F-5'-CCAAGACTGAAATTATCGTACAAAGAAATG-3' R-5'-AGAAGGAAGGTGTGGTAACTGGAG-3'	60 60
Sema3F	F- 5'-CATCTGCCTCAACGATGAGC-3' R- 5'-AGAGCCTGAAGAGGTAAAGACA-3'	60 60
Nrg1	F- 5'-AAAGTGTGCGGAGAAGGAGA-3' R- 5'-TGGCAACGATCACCAGTAAA-3'	60 60
Arx	F- 5'-GCTGGTCTGAGCACTTTTC-3' R- 5'-GGTGGGGCTGTCAGG-3'	60 60
Robo1	F- 5'-CGAACAAATCCAAGTGACCC-3' R- 5'-GGCAATCAATCAGCAACACT-3'	60 60
GAD67	F- 5'-CAAACTCAGCGGCATAGAAA-3' R- 5'-GAAGAGGTAGCCTGCACACA-3'	60 60
Nkx2.1	F- 5'-CGAGCGGCATGAATATGA-3' R-5'-GACCTGCGTGGGTGTCAG-3'	60 60
Lhx6	F - 5'-CACGGCTACATTGAGAGTCA-3' R- 5'-GACAGGCTGCTTGTTTTCAT-3'	60 60
Dlx2	F- 5'-GTGGCTGATATGCACTCGACC-3' R- 5'-GCTGGTTGGTGTAGTAGCTGC-3'	60 60

Sox6	F- 5'-TTGGGGAGTACAAGCAACTGATGC-3' R- 5'ATCTGAGGTGATGGTGTGGCTGTT-3'	60 60
Mash1	F- 5'-ACTTGAACTCTATGGCGGGTT-3' R- 5'-CCAGTTGGTAAAGTCCAGCAG-3'	60 60
Cyclin D1	F- 5'-TTGTGCATCTACACTGACAAC-3' R- 5'GAAGTGTTCGATGAAATCGT-3'	60 60
Cyclin D2	F- 5'-AGGACATCCAACCGTACAT-3' R- 5'-GGAAAGACCTCTTCTTCACA-3'	60 60
Dvl	F- 5'-AGCAGTGCCTCCCGCCTCCTCA-3' R- 5'-CCCATCACCACGCTCGTTACTTTG-3'	60 60
B-Catenin	F- 5'-GGGATGTTCACAACCGAATTGT-3' R- 5'-GCTACTCTTTGGATGTTTTCAATGG-3'	60 60
Tcf7L2	F- 5'GCACACATCGTTCAGAGCC-3' R- 5'-GGGTGTAGAAGTGCGGACA-3'	60 60
Shh	F-5'-AGGTTTCGACTGGGTCTACT-3' R- 5'-CGGTCTCCGGGACGTAAG-3'	60 60
Gli1	F- 5'- CCAAGCCAACTTTATGTCAGGG-3' R- 5'-AGCCCGCTTCTTTGTTAATTTGA-3'	60 60
Gli2	F- 5'-ACAACGCATGATTCGGACCT-3' R- 5'-AAAAGTGAAGGCTGGGCTGA-3'	60 60
Gli3	F- 5'-GGGACCAAATGGATGGAGCA-3' R- 5'-TGGACTGTGTGCCATTTCCT-3'	60 60
Ptch1	F- 5'-TGGCCGCATTGATCCCTATC-3' R- 5'-ACACAGGGGCTTGTGAAACA-3'	60 60

Abbreviations: AT, annealing temperature

Table 2. 2: Primers for genotyping

Primer Name	Sequence	Line
LTR	5'-GCGTTACTTAAGCTAGCTTGC-3'	*14-3-3ζ KO*
062F	5'-GAACTTCAGATCTGGTGAC-3'	*14-3-3ζ KO*
062R	5'- GATTGTACTCAAAATGGTGGA C-3'	*14-3-3ζ KO*
***14-3-3ζ* P1**	5'- GTTCTGGACACTGCTCATTTGG-3'	*14-3-3ζ $^{fl/fl}$*
***14-3-3ζ* P2**	5'- CAAATGAAAGACCCCCGCTGACG-3'	*14-3-3ζ $^{fl/fl}$*
***14-3-3ζ* P6**	5'- CAGTGACAGACTTCATGCAGG-3'	*14-3-3ζ $^{fl/fl}$*
Cre	F- 5'-GCCTGCATTACCGGTCGATGCAACGA-3' R- 5'-GTGGCAGATGGCGCGGCAACACCATT-3'	*Olig2- Cre* *Dlx5/6-Cre*

2.1.6 RNA probes

Table 2. 3: RNA probes for *in situ* hybridization

Probe	Type	Sequence	PM	Source
GAD67	Sense Antisense	HindIII XhoI	T7 T3	Dr Brian Condie (via Dr Eve Seuntjens, University of Leuven)
Nkx2.1	Antisense	XbaI	T3	Dr Victor Tarabykin (via Dr Eve Seuntjens, University of Leuven)
Dlx2	Sense Antisense	NotI HindIII	T7 T3	Dr. John Rubentein (via Dr Eve Seuntjens, University of Leuven)
Mash1	Sense Antisense	XhoI NotI	T7 T3	Dr Lukas Sommen (via Dr Eve Seuntjens, University of Leuven)
Shh	Antisense	SacII	Sp6	Generated using pGEM®-T easy vectors and the following primers; F- 5'-CTGTCTCGAGACCCAACTC-3' R- 5' GCTGATGACTCAGAGGTGCA-3'

Abbreviations: PM, RNA polymerase

2.1.7 Antibodies

Table 2. 4: Primary antibodies

Antibody	Clone/Lot	Species	Source
Anti-14-3-3ζ	M6	Mouse monoclonal	Centre for Cancer Biology
Anti-14-3-3ζ	C16	Rabbit polyclonal	Santa Cruz Biotechnology
Anti- TTF (Nkx2.1)	H-190	Rabbit polyclonal	Santa Cruz Biotechnology
Anti- β Actin	AC-15	Mouse monoclonal	Sigma-Aldrich
Anti-α-tubulin	DM1A	Mouse monoclonal	Abcam
Anti-Sox2	L1D6A2	Mouse monoclonal	Cell Signalling Technology
Anti-GAD67	1G10.2	Mouse monoclonal	Millipore
Anti- Parvalbumin	Ab11427	Rabbit polyclonal	Abcam
Anti-Calretinin	AB5054	Rabbit polyclonal	Millipore
Anti-Somatostatin	216002	Rabbit polyclonal	Immunostar
Anti-NPY	1112001	Rabbit Polyclonal	Immunostar
Anti-Pak1	2602	Rabbit Polyclonal	Cell Signalling Technology
Anti- pPak	2606	Rabbit	Cell Signalling Technology
Anti - BrdU	BU1/75(ICR1)	Rat monoclonal	Abcam
Anti- Gli3	H-280	Rabbit polyclonal	Santa Cruz Biotechnology
Anti β-catenin	9562	Rabbit polyclonal	Cell Signalling Technology
Anti- N-cadherin	5D5	Monoclonal mouse	Thermo Scientific
Anti- β-Gal	PA1-21447	Rabbit polyclonal	Thermo Scientific
Anti-CC3	Asp175	Rabbit polyclonal	Cell Signalling Technology
Anti- PHH3	06-570	Rabbit polyclonal	Millipore

Abbreviations: pPak, Pak1 (Ser144)/Pak2 (Ser141); TTF-1, Thyroid transcription factor; NPY- neuropeptide Y; β-Gal, β-Galactosidase; PHH3, phospho-histone H3; CC3, cleaved caspase 3.

Table 2. 5: Secondary antibodies

Antibody	Species	Source
Peroxidase anti- Rabbit	Donkey	Jackson ImmunoResearch Laboratories
Peroxidase anti- Mouse	Donkey	Jackson ImmunoResearch Laboratories
Peroxidase anti- Rat	Donkey	Jackson ImmunoResearch Laboratories
Alexa Fluor® 555 anti- mouse	Donkey	Molecular Probes, Invitrogen
Alexa Fluor® 488 anti-mouse	Donkey	Molecular Probes, Invitrogen
Alexa Fluor® 555 anti-rabbit	Donkey	Molecular Probes, Invitrogen
Alexa Fluor® 488 anti-rabbit	Donkey	Molecular Probes, Invitrogen
Alexa Fluor® 594 azide		Molecular Probes, Invitrogen

2.2 Methods

2.2.1 Genotyping

2.2.1.1 Genotyping of *14-3-3ζ* KO mice

Genotypes of mice was determined by PCR on genomic tail DNA using MyTaq™ Extract-PCR Kit (Bioline). Tails were digested as per the manufacturer's instructions. PCR was setup as follows: 12.5µl My Taq HS Red mix (2x), 6µl H20, 100ng each of primers LTR and 062F, 200ng of primer 062R2 (Table 2.2) and genomic DNA. The PCR conditions for genotyping were as follow: one cycle of 95°C, 3 minutes; followed by 34 cycles of: 95°C, 15 seconds; 55°C, 15 seconds; 72°C, 20 seconds; and a final extension 72°C for 5 minutes. PCR products were identified by 2% agarose gel electrophoresis (see section 2.2.4.10).

2.2.1.2 Genotyping of *Olig2-Cre;14-3-3ζ$^{fl/fl}$* and *Dlx5/6-Cre;14-3-3ζ$^{fl/fl}$* mice

PCR on genomic tail DNA for *Cre* and *14-3-3ζ* was used to determine genotype of mice. Tails were digested in proteinase K (50µg) and 1ml of digestion buffer (35mM Tris-Hcl, 70mM Tris-base, 6mM ethylenediaminetetraacetic acid (EDTA), 200mM NaCl and 0.2% sodium dodecyl sulfate (SDS)) at 55°C for 2 hours. DNA was precipitated with ethanol (see section 2.2.4.8) and resuspended in 100µl of RNase free water. PCR was setup as follows; 50-500µg genomic DNA, 1µl of corresponding primers each and 10µl of 2X GoTaq Green (Promega). The PCR conditions for genotyping *Cre* were as follows: one cycle of 94°C, 3 minutes; followed by 34 cycles of: 94°C, 45 seconds; 68°C, 45 seconds; 72°C, 1 minute; and a final extension 72°C for 10 minutes. The PCR conditions for genotyping *14-3-3ζ* were as follows: one cycle of 94°C, 3 minutes; followed by 34 cycles of: 94°C, 30 seconds; 58°C, 30 seconds; 72°C, 1 minute; and a final extension 72°C for 5 minutes. PCR products were identified by 2% agarose gel electrophoresis (see section 2.2.4.10).

2.2.2 Behavioural assays

Behavioural testing of control (n = 5 male and n = 6 female) and *Dlx5/6-Cre; 14-3-3ζ$^{fl/fl}$* (n = 6 males and n = 4 females) mice was carried out by Xiangjun Xu as previously described in Ramshaw et al. 2013. Briefly, locomotor activity was assessed using an open field test. The test consisted of mice being placed in a brightly lit square arena, 40 × 40 cm (Stoelting, Wood Dale, IL, USA), with clear walls 35 cm high for 10 min. The total distance and velocity at which these mice travelled within this area was measured using ANY-maze software (Wood Dale, IL, USA) as an indication of baseline locomotor activity.

2.2.3 Collection of brains and embryos

For all experiments, mice were either culled and brains dissected by Xiangjun Xu, or in the case of embryos by Dr. Quenten Schwarz. Samples were either used fresh or harvested, post-fixed in 4% paraformaldehyde (PFA) overnight at 4°C followed by infiltration of 20% sucrose at 4°C

for several hours or overnight. Samples were transferred into square disposable embedding moulds (EMS), embedded into OCT (Tissue-Tek) and frozen in acetone and dry ice. Samples were stored at -80°C until use.

2.2.4 DNA and RNA techniques

2.2.4.1 Isolating RNA from MGE tissue samples

MGE tissues were dissected out in phosphate buffered saline (PBS) under a stereo microscope (SZX10, Olympus). MGE samples were flash frozen in liquid nitrogen and stored at -80°C until use. RNA was isolated using Trizol (Invitrogen) per manufacturer's instructions. Alternatively, in preparation for microarray analysis, RNeasy Plus Micro RNA kit (Qiagen) was used according to manufacturer's instructions.

2.2.4.2 Isolating RNA from dissociated MGE cells and MGE explants

To isolate RNA from dissociated MGE cells and MGE explants, used in section 2.2.7.1 and section 2.2.7.2 respectively, Trizol was added to wells and triturated. Samples were then transferred to RNAase free microcentrifuge tubes and RNA isolated as outlined above (section 2.2.4.1)

2.2.4.3 Preparation of cDNA

cDNA was generated with 500ng-1µg of RNA using QuantiTect Reverse Transcription Kit (Qiagen) following the manufacturer's instructions. Briefly, RNA was incubated at 42°C for 2 min in C1000 Touch Thermal cycler (Bio-Rad) with gDNA wipeout buffer to remove genomic DNA. Subsequently, the sample underwent incubation for 30 min at 42°C with reverse transcriptase (RT), RT buffer and primer mix and then incubated at 95°C for 5 min to end the reaction. cDNA was diluted 1:10 in RNase free water before use.

2.2.4.4 Real-time polymerase chain reaction (qPCR)

The qPCR reaction was performed using QuantiTect SYBR Green PCR kit (Qiagen) on a Rotor-Gene thermocycler (Corbett Research, Mortlake, NSW, Australia.). Reaction parameters: 15 min at 95 °C, then cycling of 10 s at 95 °C, 20 s at 55 °C and 20 s at 72 °C; for 45 cycles followed by a melt phase. All qPCR experiments started with similar levels of RNA with runs prepared carefully to ensure equal amounts of cDNA was added. Relative gene expression levels were calculated using standard curves of cDNAs normalised to the human house-keeping genes *GAPDH* and/or *β-actin*, if any major changes were observed in *GAPDH* and/or *β-actin* experiment was repeated. Each primer (Table 2.1) set amplified a single PCR product of predicted size as determined by melt-curve analysis following PCR. Each qPCR was performed in triplicate and relative quantification was determined using Rotor-Gene Q Series software (Corbett Research).

2.2.4.5 Generating DNA plasmids for RNA probes

Following preparation of cDNA, polymerase chain reaction (PCR) was set up using appropriate primers (Table 2.3). PCR reaction contained: 1µl of a 1 in 10 dilution of the cDNA, 1µl each of appropriate forward and reverse primer, 10µl of 2X GoTaq Green (Promega) and made up to 20µl with RNase free water. Sample was incubated in C1000 Touch Thermal cycler (Bio-Rad) with the following conditions; 95°C for 2 min, 92°C for 30 s, 55-65°C for 30 s and 72°C for 1 min for 33 cycles. Subsequently, 2µl of product was visualized on 1% agarose to confirm amplification. PCR product underwent ethanol precipitation (see section 2.2.4.8) and resuspended in 3µl of RNase free water. In order to ligate insert into pGEM®-T easy plasmid (Promega), the 3µl of DNA was added to 5µl 2X ligation buffer (Promega), 1µl T4 ligase (Promega) and 1µl pGEM®-T easy plasmid. Mixture was incubated for 3 hours at room temperature. Ligation product was transformed into *E. coli* using electrocompetent cells (see section 2.2.4.9). In order to identify bacteria carrying desired insert, blue-white screening was

used, 11.8µl of 0.5M Isopropyl β-D-1- thiogalactopyranoside (IPTG) and 800ng of 5-bromo-4-chloro-3-indolyl- beta-Dgalactopyranoside (X-gal) were added to each Luria Bertani (LB) agar plate for 30 min prior to use. Electroporated bacteria were plated and incubated at 37°C overnight. The following day, 14 white colonies were collected and DNA extracted using Qiagen plasmid prep. Following DNA extraction samples were precipitated with ethanol (see section 2.2.4.8) and cloning of the PCR fragment to pGEM®-T easy plasmid was confirmed by restriction digest using Not1 and visualized on 1% agarose gel. Subsequently, the colony containing the desired insert was re-plated on an LB agar plate overnight and QIAprep Spin Miniprep Kit (Qiagen) was performed as per manufacturer's instructions in order to obtain purified DNA. Samples were then sent for sequencing (see below).

2.2.4.6 Sequencing

Samples were sequenced to ensure that they contained the correct inserts. Sequencing reactions were prepared using Big Dye Terminator v3.1 Cycle Sequencing kit (Applied Biosystems). Briefly, each reaction was set up with; 500ng of plasmid DNA, 1µl Big Dye (Applied Biosystems), 4µl 5x Big Dye Buffer (Applied Biosystems), 10ng of appropriate primer and Milli-Q Water up to 20µl. Samples were subjected to 30 cycles of 96ºC for 10 seconds, 50ºC for 10 seconds and 60ºC for 4 minutes (Applied Biosystems 2720 Thermal Cycler). Upon completion of cycling the PCR product was then transferred to a microcentrifuge tube. 1µl of glycogen (Roche) and 80µl of freshly prepared 75% isopropanol was then added and briefly vortexed. Sample was incubated at room temperature for 15 minutes to precipitate the product then spun in a microcentrifuge for 20 minutes at maximum speed. The supernatant was removed from the pellet. The DNA pellet was washed in 75% isopropanol, vortexed and centrifuged at maximum speed for five minutes. The pellet was dried in a heating block and sent to the Australian Genome Research Facility for sequencing analysis.

2.2.4.7 Generating RNA *in situ* probe

RNA probes were synthesized using supplied plasmids (Table 2.3) and the plasmid generated in section 2.2.4.5. Plasmid linearization was performed by incubating 3µg of purified DNA plasmids, 1µl of corresponding enzyme (see Table 2.3), 8µl of 10X restriction buffer (NEB), 4µl of 10X bovine serum albumin (BSA) (NEB) and made up to 40 µl with RNase free water and incubated at 37°C for 2.5 hours. To extract linearized DNA, samples were made up to 100µl and subsequently underwent ethanol precipitation (see section 2.2.4.8). RNA probe was synthesized by incubating 4µl of 10X transcription buffer (Promega), linearized DNA, 2µl of DIG labelling mix (Roche), 1µl of RNAase inhibitor (Roche), 1µl of corresponding RNA polymerase (see Table 2.3) and made up to 40µl with RNase free water. The reaction was incubated at 37°C for 2.5 hours. Subsequently, RNA probes underwent precipitation by adding 8µl of 5M lithium chloride (LiCl) to linearized DNA and proceeding with ethanol precipitation. To confirm RNA synthesis, 1µl of sample was taken at each stage and run on 1% agarose gels.

2.2.4.8 Ethanol precipitation

DNA/RNA samples were purified by ethanol precipitation. In each reaction 1µl of glycogen (Roche) was added with sodium acetate (3M, pH 5.5) (Ajax Finechem) at 1/10 of total volume and 2.5 volumes of 100% ethanol. Samples were incubated at -20ºC for one hour and centrifuged at 4ºC for 30 minutes at maximum speed. The supernatant was removed and the pellet was washed in 70% ethanol at 4ºC and centrifuged at maximum speed for ten minutes at 4ºC. The wash was repeated, before the pellet was air-dried and resuspended in Milli-Q water as required.

2.2.4.9 Electroporation into *E. coli* DH5α cells

DH5α electrocompetent bacteria were thawed on ice and 1-200ng of DNA was carefully pipetted into the cells. Mixture was transferred to pre-chilled 0.2cm bacterial electroporation cuvettes (Bio-rad, Gladesville, NSW) and placed in the Gene pulser electroporator (Bio-rad).

Voltage was set to 2.0 volts and the cuvette was then pulsed, creating an electrical current between the cuvette's electrodes. Immediately following electroporation, cells were recovered for 25 minutes in 500µl recovery medium (LB broth + 1% magnesium + 1% glucose) at 37°C. Electroporated bacteria and recovery media were plated on LB agar plates.

2.2.4.10 DNA/RNA electrophoresis

Confirmation of DNA/RNA size was performed using DNA electrophoresis. Agarose gels were prepared with 1-2% agarose in 1xTris-acetate-EDTA (TAE) buffer and boiled to melt agarose. Once cooled ethidium bromide (1µl per 4ml) was added and agarose left to set for one hour. Once the agarose gel had solidified, TAE buffer was poured into the tank covering the gel. HyperLadder (Bioline) and DNA samples mixed with 10x load buffer (Invitrogn) were loaded into the wells and then run for 40 minutes at 85 volts.

2.2.5 Histological techniques

2.2.5.1 Cryosectioning

Cryostat (Leica CM1950) was used for sectioning of frozen mouse brain samples. The chamber and stage temperatures were set to -22°C and -20°C, respectively. OCT frozen brain samples (section 2.2.3) stored in the -80°C freezer were equilibrated at -20°C for 30 min in the chamber. The sample was removed from the mould and mounted on the block holder using OCT. Excess OCT was trimmed using a single edge razor. The sample was clamped to the block holder, aligned, sectioned coronally (adult brain 10µm; embryo, 18µm) unless otherwise stated, anterior to posterior. In the case of the adult brain, every 5^{th} section was collected starting from the dorsal hippocampus and extending caudally 0.5 mm, approximately -1.28 to -1.8 relative to Bregma (Paxinos et al., 2007, Paxinos & Franklin, 2012). Samples were mounted onto Superfrost® slides (Lomb Scientific) and used fresh or allowed to dry before being stored at 20°C.

2.2.5.2 Vibratome sectioning

In the case where thicker samples were required, vibratome sectioning was used. Briefly, 4% agarose was prepared and melted in a microwave. In the meantime, samples were placed in embedding mould and excess solution was removed. Once samples were dry melted agarose was added to the mould and sample positioned within the embedding mould. After agarose had set, the block was mounted onto a mounting platform with superglue and allowed to dry for 20 min, before being placed in vibrotome (Leica VT1200). PBS was added to the chamber in order to submerge the sample. Vibrotome was set to cut at a vibration speed of 0.3m/s and for sections of 100-300µm. Sections were collected from PBS with a paint brush and stored in PBS at 4°C until use.

2.2.5.3 Immunofluorescence staining

Frozen sections were thawed for 30 min prior to use and rehydrated for 5 min in PBS. Sections were then permeabilized for 5 min with PBT (0.3% TritonX-100) and then blocked in blocking solution (10% goat serum (Sigma) in CAS-block™ (Invitrogen)) at room temperature for 30 min. Sections were incubated in primary antibodies (Table 2.4) diluted in blocking solution for 1 hour at room temperature or overnight at 4°C. Following incubation in primary antibodies sections were washed in PBT (0.3% TritonX-100) and incubated with Alexa Fluor-labelled secondary antibody (1:200, Molecular Probes) (Table 2.5) diluted in blocking solution for 1 hour at room temperature in the dark. After incubation in secondary antibody, sections were washed three times in PBT (0.3% TritonX-100) and post-fixed with 4% PFA for 10 min. Sections were subsequently mounted with Prolong Gold antifade reagent with DAPI (Molecular Probes). After mounting, sections were imaged on confocal microscope (LSM 700, Zeiss) and processed in ZEN software (blue edition). Negative controls were performed by incubating sample with Alexa Fluor-labelled secondary antibody alone for each antibody used (Figure 2.1).

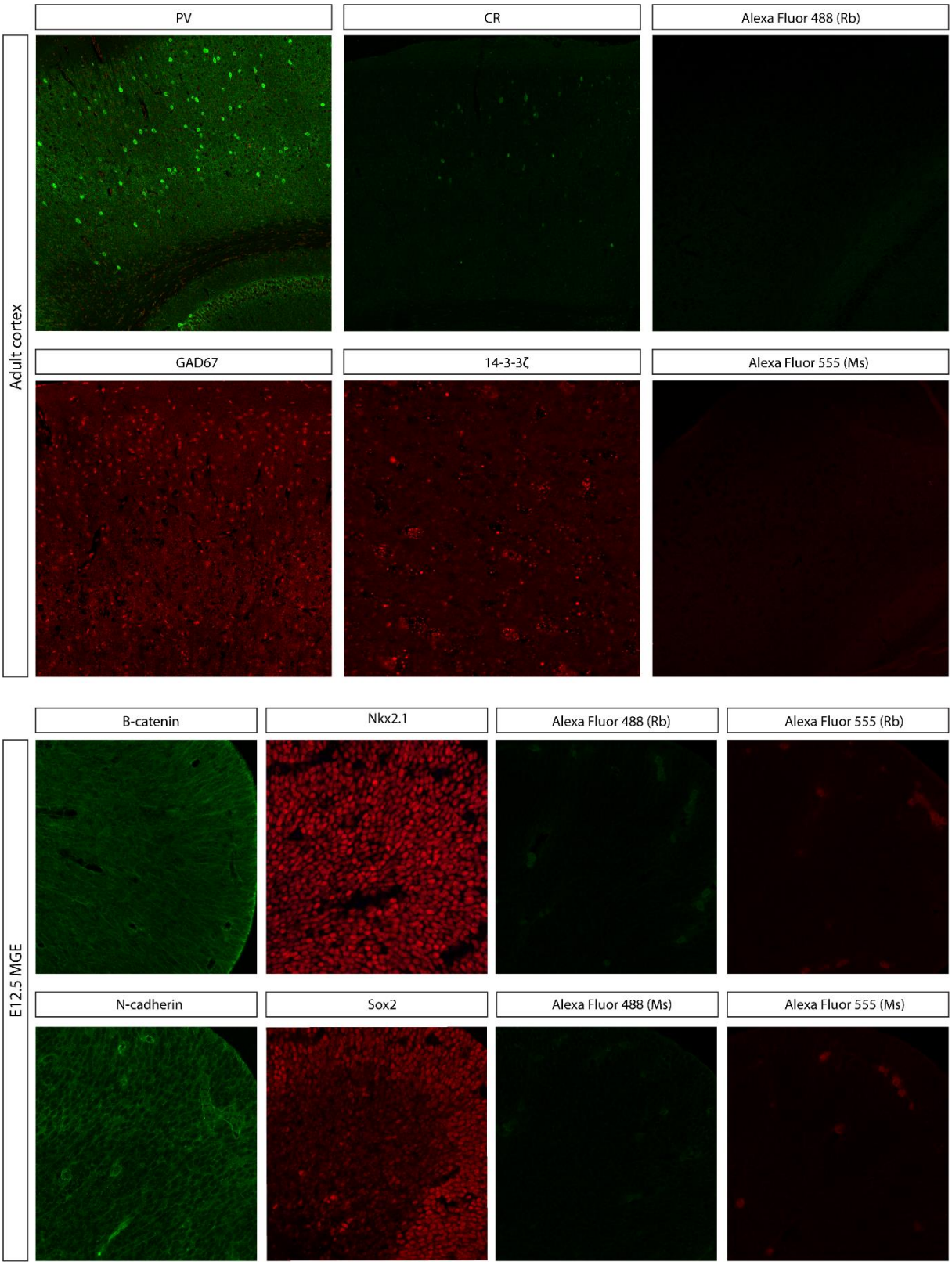


Figure 2. 1: Minimal auto-fluorescence with secondary antibodies used

For each primary antibody used for immunofluorescence in this thesis a negative control was performed by staining with Alex Fluor-labelled secondary in the absence of the primary antibody. (A) Immunofluorescence staining of each primary antibody used in the adult cortex represented next to negative control. (B) Immunofluorescence staining of each primary antibody used in the embryonic MGE represented next to negative controls.

2.2.5.4 Cell counting

All cell counts were performed using Image J software (National Institutes of Health, USA) or Photoshop CC software (Adobe Systems Incorporated, CA, USA) unless otherwise stated. For interneuron quantitation in the adult cortex, the retrosplenial area, the primary/secondary motor areas and the somatosensory area were identified by anatomical landmarks such as the appearance of the hippocampus and corpus callosum (Paxinos et al., 2007). Immunopositive neurons were counted in the defined regions with 10 sections per brain included in the analysis. Area was measured using ZEN imaging software (Zeiss) and cell counts were expressed as a cell density (cell/mm^2). Cell densities were then averaged across animals with at least 3 mice from each genotype included in the analyses.

2.2.5.5 Whole mount *in situ* hybridization

Whole embryos were fixed overnight at 4°C with 4% PFA in PBS. Following fixation, samples were gradually dehydrated in methanol (25%, 50% 75% and 100%) and stored at -20°C until use. Embryos were bleached in 6% hydrogen peroxide in methanol for 60 min before being rehydrated gradually into PBT (0.1% Tween) (25%, 50%, 75% and 100%). Samples underwent Proteinase K (Roche) (5-10 µg/ml) treatment for 3-10 min either on ice or at room temperature depending on embryo age. Samples were washed twice with PBT (0.1% Tween) for 5 min each and then post fixed with 4 % PFA in PBS for 20 min at room temperature. Samples were washed again before being immersed in hybridisation buffer (50% formamide, 5X SSC, pH 4.5, 50µg/ml tRNA, 1% SDS, 50µg/ml Heparin) for 30 min at 65°C. After prehybridization, embryos were incubated with diluted RNA probe overnight at 65°C. Probes were diluted in hybridization buffer (5µl of probe per 2ml of buffer) and denatured at 85°C for 5 min. Following hybridisation, embryos were washed 3 times in 50% formamide 5X SSC pH 4.5 and 1% SDS at 65°C and 3 times in 50% formamide and 2X SSC pH 4.5 at 65°C. Embryos were subsequently washed three times in Tris-Buffered Saline with 0.1% Tween (TBST) at room

temperature before being incubated in blocking solution (10% sheep serum (Sigma) in TBST) for 1hr at room temperature, followed by overnight incubation with anti-DIG antibody (1:5000; Roche) in 1% sheep serum in TBST at 4°C. Samples were washed three times with TBST for 5 min each then washed five times with TBST for 90 min each. Samples were then washed overnight in TBST at 4°C. Embryos were washed three times with freshly made NTMT (100mM NaCl, 100mM Tris-HCl pH 9.5, 50mM $MgCl_2$ 1% Tween-20) before being developed. Developing solution was prepared by adding: 4.5µl/ml nitro blue tetrazolium chloride and 3.5µl/ml 5-bromo-4-chloro-3-indolyl phosphate (Roche), to freshly made NTMT. Samples were incubated with developing solution until colour change was observed. Once the colorimetric reaction had taken place, samples were washed three times in PBT (0.1% Tween) for 10 min. Embryos were post fixed with 4% PFA in PBS for 1 hour and then washed twice in PBS for 5 min each. Embryos were cleared with increasing concentrations of glycerol and mounted using 90% glycerol in PBS. Embryos were imaged on stereo microscope (SZX10, Olympus). During all incubations embryos underwent gentle rocking in 2ml microcentrifuge tubes.

2.2.5.6 Section *in situ* hybridization

Sections were thawed for 30 min at room temperature then washed with PBT (0.1% Tween) for 5 min at room temperature prior to fixation with 4% PFA in PBS for 20 min. Slides were washed twice with PBT (0.1% Tween), immersed in hybridisation buffer for 1 hour before being incubated with 100µl of diluted RNA probe overnight at 65°C. Probes were diluted in hybridization buffer (15µl of probe per 1ml buffer) and denatured at 85°C for 5 min. Following hybridisation, sections were washed 3 times in 50% formamide 5X SSC pH 4.5 and 1% SDS at 65°C and 3 times in 50% formamide and 2X SSC pH 4.5 at 65°C. Sections were subsequently washed three times in TBST at room temperature before being incubated in blocking solution (10% sheep serum in TBST) for 1 hr, followed by overnight incubation in anti-DIG antibody (1:2000; Roche) in 1% sheep serum in TBST at 4°C. Sections were washed several times in

TBST following antibody incubation. Developing solution was prepared by adding: 4.5µl/ml nitro blue tetrazolium chloride and 3.5µl/ml 5-bromo-4-chloro-3-indolyl phosphate (Roche), to freshly made NTMT. Slides were incubated with developing solution until colour change was observed. Once colorimetric reaction had taken place, slides were washed in three times in TBST for 10 min and then twice in PBS for 10 min. Sections were post fixed with 4% PFA in PBS before being mounted using 90% glycerol in PBS and imaged on stereo microscope (SZX10, Olympus).

2.2.5.7 β-Galactosidase Staining

Embryos were fixed for 2 hr in 4% PFA in PBS. Cryosections or vibratome sections were incubated in staining solution: 19 mM sodium dihydrogen phosphate, 81 mM disodium hydrogen phosphate, 2 mM $MgCl_2$, 5 mM EGTA, 0.01% sodium deoxycholate, 0.02% Nonidet P-40, 5 mM potassium ferricyanide, 5 mM potassium ferrocyanide, and 1 mg/mL X-gal substrate at 37°C until blue staining was clearly visible. After staining samples were washed in PBS and mounted on slides in 90% glycerol.

2.2.5.8 EdU short pulse labelling

EdU incorporation was used to identify proliferating cells in E12.5 and E13.5 embryonic brains, using the Click-iT® 594 Imaging kit (Molecular Probes, Life Technologies). Briefly, 10mg/ml EdU was prepared in sterile PBS and stored in -20°C. Pre-warmed EdU was intraperitoneally injected into pregnant dams (100mg/kg EdU per bodyweight). After 30 min or 1 hr embryos were harvested, fixed and sectioned as described in sections 2.2.3 and 2.2.5.1. Sections were stained with Click-iT® 594 Imaging kit, following the manufacturer's protocol. Images were taken by confocal laser microscopy (LSM 700, Zeiss) and processed with ZEN imaging software (Zeiss).

2.2.5.9 Dual pulse labelling using EdU and BrdU incorporation

To determine the number of cells exiting the cell cycle in MGE derived interneurons a combination of EdU and BrdU incorporation was used based on protocol described in Etienne et al. 2014. Briefly, BrdU (Roche) (100mg/kg BrdU per bodyweight) was intraperitoneally injected into the E11.5 and E12.5 pregnant dams. After 24 hr, EdU (100mg/kg EdU per bodyweight) was intraperitoneally injected into the same pregnant dams. After 30 min or 1 hr embryos were harvested and sectioned as described in sections 2.2.3 and 2.2.5.1. Sections were stained for EdU-positive cells using Click-iT® 594 Imaging kit, following the manufacturer's protocol. Following EdU staining, anti-BrdU antibody was used to detect BrdU staining. The DNA was denatured by incubating the slides with 4M HCl for 20 min at room temperature and washed once in PBT (0.3% TritonX-100) for 2 min with gentle shaking. HCl was then neutralised by adding 0.5M phosphate citrate buffer (pH 5) for 5 min at room temperature, then washed three times in PBT (0.3% TritonX-100) for 5 min each. Slides were then stained according to section 2.2.4.3 with rat monoclonal anti-BrdU antibody (1:250).

2.2.5.10 Terminal deoxynucleotidyl transferase dUTP nick end labelling (TUNEL)

TUNEL staining was performed using TMR red *In Situ* Cell Death detection kit (Roche) as per manufacturer's instructions. Briefly, following immunofluorescent staining (section 2.2.5.3) TUNEL reagents were combined and incubated for 1 hr. Following incubation, sections were washed three times with PBT (0.3% TritonX-100) and fixed for 20 min with 4% PFA in PBS. Sections were mounted with Prolong Gold antifade reagent with DAPI (Molecular Probes). After mounting, sections were imaged on confocal microscope (LSM 700, Zeiss) and processed in ZEN software (blue edition).

2.2.6 Western blotting

2.2.6.1 Sample preparation

Cells and tissue were homogenized in NP-40 lysis buffer (137mM NaCl, 10mM Tris pH 7.4, 10% glycerol and 1% NP-40) with protease and phosphatase inhibitors (10 mM sodium pyrophosphate, 2mM sodium orthovandate, 2mM sodium fluoride, 10mM β-glycerol phosphate, 2mM phenylmethylsulfonyl fluoride (PMSF), 1µg/ml leupeptin and 1 Complete, Mini, EDTA-free protease inhibitor tablet (Roche)). 10-40µg of protein was made up to 10µl with NP-40 lysis buffer and 30% 5x loading buffer (Tris pH 6, 10% SDS, Bromophenol blue and glycerol) with 5% -mercaptoethanol (Sigma, St. Louis, MO) added prior to use. Samples were denatured at 95°C for 5 minutes prior to loading on gels. The same amount of protein was added for all treatment groups in each experiment.

2.2.6.2 BCA protein Assay

Protein concentration of lysates was determined using the Pierce BCA protein assay (Thermo Fisher Scientific) according to manufacturer's instructions. Briefly, protein lysates from section 2.2.6.1 were added into a 96-well plate neat or at 1:10 dilution in NP-40 lysis buffer. A standard was then prepared using BSA diluted in 1x PBS (0µg/mL, 0.125µg/mL, 0.25µg/mL, 0.5µg/mL, 1µg/mL, 2µg/mL, 5µg/mL, & 10µg/mL) and 10µl aliquoted per well. Reagent A (50 parts) and Reagent B (1 part) were combined and 200µl added to each well. The plate was incubated at 37°C for 20 min and following incubation immediately measured at 540nm using the Epoch Microplate Spectrophotometer (Biotek) and processed using Gen5™ (Biotek) analysis software. Standard graph and protein concentration was generated using Gen5 software.

2.2.6.3 Sodium dodecyl sulphate polyacrylamide gel electrophoresis (SDS-PAGE)

Acrylamide gels between 10% and 15% (377mM tris pH 8.8, 0.1% SDS, 0.1% ammonium persulphate, 0.04% tetramethylethylenediamine (TEMED)) were prepared, with the percentage of acrylamide being dependent on the size of the protein of interest. Stacking gels contained

5% acrylamide in Tris pH 6.8, SDS, ammonium persulfate, and TEMED. Alternatively, pre-poured gradient Bolt™ 4-12% Bis-tris gels (Life Technologies) were used. Gels were loaded in Bolt™ Mini Gel Tank (Novex, Life technologies) and immersed in MES running buffer (Life Technologies). Precision Plus Protein Kaleidoscope standard molecular weight markers (Bio-rad, Gladesville, New South Wales) were run alongside samples at 160V for 30 min.

2.2.6.4 Transfer of proteins to PVDF membranes

Resolved proteins were transferred from SDS-PAGE gels to PVDF membranes using the wet transfer method, originally described by Towbin et al. (1979). Sponges and Whatman filter paper were pre-soaked in Nu PAGE 1 x transfer buffer (25mM Bicine, 25mM Bis-Tris, 1.25mM EDTA and 20% methanol) and placed into Bolt™ Mini Blot module (Life Technologies) transfer apparatus in the following setup: 1 x Sponge, 3 x Whatman Paper, SDS-PAGE gel, PVDF membrane (GE Healthcare Life sciences, United Kingdom), 3 x Whatman Paper and 1 x Sponge. PVDF membranes were pre-soaked in 100% methanol. Proteins were transferred for 1 hour at 20V.

2.2.6.5 Protein detection

Following transfer, membranes were immediately added to blocking solution (1% skim milk in TBST or 5% BSA with TBST) and incubated on rotating table for 30 minutes at room temperature. Membranes were incubated with primary antibodies (see Table 2.4) diluted in blocking solution for one hour at room temperature or overnight at 4°C. Subsequently, PVDF membranes were washed three times with TBST over a period of 30 minutes at room temperature, prior to incubation with secondary antibody (see Table 2.5) diluted in blocking solution for one hour at room temperature on rotating platform. Membranes were washed as above prior to developing with 1:1 ratio of Amersham enhanced chemiluminescence (ECL) reagents (GE healthcare), incubated for one minute and then exposed on the LAS 4000 (Fujifilm, Tokyo, Japan) with varying exposure times ranging from 5 seconds – 10 minutes.

2.2.6.6 Digital image processing

Images were orientated in multigauge (GE healthcare) and then exported as tiff files for quantification on ImageQuant TL (GE Life Sciences) and digitised with Photoshop CS4 software (Adobe Systems Incorporated, CA, USA).

2.2.7 *In vitro* cell culture experiments

2.2.7.1 Dissociated MGE cell cultures

Dissociated cell cultures were prepared from E13.5 mouse brains according to the method of Cavanagh et al. (1997). Briefly, MGE tissues were dissected out in PBS under a stereo microscope (SZX10, Olympus) and incubated in trypsinisation medium (0.05% trypsin (Sigma) with 100 µg/ml DNaseI (Worthington Biobchemical) in Neurobasal media (Gibco, Invitrogen)) for 15 minutes at 37°C. Trypsinisation was stopped with neutralisation medium (10% of FCS (Gibco, Invitrogen) in Neurobasal medium) for 5 minutes at 37°C. MGE tissues were then triturated with a fire polished Pasteur pipette several times. The cells were subsequently pelleted by centrifugation at 1,000 x g for 3 minutes and supernatant removed. Cells were resuspended in culture media (Neurobasal media containing B27 supplement, 100 µg/ml penicillin/streptomycin (Invitrogen) and 2 mM L-glutamine (Invitrogen)) for calculation of cell number. Cells were plated at a density of 2 X 10^5 per well on a 24-well plate pre-coated with 10 µg/ml poly-L-lysine (Sigma) and 10 µg/ml laminin (Invitrogen). Culture media was prepared with or without inhibitors to 14-3-3ζ, Rac1 and Shh pathway, which were added at pre-determined optimal concentrations (see section 2.2.7.3) and recombinant Shh (C25II) (R&D systems) which was added at a final concentration of 2µM. Cells were incubated in a humidified incubator at 37°C/5% CO_2. Dissociated culture medium was changed daily and after 2-3DIV RNA and protein was collected for qPCR and western blotting (see above).

2.2.7.2 Matrigel assays

E13.5 mouse embryos were harvested from sacrificed dams and their brains were dissected out in PBS under a stereo microscope (SZX10, Olympus). Small pieces of MGE (approximately 250-300 µm across) were placed in µ-slide 8 well (Ibidi) coated with 10 µg/ml poly-L-lysine and 10 µg/ml laminin. Explants were embedded in a mixture of 75% Matrigel® solution (BD Biosciences, CA, USA) and 25% Neurobasal medium supplemented with B27 and Glutamine (Gibco). After a period of 30 minutes in which the Matrigel® was solidified, 500µl of culture media was added with or without 2µM recombinant Shh. Explants were cultured for 48hrs at 37°C 5%CO_2 in CellVoyager™ CV1000 spinning disc microscope (Yokogawa) and time lapsed imaging of cell migration from MGE explants was captured. After imaging, qPCR was performed on samples. CV1000 software (Yokogawa) was used to generate images and movies which were then quantified using ImageJ software to define the area covered during cell migration from the original explant.

2.2.7.3 Dose response experiments to determine concentrations of inhibitors

To determine optimal concentrations of 14-3-3 inhibitor (RB-012) (Woodcock et al., 2015), Rac1 inhibitor (NSC23766) (Sigma) and cyclopamine hydrate (Sigma), titration experiments on dissociated MGE cells (section 2.2.7.1) were used. A range of concentrations were trialled for each inhibitor based on the current literature and manufacturer's recommendations. Dissociated MGE cells were treated as described in section 2.2.7.1, with the following concentrations; Rac1 inhibitor, 50µM, 10µM, 5µM, 1µM; 14-3-3 inhibitor, 5µM, 1µM, 0.5µM, 0.1µM; Cyclopamine, 5µM, 2µM, 1µM, 0.5µM. Optimal concentration for Rac1 inhibitor, 14-3-3 inhibitor and cyclopamine were 10µM 5µM, 2µM respectively.

2.2.8 Statistics

Statistical analyses were performed by GraphPad 3 software (GraphPad Software, Inc., CA, USA). All data is reported as mean number and standard error of the mean (SEM). The

statistical significance between group means was tested via student t-test unless otherwise stated. In order to test the null hypothesis that genotype is independent of branching in Figure 4.5C, an independent chi-square (χ^2) analysis was used. Significance was set at a p value of ≤ 0.05.

2.2.9 Figure preparation

All illustrations, figures and images were prepared using Photoshop C5 (Adobe) and Illustrator (Adobe).

Chapter 3: Characterization of interneuron deficiency in *14-3-3ζ* KO mice

3.1 Background

As described in chapter 1, aberrant interneuron function is consistently associated with neuropsychiatric and neurodevelopmental disorders. There have been several studies, using *in vivo* disease models and patient cohorts, in which this has been reported (Beasley et al., 2002; Hashimoto et al., 2003; Konradi et al., 2011; Hashimoto et al., 2008a; Hashimoto, 2008b; Fisahn et al., 2009; Lodge, 2009). Though there is a large variety of different interneurons, they have traditionally been sub-divided into three largely non-overlapping groups based on their expression of calcium binding proteins parvalbumin (PV), calretinin (CR) and the neuropeptide somatostatin (SST) (Gonchar & Burkhalter,1997; Ascoli et al., 2008, DeFelipe et al., 2013). PV expressing interneurons are characterized as fast-spiking neurons essential for gamma oscillations (Kawaguchi et al., 1987; Geiger et al., 1995; Geiger et al., 1997; Cardin et al., 2009; Sohal et al., 2009) and are the most well characterized subgroup due to their unique functions and consistent link to schizophrenia. PV and SST expressing interneurons usually originate in the medial ganglionic eminence (MGE), while CR expressing interneurons originate primarily from the caudal ganglionic eminence (CGE) (Wichterle et al., 2001; Xu et al., 2004). The alternative interneuron phenotypes arising from the MGE and CGE come from distinct transcriptional profiles, within each region. Thus, *Nkx2.1* is expressed predominantly in the MGE and drives a PV and SST cell fate (Butt et al., 2008) by initiating a cascade of several other transcription factors, including *Lhx6* and *Sox6*. Alternatively, in the CGE, Gsx1/2 drives CR cell fate through expression of transcription factor *Mash1*. The range of interneuron subtypes formed within the MGE and CGE/LGE help to account for the diversity of inhibition that is essential for cortical brain functions. The aim of this chapter was to establish the

necessity of 14-3-3ζ in interneuron formation. Furthermore, work in this chapter aimed to identify whether 14-3-3ζ is essential in the global interneuron population or if it is required for only a subtype of interneurons.

3.2 Results

3.2.1 *14-3-3ζ* is expressed in interneurons

Our previous studies have identified a key role for 14-3-3ζ in pyramidal neuron development, however, to date no reports have investigated the role of 14-3-3ζ in interneurons or interneuron development. Previously, our laboratory generated *14-3-3ζ* constitutive KO mice using genetic engineering technology (described in Cheah et al., 2012). *14-3-3ζ* KO mice carry a gene trap construct inserted into the first intron of *14-3-3ζ*. This gene trap cassette contains a reporter gene, *βgeo*, downstream of the splice acceptor and hence when the gene is spliced to this cassette, staining for β-galactosidase activity identifies where the gene is expressed. Mice were backcrossed to the BALB/c background for at least ten generations and used for all of the analyses presented herein. Though all mouse strains have shown similar defects, BALB/c mice were used as they have larger litters and generate increased numbers of *14-3-3ζ* KO mice.

Before exploring the role of 14-3-3ζ in interneurons, or more specifically the loss of 14-3-3ζ on the interneuron populations, I first established that *14-3-3ζ* is indeed expressed in this population of cells. Taking advantage of the presence of a *βgeo* reporter to trace native *14-3-3ζ* expression, E12.5 and E16.5 *14-3-3ζ* HET embryos were stained with X-gal solution. At E12.5, when expansion and maintenance of early progenitors is taking place, X-gal staining was present in the ganglionic eminences and POA regions, the birth place of interneurons. Counterstaining sections with 14-3-3ζ specific antibodies and Nkx2.1, a marker of MGE progenitor cells, further showed that 14-3-3ζ was expressed in interneurons and their progenitors in the VZ. Conversely, at E16.5 when the majority of interneurons have begun to migrate, X-gal staining was seen in the GE, POA and in the MZ. From this analysis, I found

that *14-3-3ζ* is expressed in interneuron populations during embryonic development (Figure 3.1A-C). I next examined 14-3-3ζ expression in interneurons of adult samples. Sections from P56 mouse brains were counterstained for 14-3-3ζ and the interneuron marker PV (Figure 3.1D). Similar to what was seen at the earlier stages, this analysis indicated that 14-3-3ζ is expressed in mature interneurons. As 14-3-3ζ showed broad expression in tissue samples, I next performed immunostaining on purified cells to examine if 14-3-3ζ is indeed expressed by interneurons. For this analysis interneurons were dissociated from microdissected E12.5 MGE and cultured for 5 days *in vitro*. Interneurons were then immunofluorescently stained for 14-3-3ζ and PV (Figure 3.1E). Almost 80% of the cells dissociated from the MGE were positive for PV showing that this isolation method enriches for MGE derived interneurons. Importantly, counterstaining for 14-3-3ζ and PV showed co-expression of the two markers. Taken together, this data shows that *14-3-3ζ* is expressed throughout all stages of PV+ interneuron development including their formation, migration and differentiation.

3.2.2 Loss of GABAergic interneurons in the cortex of *14-3-3ζ* KO mice

To further investigate whether 14-3-3ζ plays a unique functional role in interneuron development, I assessed if there was a difference in the total number of interneurons in *14-3-3ζ* KO mice compared to their WT littermates. GAD67, an enzyme which is essential for the synthesis of GABA from glutamic acid, is present in all inhibitory interneurons and was used as a global marker of interneuron identity. Coronal sections of the cortex immunostained for GAD67 identified a significant reduction in the total number of GAD67+ cells in the cortex of adult P56 *14-3-3ζ* KO mice compared to WT controls (WT, 2171 cells/mm^2; KO, 1353 cells/mm^2; $p<0.01$) (n=3) (Figure 3.2). Western blot analysis of whole forebrain lysates confirmed an overall loss of GAD67 protein in *14-3-3ζ* KO mice compared to WT (Figure 3.2D). Taken together, this data indicates that there is a reduction in the overall number of GAD67+ interneurons.

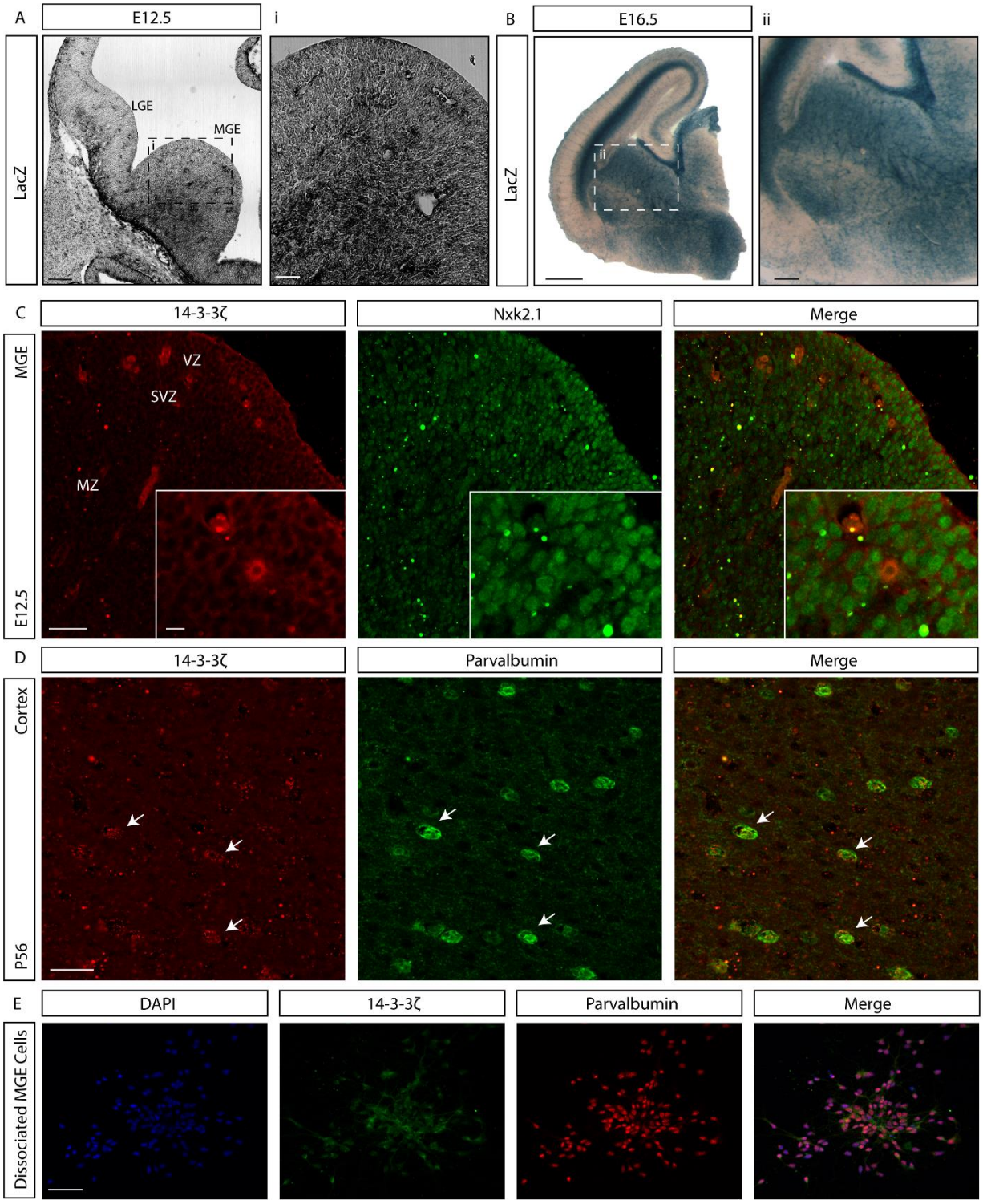


Figure 3.1: *14-3-3ζ* is expressed in PV+ interneurons.

(A) X-gal staining of *14-3-3ζ* HET E12.5 embryo coronal sections. Scale bar, 100µm. (A') High magnification image of A. Scale bar, 50µm. (B) X-gal staining of vibratome sectioned E16.5 *14-3-3ζ* HET embryos to determine the expression profile of 14-3-3ζ. Boxed region and dashed circle highlight the presence of *14-3-3ζ* expression in the ganglionic eminences and POA respectively. Scale bar, 500µm. (B') High magnification image of B. Scale bar, 200µm. (C) Co-staining for 14-3-3ζ and Nkx2.1. Scale bar, 50µm (Left) and 20µm (inset). (D) Co-staining for 14-3-3ζ and PV in the Cortex of WT sections. Scale bar, 50µm. (E) Dissociated MGE cells from E13.5 embryos were cultured (DIV5) and stained for 14-3-3ζ and PV. Scale bar, 50µm.

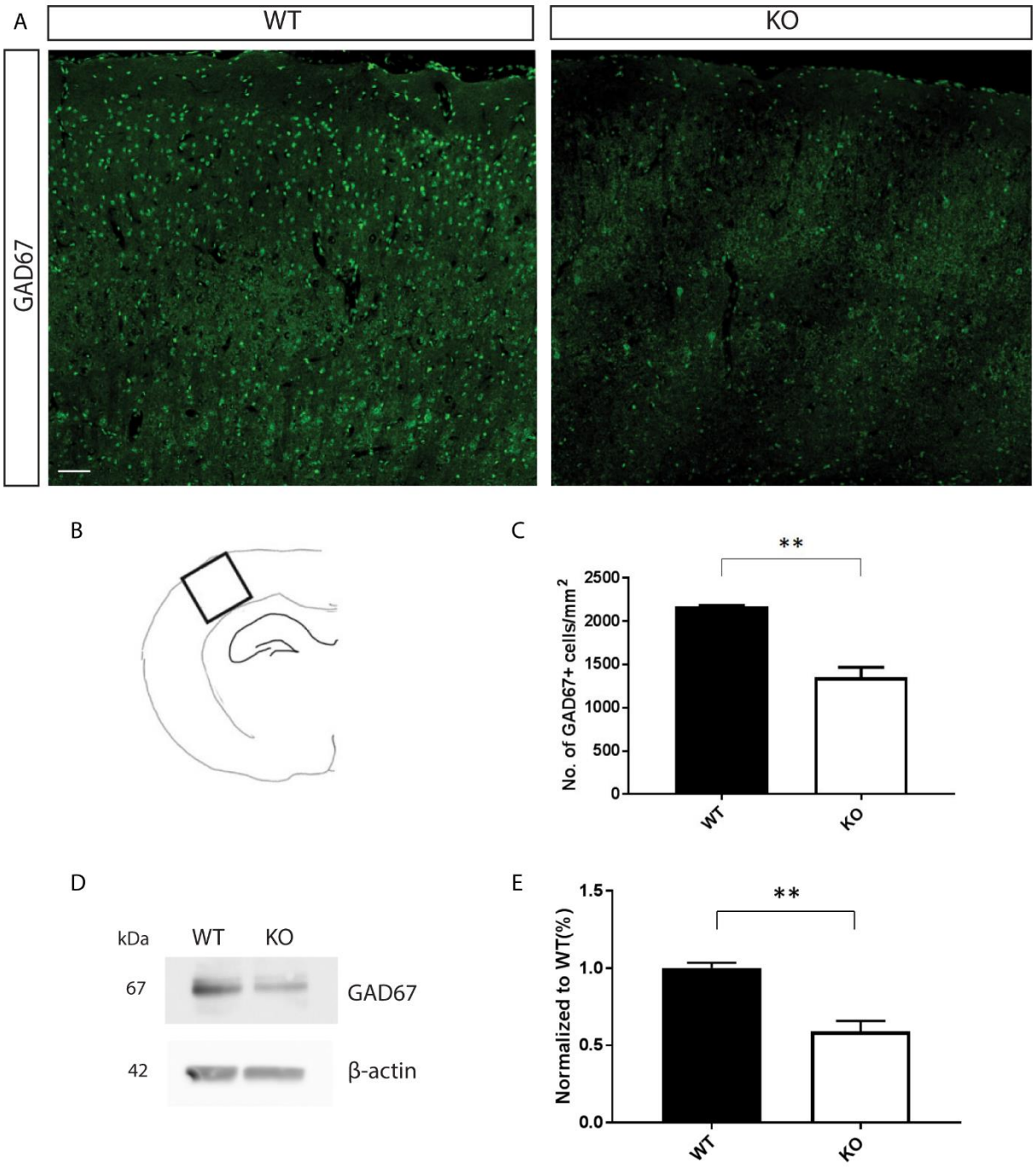


Figure 3.2: GAD67 is reduced in the brains of adult *14-3-3ζ* KO mice.

(A) Representative coronal brain sections from P56 WT and *14-3-3ζ* KO mice that were immunofluorescently stained to examine GAD67+ interneurons (n=3). (B) Schematic representation of the adult mouse brain, with the boxed region representing the region quantified. (C) Quantification of GAD67+ cells in WT and *14-3-3ζ* KO samples. (D) Western blot analysis of total brain lysate in adult WT and *14-3-3ζ* KO mice. (E) Densitometry of GAD67 western blot represented as relative intensity of each band as a percentage of WT following quantification with β-actin (n=4). Error bars represent ±SEM. Statistical significance was determined via t-test. (**$p<0.01$). Scale bar, 50μm.

To explore whether this defect was also present at earlier stages of development I performed *in situ* hybridization on coronal sections through the cortex of E16.5 WT and *14-3-3ζ* KO embryos with a riboprobe for *GAD67*. As GAD67 protein is only stabilised in mid/late embryonic development during which interneurons have already migrated substantial distances, this precluded the use of antibody staining. Similar to adults, this analysis identified a reduction in the number of interneurons during embryonic development (Figure 3.3). Furthermore, there also appeared to be a more severe reduction in *GAD67*+ cells migrating ventral to the striatum. Interestingly, interneurons migrate via two distinct paths. The early migrating cells consisting of MGE derived cells migrate ventral to the striatum and via the marginal zone to reach the cortex, whereas the later migrating interneurons comprising CGE derived interneurons migrate dorsal to the striatum and travel via the sub-ventricular zone to reach the cortex. The loss of *GAD67*+ cells specifically in this ventral region suggests a loss of MGE derived interneurons in the marginal zone migratory stream raising the notion that only a specific population of interneurons may be affected in the *14-3-3ζ* KO mice.

3.2.3 *14-3-3ζ* KO mice display a subtype specific reduction in PV+ interneurons

The function, physiology and morphology of interneurons are strongly dependent on both their origin and the markers they express. Cortical PV expressing interneurons are almost exclusively derived from the MGE, whereas CR expressing interneurons are predominantly derived from the CGE. In order to identify if 14-3-3ζ plays a subtype specific role in interneurons, I investigated whether *14-3-3ζ* KO mice show reductions in either or all of these populations.

For these analyses three regions of interest which define the migration path of interneurons during development were investigated, including the retrosplenial area (lateral), the primary/secondary motor areas (intermediate) and the somatosensory area (medial). CGE derived cells were examined by immunostaining cortical sections of WT and *14-3-3ζ* KO mice

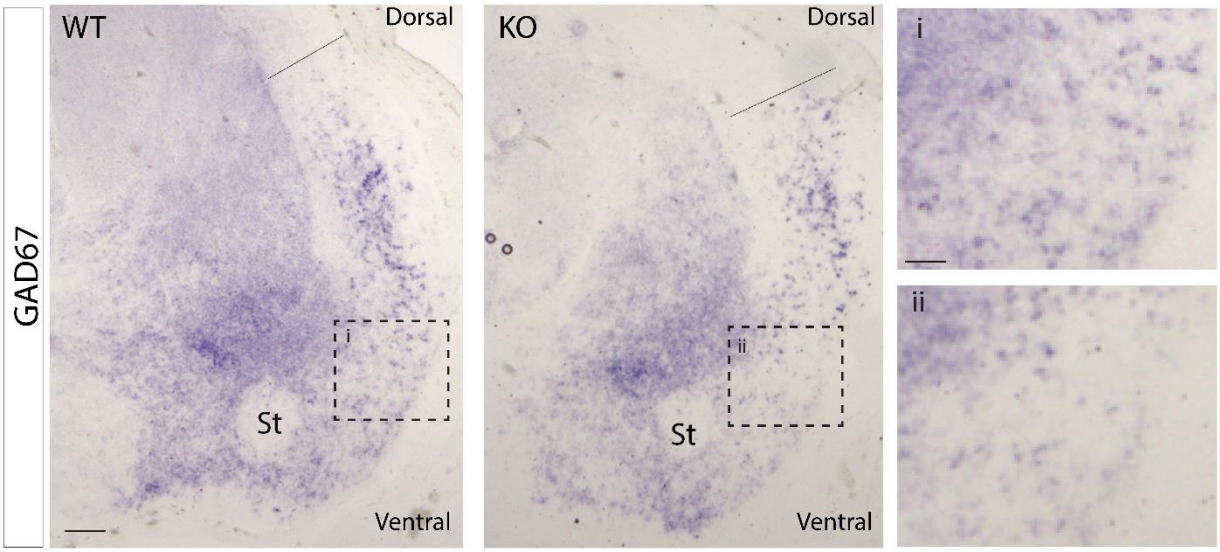


Figure 3.3: Loss of *GAD67+* cells during embryonic development.

Section *in situ* hybridization of E16.5 WT and *14-3-3ζ* KO embryos with *GAD67* riboprobe to identify *GAD67+* interneurons. Line indicates point of furthest migration by interneurons. (i) Enlarged image of boxed region in WT. (ii) enlarged image of boxed region in KO. Scale bar, 200μm (left) and 75μm (inset). St, striatum

for CR. The number of cells in each region was measured using manual counting in ImageJ and compared between WT (lateral, 17.7 cells/mm^2; intermediate, 28.3 cells/mm^2; medial 34.0 cells/mm^2) and *14-3-3ζ* KO mice (lateral, 16.4 cells/mm^2; intermediate,29.5 cells/mm^2; medial, 30.7 cells/mm^2) (Figure 3.4). There were no significant differences in the number of CR expressing cells in any region examined ($p>0.05$). A similar analysis was performed on WT (lateral, 54.2 cells/mm^2; intermediate, 70.3 cells/mm^2; medial, 50.5 cells/mm^2) and *14-3-3ζ* KO (lateral, 43.1 cells/mm^2; intermediate, 44.7 cells/mm^2; medial, 33.6 cells/mm^2) mice immunostained for PV with cell numbers determined by manual counting in ImageJ (n=4). This analysis identified a significant reduction in PV+ interneurons in both the medial and intermediate regions of *14-3-3ζ* KO mice compared to WT littermates (intermediate, $p<0.05$; medial, $p<0.05$) (Figure 3.5). While the lateral region also displayed a reduction in PV+ interneurons this failed to reach significance (lateral, $p>0.05$). In support of a reduced number of PV+ interneurons in the adult brain, western blotting confirmed reduced expression of PV in *14-3-3ζ* KO compared to WT (Figure 3.5D). Together, this data confirms that *14-3-3ζ* KO mice show a PV subtype specific reduction of interneurons.

Hippocampal interneurons have a similar origin to cortical interneurons, with PV and SST+ interneurons occupying the cornis armonis (CA) and calretinin interneurons occupying the dentate gyrus (DG). With this in mind I also examined whether this subtype specific interneuron deficiency extended to the hippocampus (n=4). Hippocampal coronal sections of P56 WT (CA, 533.4 cells/mm^2; DG, 161.0 cells/mm^2) and *14-3-3ζ* KO (CA, 275.2 cells/mm^2; DG, 108.5 cells/mm^2) mice were stained for PV and positive cells within the CA regions and DG counted (Figure 3.6). Interestingly, this analysis identified a significant reduction in the number of interneurons within the CA region of *14-3-3ζ* KO mice but not the DG (CA, $p<0.001$; DG, $p>0.05$). Using ZEN (Zeiss) software I was also able to examine the overall intensity of PV expression. Although these values did not reach significance, the overall intensity of PV

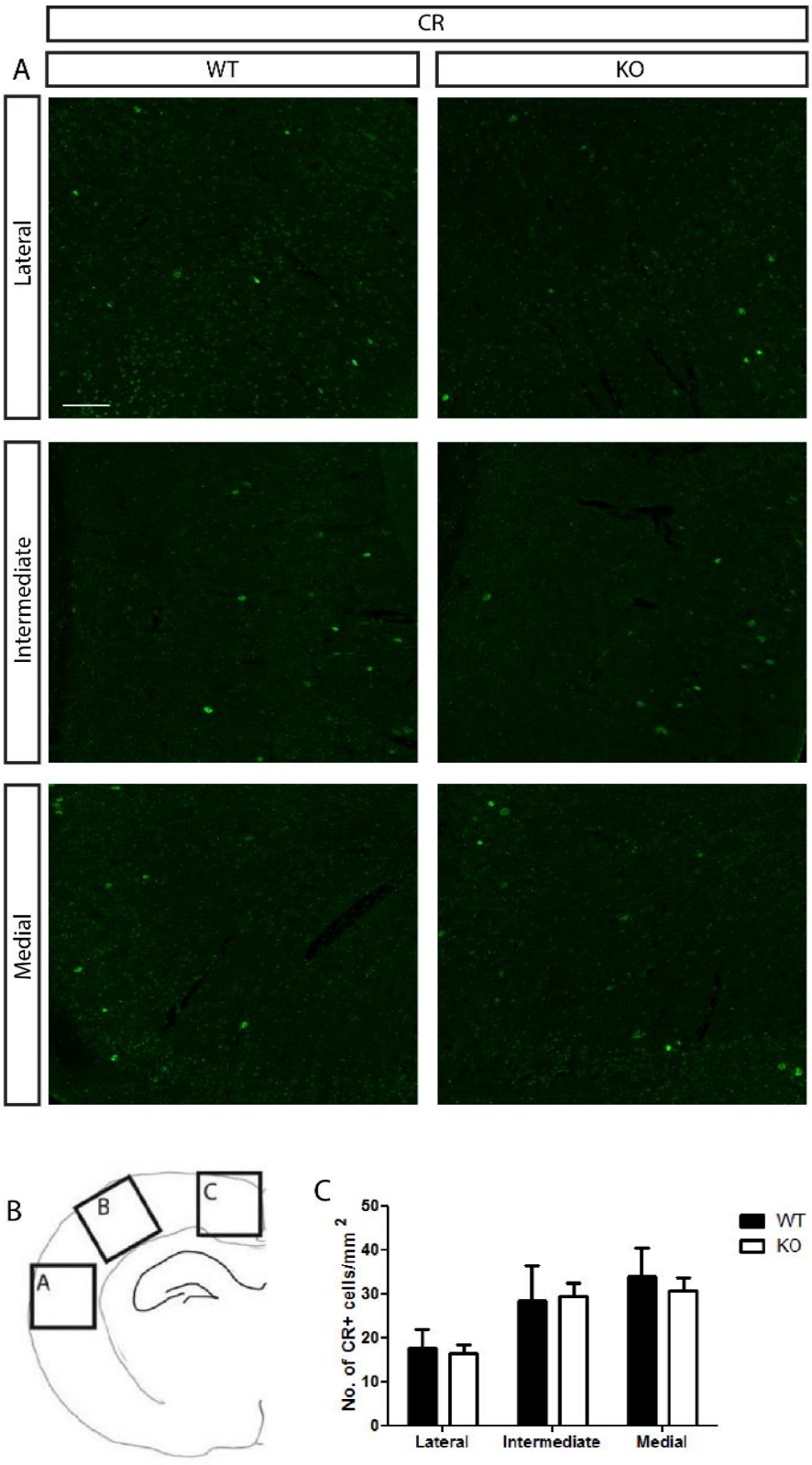


Figure 3.4: No change in the number of CR+ cells in *14-3-3ζ* KO mice.

(A) Representative coronal brain sections from P56 WT and *14-3-3ζ* KO mice that were immunofluorescently labelled for CR. Scale bar, 100μm. (B) Schematic representation of the adult mouse brain, with the boxed regions representing the regions quantified where A=lateral, B=intermediate and C=medial. (C) Quantification of CR cells in WT and KO samples (n=4). Error bars represent ±SEM. Statistical significance was determined via student t-test.

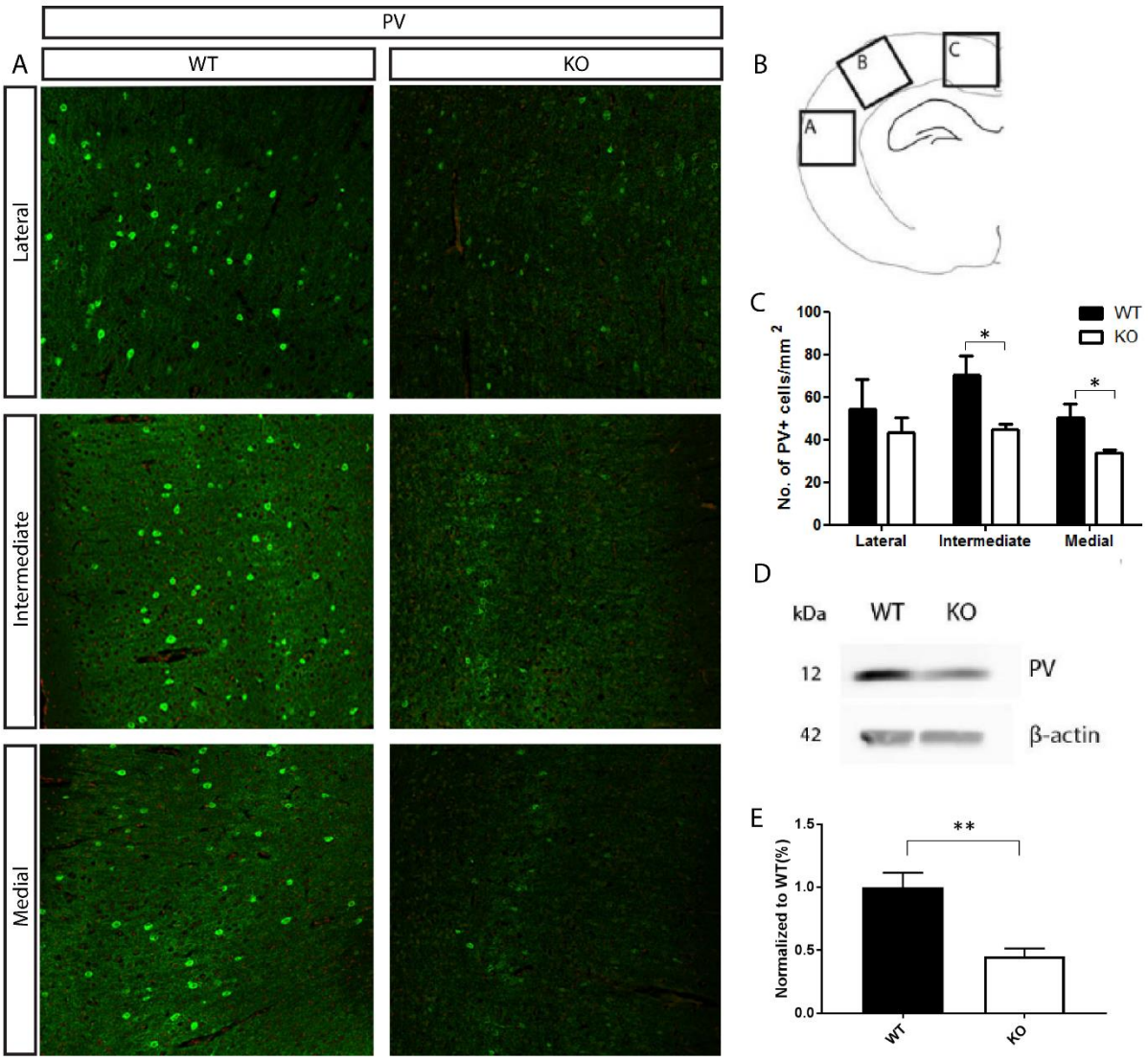


Figure 3.5: Subtype specific loss of PV+ interneurons in absence of *14-3-3ζ*.

(A) Representative coronal brain sections from P56 WT and *14-3-3ζ* KO mice that were immunofluorescently labelled for PV. Scale bar, 100μm. (B) Schematic representation of the adult mouse brain, with the boxed regions representing the regions quantified where A=lateral, B=intermediate and C=medial. (C) Quantification of PV+ cells in WT and KO samples. (D) Western blot analysis of total brain lysate in adult WT and *14-3-3ζ* KO mice probed with anti-PV antibody and β-actin used as load controls. (E) Densitometry of PV western blot represented as relative intensity of each band as a percentage of WT following quantification with β-actin (n=4). Error bars represent ±SEM. Statistical significance was determined via student t-test. (*p<0.05, **p<0.01).

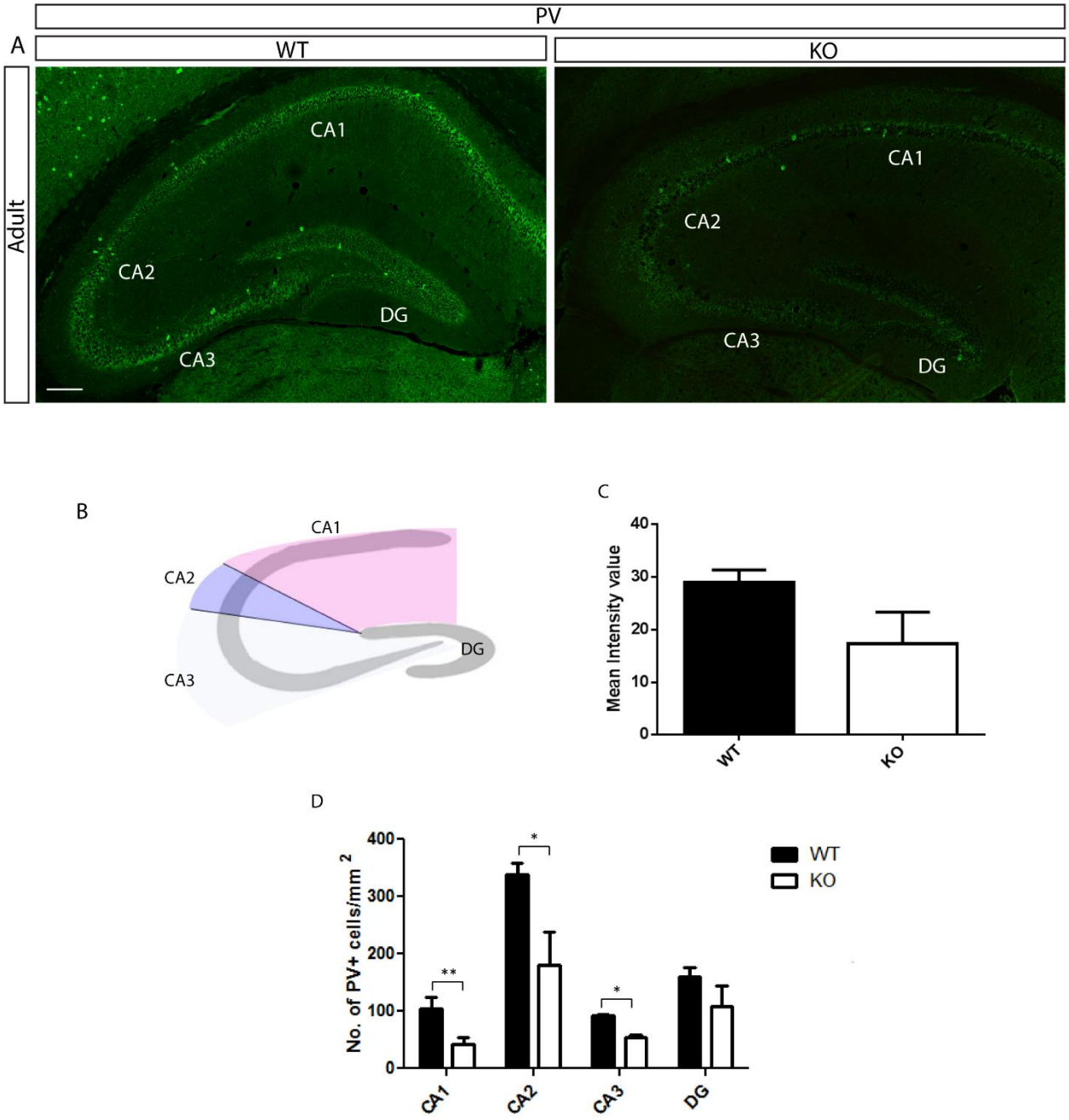


Figure 3.6: Loss of PV+ cells in the hippocampus of *14-3-3ζ* KO mice.

(A) Representative coronal brain sections from P56 WT and *14-3-3ζ* KO mice that were immunofluorescently labelled for PV. Scale bar, 100µm. (B) Schematic representation of the hippocampus. (C) Quantitation of the fluorescent intensity of WT compared to KO using ZEN software. (D) Quantitation of PV positive cells in the Hippocampus. (n=4). Error bars represent ±SEM. Statistical significance was determined via student t-test. (*p<0.05, **p<0.01).

was also reduced in the *14-3-3ζ* KO mice (mean intensity value; WT, 29.0; KO, 17.3) ($p>0.05$) (Figure 3.6C).

To ensure the reduction in interneurons is not limited to a specific region of the cortex, sagittal sections were taken and examined for the numbers of PV+ cells (Figure 3.7). Preliminary data shows that the same reduction as quantified previously from coronal sections was also seen along the entire rostral-caudal axis of the cortex (WT, 77.8 cells/mm^2; KO, 57.5 cells/mm^2) ($p<0.05$) (n=3).

3.2.4 Ablation of *14-3-3ζ* leads to minor defects in laminar distribution of PV+ interneurons.

The final position of interneurons within the cortex is crucial for their ultimate function. Once interneurons reach the cortex during embryonic development they undergo radial migration to distribute between the five cortical layers in an inside out fashion. Previous studies have identified defects in radial migration of pyramidal neurons in *14-3-3ζ* KO mice (Cheah et al., 2012; Toyo-oka et al., 2014). Though interneurons and pyramidal neurons use different mechanisms to migrate radially, I investigated if there were any defects in the laminar distribution of interneurons within the cortex of the *14-3-3ζ* KO mice. In order to examine the laminar distribution of interneurons in these mice, the cortex was divided into 10 evenly distributed horizontal bins. Cells within each bin were counted and normalized to the total number of neurons in each sample. The number of neurons within each bin was then expressed as a percentage of the total number of cells (n=4) (Figure 3.8) to control for *14-3-3ζ* KO mice having a reduction in the total number of interneurons. Though distribution was similar between genotypes, *14-3-3ζ* KO mice had a significant increase in interneurons within bin 3 and a decrease in bin 6 compared to WT littermates (KO, bin 3, 10.4%; bin 6, 15.7%) (WT, bin 3, 9.0%; bin 6, 17.5%) ($p<0.05$). While this mild difference in laminar distribution indicates that 14-3-3ζ has a role in radial migration, I have chosen to focus my investigation in the remainder of this thesis on defining how 14-3-3ζ regulates the abundance of interneurons.

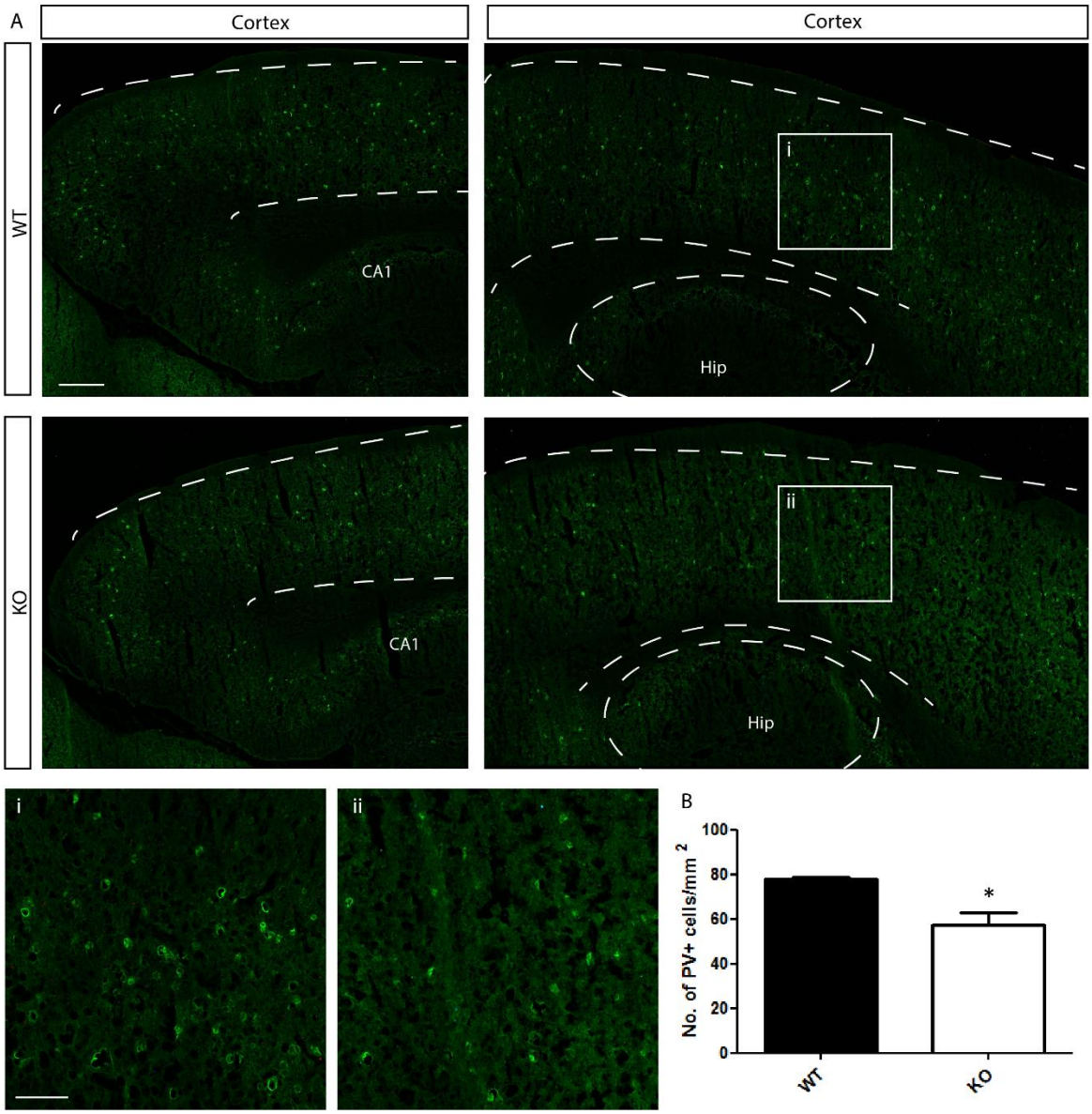


Figure 3.7: PV+ cells decreased over entire cortex of *14-3-3ζ* KO mice.

(A) Representative sagittal brain sections from P56 WT and *14-3-3ζ* KO mice that were immunofluorescently labelled for PV. (i,ii) High magnification images of boxed areas. Scale bars, 300μm (top) and 100μm (bottom). (B) Quantitation of PV+ cells in the cortex. (n=3).

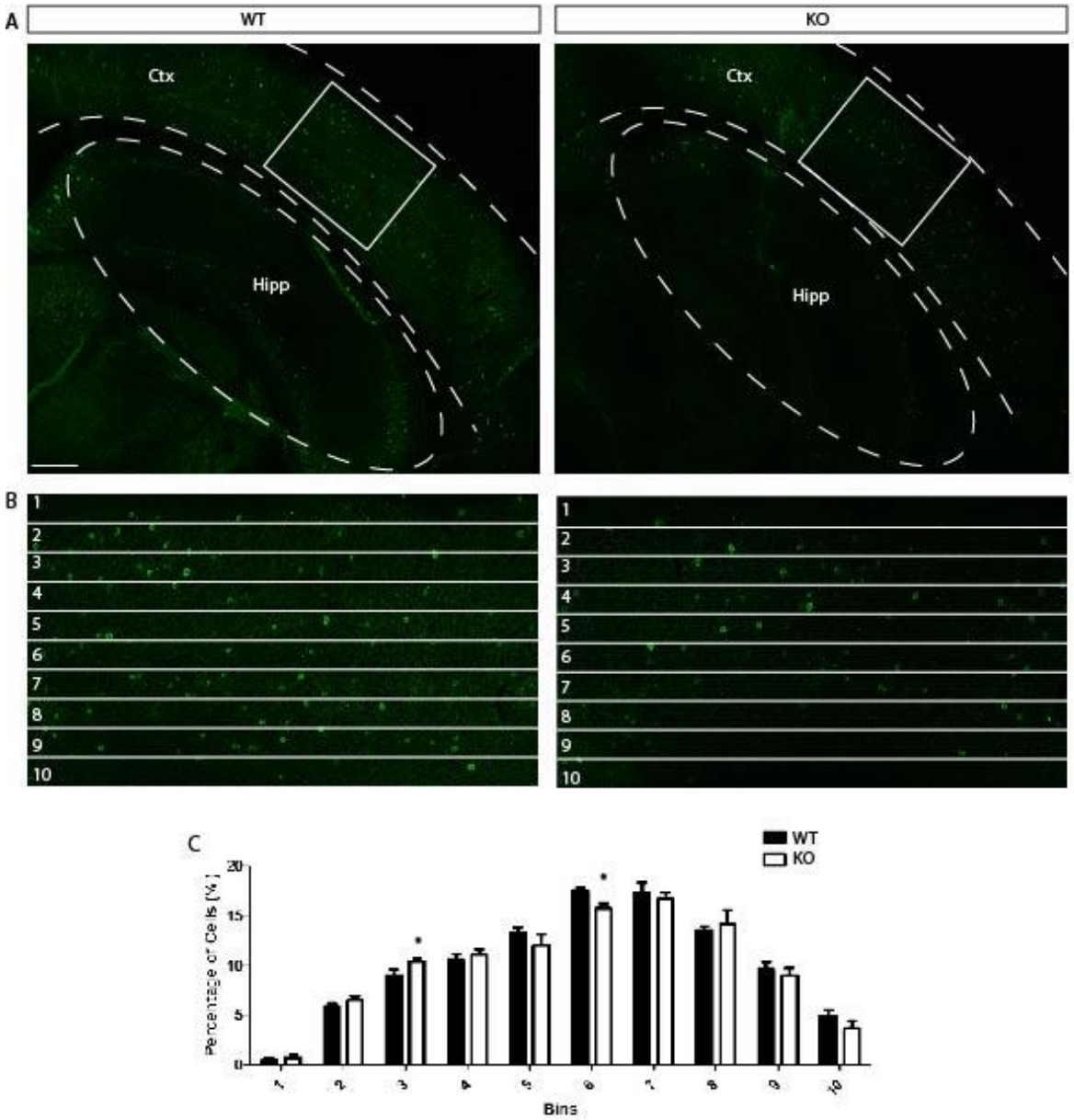


Figure 3.8: Aberrant laminar distribution of PV+ interneurons in the absence of *14-3-3ζ*.

Quantification of PV+ cells was achieved by counting the number of fluorescent cells in each bin and expressed as a percentage of total number across the neocortex. (A, B) Representative section used for counting PV+ cell densities are shown with boxes depicting the areas analysed. Scale bar, 300μm. (C) Quantification PV+ interneurons in each bin (student t-test, $p<0.05$) (n=4). Error bars represent ±SEM. Statistical significance was determined via student t-test. (*$p<0.05$). Hipp, hippocampus; Ctx, cortex.

3.2.5 Loss of PV+ interneurons does not arise from increased cell death in the hippocampus or cortex.

In order to understand the cellular mechanism underlying a reduction in PV+ interneurons, I first investigated whether *14-3-3ζ* KO mice displayed an increase in cell death. Using co-staining of TUNEL and PV on coronal sections of P56 (Figure 3.9) and P14 (Figure 3.10) mice I found no change in the number of PV+ neurons undergoing apoptosis in the hippocampus or cortex of *14-3-3ζ* KO mice compared to WT littermates. This was also confirmed with activated caspase-3 staining, another marker of apoptosis.

3.2.6 Loss of PV+ interneurons does not arise from neurodegeneration but from defects in neurodevelopment.

Since no increase in cell death was observed in *14-3-3ζ* KO mice, I next investigated whether these defects are neurodegenerative or neurodevelopmental in origin. This was done by examining the cortex of *14-3-3ζ* KO mice at several time points throughout postnatal development. I performed the same analysis on the cortex as described in section 3.2.3 on P9 and P14 coronal sections (Figure 3.11). Due to the size of the developing brain at P9 quantification was only performed in medial and intermediate regions (n=3). Similar to that seen in the adult, there was a significant reduction of PV+ interneurons ($p<0.05$) in the intermediate and medial regions of *14-3-3ζ* KO mice (P9; intermediate, 6.5 cells/mm^2; medial, 45.8 cells/mm^2)(P14; lateral, 65.1 cells/mm^2; intermediate, 54.3 cells/mm^2; medial, 65.0 cells/mm^2) compared to WT littermates (P9; intermediate, 14.8 cells/mm^2; medial, 70.3 cells/mm^2) (P14; lateral, 89.9 cells/mm^2; intermediate, 79.2 cells/mm^2; medial, 83.1 cells/mm^2) at both P9 and P14. There was no significant difference in the lateral region of P14 *14-3-3ζ* KO mice compared to WT ($p<0.05$). This analysis suggests that PV deficiency observed in *14-3-3ζ* KO mice arises from neurodevelopmental defects and not from aberrant cell death.

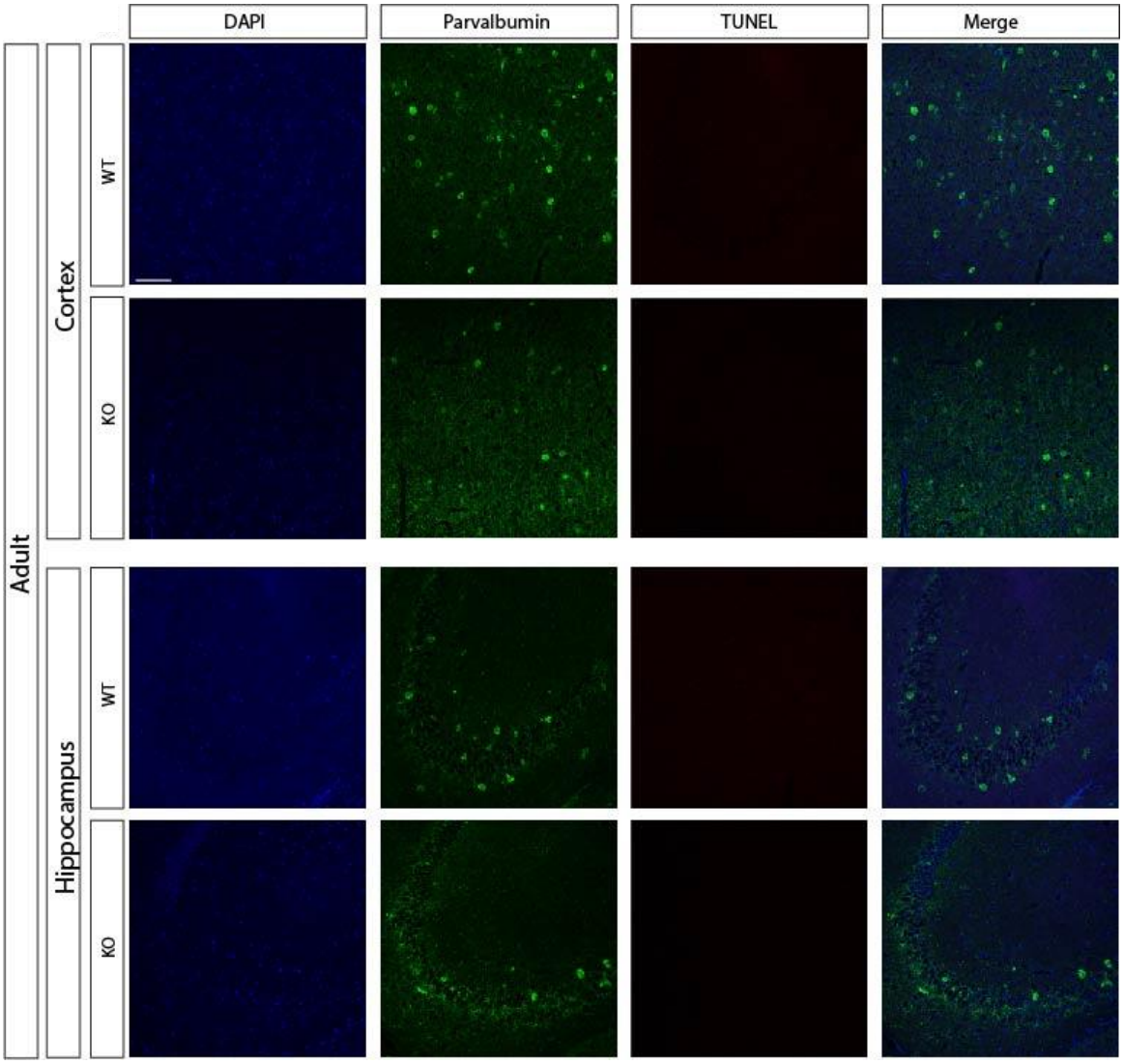


Figure 3.9: Loss of interneurons does not result from an increase in cell death in adult *14-3-3ζ* KO mice.

Brain sections from the cortex and hippocampus of adult WT and *14-3-3ζ* KO mice stained for TUNEL, PV and DAPI. Scale bar, 100μm (n=4).

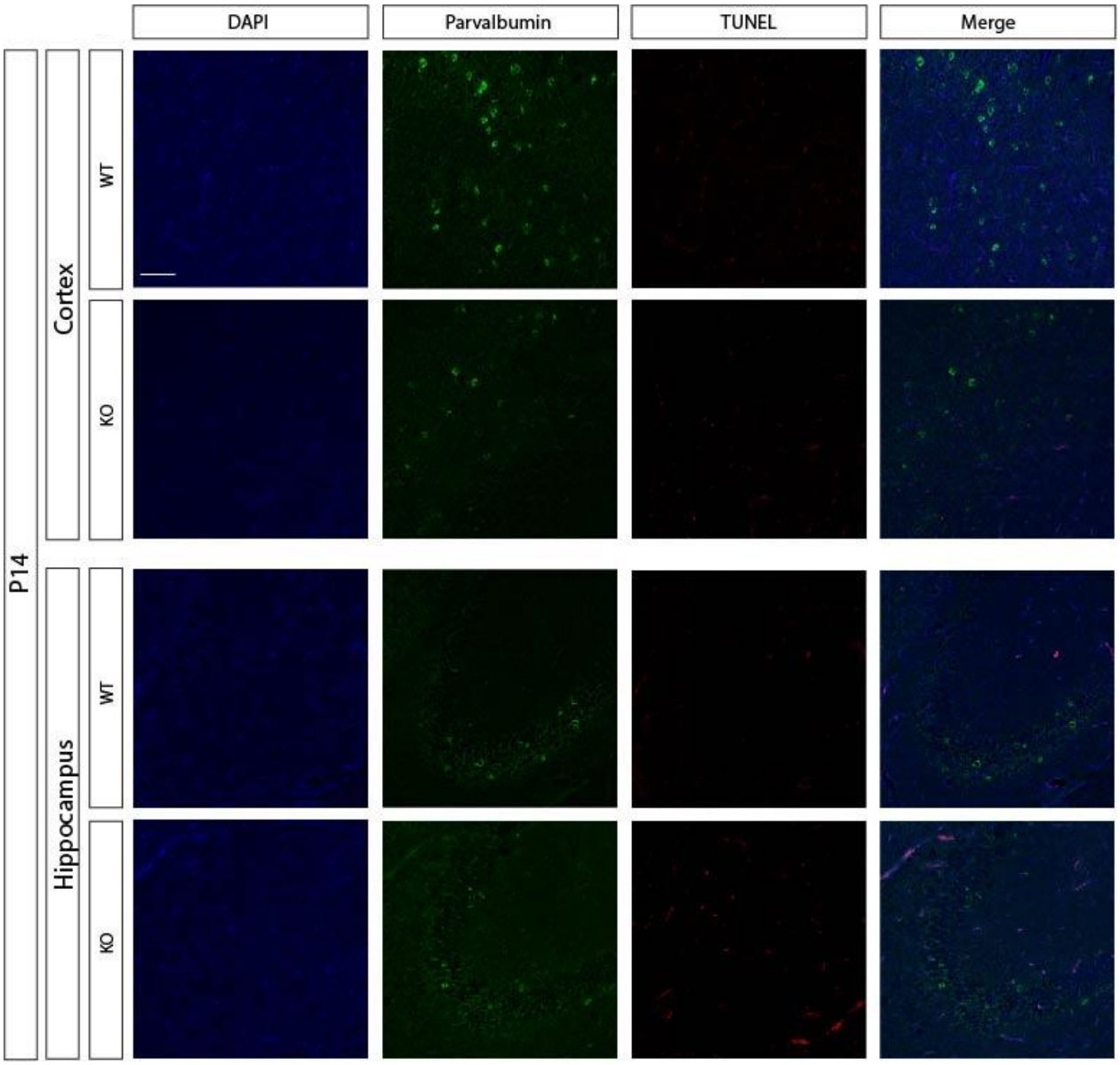


Figure 3.10: Loss of interneurons does not result from an increase in cell death in adolescent *14-3-3ζ* KO mice.

Brain sections from the cortex and hippocampus of P14 WT and *14-3-3ζ* KO mice stained for TUNEL, PV and DAPI. Scale bar, 100µm (n=4).

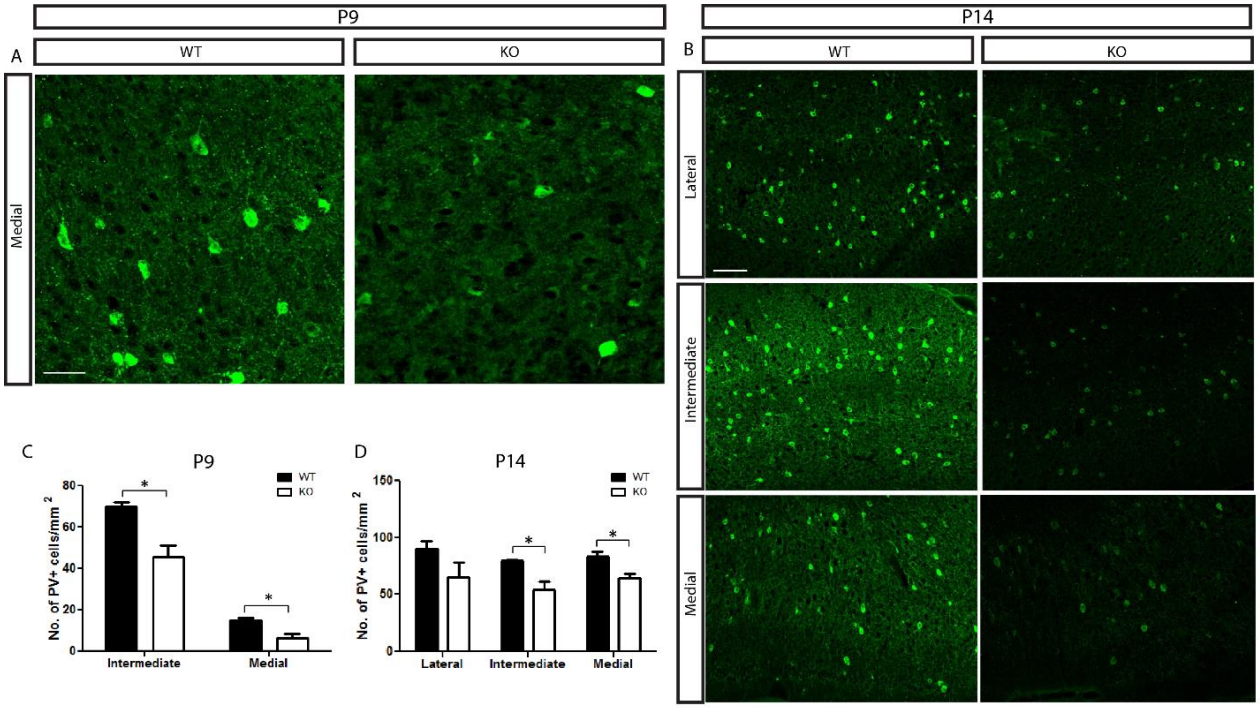


Figure 3.11: Loss of PV+ interneurons does not result from neurodegeneration.

(A, B) Representative coronal brain sections from P9 and P14 WT and *14-3-3ζ* KO mice that were immunofluorescently labelled for PV. Scale bars, 40µm (A) and 100µm (B). (C,D) Quantification of PV+ cells in WT and *14-3-3ζ* KO in P9 and P14 samples. (n=3) Error bars represent ±SEM. Statistical significance was determined via student t-test (*p<0.05).

3.3 Discussion

Correct interneuron formation during development is essential for normal brain function with even mild deficits in number or function having a profound effect on the intricate functioning of the brain (Flandin et al., 2011; Vidaki et al., 2012; Zhao et al., 2014). The aim of this chapter was to characterize the interneuron phenotype of *14-3-3ζ* KO mice. Here we demonstrate that the *14-3-3ζ* KO mice show a subtype specific reduction in PV expressing interneurons throughout the cortex. We extended this to show a loss of MGE derived cells in the *14-3-3ζ* KO mice with no significant change in the number of interneurons derived from the CGE. Due to their vastly different transcriptional profiles MGE cells play a unique and important role in normal brain dynamics, including a large contribution to the fast acting PV interneurons. Interestingly, this reduction of PV expressing interneurons is similar to that seen in schizophrenia (Hashimoto et al., 2003). Several mouse models of schizophrenia, including MAM model and ErbB4 KO mice, have shown a reduction of MGE derived interneurons, with no change reported in CGE derived interneurons (Penschuck et al., 2006; Fisahn et al., 2009). Furthermore, several studies which have looked at post-mortem human schizophrenic brain samples have reported a decrease in PV interneurons with no change in CR interneurons. Our data shows for the first time that loss of *14-3-3ζ* recapitulates this loss of interneurons and further validates *14-3-3ζ* KO mice as an appropriate model for schizophrenia. Due to the diverse roles of 14-3-3ζ in a large number of cellular processes and protein interactions there are several hypotheses as to how 14-3-3ζ may be playing a role in interneuron development, several of which will be expanded on in the following chapters. However, it is notable that a reduction of interneurons has also been seen in several other mouse models in which known interactors of 14-3-3ζ have been knocked out, including *DISC1* (Steinecke et al., 2012).

It is widely known that the cortical layer in which interneurons reside is crucial to their connections and function. For example, interneurons within layer IV predominantly inhibit other interneurons. Interestingly, *14-3-3ζ* KO interneurons showed a change in the laminar

distribution of the interneurons throughout the cortex. Furthermore, within the cortex *14-3-3ζ* KO mice had an increase in the proportion of interneurons in the lateral regions compared to WT. Both of these findings suggest that in addition to a reduction in number, the distribution of interneurons in *14-3-3ζ* KO mice is also affected. The change in distribution is likely to be a result of impaired radial migration, in which interneurons are able to migrate through the cortex to their final laminar position via a process called branching. We have previously identified defects in radial migration of pyramidal cells in *14-3-3ζ* KO mice, however the mechanism controlling radial migration of interneurons is different to that seen in excitatory neurons and hence may not be the same pathway. Interestingly, there have been several molecules to have roles in both interneurons and pyramidal radial migration, including cyclin dependent kinase CDK5 and p35 (Toyo-oka et al., 2003; Rakic et al., 2009). Furthermore, CDK5/p35 complex which is critical in interneuron laminar distribution has been found to bind to 14-3-3ε (Toyo-oka et al., 2003).

Our data demonstrates that there is no increase in PV+ interneuron cell death in *14-3-3ζ* KO mice and that the postnatal deficiency of interneurons arises during development. We demonstrate not only that the defect is present in early post-natal development but that there is a reduction in interneurons during embryonic development. Thus, we propose that there is an early embryonic defect in the formation of interneurons specific to the MGE, rather than a neurodegenerative or functional deficiency.

Though we have shown a role of 14-3-3ζ in the development of interneurons it is not yet clear whether this is due to a cell autonomous effect or if the role of 14-3-3ζ in excitatory neurons and other cell types perhaps leads to a secondary loss of interneurons. However, given the expression of 14-3-3ζ in interneurons through all stages of development it is therefore likely to act through a cell autonomous role. This topic will be expanded upon in subsequent chapters.

While this chapter reports a role for 14-3-3ζ in interneuron development for the first time, several binding partners, including, DISC1, have been previously shown to have a role regulating interneuron development. Taken together my data provides new insights to the aetiology of neurodevelopmental disorders such as schizophrenia and provides a basis for the schizophrenia-like deficiency arising from deletion of *14-3-3ζ*. The underlying cellular and molecular mechanisms by which 14-3-3ζ controls interneuron development will be discussed in subsequent chapters.

Chapter 4: Ablation of *14-3-3ζ* impedes formation of MGE derived interneurons

4.1 Background

The MGE is comprised of the ventricular zone (VZ) and subventricular zone (SVZ) as two distinct proliferative compartments (Sheth and Bhide, 1997). The initial patterning of the MGE takes place in response to Shh signalling, which leads to the expression of transcription factor *Nkx2.1*, while also acting as a repressor to Wnt signalling. *Nkx2.1* is expressed in the MGE but not the LGE or CGE and underlies the remarkable plasticity of progenitors to generate different interneuron subgroups such as those expressing PV and SST (Xu et al., 2010; DeBoer & Anderson, 2015). Aberrant Shh signalling from MGE-derived cells results in a switch of fates from MGE derived (PV or SST expressing) interneurons to CGE derived interneurons (Xu et al., 2010).

Interneuron development and maturation are precise processes with movement through the VZ and SVZ of the MGE coinciding with neurogenesis. Cells in the ventricular zone of the MGE transition from neural progenitors to intermediate progenitors and then into bona fide interneurons via a signalling cascade initiated by Nkx2.1. As these cells transition, they move ventrally through the layers of the MGE where they exit the cell cycle and then undergo tangential migration to the developing cortex. Simultaneously, they initiate expression of transcription factors such as *Lhx6*, *Dlx5* and *Dlx6*. *Lhx6* expression is critical for interneuron migration by controlling a downstream cascade of transcription factors including *Sox6* (Flandin et al., 2011; Fragkouli et al., 2009; Lavdas et al., 1999; Liodis et al., 2007; Zhao et al., 2008, DeBoer & Anderson, 2015).

Transition through the cell cycle is a key process in interneuron development and is modulated by both intrinsic and extrinsic influences. Interestingly, in contrast to excitatory

neurons, cell cycle exit is essential for interneurons to initiate tangential migration. Cyclins and cyclin dependent kinases (CDKs), act together to enable cells to progress through the cell cycle checkpoints. G1-phase is key in governing the cell cycle and acts in a gatekeeping capacity. Perturbation at this point can result in premature or delayed exit from the cell cycle and ultimate loss of interneurons, as seen in *Nkx2.1-Cre; Rac1*$^{fl/fl}$ mice (Vidaki et al., 2012).

Tangential migration of interneurons is under control of several molecular cues from the neocortex, striatum and GE (Marin et al., 2001; Flames et al., 2004; Faux et al., 2012; Marin et al., 2013). Class 3 semaphorins and neuregulin are known to play pivotal roles in the attraction and repulsion of interneurons toward their final destination through interactions with their respective receptors, the Neuropilins and ErbB family proteins (Marin et al., 2001; Tamamaki et al., 2003; Flames et al., 2004). The first interneurons to migrate away from the ganglionic eminences arise from the MGE and migrate in a stream ventral to the striatum and into the neocortex through the subventricular zone (Marin et al., 2000; Marin et al., 2001). LGE and CGE derived interneurons begin migration later and mostly migrate along an alternative path into the neocotex via the marginal zone.

The previous chapter identified a subtype specific reduction of MGE derived interneurons in *14-3-3ζ* KO mice. In this chapter I have explored the cellular mechanisms underlying the deficit of MGE derived interneurons and the developmental stage at which this occurs.

4.2 Results

4.2.1 Ablation of *14-3-3ζ* results in interneuron migration defects during development.

The birth place of interneurons is critical to their identity and function. Interneurons derived from different regions of the ganglionic eminences have different migration paths, transcriptional profiles and overall identity. As there is a reduction of interneurons in *14-3-3ζ* KO mice both in adulthood and in the post-migratory phase during development, this suggests

that the deficit arises at an earlier time-point during development. In order to explore this, I first examined the migratory process of interneurons, using *in situ* hybridisation of *GAD67* on E16.5 coronal brain sections to recognise all post-mitotic interneurons. To determine whether migration of interneurons was affected in the *14-3-3ζ* KO mice the distance which interneurons migrated by the mid-migratory phase was examined *in vivo.* By measuring the distance of the furthest *GAD67* positive cell from the striatum at E16.5 (Figure 4.1) I identified a significant decrease in the distance travelled in *14-3-3ζ* KO embryos compared to their WT littermates (WT, 20.82 mm vs KO, 19.58 mm; $p<0.01$) (n=3). However, when factors associated with interneuron migration were examined in E12.5 brain samples by qPCR there was no difference in the expression of *Neuregulin* or class 3 semaphorins (*Sema3A* and *Sema3F*) suggesting that this defect is independent of these guidance cues (Figure 4.2). Furthermore, transcription factor *Arx* and Slit ligand, *Robo1*, both with known roles in migration (Hernandez-Miranda et al., 2011), were also unaffected in *14-3-3ζ* KO mice. Taken together, the data suggests that although interneuron migration is affected in *14-3-3ζ* KO mice there is no change in guidance cues or transcription factors directly related to this process. Moreover, this possibly suggests the aberrant migration arises from a cell autonomous defect rather than altered expression of guidance cues within their migratory environment.

To investigate a potential cell autonomous role for *14-3-3ζ* in promoting interneuron migration and neurogenesis an *ex vivo* model was established. For this, I optimised a cell culture model in which E13.5 MGE explants were analysed in real-time by spinning disc confocal microscopy. The MGE was microdissected away from the CGE and LGE and 250µm plugs incubated in matrigel matrix. Real time imaging of these explants was performed over a 48 hr period with images taken every 30 min (Figure 4.3). Analysis of this data identified a reduction in the number of interneurons arising from the MGE of *14-3-3ζ* KO mice and showed that the

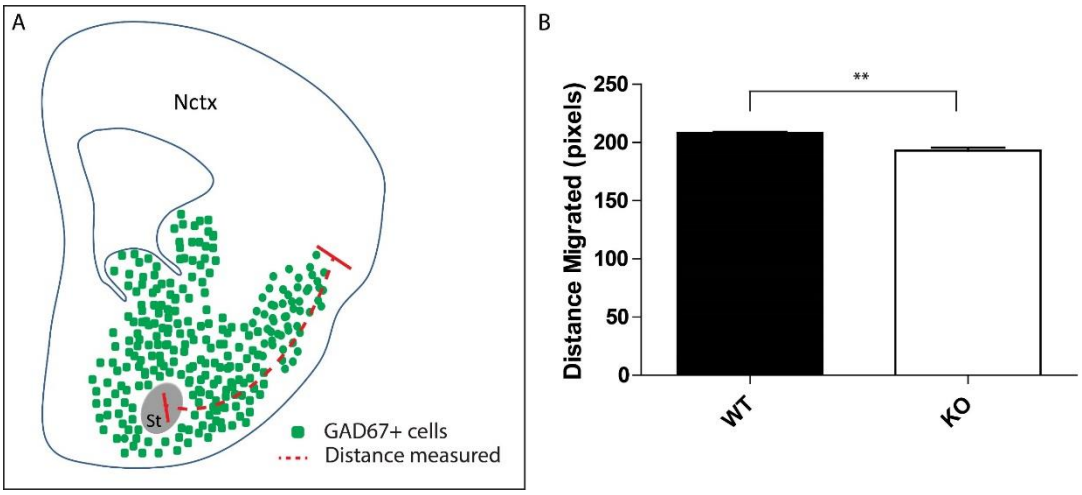


Figure 4.1: Ablation of *14-3-3ζ* leads to aberrant migration of GABAergic interneurons into the developing neocortex.

The distance of *GAD67+* cells, in E16.5 WT and *14-3-3ζ* KO embryos shown previously in Figure 3.3, was measured. (A) Schematic diagram of the distance measured. Dashed red line indicates distance measured using Photoshop software. (B) Quantification of the furthest distance an interneuron travelled in WT and KO mice (n=4). Statistical analysis was performed using Student's t-test (P= 0.0015). Error bars represent ±SEM. Statistical significance was determined via student t-test. (*p<0.05, **p<0.01, ***p<0.001).

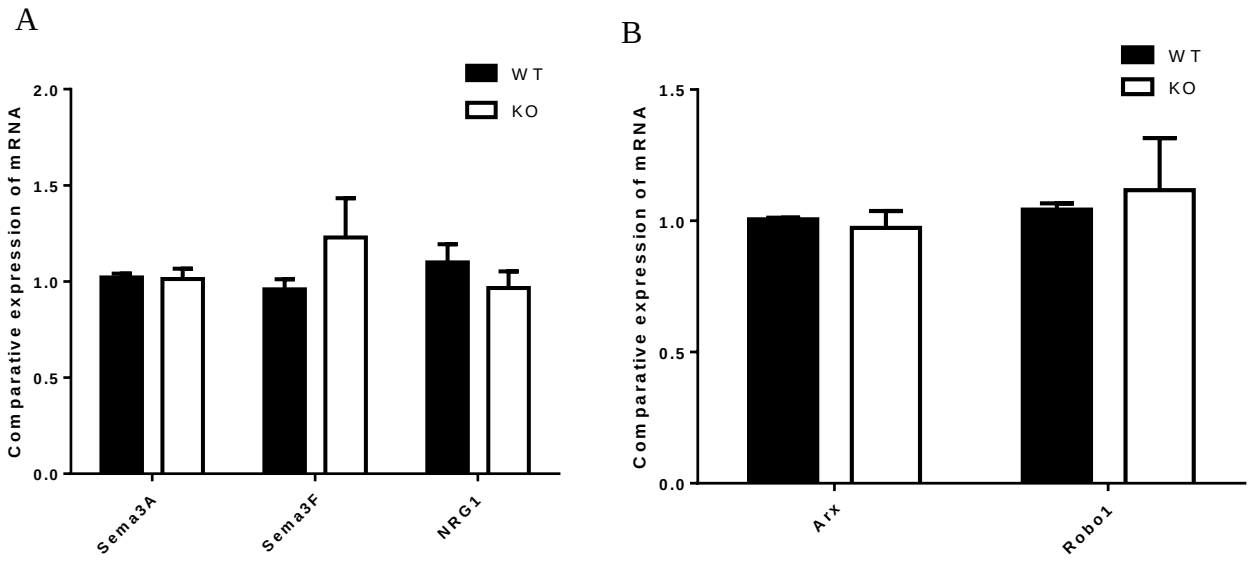


Figure 4.2: *14-3-3ζ* is not required for expression of common factors involved in tangential migration.

Real time PCR analysis of RNA expression in WT and *14-3-3ζ* KO mice. (A) adult cortex from WT and *14-3-3ζ* KO mouse brain quantifying mRNA expression of genes with known chemoattractive and chemorepulsive roles and involved in guidance of interneurons to the cortex (*Sema3A, Sema3F and NRG1*) (n=3). (B) Real time PCR analysis of WT and *14-3-3ζ* KO E12.5 MGE samples quantifying expression of molecules which facilitate migration (*Arx* and *Robo1*) (n=3). Error bars represent ±SEM. Statistical significance was determined via student t-test. *Arx* p=0.837, *Robo1* p=0.589, *Sema3A* p=0.77, *Sema3F* p=0.716, *NRG1* p=0.559.

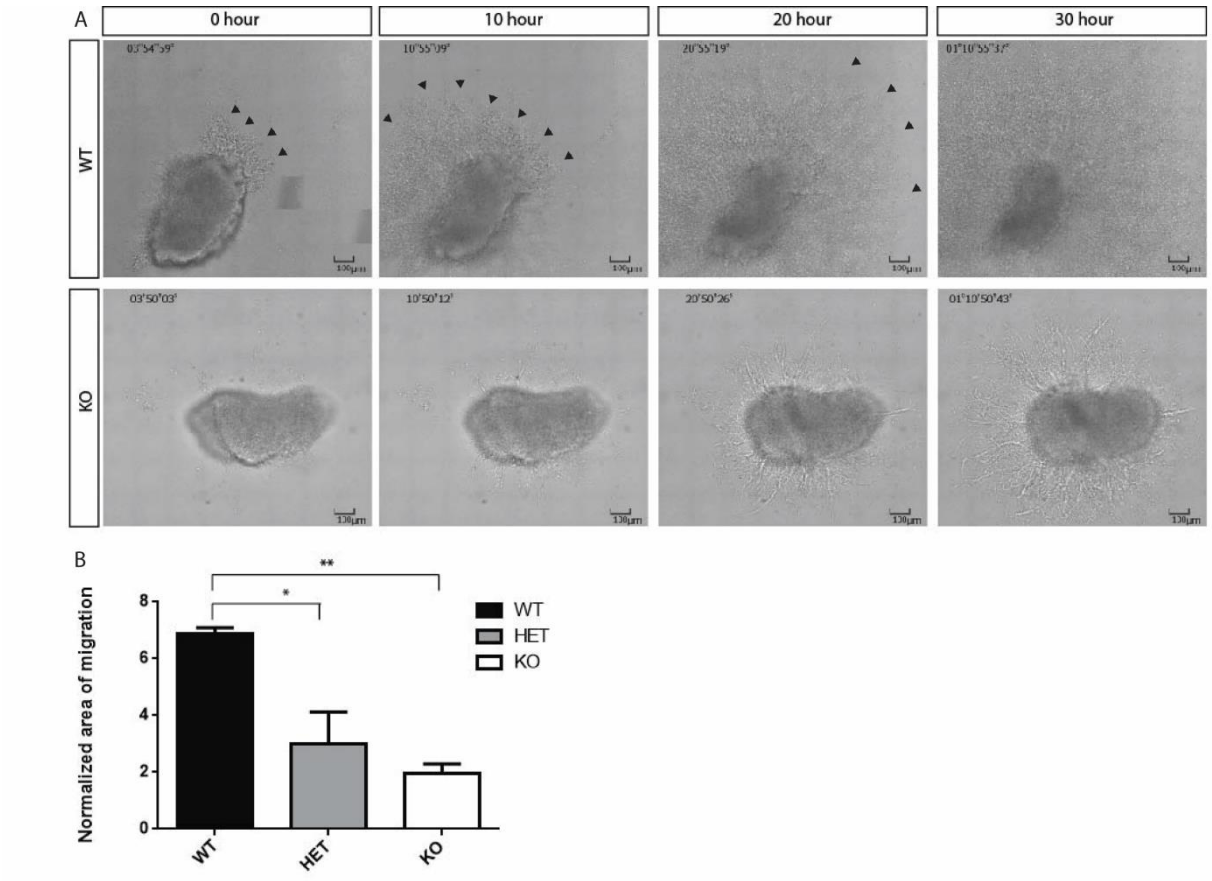


Figure 4.3: MGE-derived cell migration defects observed in the absence of *14-3-3ζ*.

MGE explants from E13.5 WT and *14-3-3ζ* KO mice were cultured in matrigel for 48 hours and imaged on CV1000 spinning disc microscope. (A) Representative images of time points 0 hour, 10 hour, 20 hour and 30 hour of WT and KO explants. (B) Quantification of area travelled by WT, HET and KO interneurons normalized to explant size. (n=3) Error bars represent ±SEM. Statistical significance was determined via t-test. (*p<0.05, **p<0.01). Scale bars 100μm (top), 25μm (bottom).

neurons which had formed migrated a shorter distance from the explant (WT, 6.9; HET, 3.0; KO, 1.9; P<0.05; n=4). Migration dynamics were also analysed with ImageJ software. By tracking the migration path of at least 50 neurons from each sample (n=3), I found that although interneurons of *14-3-3ζ* KO mice had no change in directionality, their migration speed was significantly reduced (WT, 0.77μm/min; KO, 0.34μm/min; p=0.04) (Figure 4.4). These findings are consistent with our *in vivo* analyses and raise the hypothesis that 14-3-3ζ is essential for the formation and migration of MGE-derived interneurons.

4.2.2 Loss of *14-3-3ζ* leads to morphological changes in cortical interneurons.

Whilst fully differentiated interneurons display a wide range of phenotypes, migrating MGE derived interneurons display a distinctive morphology characterised by the presence of 2 leading processes extending from the cell body. Interneurons from E12.5 WT explants have two prongs at the leading migration front, whereas interneurons from *14-3-3ζ* KO mice had longer projections and migrated via branch like processes (Figure 4.5A). The morphology of individual interneurons was further examined by quantifying the number of primary branch points from at least 50 neurons per sample (n=3). Interneurons from *14-3-3ζ* KO mice have a significant increase in the number of primary branches compared to WT (WT, 1.66 branches/cell; KO, 2.26 branches/cell; P=0.002) and also showed a marked change in distribution (χ^2, P<0.001) (Figure 4.5B,C). Taken together, this suggests that interneurons derived from the MGE show defects in specification and and/or identity in *14-3-3ζ* KO mice.

4.2.3 Altered transcriptional profile and formation defects observed in MGE-derived interneurons in *14-3-3ζ* KO mice.

The reduced number and altered morphology of interneurons in *14-3-3ζ* KO mice suggests that specification of cells within the VZ of the MGE may be affected. Indeed, defects during the earliest stages of neurogenesis could also underlie the aberrant migration and loss of embryonic and postnatal MGE-derived interneurons in *14-3-3ζ* KO mice. In order to explore

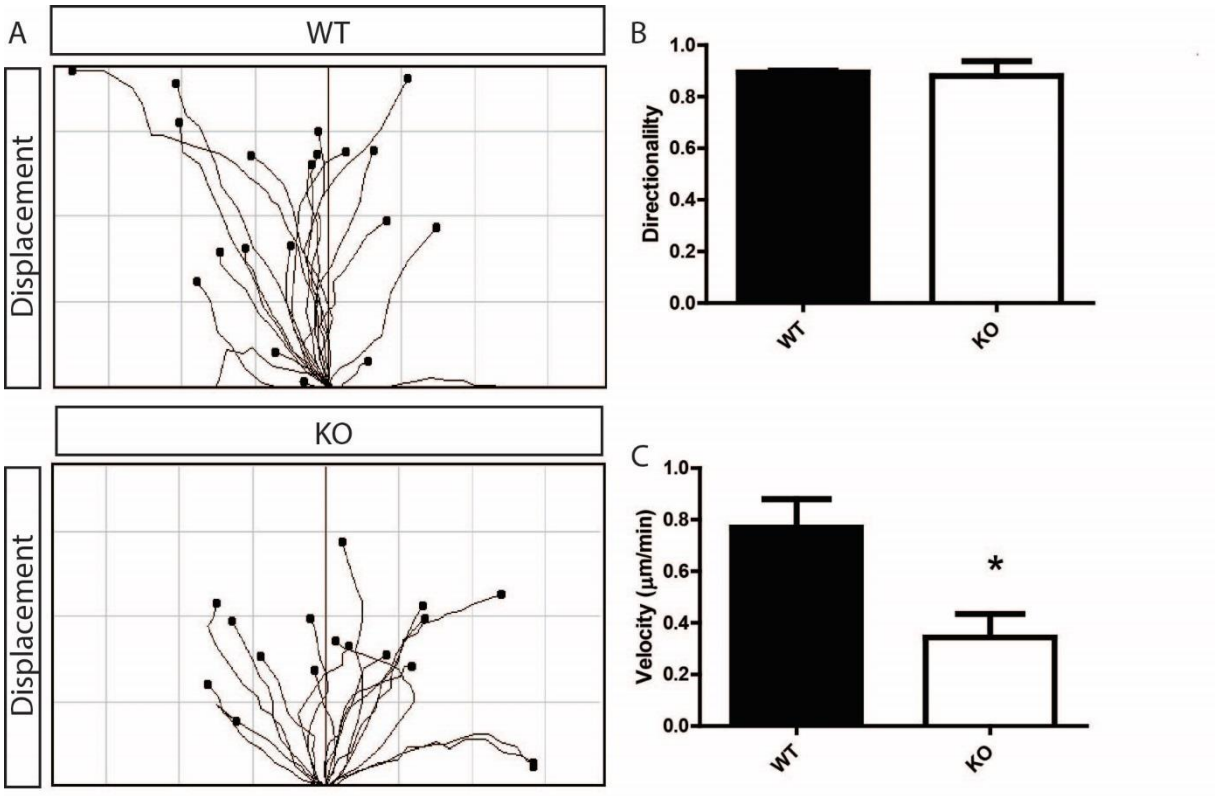


Figure 4.4: Analysis of migration dynamics in *14-3-3ζ* KO interneurons.

Neurons from cultured MGE explants were analysed. At least 50 neurons per sample were tracked using image J software. (A) Representative trace of interneuron displacement from one WT and *14-3-3ζ* KO explant. (B) Representation of cell directionality from explant. (C) Quantification of velocity of cells migrating from explant (n=3). Error bars represent ±SEM. Statistical significance was determined via t-test. (*$p<0.05$).

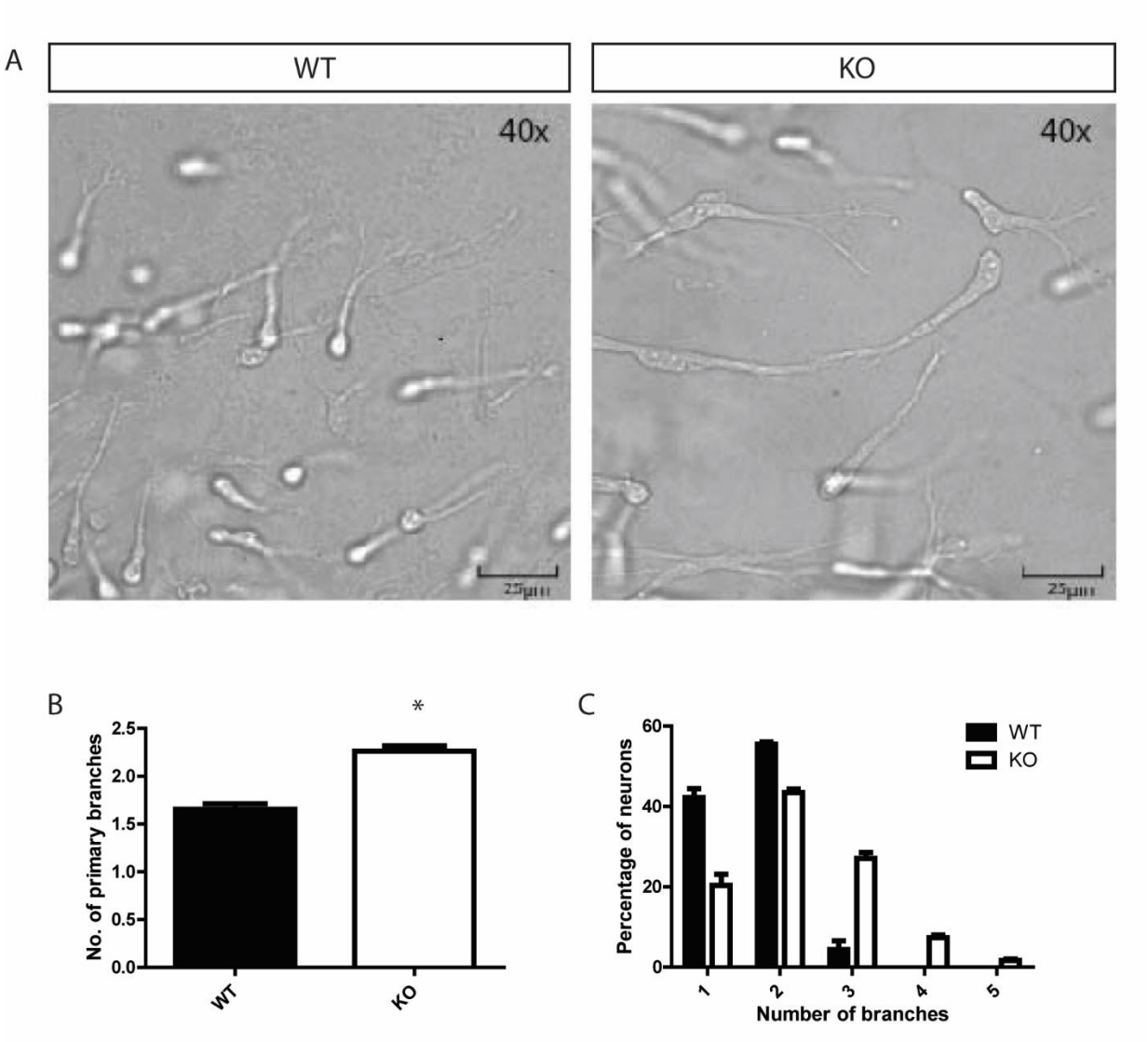


Figure 4.5: *14-3-3ζ* KO MGE derived cells display morphological changes.

Morphology of neurons from cultured MGE explants were analysed. (A) High magnification (40x) of single frame images at 30-hour time point for WT and KO. (B, C) Primary branches of individual cells were manually counted for WT and KO explants with at least 100 neurons counted per sample (n=3). Error bars represent ±SEM. Statistical significance in (B) was determined via t-test. (*$p<0.05$). Statistical significance in (C) was determined via independent chi square ($p<0.001$).

this, I investigated the transcriptional profile of interneurons in *14-3-3ζ* KO mice compared to WT. This was completed using *in situ* hybridization on sectioned E12.5 embryos and qPCR of microdissected MGE (Figure 4.6). Transcription factors *Nkx2*.1 and *Dlx2*, which are associated with the MGE-derived lineage, were examined alongside *Mash1* which is associated with the CGE lineage. *Nkx2.1* expression was substantially reduced in *14-3-3ζ* KO mice at both the transcript and protein level (Figure 4.6). *Dlx2* expression was also reduced in *14-3-3ζ* KO mice (Figure 4.6A). Interestingly, staining of both Nkx2.1 and *Dlx2* showed that a smaller proportion of immature interneurons had transitioned from the VZ into the SVZ. Conversely, *Mash1* which is important in CGE identity and not in MGE identity showed no change in expression levels or patterning in *14-3-3ζ* KO embryos (Figure 4.6A). Quantitative real time PCR was also performed on the MGE to analyse expression of transcription factors involved in interneurons development. This analysis confirmed a reduction of *Nkx2.1* and its downstream effectors *Lhx6*, *Sox6*, and *Dlx2* in *14-3-3ζ* KO mice (Figure 4.6C). Furthermore, this analysis confirmed the normal expression of *Mash1*. Taken together, this data supports a role for 14-3-3ζ in promoting specification of MGE derived interneurons.

4.2.4 Ablation of *14-3-3ζ* does not affect the proliferation of MGE-derived progenitors.

Given that correct specification is essential for neurogenesis in the MGE, I next analysed proliferation in *14-3-3ζ* KO mice using pulse labelling with the thymidine analog EdU to identify proliferating cells. EdU was injected into pregnant dams either 1 hour or 30 minute prior to harvesting embryos at E12.5. Proliferating cells within the MGE were then identified by staining coronal sections using the Click-it EdU assay (Section 2.2.5.8, Figure 4.7A). Due to the high number of progenitor cells undergoing proliferation within the VZ, as recognised by counter staining for Sox2, absolute cell counts were not possible (Figure 4.7A). Although qualitative analysis identified no gross changes in proliferation between the *14-3-3ζ* KO and WT mice, a common observation throughout my investigation was a compact proliferative layer

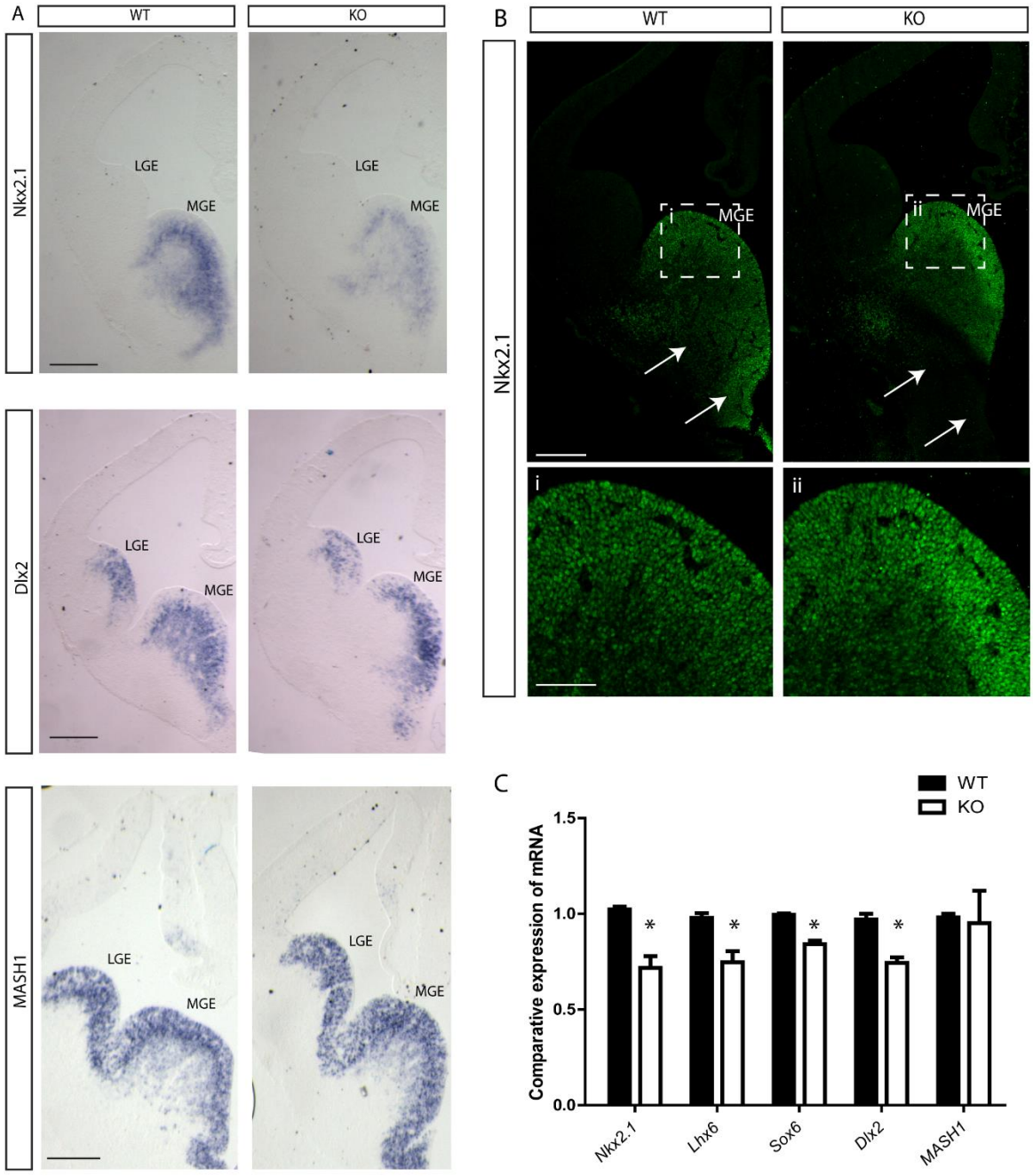


Figure 4.6: Loss of MGE identity in *14-3-3ζ* KO mice.

(A) *In situ* hybridization on coronal brain sections of E12.5 WT and *14-3-3ζ* KO mice with riboprobes against *Nkx2.1, Dlx2 and Mash1* (n=3). Scale bars, 200µm. (B) Brain sections from E12.5 WT and KO mice immunofluorescently labelled for Nkx2.1 (n=3). Scale bars, 200µm (top) and 100µm (i,ii). (C) Real time PCR analysis of transcription factors involved in specification from E12.5 MGE samples (n=3). Error bars represent ±SEM. Statistical significance was determined via t-test. (*$p<0.05$).

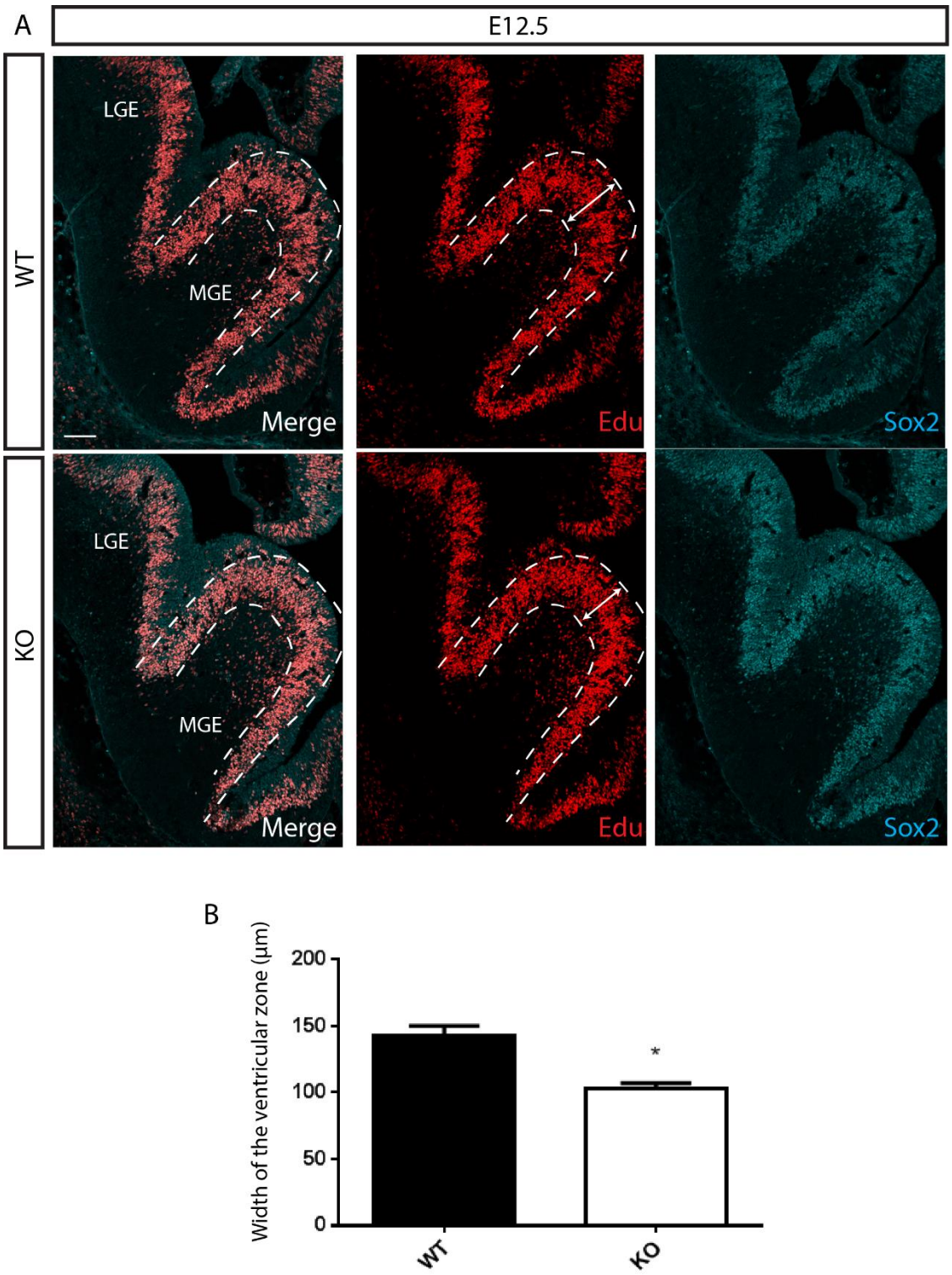


Figure 4.7: EdU incorporation shows no change in proliferation of interneurons in *14-3-3ζ* KO mice.

(A) Representative coronal brain sections of E12.5 WT and *14-3-3ζ* KO mice. Mice were intraperitoneally injected with EdU at E12.5 and collected 30 minutes later. EdU incorporation was visualized with alexafluor 555 (red) and counterstained with anti-Sox2 antibody to examine proliferation (n=3). Dashed lines represent the boundaries of the VZ and SVZ. Arrows indicate were measurement was taken. (B) Quantification of the VZ width in WT and *14-3-3ζ* KO mice (n=3). Statistical analysis was performed using Student's t-test. Error bars represent ±SEM. Statistical significance was determined via student t-test. (*p<0.05). Scale bar, 100µm.

in the *14-3-3ζ* KO mice. The width of the VZ in the MGE was measured at E12.5 and the *14-3-3ζ* KO mice had considerably thinner and denser VZ compared to WT which was far more disperse (WT, 142.5µm; KO, 102.5µm; n=3; p=0.04) (Figure 4.7B). In association with the finding that cells fail to transition from the VZ to the SVZ (Section 4.2.3), the presence of a thinner VZ fits with the notion that cells are unable to migrate through the MGE and could also indicate a defect in the cell cycle exit.

4.2.5 Loss of *14-3-3ζ* results in dysregulation of cell cycle exit.

The movement of cells from the VZ to the marginal zone is tightly associated with cell cycle exit. To explore a potential defect in cells exiting the cell cycle I next performed a dual thymidine analogue incorporation assay by injection of BrdU and EdU with embryo harvest 30 min after the final injection at E12.5 (Figure 4.8) and E13.5 (Figure 4.9). In this assay, cells positive for both EdU and BrdU have remained in the cell cycle, whilst cells positive for only BrdU have divided and now exited the cell cycle. In a similar manner to the previous proliferation assay it was not possible to accurately count cells in the MGE which precluded a quantitative analysis. However, when analysing the staining there appeared to be an increase in the number of double positive cells in *14-3-3ζ* KO mice at E13.5 (Figure 4.9). An increased proportion of cells expressing both BrdU and EdU compared to BrdU alone indicates a reduced number of cells exiting the cell cycle. Although these pilot studies suggest the cell cycle is affected in the MGE of *14-3-3ζ* KO mice future studies would benefit from a quantitative analysis which may be possible with assays at different ages (E14.5 vs E12.5), using different staining procedures (Ki67 and pHH3 vs EdU) or by using thinner sections and higher magnification images.

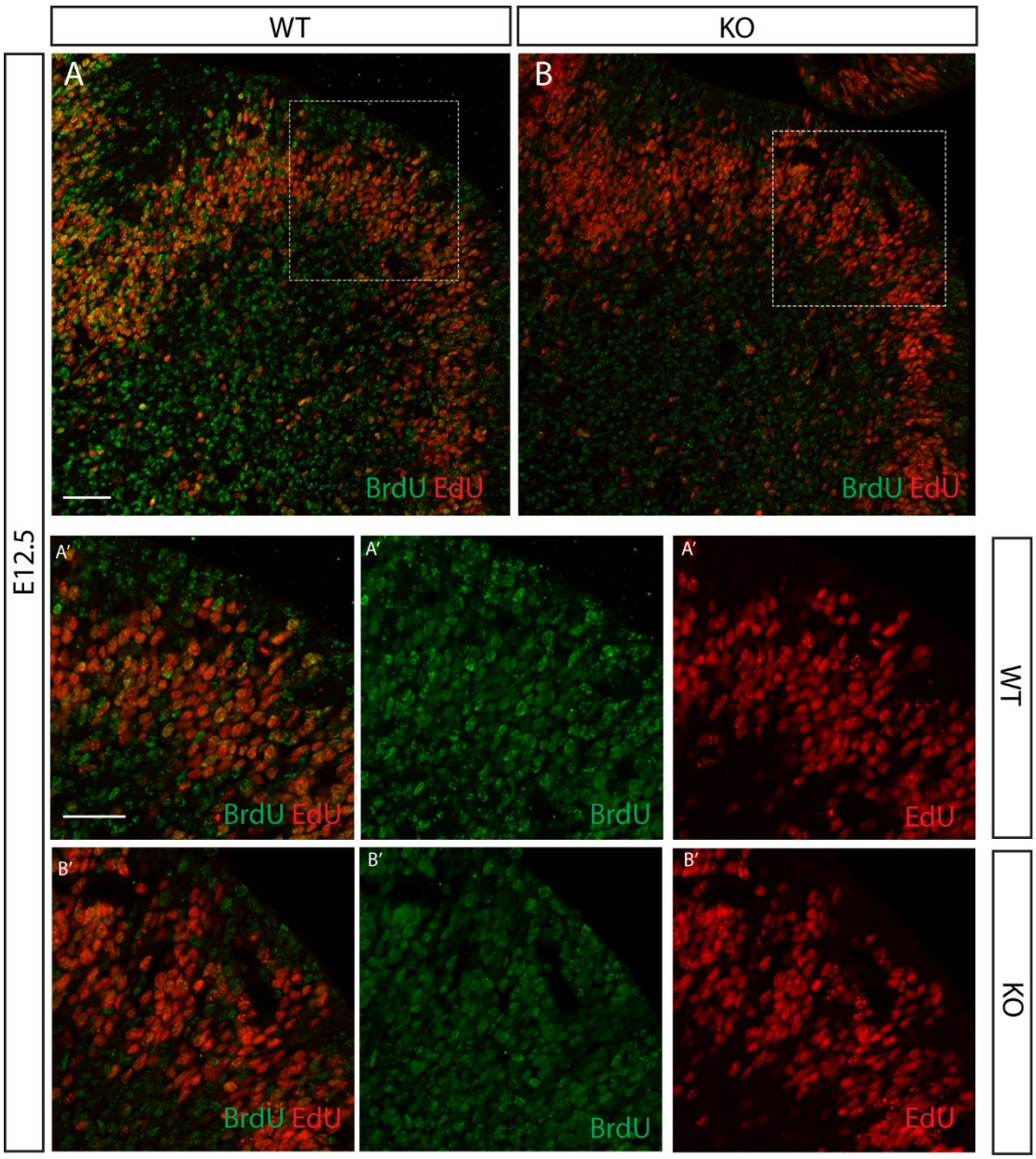


Figure 4.8: No significant change in cell cycle exit at E12.5 in *14-3-3ζ* KO mice.

Dual pulse labelling with EdU and BrdU was used to determine the percentage of cells exiting the cell cycle. (A, B) WT and *14-3-3ζ* KO mice injected at E11.5 with BrdU (green) for 24 hr and at E12.5 with EdU (red) for 30min prior to harvesting (n=3). Boxed region indicates position of high magnification images. Scale bars, 100µm (top) and 50µm (bottom).

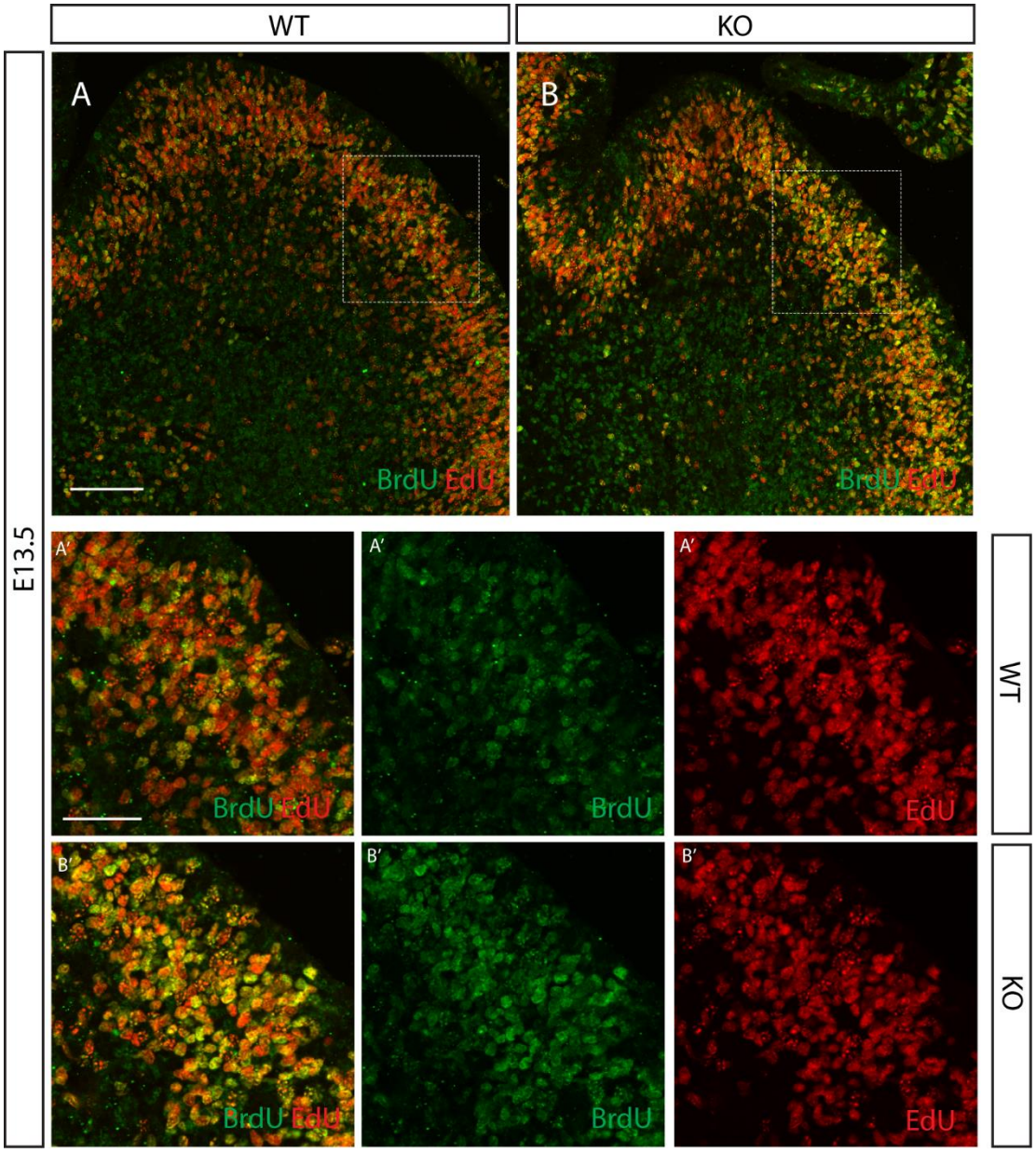


Figure 4.9: Interneurons display delayed cell cycle exit at E13.5 in *14-3-3ζ* KO mice.

Dual pulse labelling with EdU and BrdU was used to determine the percentage of cells exiting the cell cycle. (A,B) WT and *14-3-3ζ* KO mice injected at E12.5 with BrdU (green) for 24 hr and at E13.5 with EdU (red) for 30min prior to harvesting (n=3). Boxed region indicates position of high magnification images. Scale bars, 100µm (top) and 50µm (bottom).

4.2.6 14-3-3ζ plays an important role in interneuron development prior to cell cycle exit.

In order to verify the necessity of 14-3-3ζ in MGE progenitors prior to cell cycle exit, I explored the consequences of removing *14-3-3ζ* in both pre-mitotic and post-mitotic interneurons. During the course of my PhD, a conditional floxed *14-3-3ζ* mouse line (*14-3-3ζ$^{fl/fl}$*) was generated in the Neurovascular Research Laboratory that could be used for this analysis. By crossing *14-3-3ζ$^{fl/fl}$* mice to *Olig2-Cre* mice and *Dlx5/6-Cre* mice, *14-3-3ζ* was removed in both pre- and post-mitotic interneurons, respectively. To analyse the role of 14-3-3ζ in post mitotic interneurons we first intercrossed *Dlx5/6-Cre;14-3-3$^{fl/+}$* males with *14-3-3$^{fl/fl}$* females. In order to explore if these mice display similar morphological defects as in *14-3-3ζ* KO mice, PV was immunofluorescently labelled in coronal sections through the cortex of adult control mice and *Dlx5/6-Cre;14-3-3ζ$^{fl/fl}$* mice (Figure 4.10). Cell counts were performed in 3 regions (lateral, intermediate and medial) within the cortex (as described in chapter 3). There were no significant changes observed between *Dlx5/6-Cre;14-3-3ζ$^{fl/fl}$* (lateral, 73.1 cells/mm^2; intermediate, 67.5 cells/mm^2; medial, 55.6 cells/mm^2) compared to control (lateral; 83.8 cells/mm^2, intermediate; 70.0 cells/mm^2, medial; 53.2 cells/mm^2) (p(lateral)= 0.77; p(intermediate)=0.85; p(medial)=0.77; n=6). This shows that 14-3-3ζ is not required for MGE-derived interneuron development after neural progenitor cells transition to post-mitotic interneurons. As *14-3-3ζ* KO mice display behavioural changes we also examined this mouse line for hyperactivity, a common readout for schizophrenia-like behaviour (Lipska & Weinberger, 2000; Cheah et al., 2012). However, there was no significant defect in locomotor function or hyperactivity in *Dlx5/6-Cre;14-3-3ζ$^{fl/fl}$* mice compared to the control group (p(mean distance) =0.58; p(mean speed) =0.47) (Figure 4.11) suggesting that 14-3-3ζ is not required by post mitotic interneurons for regulating locomotor activity. *14-3-3ζ* was next removed from pre-mitotic cells by crossing *Olig2-Cre;14-3-3$^{fl/+}$* males to *14-3-3$^{fl/fl}$* females. The *Olig2* promotor drives expression of Cre in the VZ of the MGE (Miyoshi et al., 2007; Ono et al., 2008).

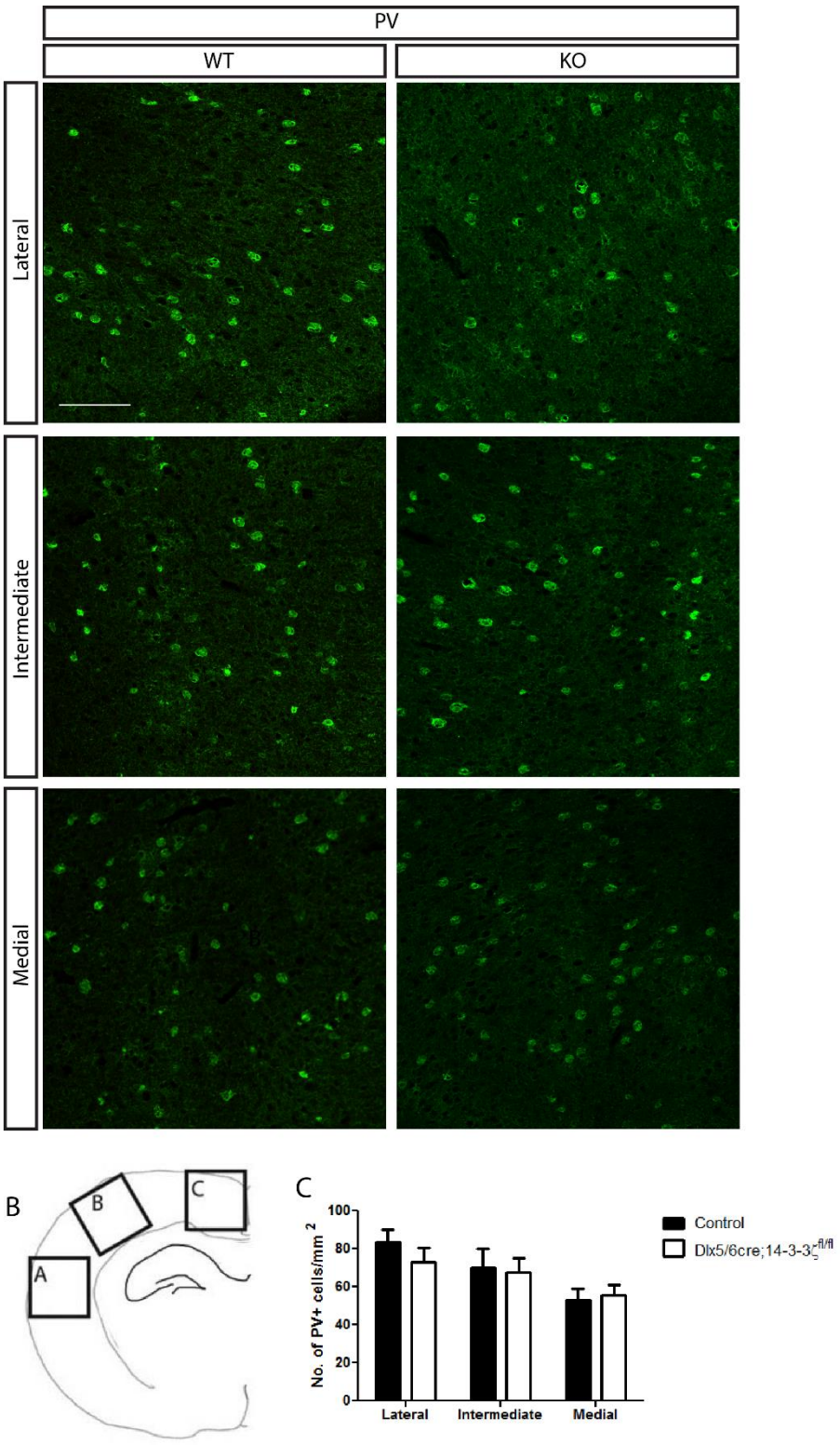


Figure 4.10: *14-3-3ζ* is not required for interneuron development in post mitotic MGE-derived cells.

Representative coronal brain sections from P56 control and *Dlx5/6-Cre;14-3-3ζ*$^{fl/fl}$ mice immunofluorescently labelled for PV. Scale bar, 100µm. (B) Schematic representation of the adult mouse brain, with the boxed regions representing the regions quantified where A=lateral, B=intermediate and C=medial. (C) Quantification of PV+ cells in control and *Dlx5/6-Cre;14-3-3ζ*$^{fl/fl}$ samples (n=6). Scale bar, 100µm. Error bars represent ±SEM. Statistical significance was determined via student t-test. P values were not significant.

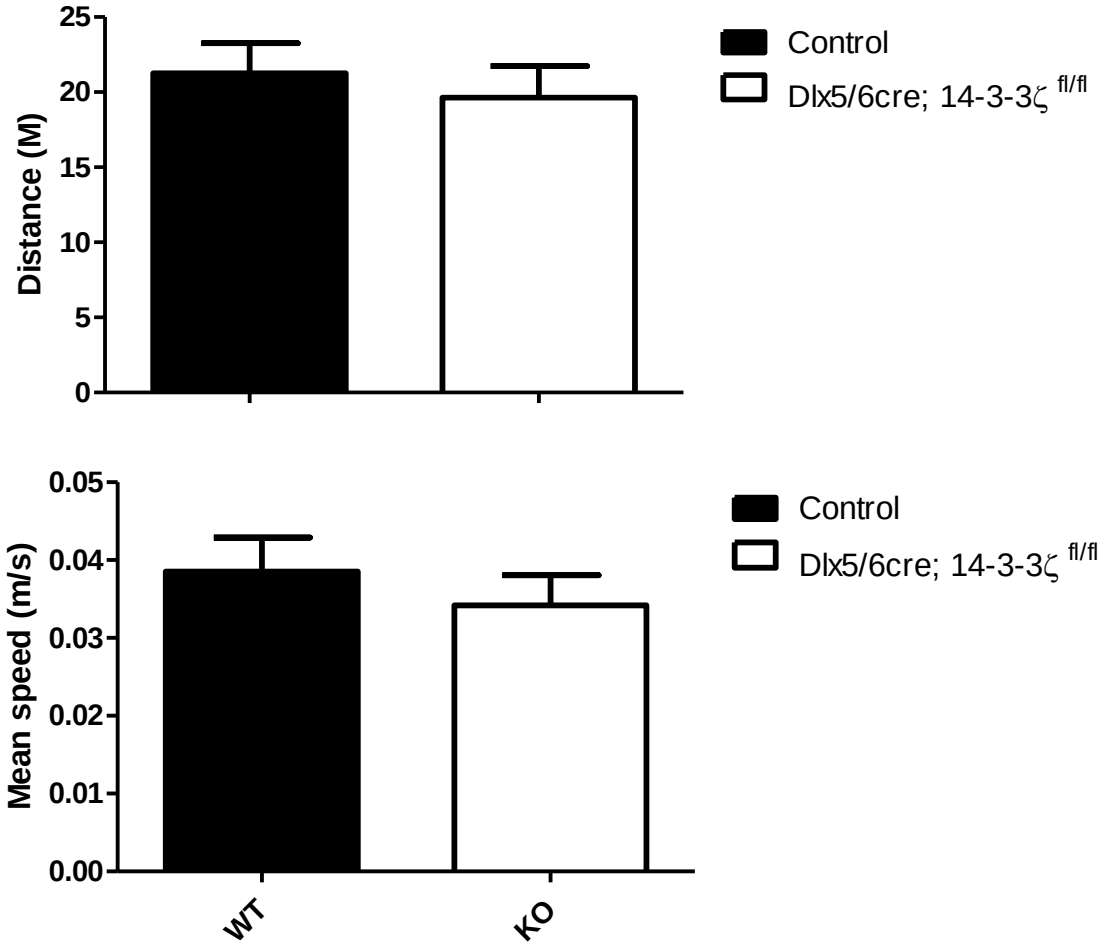


Figure 4.11: *Dlx5/6-Cre; 14-3-3ζ$^{fl/fl}$* mice do not display locomotive defects or hyperactivity.

Locomotor function of control and *Dlx5/6-Cre; 14-3-3ζ$^{fl/fl}$* mice were examined using ANY-maze software. (A) Total distance travelled over a 10 min period by *Dlx5/6-Cre; 14-3-3ζ$^{fl/fl}$* mice compared to control. (B) Mean speed in which mice travelled over 10 min period by *Dlx5/6-Cre; 14-3-3ζ$^{fl/fl}$* mice compared to control.

Using the same analysis as above, I identified a reduction in the number of PV+ interneurons in the medial and intermediate regions of the cortex but not the lateral region (lateral, 59.1 cells/mm^2; intermediate, 55.5 cells/mm^2; medial, 52.3 cells/mm^2) compared to control mice (lateral, 63.4 cells/mm^2; intermediate, 85.1 cells/mm^2; medial, 74.1 cells/mm^2) (p(lateral)= 0.50; p(intermediate)=0.014; p(medial)=0.015; n=3), similar to that seen in the constitutive *14-3-3ζ* KO mice (Figure 4.12). This indicates that 14-3-3ζ is required in mitotic cells but not post mitotic cells. We therefore hypothesise that the primary role for 14-3-3ζ is to promote the transition of neural stem cells into post-mitotic interneurons and therefore correct migration and positioning of interneurons in the cortex.

4.2.7 Microarray analysis reveals changes in the Shh signalling pathway in *14-3-3ζ* KO mice.

Though our data identifies significant changes in the overall formation of interneurons in *14-3-3ζ* KO mice, we are yet to establish the underlying molecular pathway/s involved. In order to investigate what is underpinning loss of *Nkx2.1* and overall loss of MGE identity, a microarray analysis was performed. The MGE from 3 pairs of WT and *14-3-3ζ* KO E12.5 embryos were microdissected away from all other brain regions. Initial analysis of RNA quality returned a RIN measure of between 8.1 and 9.4 for all samples. Gene ST 2.0 microarray (Affymetrix) analysis was then performed at the Australian Cancer Research Foundation (ACRF) Cancer Genomics Facility, where expression of 20,000+ transcripts were investigated. Microarray analysis returned varied results with inconsistencies between samples of the same genotype that may have resulted from gender differences. Analysis of *Xist* expression indicated that our analysis included 2 male/1 female *14-3-3ζ* KO embryos and 1 male/2 female WT embryos. Indeed, the grouping of samples in Principle Component Analysis suggests that difference in sex accounts for some of the major expression variations across samples (Figure 4.13). In future, analyses on matched sexes and an increase sample size would be recommended for this approach. Due to the variation between samples, the use of standard statistical

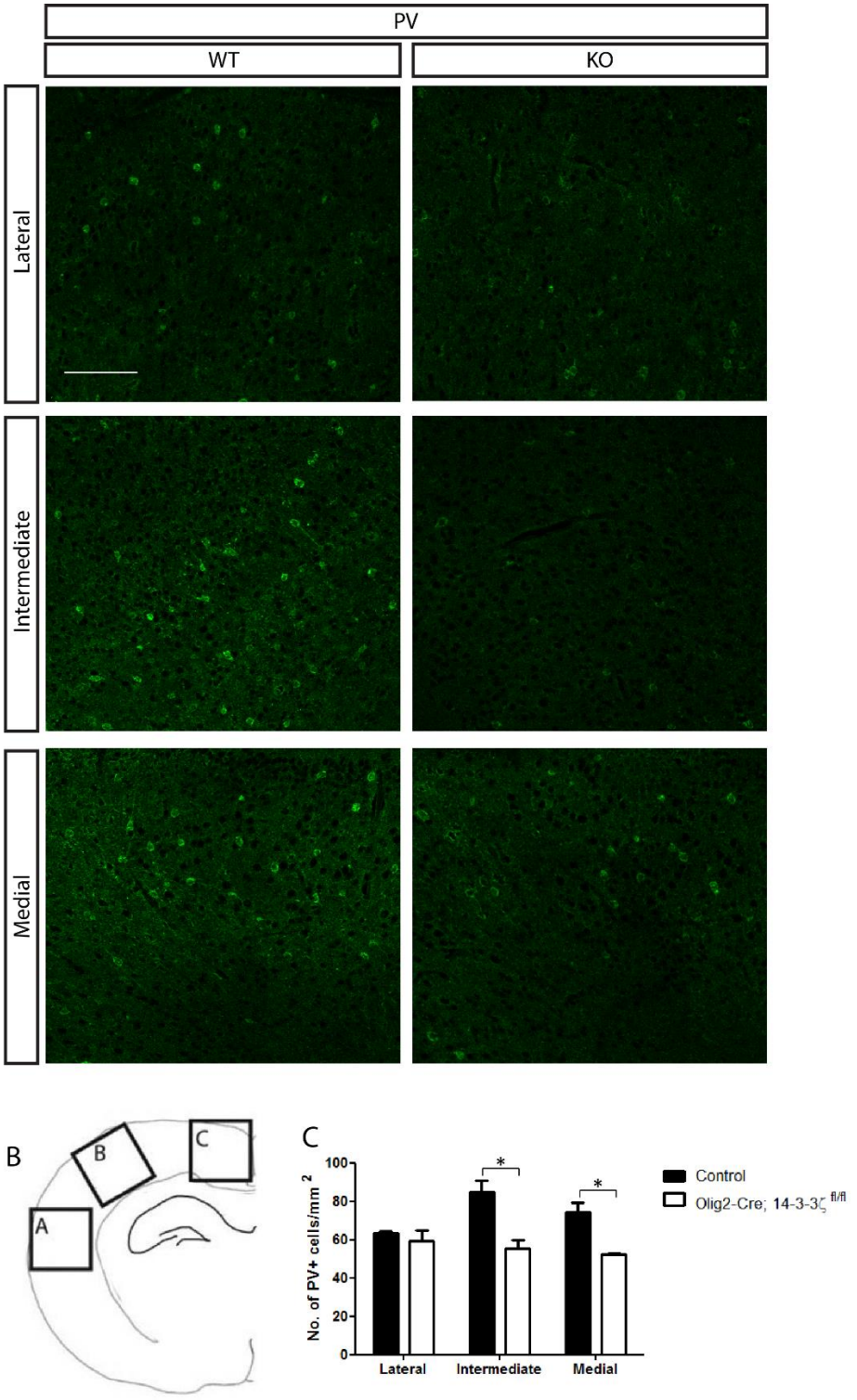


Figure 4.12: Ablation of *14-3-3ζ* in mitotic cells leads to a reduction in PV+ interneurons.

(A) Representative coronal brain sections from P25 control and *Olig2-Cre;14-3-3ζ*$^{fl/fl}$ mice immunofluorescently labelled for PV. Scale bar, 100µm. (B) Schematic representation of the adult mouse brain, with the boxed regions representing the regions quantified where A=lateral, B=intermediate and C=medial (C) Quantification of PV+ cells in control and *Olig2-Cre;14-3-3ζ*$^{fl/fl}$ samples (n=3). Scale bar, 100µm. Error bars represent ±SEM. Statistical significance was determined via student t-test. (*p<0.05).

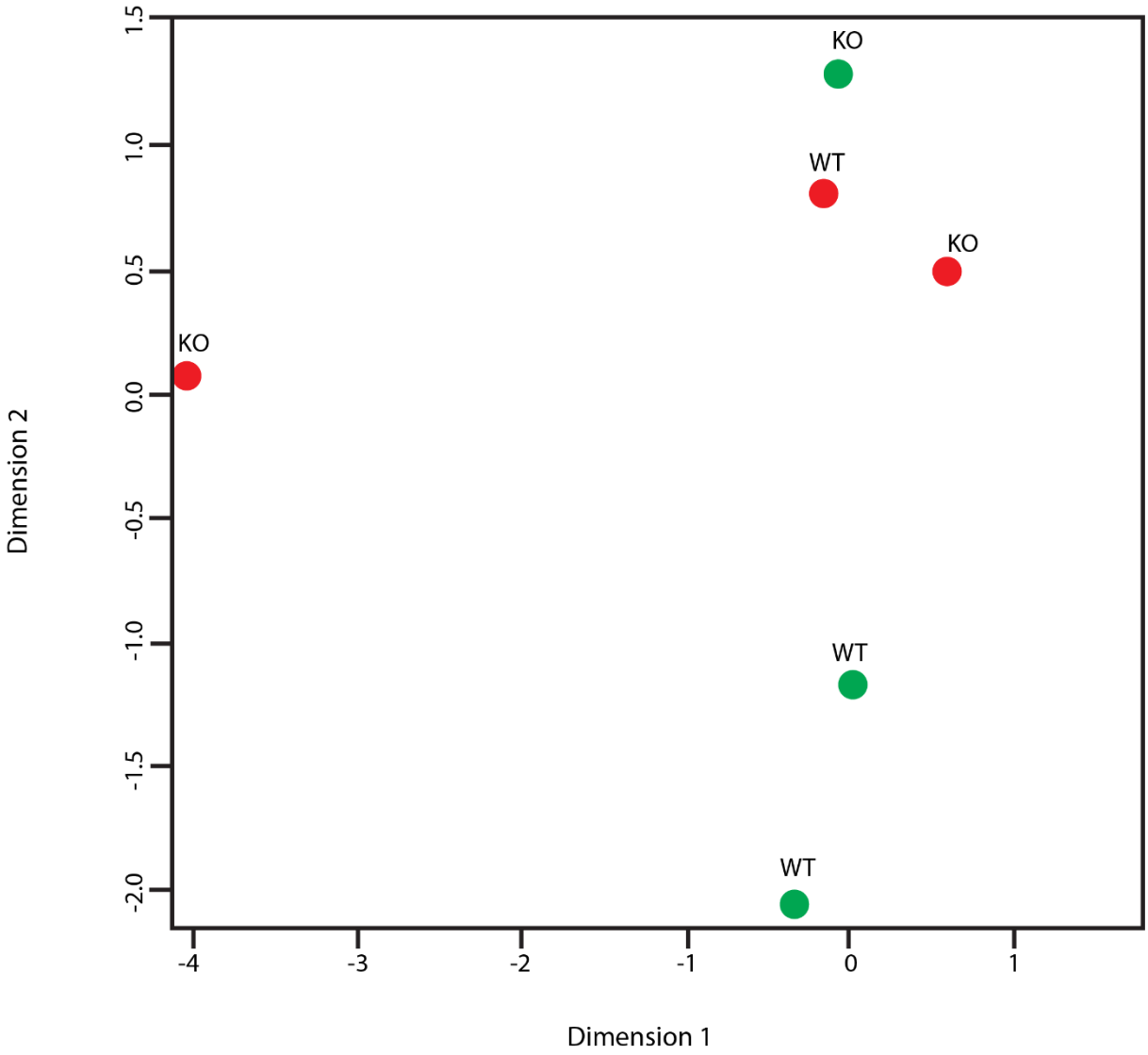


Figure 4.13: Sex differences potentially account for microarray variability.

GeneChip Mouse Gene 2.0 ST Array was used to perform a microarray analysis for identification of 14-3-3ζ dependent gene expression. Partek Genomics Suite v6.6 was used to generate a Principal Components Analysis (PCA) to plot the biological samples with each axis being a linear combination of all 20,000+ transcripts. Red=male, green=female

techniques such as the Step-up P-value which reduces the false discovery rate could not be used as this returned no significant changes in gene expression, albeit that *14-3-3ζ* expression was consistently reduced across all KOs. Since the main aim of this analysis was to identify potential signalling pathways or interacting genes, a more "liberal" approach was taken. Thus, rather than using the Step-up P-value for prioritising samples, the P-value was used as a measure of significance. Furthermore, we also incorporated a second criteria for sorting the data based on the known expression change of *Nkx2.1*, which was shown to be decreased at the mRNA level in *14-3-3ζ* KO embryos earlier in this chapter. By looking at differentially expressed genes with a P-value lower than 0.05, this approach identified 678 genes upregulated and 336 genes down regulated in KO samples compared to WT. Gene ontology analysis of these differentially expressed genes (MetaCore and PANTHER) identified over representation of genes within several pathways and processes of interest, including cytoskeletal regulation by Rho GTPase and cell cycling. Although this method is the most straight forward it fails to take into consideration fold change and that some of the genes identified have only marginal changes. Further refinement of the list based on using the fold change of *Nkx2.1* (1.159) as a cut off for genes that are decreased in expression identified 202 genes significantly reduced in *14-3-3ζ* KO samples (Appendix A.1). Within this list, we identified 50-fold reduction of *14-3-3ζ* which was expected given that one sample set was taken from mouse embryos lacking this gene. Other notable changes included reduced expression of *Fgf16* and *Sema5a* which are involved in interneuron specification and migration, respectively. Gene ontology analysis of these 202 genes identified several pathways of interest. For example, when the fold enrichment (number of genes expected vs number of genes identified) was taken into account, the Shh signalling pathway, cell cycle and ATP synthesis were all significantly altered. Using this same analysis, 31 genes within the Wnt signalling pathway were also identified, however, this is less than the number of genes expected and hence underrepresented. To explore the microarray data further we also prioritised the data set based on P-values below that of *Nkx2.1* (P=0.189). Using this

criterion, 2868 genes were up regulated and 1706 genes down regulated in *14-3-3ζ* KO samples. Pathways with positive fold enrichment (i.e. a greater number of genes changed than expected) across both analyses (Table 4.1) identified the Shh signalling pathway as a major contributor to the 14-3-3ζ phenotype. In contrast, genes in the Wnt signalling pathway were found to be underrepresented, despite having the largest number of genes changed overall. While the analysis of Shh signalling forms the basis of the following chapter, the remainder of this chapter has focussed on further analysis of the Wnt signalling pathway, due to its known roles in interneuron development.

Microarray analysis identified reduction of several Wnt signalling molecules including *β-Catenin*, *Dvl*, *Tcf7L2* and *cyclin D1*. For validation purposes qPCR was performed on cDNA synthesised from E12.5 MGE samples with only *cyclin D1* (49% reduction) found to be significantly decreased. B-catenin showed a marked reduction in *14-3-3ζ* KO samples (only 27% of WT) but due to high variability this qPCR analysis did not reach significance (Figure 4.14). Given the lack of Wnt target genes in the microarray and that *cyclin D1* and *β-catenin* both have well established roles downstream of multiple signalling pathways, including Shh signalling, these results suggest that the Wnt signalling pathway does not underlie the interneurons defects in *14-3-3ζ* KO mice.

4.2.8 Structural disorganization and impaired formation of the MGE in *14-3-3ζ* KO mice.

β-catenin has essential roles in signalling and cell junctions. To further explore if this protein may be deficient in *14-3-3ζ* KO embryos immunofluorescence staining for β-catenin and Sox2 was performed on the GEs of E12.5 embryos. This analysis uncovered a dramatic decrease in β-catenin expression in *14-3-3ζ* KO mice compared to WT, and also showed overall higher expression in LGE compared to the MGE in both WT and *14-3-3ζ* KO mice (Figure 4.15). Moreover, β-catenin staining revealed defects in the structural organization of the MGE derived cells. While organization of the MGE was altered in *14-3-3ζ* KO embryos there were

Table 4. 1: Gene ontology analysis of molecular pathways

Pathways	Genes in pathway	Expected gene change	Change in genes	Fold enrichment
Aminobutyrate degradation	3	.28	3	10.72
Tetrahydrofolate biosynthesis	4	.37	2	5.36
Formyltetrahydroformate biosynthesis	7	.65	3	4.59
Atp synthesis	9	.84	3	3.57
Cell cycle	21	1.96	7	3.57
Flavin biosynthesis	3	.28	1	3.57
Gamma-aminobutyric acid synthesis	6	.56	2	3.57
Sulfate assimilation	3	.28	1	3.57
De novo purine biosynthesis	31	2.89	9	3.11
Salvage pyrimidine ribonucleotides	15	1.40	4	2.86
Hedgehog signaling pathway	20	1.87	5	2.68
5-hydroxytryptamine degredation	21	1.96	5	2.55
P53 pathway feedback loops 2	51	4.76	12	2.52
Axon guidance mediated by semaphorins	22	2.05	5	2.44
Synaptic vesicle trafficking	28	2.61	6	2.30

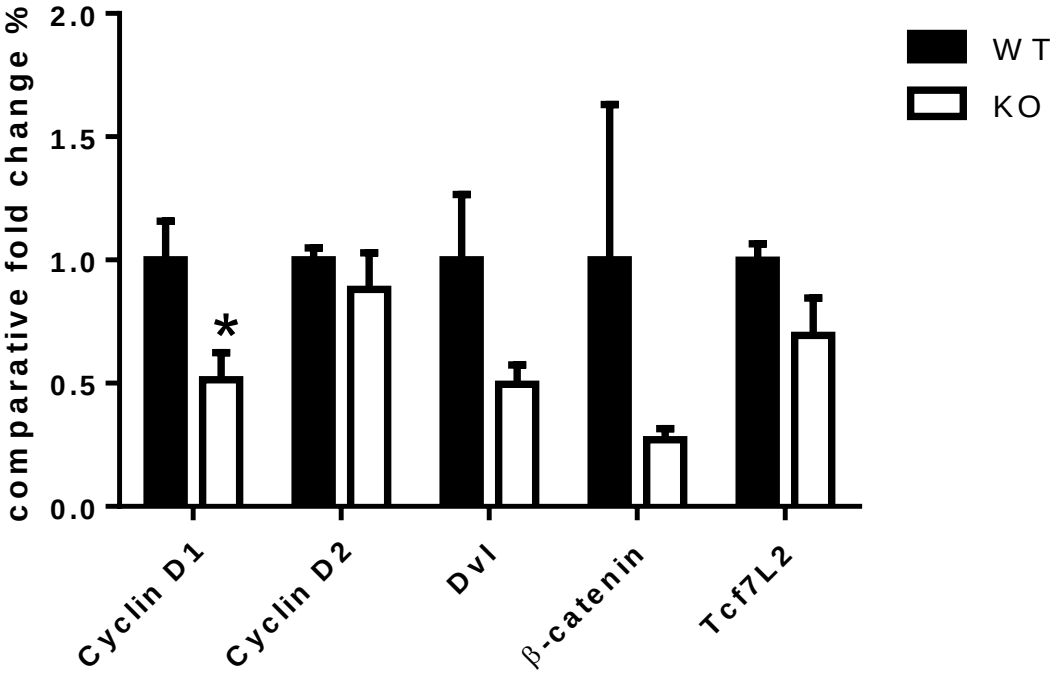


Figure 4.14: Validation of Wnt signalling genes identified by microarray.

Real time PCR analysis was performed on Wnt signalling genes identified in microarray. RNA from E12.5 MGE of WT and *14-3-3ζ* KO mice was used to validate genes (n=3). Error bars represent ±SEM. Statistical significance was determined via t-test. (*$p<0.05$)

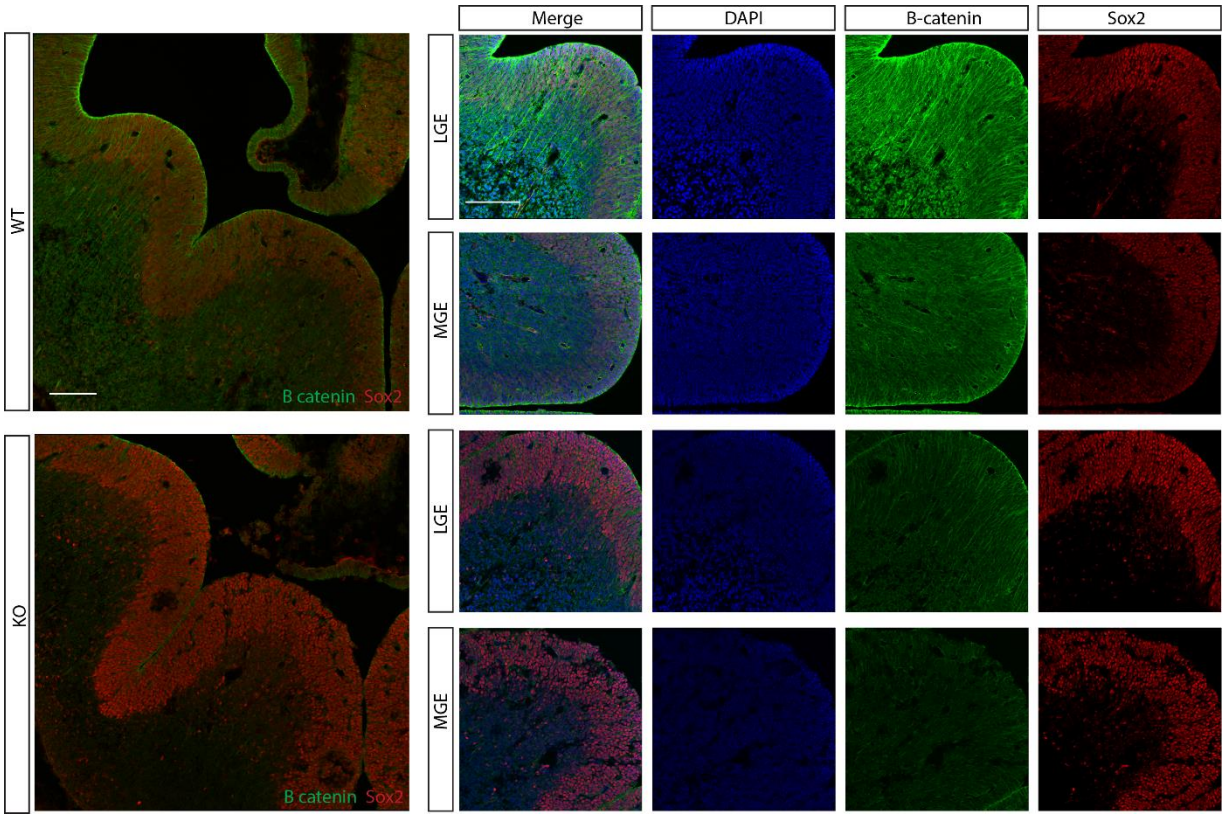


Figure 4.15: Loss of β-catenin in GE of *14-3-3ζ* KO mice.

(A) Representative coronal brain sections from E12.5 WT and KO mice labelled to examine β-catenin and Sox2. Both the MGE and LGE were imaged via confocal microscopy. Scale bar, 100µm (left) and 200µm (right).

no notable changes in the LGE (Figure 4.16). B-catenin is known to form a complex with N-cadherin in adherens junctions. Sections of E12.5 WT and KO embryos were stained for N-cadherin which identified a similar defect to that seen with β-catenin (Figure 4.17). Notably, the overall levels of N-cadherin were reduced and the structural organization of the MGE was also affected.

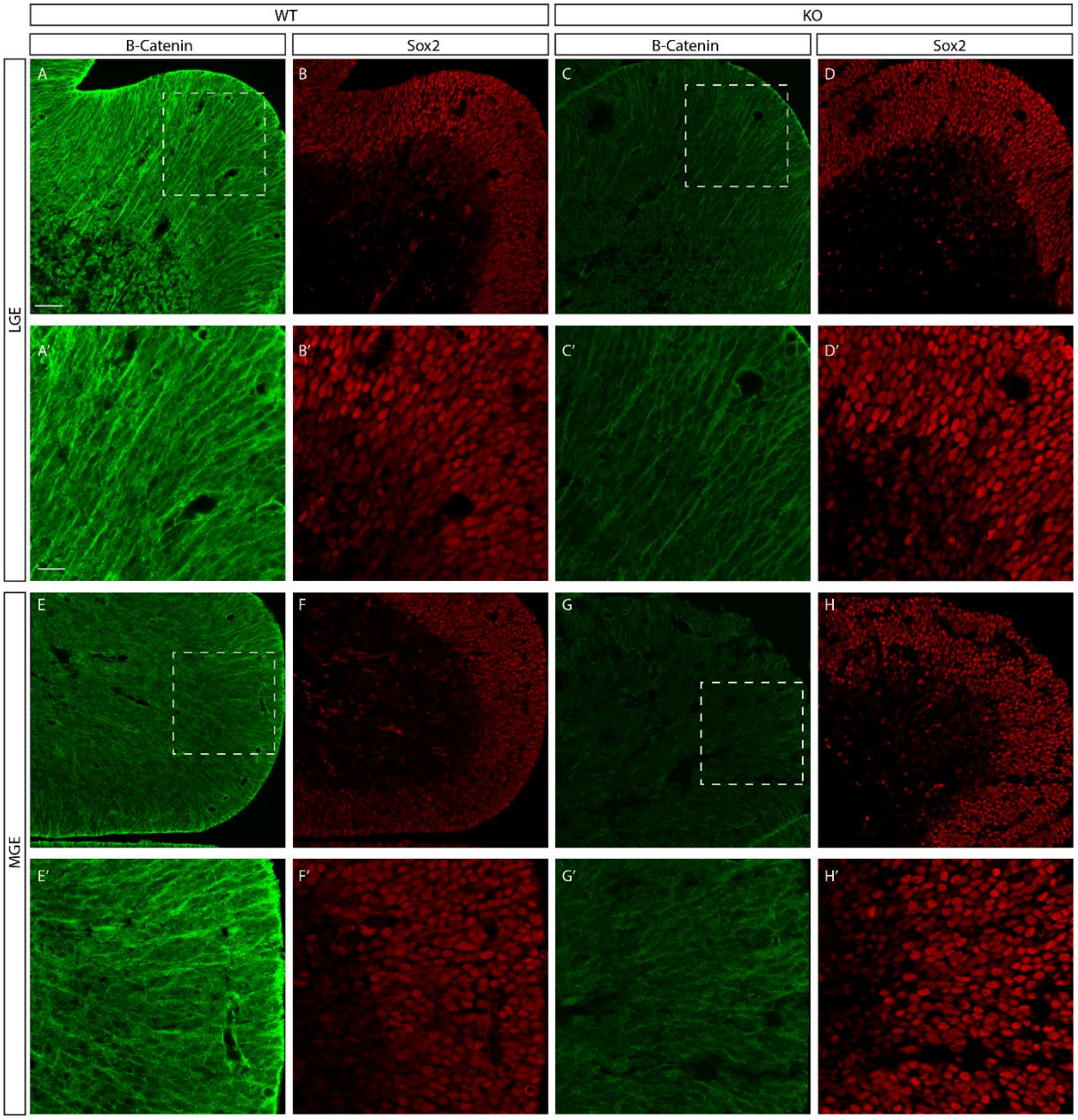


Figure 4.16: Defects in the organization of the MGE in *14-3-3ζ* KO mice.

(A-H) High magnification images of the LGE and MGE of WT and *14-3-3ζ* KO mice from Figure 4.14 identified structural defects of GE. Scale bars, 50µm (A-D) and 20µm (A'-D').

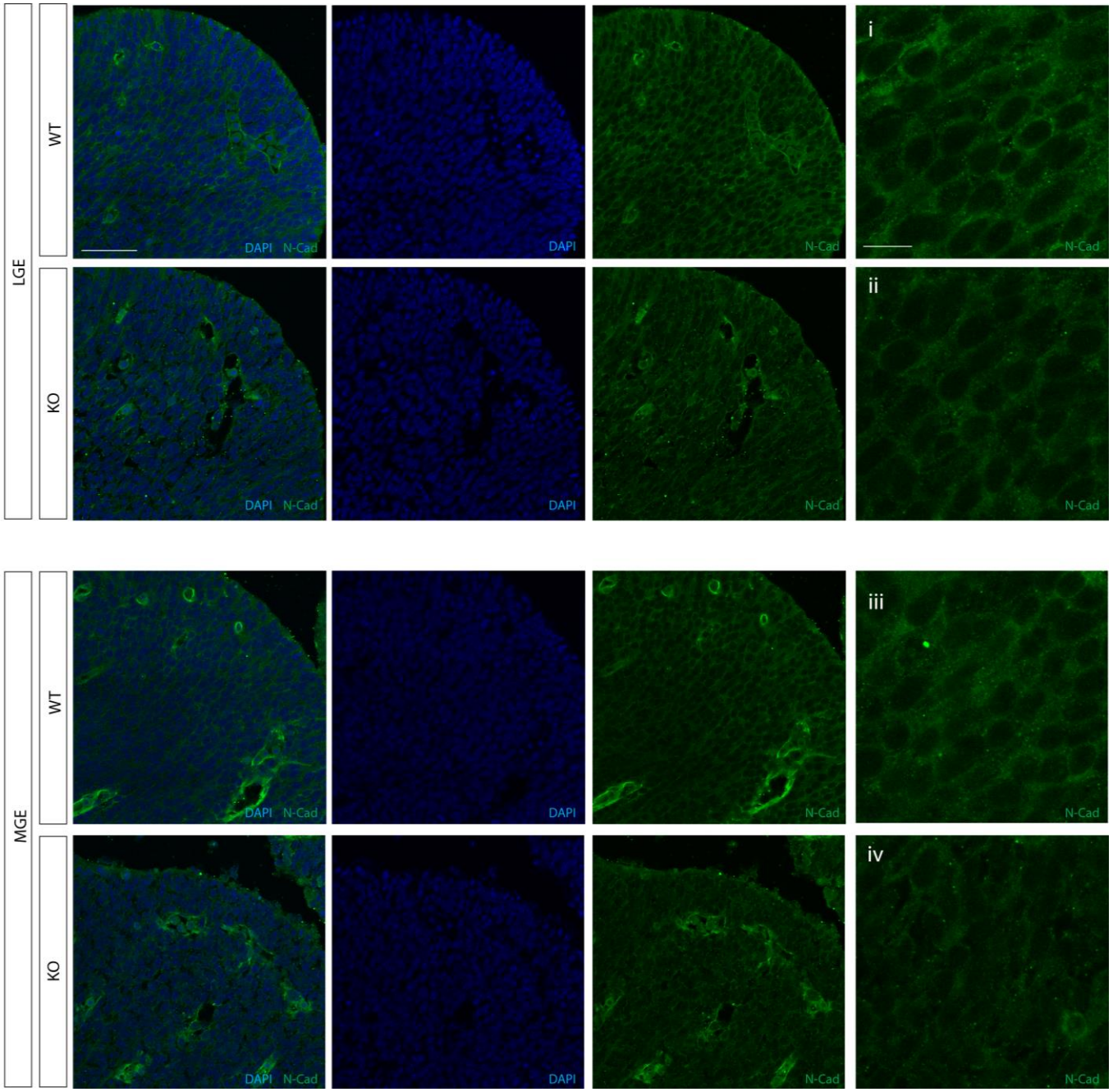


Figure 4.17: N-cadherin staining confirms abnormal architecture of the MGE in *14-3-3ζ* KO mice.

Representative coronal brain sections from E12.5 WT and *14-3-3ζ* KO mice that were immunofluorescently labelled to examine N-cadherin expression. Both the MGE and LGE were imaged via confocal microscopy. (i-iv) High magnification images of N-cadherin staining. Scale bar, 50µm and 10µm (i-iv).

4.3 Discussion

Precise formation of interneurons during embryonic development is critical for their role in the postnatal brain. In the absence of *14-3-3ζ*, MGE-derived interneurons fail to form correctly during development and this deficiency is maintained through to adulthood. The aim of this chapter was to determine which cellular process/es underlie deficiency of MGE-derived interneurons in *14-3-3ζ* KO mice and the developmental stage at which such an insult occurs. Interestingly, and perhaps not surprising, we identified multiple abnormalities in different cellular processes which may account for the interneuron deficit observed in adults. These findings further highlight that interneuron development necessitates a series of complex and overlapping cellular processes that are influenced by multiple factors.

The data presented here identify an essential role for 14-3-3ζ in the control of interneuron migration, with *14-3-3ζ* KO mice showing a reduction in the distance and velocity at which the interneurons migrate. Several studies have reported that interneurons, likely due to longer migration paths, migrate faster than other neuronal types (Komuro & Rakic, 1993; Komuro & Rakic, 1992; Miller, 1999; Wichterle et al., 2001; Polleux et al., 2002). Thus, one possibility for a change in velocity could be that interneurons arising from the MGE in *14-3-3ζ* KO mice fail to be specified correctly and hence fail to exhibit the normal characteristics of an interneuron. This hypothesis is supported by the change in morphology and increase in primary branch points of interneurons in *14-3-3ζ* KO mice. Alternatively, within the interneuron subtypes, MGE-derived interneurons are also known to travel with a greater velocity than CGE/LGE- derived interneurons and display a distinct morphology (Wichterle et al., 1999). Thus, my data raises the hypothesis that the absence of 14-3-3ζ may lead to a fate change or loss of MGE identity which may mark a switch to a CGE like fate. Moreover, particular subtypes of LGE derived interneurons (i.e. olfactory bulb interneurons migrating via the rostral migratory stream) are known to migrate via chain migration which was also a characteristic of

14-3-3ζ KO MGE-derived interneurons in this study (Figure 4.5). This strengthens the hypothesis that deficiency of 14-3-3ζ changes the identity of MGE-derived interneurons to a LGE/CGE like fate. Interestingly, Xu et al. 2010 described an interneuron cell fate switch from MGE to CGE-like interneurons in the absence of Shh signalling (Xu et al., 2010), which was also identified as a molecular pathway affected in the absence of *14-3-3ζ* in this chapter.

The defects observed in the migration dynamics and morphology of interneurons from *14-3-3ζ* KO mice, coupled with their inability to progress through the VZ of the MGE, strongly suggests defects in the correct specification of these cells. Indeed, a lack of behavioural or anatomical defects after the conditional removal of *14-3-3ζ* from post mitotic interneurons strongly suggests that the predominant role of 14-3-3ζ is to promote specification of interneurons from their neuronal precursors within the VZ. Despite the altered migration dynamics in *14-3-3ζ* KO mice it appears that 14-3-3ζ is not crucial for post mitotic migration, but rather this is a secondary effect of abnormal formation, thus underlying a stage-specific requirement for 14-3-3ζ activity which is consistent with other models displaying mitotic specific defects (Vidaki et al., 2012). Furthermore, 14-3-3ζ is having a critical function while cells are still mitotic in the VZ and ablation of *14-3-3ζ* results in cells being unable to progress to the SVZ. Notably, Xu et al. 2005 found that disruption of the Shh signalling pathway in post mitotic interneurons resulted in no change in MGE-derived interneurons, however when Shh signalling was disrupted in neural progenitor cells, cortical examination revealed a loss of MGE-derived cells (Xu et al., 2005). Taken together, investigation into the Shh signalling pathway in *14-3-3ζ* KO interneurons may be of interest due to the similar findings in other mouse models.

Precise regulation of the cell cycle is critical for neurogenesis, with disruption of cell cycle length changing the balance of different interneuron subtypes (Ross, 2011). 14-3-3 family proteins have a well-known role in regulating cell cycle (reviewed in Hermeking & Benzinger, 2006), with 14-3-3ζ having previously been shown to regulate $p27^{Kip1}$ which controls the G1-

to S-phase transition in murine pre-adipocytes (Lim et al., 2015). The GE-derived cells in this context are particularly important since disruption of the normal cell cycle changes the balance of different interneuron subtypes. Herein, I have described a critical role of 14-3-3ζ in MGE-derived interneurons prior to cell cycle exit, with the logical next step to examine cell cycle regulation in the *14-3-3ζ* KO mice. Previous studies have suggested an important role of cyclin D molecules in interneuron development acting via multiple pathways to regulate interneuron development (Glickstein et al., 2007b; Gilani et al., 2014). Cyclin D1 and D2 are both known to be involved in cell cycle regulation and are key influences in the progression of progenitors through G1 phase and their dysregulation leads to prolonged time within this phase (Lange et al., 2009; Pilaz et al., 2009; Glickstein et al., 2007a; Glickstein et al., 2007b; Glickstein et al., 2009). Furthermore, cyclin D molecules are known to form a complex with CDK4/6 to phosphorylate the cell cycle inhibitor retinoblastoma protein rendering it inactive. However, there are also cell type specific roles for these cyclins with cyclin D1 being associated with functions in the VZ and cyclin D2 being associated with cells in the SVZ, suggesting cyclin D1 to be important in early progenitor populations (Glickstein, 2007). Hence, the loss of *cyclin D1* observed in this thesis, is fitting with the data thus far and strongly suggests that G1 phase may be compromised in *14-3-3ζ* KO mice. Shh signalling also preferentially targets cyclin D1 and further implicates this pathway as a target of 14-3-3ζ regulation. Though our findings fit with a potential change in the regulation of G1, we were unable to definitively identify a cycling defect in this study. The data suggests a decreased number of cells exiting the cell cycle in the *14-3-3ζ* KO mice, though quantitative analysis would be necessary to for this to be conclusive. Taken together, the G1 phase may indeed be stalled leading to cells being unable progress through the cell cycle and hence delay their exit. This is contrary to what is known about cell cycling dynamics, that when a cell is unable to progress through its check point it should either exit the cell cycle early or become quiescent. Interestingly, the reduced cell cycle exit that is seen in the *14-3-3ζ* KO progenitor cells, is also seen in other mouse models, such as $Nkx2.1^{Tg(Cre);}Rac1^{fl/fl}$,

where cyclin D is reduced in the MGE. The delay in cell cycle exit may also explain the inability of MGE progenitor cells to progress through the layers of the MGE and result in the increased number of cells in the VZ of *14-3-3ζ* KO mice. There are several possibilities as to why cells are 'stuck' in the VZ due to extended cell cycling; 1) They may not exit at all and hence not be able to progress to the SVZ, 2) by exiting the cell cycle late, cells may fail to receive crucial cues from the SVZ directing them to the cortex and 3) cells may exit the cell cycle and progress but are not correctly specified.

Despite their critical importance to cortical function and neurodevelopmental disorders relatively little is known about the molecular mechanisms regulating cortical interneuron formation. The data presented here overwhelmingly suggests a potential role for 14-3-3ζ in modulating Shh signalling. Our microarray analysis identified several Shh pathway molecules which are changed at the mRNA level in the MGE of *14-3-3ζ* KO mice. In this chapter, we also briefly considered 14-3-3ζ playing a role in the Wnt signalling pathway. Though complicated by the presence of multifactorial molecules, such as cyclin D1 and β-catenin, and the reciprocal nature of Shh and Wnt signalling, there was no direct evidence to implicate 14-3-3ζ in regulating Wnt signalling pathway in this system. Future investigation should examine the exact relationship between Wnt signalling and 14-3-3ζ. Furthermore, the Shh pathway is a logical suspect, given that it is the only known up stream regulator of *Nkx2.1* and the gravity of evidence linking 14-3-3ζ to augmenting its role in interneuron development.

Due to the complex and dependent relationship of interneuron formation, interneuron defects can either arise from a cell autonomous or non-cell autonomous deficiency. Several findings in this chapter have suggested that defects in interneuron progression are cell autonomous. For example, MGE explants, which consist predominantly of interneuron progenitor cells, showed defects in migration and specification, while there were no change in extracellular migration factors observed. Furthermore, changes in transcription factors such as, *Nkx2.1, Lhx6, Dlx2* and *Sox6,* and transcription profiles of the MGE further suggested that the

defects were arising from the MGE and hence suggesting 14-3-3ζ plays a cell autonomous role in interneuron deficiencies. Moreover, analysis of the *Olig2-Cre;14-3-3ζ*$^{fl/fl}$ mice, in which *14-3-3ζ* has been removed in MGE progenitors, not only identified the necessity of *14-3-3ζ* in mitotic MGE cells but identified that removal of *14-3-3ζ* in interneurons alone recapitulates the defect seen in the constitutive *14-3-3ζ* KO mice and hence I concluded from these observations a cell autonomous defect in *14-3-3ζ* deficient interneurons.

Though many of our findings have focused on the cell autonomous roles of 14-3-3ζ in interneurons, the intercellular dynamics and organization of cells within the MGE are also critical for interneuron formation. Cells within the MGE maintain close connections via adherens junctions which are regulated via β-catenin and N-cadherin. Our data identifies an essential role for 14-3-3ζ in promoting the formation of cellular junctions and organization in the MGE, suggesting that a loss of adherens junctions leads to disorganization of the MGE in *14-3-3ζ* KO mice. This is consistent with previous findings which identified a multifactorial role of junctions between neural progenitors, with crucial roles not only in the architecture but also contributing to differentiation and formation (Reviewed in Miyamoto et al., 2015). Taken together, impaired organization of the MGE may also be involved in the impaired progression of interneurons through the layers of the MGE.

This chapter suggests that MGE-derived neuronal precursors in *14-3-3ζ* KO mice are not able to transition correctly into bona fide interneurons but rather incur a fate switch to CGE like interneurons. Though several processes have been implicated, we are yet to identify what role 14-3-3ζ has in controlling interneuron development. Evidence suggests that Shh signalling pathway is perturbed in MGE interneurons lacking 14-3-3ζ and this will be explored further in the following chapter. Understanding the molecular mechanism(s) by which 14-3-3ζ controls interneuron development is critical in gaining a global perspective of the fate of interneurons in the absence of *14-3-3ζ*. In the subsequent chapter I investigate the molecular mechanism(s) of 14-3-3ζ in interneuron development.

Chapter 5: A novel role for 14-3-3ζ in augmenting non-canonical Shh signalling within the ventral telencephalon.

5.1 Background

As shown in Chapter 4, *Nkx2.1* expression is significantly decreased in the absence of *14-3-3ζ* and several cellular processes, including migration, specification and formation, were found to be dysfunctional. Understanding the molecular mechanism by which 14-3-3ζ controls these processes is crucial in our overall understanding of interneuron development. The Shh signalling pathway is essential for the initial patterning and maintenance of *Nkx2.1* expression in the MGE (Figure 5.1). Notably, my microarray analysis (Chapter 4.2.7) implicates a role for 14-3-3ζ in regulating the Shh signalling pathway.

Shh is initially secreted from the floor plate at embryonic day E8.5–E9.0. It functions to promote patterning and outgrowth of the MGE through regulating expression of *Nkx2.1* and by inducing its own expression in the proliferative zone and mantle zone via a positive feedback loop (Sussel et al., 1999; Xu et al., 2005; Xu et al., 2010; Flandin et al., 2011). Following the initial patterning of the MGE, Shh expression within the proliferative and mantle zones is required to maintain *Nkx2.1* expression and the identity of neural progenitors in the ventricular zone. The earliest role of Shh in patterning the MGE is mediated via a Gli dependent mechanism in which Shh binds to the inhibitory cell surface receptor Patched (Ptch1) to release Smoothened (Smo) from a state of inhibition. Disinhibition of Smo promotes activation of Gli3 which controls transcription of Shh target genes such as *Gli1* and *Ptch1*. In contrast, the role of Shh in maintaining *Nkx2.1* expression and progenitor identity at later developmental stages occurs through a non-canonical and Gli-independent mechanism that is currently ill-defined. While

the role for Shh in maintaining progenitor identity and promoting neurogenesis is supported by conditional mouse models (i.e. *Nestin-Cre; Shh$^{fl/fl}$*), removal of Smo in post mitotic neurons (i.e. *Dlx5/6-Cre; Smo$^{fl/fl}$*) suggests that Shh signalling is not required for cell motility as interneurons migrate to the cortical plate (Xu et al., 2005).

In addition to Shh signalling, key regulators of cytoskeletal dynamics are also important for neurogenesis in the MGE. The small GTPases Rac1, RhoA and Cdc42 are required by neural progenitors in the ventricular zone to develop migratory competence during progenitor differentiation. Deficiency of Rho family genes in neural progenitors (i.e. *Olig2-Cre; RhoA$^{fl/fl}$* or *Nkx2.1-Cre; Rac1$^{fl/fl}$*) leads to aberrant interneuron migration and a lack of interneurons in the cortex (Vidaki et al., 2012; Katayama et al., 2013). However, in a similar manner to the Shh and 14-3-3ζ signalling pathways, the Rho family of genes are not required for cell motility in post-mitotic interneurons as they migrate to the cortical plate as *Lhx6-Cre; Rac1$^{fl/fl}$* mice have no interneuron deficiencies (Vidaki et al., 2012).

The striking similarities between the phenotypes of *14-3-3ζ*, *Shh* and *Rac / Rho / Cdc42* KO mice suggest interactions between these molecular pathways may occur during interneuron development. Indeed, ablation of *Rac1* in progenitor populations leads to perturbed G1 phase cell cycle progression (Vidaki et al., 2012). Furthermore, Rac1 has been shown to regulate non-cononical Shh signalling in other cell types and Rac1 activity is regulated by 14-3-3ζ in several cell types including neuronal cells (Choi et al., 2010; Polizio et al., 2011a; Polizio et al., 2011b; Goc et al., 2012; Brennan et al.,2012).

In this chapter I explore the role of 14-3-3ζ in regulating Shh signalling to control interneuron development and provide novel insight to define how Shh signals via a non-canonical pathway to regulate *Nkx2.1* expression in the MGE.

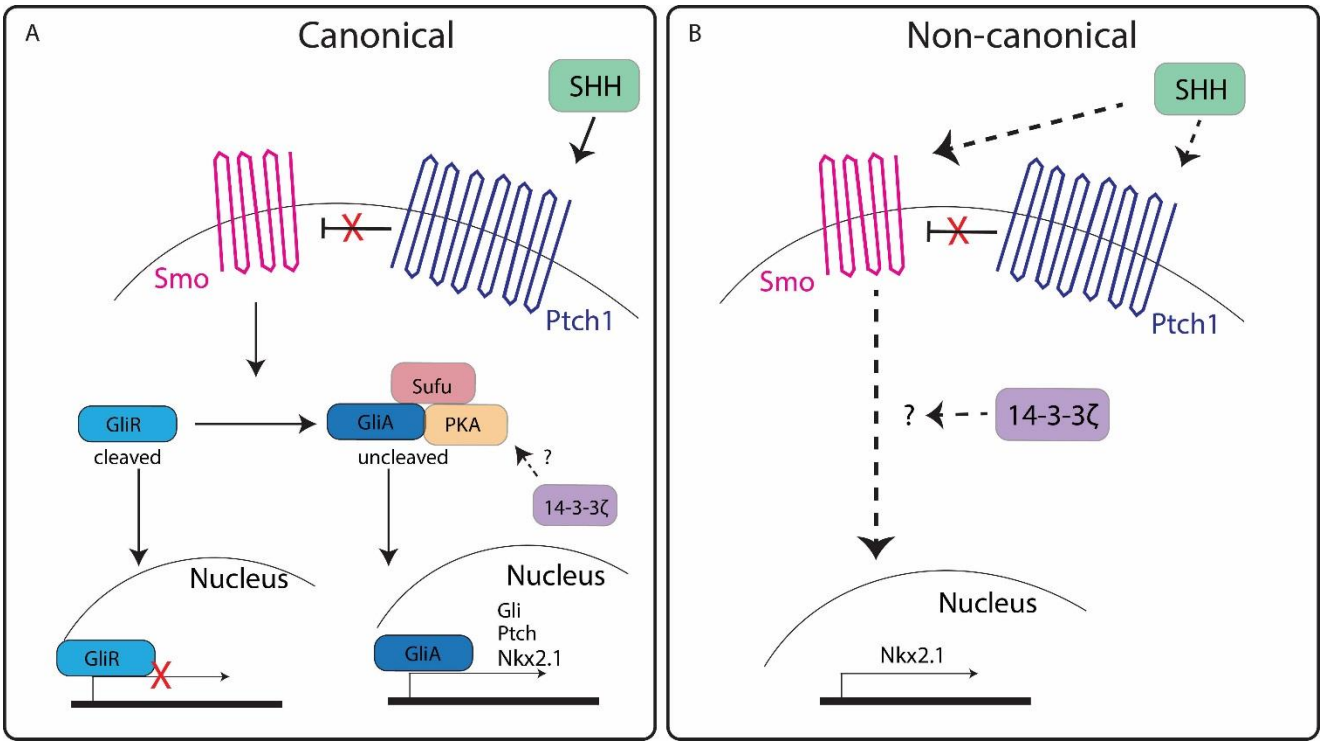


Figure 5.1: Canonical and non-canonical Shh signalling pathways.

Schematic summary of both the canonical and non-canonical Shh signalling pathways in the MGE and the potential role of 14-3-3ζ in each pathway. (A) In the canonical Shh signalling pathway, when Shh is present it binds Ptch1 which disinhibits smoothened to promote Gli. When Gli is activated (GliA) it relocates to the nucleus where it initiates transcription. Alternatively, when Shh is absent Gli is cleaved to its repressor form, GliR, and is unable to initiate gene transcription. (B) The non-canonical Shh signalling pathway in the MGE is largely uncharacterized. Shh can act via Ptch1 to disinhibit Smo or by Smo directly. GliA, Gli activator; GliR, Gli repressor.

5.2 Results

5.2.1 Non-canonical Shh signalling is disrupted in *14-3-3ζ* KO mice.

The findings presented in Chapter 4 suggest that the Shh signalling pathway is dysregulated in *14-3-3ζ* KO mice at E12.5 leading to the aberrant formation of interneurons. To further explore both the canonical pathway, which controls the initial patterning of the MGE, and the non-canonical pathway which maintains *Nkx2.1* expression in the MGE, I completed *in situ* hybridisation analysis with a *Shh* riboprobe on E9.5 and E12.5 embryos (Figure 5.2). This analysis indicated that *Shh* was expressed normally within the telencephalon at E9.5. However, at E12.5 *Shh* expression was dramatically decreased throughout the MGE of *14-3-3ζ* KO mice. Real time PCR analysis with MGE samples dissected from E12.5 embryos confirmed a significant reduction of *Shh* at this time point (Figure 5.2C). Furthermore, the Shh responsive transcription factors; *Gli1*, *Gli2* and *Gli3* were expressed normally. However, in contrast to a reduction in Shh, another Shh target gene, *Ptch1*, was found to be significantly increased (Figure 5.2C) fitting with the notion that canonical Shh signalling is unaffected in *14-3-3ζ* KO mice. Though there were no changes in the overall expression of Gli, to further explore the canonical Shh signalling pathway I also quantitated the levels of Gli3 repressor (Gli3R) to Gli3 activator (Gli3A). In the presence of Shh, full length Gli3 (Gli3A) activates transcription, whereas in the absence of Shh, Gli3 is cleaved (Gli3R) to repress transcription. Western blot analysis of E12.5 whole forebrain samples was unable to identify any change in the total amounts of Gli3A to Gli3R in *14-3-3ζ* KO embryonic brain compared to WT and more importantly there was no change in the ratio between Gli3A and Gli3R (Figure 5.3). Taken together these analyses strongly suggest that the non-canonical Shh signalling pathway, but not the canonical signalling pathway, is affected in *14-3-3ζ* KO mice.

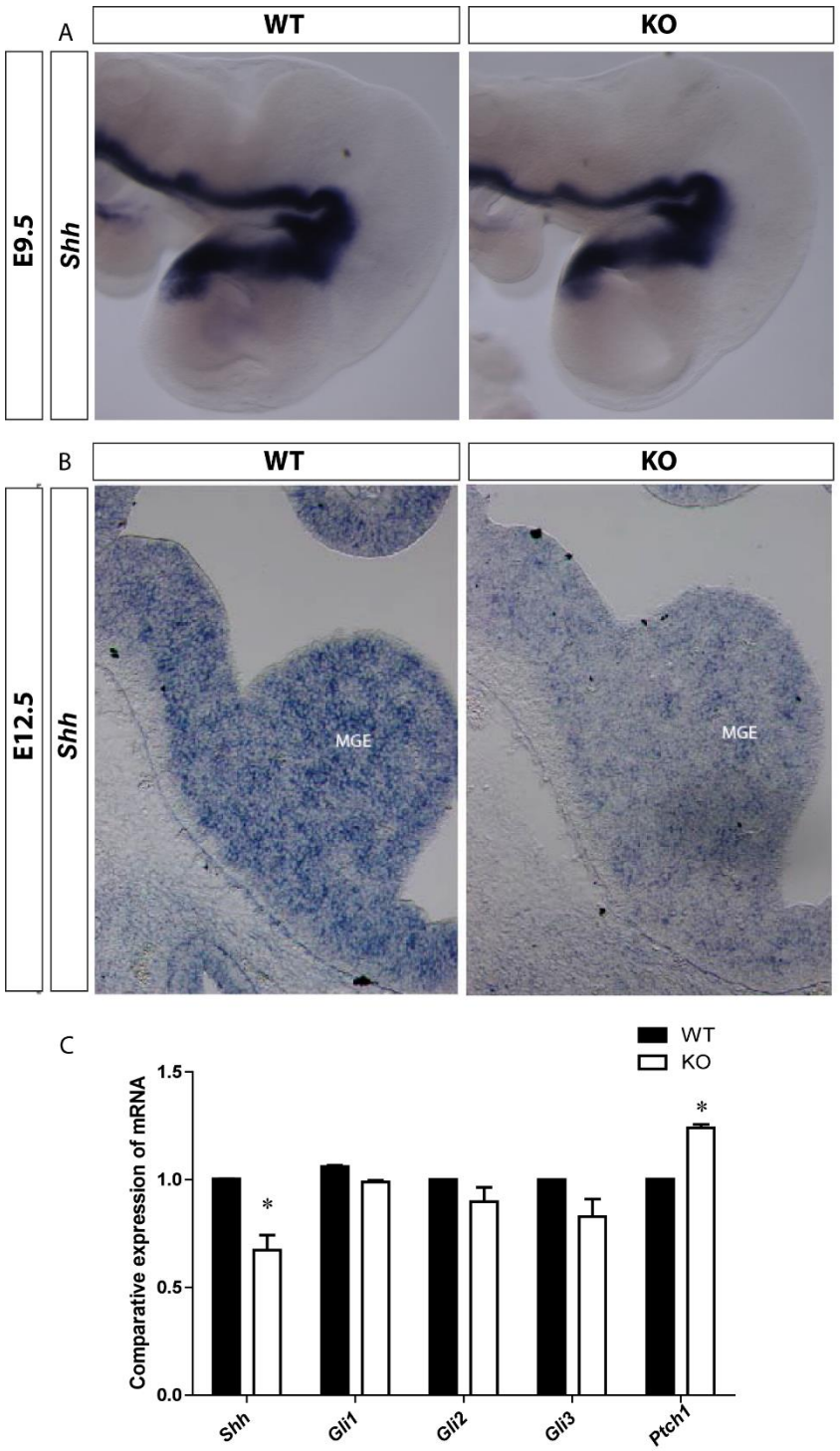


Figure 5.2: Ablation of *14-3-3ζ* leads to aberrant non-canonical Shh signalling.

(A) Representative whole mount *in situ* hybridization of E9.5 WT and *14-3-3ζ* KO embryos using *Shh* riboprobe (n=4). (B) Representative *in situ* hybridization on coronal brain sections of E12.5 WT and *14-3-3ζ* KO mice using *Shh* riboprobe (n=4). (C) Real time PCR analysis of canonical Shh signalling using RNA from E12.5 MGE WT and *14-3-3ζ* KO embryos (n=3). Error bars represent ±SEM. Statistical significance was determined via t-test. (*$p<0.05$)

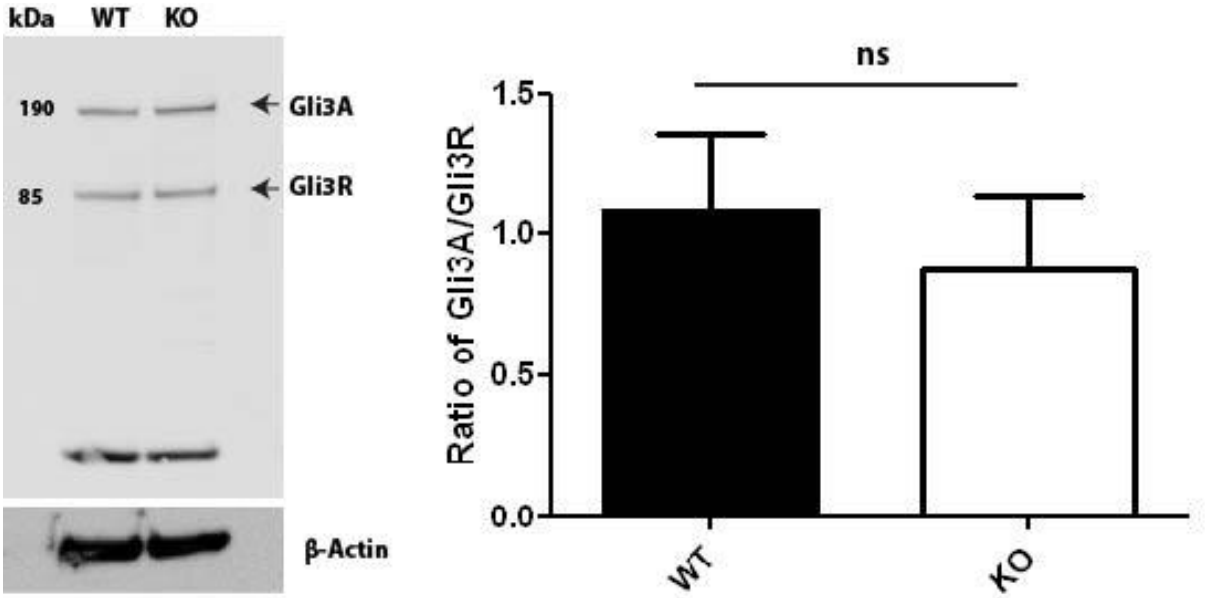


Figure 5.3: Gli3 processing is unaffected in *14-3-3ζ* KO mice.

Western blot analysis of protein extracts from E13.5 WT and *14-3-3ζ* KO brain lysates using N-terminal Gli3 antibody. (A) Approximately 20μg of protein extracted from brain lysates was used in each lane; protein bands were immunoblotted and probed for anti Gli3 antibodies which identify a 190 kDa band and 85 kDa band, corresponding to full-length (Gli3A) and processed repressor form (Gli3R), respectively. (C) Relative intensity of each band in arbitrary units following quantification and normalization to the intensity of the activator band. Error bars represent ±SEM. Statistical significance was determined via student t-test. (n=4) (ns = no significance).

5.2.2 Addition of exogenous Shh normalizes interneuron formation defects in *14-3-3ζ* KO mice *in vitro*.

Evidence suggests that *14-3-3ζ* KO mice display aberrant Shh signalling after the initial patterning of the GE and hence acting via a Gli-independent non-canonical pathway. In order to establish the functional significance of reduced Shh signalling, exogenous Shh was added to the MGE explant assay described in Chapter 4. Briefly, MGE explants from E13.5 embryos were dissected and grown in matrigel with or without Shh added to the growth media. Explants were imaged over a 48hr time period and migration distance calculated based on the distance migrated comparative to the size of the explant. There was a significant reduction in the distance in which the *14-3-3ζ* KO interneurons travelled from the explant compared to the WT interneurons, consistent with previous findings (Figure 5.4). Interestingly, the addition of Shh to explants normalized migration of the *14-3-3ζ* KO interneurons (WT, 10.5; KO, 2.9; KO+SHH, 8.4; n=3; p(WT vs KO)=0.027; p(WT vs KO+SHH)=0.31; p(KO vs KO+SHH)=0.008). Real time PCR performed on the RNA from MGE explants found the addition of exogenous Shh also normalized the expression of *Nkx2.1* (Figure 5.4C).

To further explore the role of 14-3-3ζ in the Shh signalling pathway it would have been beneficial to use a cell line in order to manipulate the pathway. However, as there were no cell lines available to me, I sought to use an alternative model. I established an *in vitro* model in which cells dissociated from E13.5 WT MGE, which are predominately interneuron progenitor cells, were grown for 48hr in the absence or presence of 14-3-3 inhibitors and exogenous Shh. This approach allowed for me to better interrogate the Shh signalling pathway, as it was impossible to acquire enough material from the 14-3-3ζ KO mice, hence pooling together several E13.5 WT MGE's and dissociating the cells was more appropriate way to perform the analyses. Initially in order to establish if this model was relevant to my investigation, 14-3-3 function was inhibited to see if we could recapitulate results seen *in vivo*. For these assays, all 14-3-3 isoforms were inhibited using a small molecule inhibitor (RB-012) that destabilizes

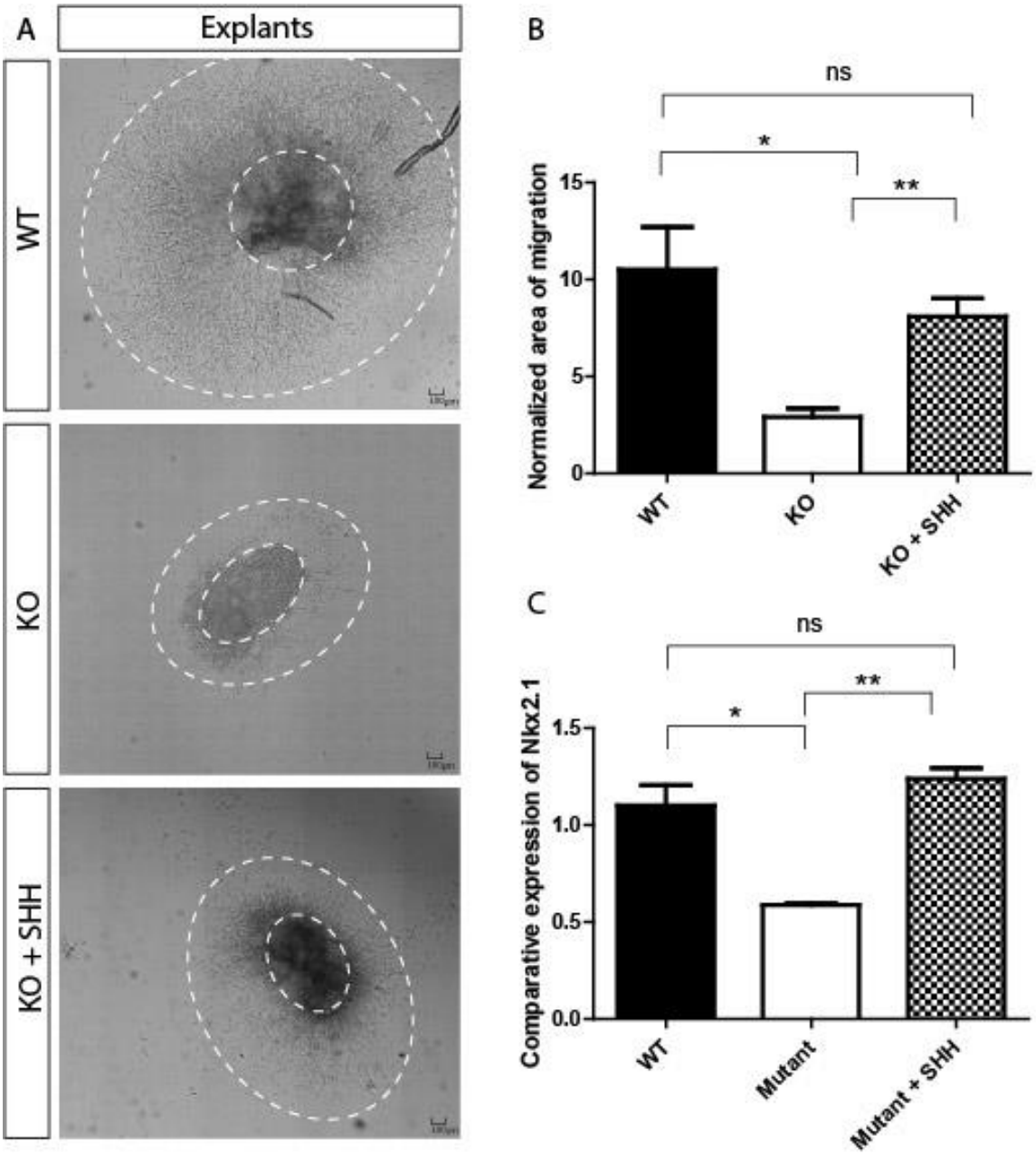


Figure 5.4: Exogenous Shh rescues *Nkx2.1* expression in the GE of *14-3-3ζ* KO mice *ex vivo*.

MGE explants from E13.5 WT and *14-3-3ζ* KO mice were cultured in matrigel for 48 hours and imaged on CV1000 spinning disc microscope. (A) Representative images of 48 hr time point of WT and *14-3-3ζ* KO mice with and without Shh treatment. (B) Quantification of area travelled by interneurons normalized to explant size from WT, *14-3-3ζ* KO and *14-3-3ζ* KO +Shh. (C) Real time PCR analysis of transcription factor *Nkx2.1* from explant samples after 48 hr in matrigel (n=3). Error bars represent ±SEM. Statistical significance was determined via t-test. (*$p<0.05$, $p<0.01$**). Scale bars 100μm.

the 14-3-3 dimer. Since RB-012 is readily taken up by cells and is highly efficient (Woodcock et al., 2015), it was preferential to more traditional methods, such as siRNAs as these methods have poorer efficacy on primary cells. I initially tested a range of concentrations with 1μM RB-012 being identified as the optimal dose for inhibition in primary MGE derived cells. Real time PCR analysis showed that inhibition of 14-3-3 resulted in decreased expression of *Nkx2.1* which was normalized by the addition of 2μM of Shh, consistent with *ex vivo* findings (Figure 5.5). Taken together, this data indicates: 1) loss of Shh is functionally significant in the interneuron phenotype of *14-3-3ζ* KO mice, 2) loss of 14-3-3ζ leads to a cell autonomous impairment of Shh signalling, and 3) 14-3-3ζ modulates non-canonical Shh signalling to control *Nkx2.1* expression in the MGE.

5.2.3 Small GTPase Rac1 regulates *Nkx2.1* to control interneuron development.

Although it is well established that Shh acts via a non-canonical Gli-independent pathway to maintain expression of *Nkx2.1* in the MGE the molecular mechanisms controlling this process remains ill-defined. The strikingly similar phenotypes of Shh and Rac1 KO mice, and the finding that Shh signals via Rac1 in other contexts, presents Rac1 as a strong candidate to mediate Shh signalling in the MGE. To establish the necessity of Rac1 in promoting *Nkx2.1* expression, MGE cells were dissociated and grown in the absence or presence of the Rac1 inhibitor (NSC23766) for 48 hr. Real time PCR analysis was performed and the expression level of *Nkx2.1* in each sample was examined (Figure 5.6). Analysis showed that when Rac1 is inhibited, *Nkx2.1* expression was significantly decreased ($p=0.0099$) suggesting that Rac1 may regulate Shh signalling to control *Nkx2.1* expression and hence play a crucial role in interneuron development and MGE identity.

5.2.4 Shh acts upstream of Rac1 signalling.

In order to determine if Shh acts via Rac1 to control *Nkx2.1* expression and thereby promote interneuron formation, dissociated MGE cells were grown in the presence or absence of

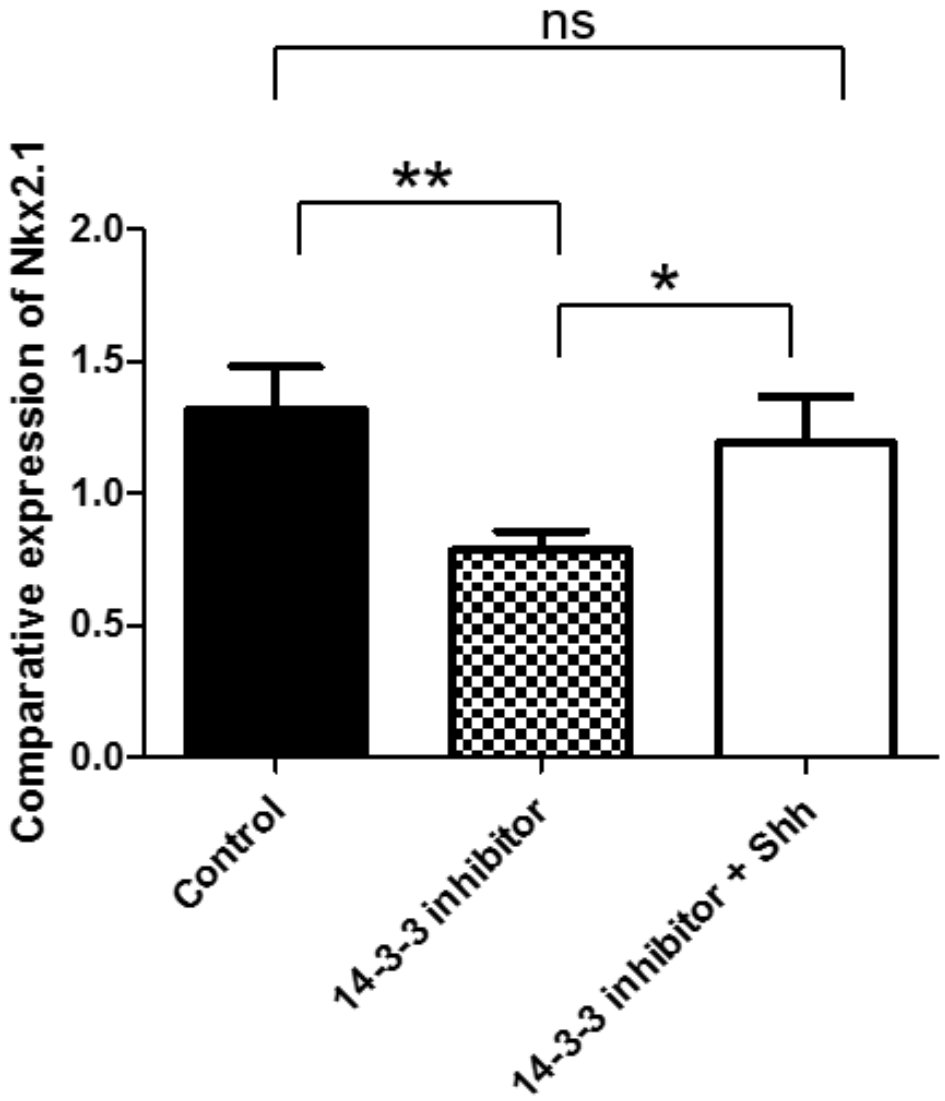


Figure 5.5: Exogenous Shh rescues *Nkx2.1* expression in MGE cells *in vitro*.

Dissociated cells from the MGE of E13.5 embryos cultured for 48 hr. Real time PCR analysis of transcription factor *Nkx2.1* from dissociated cells after 48 hr with and without 14-3-3 inhibitor and exogenous Shh (n=5). Error bars represent ±SEM. Statistical significance was determined via t-test. (*$p<0.05$, $p<0.01$**).

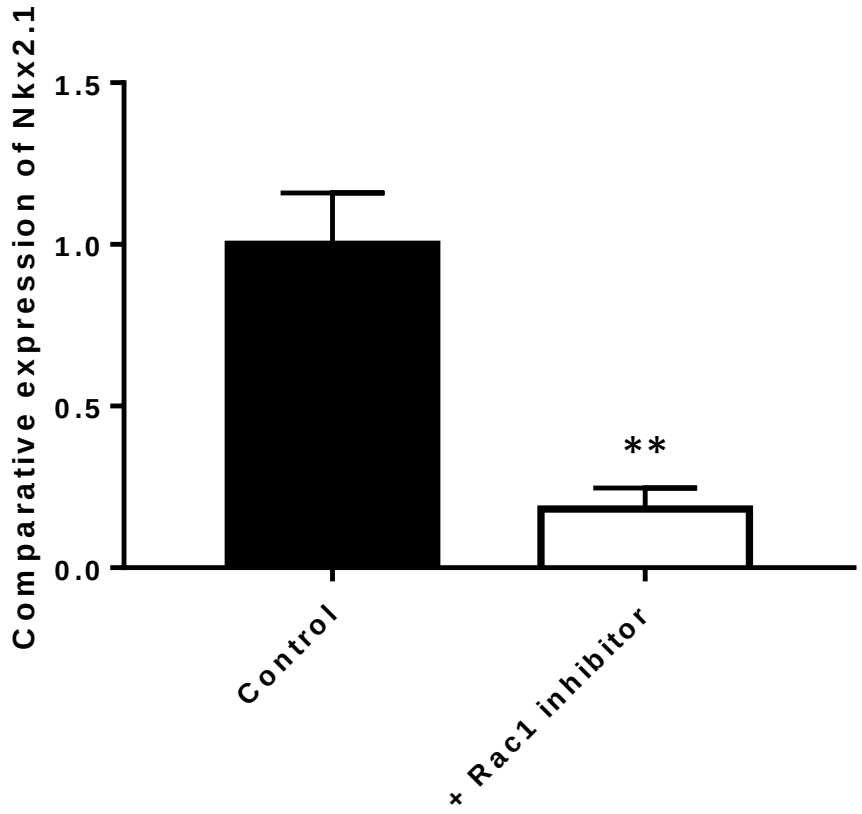


Figure 5.6: Inhibition of Rac1 activity reduces the expression of *Nkx2.1* in GE derived cells.

Dissociated cells from the MGE of E13.5 embryos cultured for 48 hr. Real time PCR analysis of transcription factor *Nkx2.1* from dissociated cells after 48 hr with and without the Rac1 inhibitor (NSC23766) (n=3). Error bars represent ±SEM. Statistical significance was determined via t-test. ($p<0.01$**).

exogenous Shh. To assay the activity of Rac1, samples collected at 0, 15 min, 30 min, 1 hr and 12 hr after addition of Shh were immunoblotted for phospho P21 activated kinase (pPak1) which is directly activated by Rac1 as well as being activated by other pathways (Figure 5.7). Western blot analysis revealed a time-dependent increase in pPak1 in response to Shh stimulation with maximal activity reached at 1 hr. This indicates that Shh acts as a positive regulator of pPak1 and potentially Rac1. Though pPak1 is a target of Rac1 signalling, in the future it would be of interest to assay directly for active Rac1 activity to ensure the changes we observe in pPak1 are as a direct result of Rac1 signalling.

5.2.5 Non-canonical Shh signalling pathway is augmented by 14-3-3ζ and Rac1 to control interneuron development.

The question remains to whether 14-3-3ζ has any role in regulating Rac1 to control non-canonical Shh signalling pathway. Earlier in this chapter I showed that in the absence of *14-3-3ζ*, *Shh* expression is decreased. In order to ascertain whether the ablation of *14-3-3ζ* leads to a change in Rac1 signalling, pPak1 was used as a read out of the Rac1 activity. Western blot analysis performed on WT and *14-3-3ζ* KO E12.5 MGE revealed a significant decrease in the expression of pPak1 with no change in total Pak1 levels (Figure 5.8). This is fitting with the well-established role of Rac1 in facilitating auto-phosphorylation of Pak1. Taken together, these results support the hypothesis that Shh signals via Ptch1 to disinhibit smoothened which acts on Rac1 to drive phosphorylation of Pak1 and expression of *Nkx2.1* (Figure 5.9). Moreover, my results also suggest that 14-3-3ζ modulates this pathway to control *Nkx2.1* expression and interneuron development.

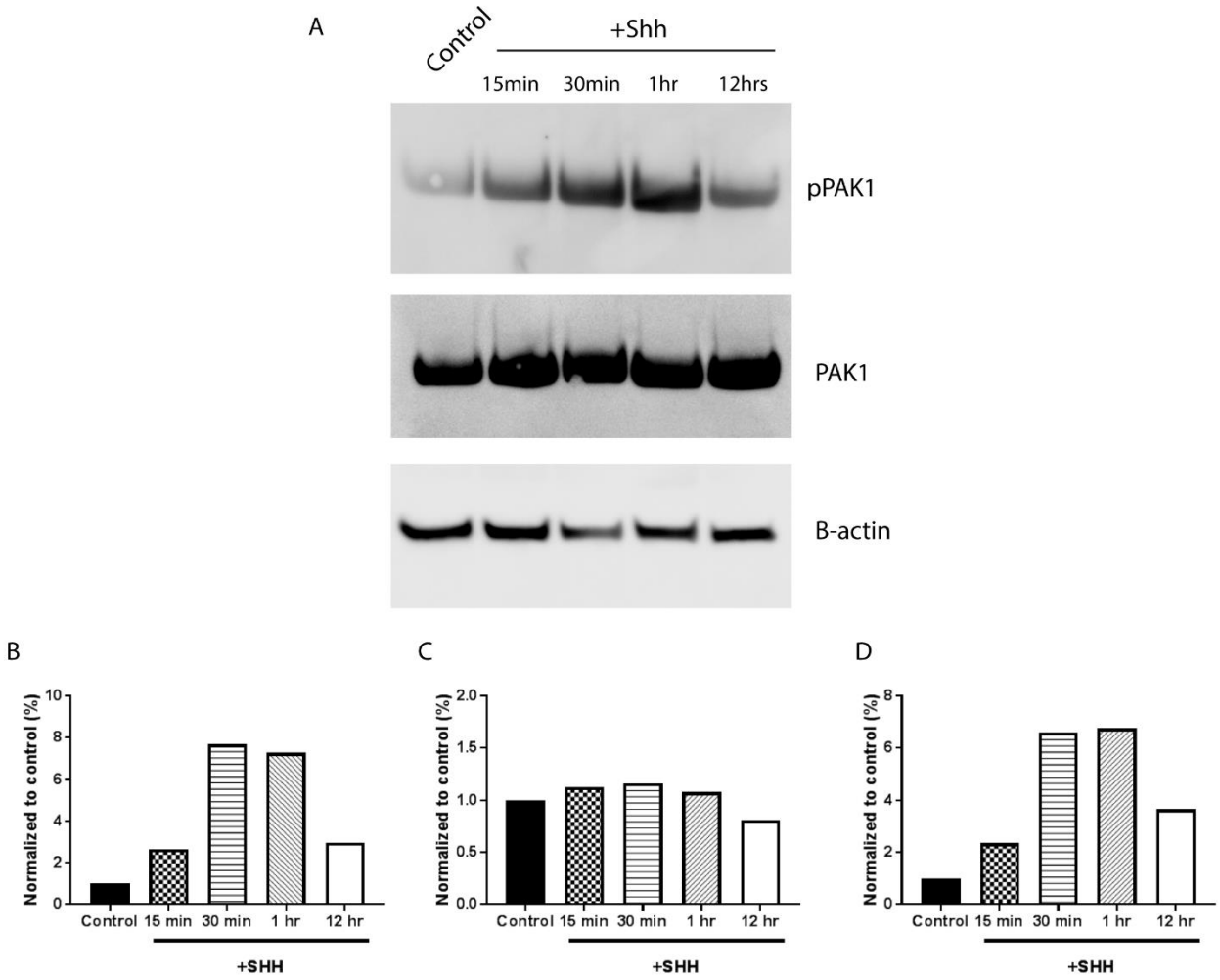


Figure 5.7: Exogenous Shh leads to increased activation of Pak1.

Dissociated cells from the MGE of E12.5 embryos cultured for 48hr. Exogenous Shh was added 15 min, 30 min, 1hr and 12 hr before collection. (A) Western blot analysis was performed on samples and pPak1 was used as a readout of Rac1 activation. (B) Densitometry of pPak1 western blot normalized to β-actin. (C) Densitometry of total Pak1 western blot normalized to β-actin. (D) Densitometry of pPak1 normalized to total Pak1 levels.

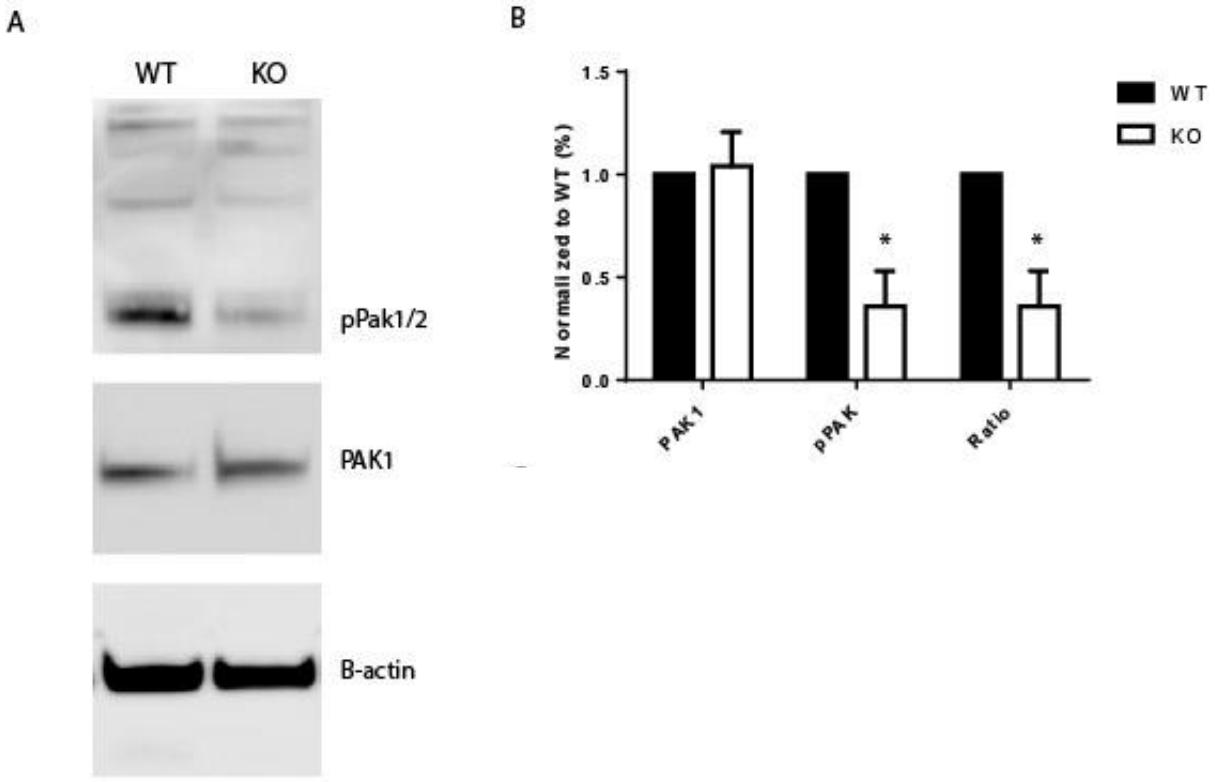


Figure 5.8: Ablation of *14-3-3ζ* leads to reduced Rac1 signalling *in vivo*.

Western blot analysis of protein extracts from the MGE of E12.5 WT and *14-3-3ζ* KO embryos using Pak1 and pPak1 antibodies. (A) Approximately 30μg of protein extracted from MGE lysates was used in each lane and immunoblotted with Pak1, pPak1 and β-actin (load control). (B) The graph shows the relative intensity of each band as a percentage of WT following quantification with β-actin. Error bars represent ±SEM. Statistical significance was determined via student t-test (n=4). (*$p<0.05$).

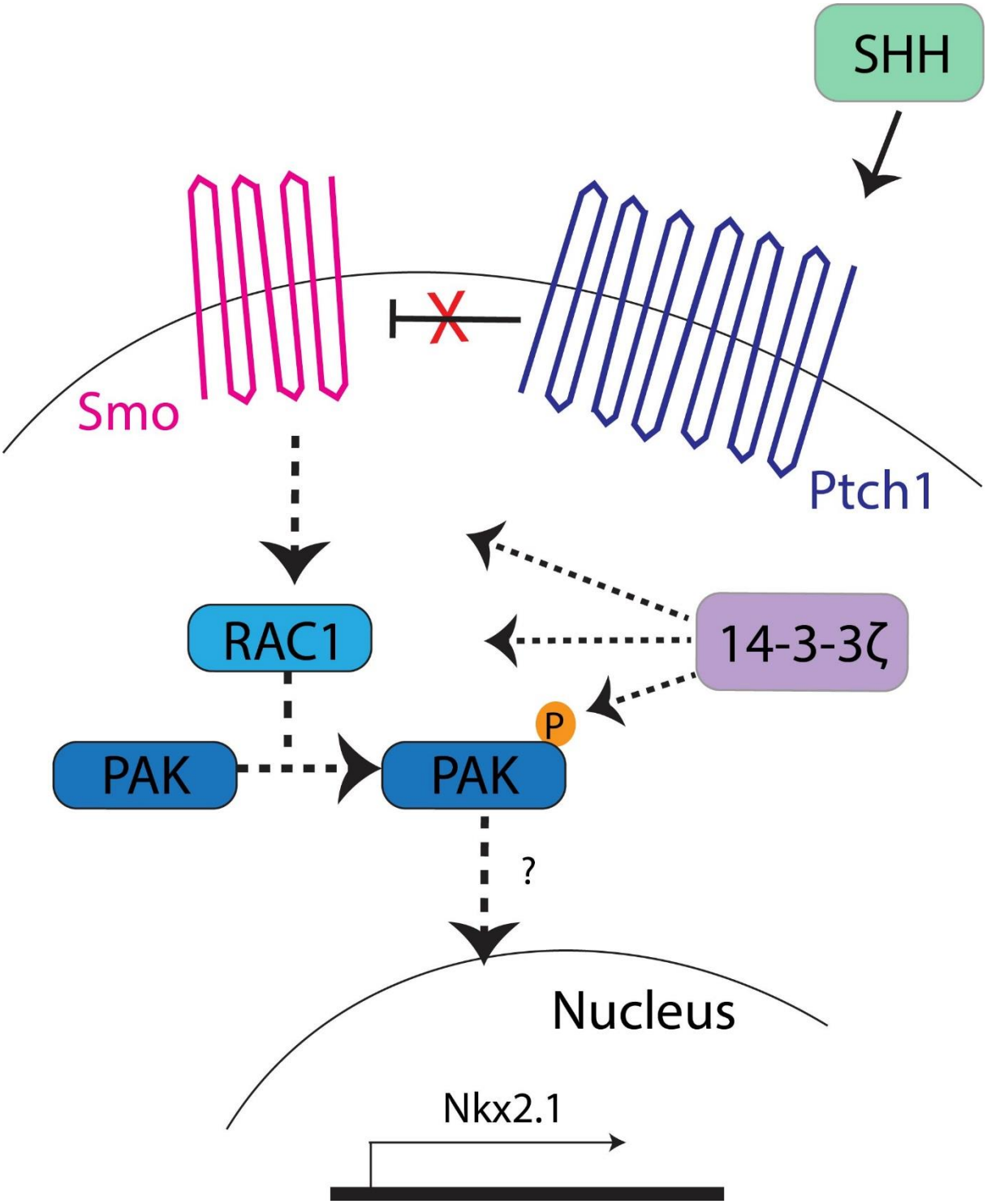


Figure 5.9: Working model of how 14-3-3ζ augments the Shh signalling pathway.

Schematic model of non-canonical Shh signalling pathway. Shh activates Ptch1 which causes it to release Smo from a state of inhibition. Smo activates Rac1, which facilitates the auto-phosphorylation of Pak1 to control expression of *Nkx2.1*. We propose that 14-3-3ζ regulates this pathway through interactions with pPak1, Rac1 or downstream of Smo.

5.3 Discussion

The aim of this chapter was to identify the molecular mechanism(s) by which 14-3-3ζ controls interneuron development and further explore how the Shh signalling pathway acts to control *Nkx2.1* expression. Interestingly, my results identified a novel role for 14-3-3ζ in regulating non-canonical Shh signalling. Canonical Shh signalling has well established roles in interneuron development and regulation of *Nkx2.1*, with ablation of Shh signalling leading to a complete loss of the GEs (Xu et al., 2005; Xu et al., 2010). However, although the canonical functions of Shh signalling in the initial patterning of the GEs has long been known, it was more recently established that an alternative role of Shh is required for the proliferation and maintenance of multipotent progenitor populations at later stages of development (Britto et al., 2002; Machold et al., 2003; Gulasci et al., 2006).

Gulacsi and colleagues, first identified that removal of Gli3 after the initial patterning of the MGE did not result in the loss of interneurons and suggested that Shh acts via an undefined non-canonical Gli-independent pathway (Gulacsi et al., 2006). The defects in *14-3-3ζ* KO mice identified in previous chapters can be explained by the loss of Shh signalling after the initial patterning of the MGE. Thus, loss of *14-3-3ζ* leads to dysregulation of non-canonical Shh signalling pathway which compounds in reduced expression of *Nkx2.1* and *cyclin D1*. The reduction in *Nkx2.1* underlies abberant specification of MGE-derived interneurons which display abnormal morphological and migratory characteristics and loss of *cyclin D1* underlies aberrant G1 to S-phase progression and late cell cycle exit. The delay in cell cycle exit likely affects transition through the different layers of the MGE and underlies defects in migration and hence a loss of MGE-derived interneurons in adulthood.

The finding that non-canonical Shh signalling is affected in *14-3-3ζ* KO mice is fitting with what was observed in previous chapters and the observations in schizophrenia patients. Ablation of *14-3-3ζ* does not result in a complete loss of MGE-derived interneurons and mice

do not display obvious seizures, which is commonly associated with severe loss of this cell type. In contrast, the phenotype is consistent with that seen in schizophrenia patients, in that there is a moderate loss of PV+ interneurons which is thought to lead to behavioural and cognitive symptoms. When Shh signalling is lost during the initial patterning of the MGE, the phenotype is severe and embryonically lethal, hence, it would not be expected that the severe decrease in Shh expression would be via the early canonical signalling pathway without generating a much severer phenotype. The loss of Shh signalling after the initial patterning of the GE, when Shh signalling is maintaining *Nkx2.1* expression, would likely result in a decreased number of interneurons as identified in *14-3-3ζ* KO mice.

Non-canonical Shh signalling has been identified in several other cellular contexts and has been found to progress through two independent mechanisms: 1) by direct activation of Ptch1 which itself promotes downstream signalling cascade, or 2) through the de-repression of Smo via Ptch1 activation but independent of Gli (Brennan et al., 2012). When I examined the Shh signalling pathway in *14-3-3ζ* KO mice, *Shh* was down regulated with no change to Gli transcripts, however, *Ptch1* was found to be increased. Increased expression of *Ptch1* fits well with the notion that 14-3-3ζ regulates a non-canonical Shh pathway given its role inhibiting Smo activity. This also supports the hypothesis that Shh acts via Ptch1 to disinhibit Smo in the non-canonical Shh signalling pathway in the MGE, given that an increase in Ptch1 acting independently to Smo would result in increased Shh activity. To test the hypothesis that non-canonical Shh signalling pathway is Smo dependent, it would now be worthy of intercrossing *14-3-3ζ* KO mice to *Ptch1* heterozygous mice. Heterozygosity of *Ptch1* in *14-3-3ζ* KO mice would be expected to either exacerbate or rescue the MGE and interneuron defects depending on which mechanism is required for maintenance of MGE identify. For example, should Shh act via Smo then we would expect *Ptch1* heterozygous mice to increase activation of the non-canonical Shh pathway and ameliorate the *14-3-3ζ* KO phenotype. Conversely, should Shh act directly through Ptch1 then we would expect Ptch1 heterozygous mice to decrease activation

of the non-canonical Shh pathway and exacerbate the *14-3-3ζ* KO phenotype. Alternatively, Smo specific agonists (SAG) could be used to see if treatment with SAG increases non-canonical Shh activity. Interestingly, the NSC23766 Rac1 inhibitor used in this analysis acts on guanine exchange factors (GEFs) which have been shown to act downstream of Smo (Gao et al., 2004), adding further evidence to the involvement of Smo in non-canonical Shh signalling in the MGE.

The molecular pathway by which Shh signals independently of Gli to maintain *Nkx2.1* expression is unknown. In other contexts, Rac1 has been found to have a role in Shh signalling and is also a known interactor of 14-3-3ζ. Smo has been shown to activate Rac1 to control dendritic spine formation (Brennan et al., 2012) and *14-3-3ζ/ε* KO mice show a significant decrease in Rac1 activity (Toyo-oka et al., 2014). Polizio et al. 2011 proposed that Rac1 was acting downstream of Smo to control cytoskeleton dynamics in endothelial cells in a non-canoncial gli-independent pathway (Polizio et al., 2011b). Furthermore, the ablation of Rac1 in mitotic MGE progenitors leads to a reduction in interneurons (Vidaki et al. 2012). Given, these findings it was exciting though perhaps not surprising that Rac1 signalling was disrupted in MGE of *14-3-3ζ* KO mice. Rac1 acts by facilitating the auto-phosphorylation of Pak1 (Lei et al., 2000) and hence reduction in pPak1 in the MGE of *14-3-3ζ* KO mice and reduction in *Nkx2.1* after inhibition with a Rac1 inhibitor supports the hypothesis that 14-3-3ζ modulates non-canonical Shh signalling and Rac1 in interneuron development.

Here we identify a role for 14-3-3ζ in interneuron development by augmenting non-canonical Shh signalling. However, given the promiscuity of 14-3-3ζ and the vast unknowns in the pathway, I was unable to identify the exact mechanism by which 14-3-3ζ modulated this pathway. I identified that 14-3-3ζ is regulating non-canonical Shh signalling somewhere upstream of Pak1. Based on this and other findings from this chapter there are several hypotheses which can be formed: Firstly, 14-3-3ζ is acting directly on Pak1. Pak1 is known to have a 14-3-3ζ binding site and given that 14-3-3ζ is a phospho serine-theonine binding protein

and pPak1 is the active form of Pak1, it may well be the case that 14-3-3ζ binds to pPak1 to prevent its degradation or enable its function (Somanath et al., 2009). Secondly, 14-3-3ζ could act directly on Rac1 (Toyo-oka et al., 2014). This hypothesis is currently the best supported, with 14-3-3ζ and Rac1 having been linked in several cell systems. 14-3-3ζ dimerization is known to drive Rac1 activity, with overexpression of 14-3-3ζ leading to increased Rac1 activity (Goc et al., 2012). Thirdly, 14-3-3ζ could act upstream of Rac1, on Smo or GEFs. This is the least explored hypothesis, however Smo is a G-coupled protein receptor with 14-3-3ζ having known roles in binding and regulation of G-coupled proteins. Furthermore, T-lymphoma invasion and metastasis-inducing protein-1 (Tiam-1), a Rac1 specific GEF targeted by the Rac1 inhibitor used in our analysis, is known to interact with 14-3-3 proteins in other cell types (You et al., 2013).

Notably, *Shh*, *Nkx2.1* and pPak1 are all reduced in the MGE of *14-3-3ζ* KO mice. The *14-3-3ζ* KO mouse model therefore provides a unique opportunity to investigate if Shh signals via Rac1 to control *Nkx2.1* expression. Shh provided exogenously to *14-3-3ζ* KO MGE explants increases expression of *Nkx2.1* and interneuron outgrowth to the same level as controls. These findings suggest that Rac1 mediates this increase in *Nkx2.1* expression and interneuron mobility. Moreover, our cell and explant system provide an ideal resource to explore this pathway further.

In this chapter, I showed that the addition of exogenous Shh was able to rescue the *14-3-3ζ* KO phenotype when supplemented in early development. One question that arises from the use of exogenous Shh in *in vitro* systems is, the extent to which the normalization of *Nkx2.1* is due to the activation Gli-dependent canonical mechanism in the MGE as opposed to the rescue of the non-canonical pathway. Given that Shh does act on Gli it is likely that the increase in *Nkx2.1* is at least in part due to increased canonical signalling within the cells, however that would not result in the rescue in the formation phenotype in the *14-3-3ζ* KO mice. Hence, even

if canonical Shh signalling is activated, the predominant mechanism is still activation of non-canonical Shh signalling, which rescues the *14-3-3ζ* KO phenotype.

In summary, this chapter proposes a previously undescribed pathway of non-canonical Shh signalling controlling interneuron development. There were three key findings of this chapter; 1) the ablation of *14-3-3ζ* leads to reduced Shh signalling, 2) Rac1 is involved in non-canonical Shh signalling pathway, and 3) 14-3-3ζ modulates the non-canonical Shh signalling pathway. Here, evidence has been given for the first time implicating 14-3-3ζ as a key regulator of this pathway, though its exact function remains unknown. Indeed, there is still much to discover about non-canonical Shh signalling and its function in interneuron development. At present these findings give new insight into the dynamics of interneuron development, their role in the aetiology of schizophrenia and possible targets for new treatments.

Chapter 6: Discussion

6.1 Final discussion

The remarkable diversity of interneurons accounts for the complexity of the inhibition required for correct brain function, however this complexity also makes the study of interneurons difficult and leaves many unanswered questions in the field. Interneurons differ from other locally derived cortical excitatory neurons in that they migrate large distances from their place of origin in the subpallium. To reach their target sites interneurons first undertake tangential migration into the neocortex and then switch to a radial migration phase to find their correct neocortical layer. In contrast, other neuronal cell types will undergo only a comparatively short migration along radial glial scaffolds to their target neocortical layer. This intricate migration combined with a complex specification process opens many avenues through which deficits can disrupt their development. Indeed, more and more research implicates early developmental insult with irreversible dysfunction in adulthood as the likely mode of pathogenesis of neurodevelopmental disorders.

Dysfunction in GABAergic cortical interneurons has been implicated in several developmental disorders including schizophrenia, epilepsy, autism spectrum disorder and Down syndrome (Levitt et al., 2004; Lewis, 2000; Rubenstien & Merzenich, 2003). Now widely regarded as one of the main pathologies associated with schizophrenia, interneurons were brought to the forefront of interest when post-mortem schizophrenic brains were found to have decreased levels of GABA (Perry et al., 1979). Numerous findings since then have also highlighted a subtype specific reduction in interneurons in the post-mortem schizophrenic brain (Hashimoto et al., 2003) and underpin the GABAergic/interneuron hypothesis of disease progression (Nakazawa et al.,

2012). Given the recent findings of 14-3-3ζ's role in neurodevelopmental disorders and that *14-3-3ζ* KO mice are a model for schizophrenia, we undertook an in depth look at the effect of *14-3-3ζ* ablation on interneuron development and sought to identify 14-3-3ζ's role in interneuron formation and specification. Here we discuss the role of 14-3-3ζ in interneuron development and how these findings provide new insight towards the aetiology and pathophysiology of schizophrenia.

The aim of Chapter 3 was to address whether there were any changes in the population of interneurons when *14-3-3ζ* was removed in mice. Interestingly, a subtype specific reduction in PV expressing interneurons throughout the cortex was identified. We extended this to show a loss of MGE derived cells in the *14-3-3ζ* KO mice with no significant change in the number of interneurons which are CGE derived. Given the function of fast spiking PV+ interneurons in controlling brain dynamics and their implication in disease, these findings further show links between 14-3-3ζ and schizophrenia. Moreover, these defects were found not to result from neurodegeneration but found throughout development. The differences between *14-3-3ζ* KO and WT mice in development, as well as the notion that schizophrenia is a neurodevelopmental disorder, opened the door to investigating how interneurons develop in the *14-3-3ζ* KO mice.

The Shh signalling pathway controls early regionalisation of the ventral telencephalon by modulating the expression of transcription factor *Nkx2.1*. This transcriptional profile controls cell identity and ultimately the distribution of interneuron subclasses, including PV, SST and CR in the adult cortex. When investigating the development of interneurons in Chapter 4, it was apparent that the MGE derived interneurons showed abnormalities in several processes. Though MGE derived interneurons displayed deficits in cell migration, specification and formation, their primary defect was their inability to exit the cell cycle and hence to become correctly specified. This leads to several downstream complications including the observed migration defects. The resulting loss in identity led to the overall loss of PV+ interneurons previously identified in chapter 3.

Understanding the molecular mechanism of 14-3-3ζ in regulating these processes is crucial to understanding the overall impact of 14-3-3ζ in interneuron development, as well as understanding how to manipulate this pathway as a potential tool for therapeutics. Deficiency of interneurons in *Nkx2.1-Cre; Rac1$^{fl/fl}$* and *Nestin-Cre; Shh$^{fl/fl}$* mice have been suggested to arise from aberrant exit of the cell cycle and from a reduction in the proportion of S-phase progenitors expressing *Nkx2.1*, similar to what was seen in the *14-3-3ζ* KO mice. With this in mind Chapter 5 investigated Shh and Rac1 signalling pathways in the *14-3-3ζ* KO mice. Interestingly, *14-3-3ζ* KO mice showed dysfunction in both the non-canonical Shh and the Rac1 signalling pathways, suggesting that 14-3-3ζ controls interneuron development by regulating Rac1 and the non-canonical Shh signalling pathway.

Schizophrenia is a complex disorder with both genetic and environmental factors known to contribute to its pathogenesis, with a common hypothesis being that both gene susceptibility and environmental insult later in life are required to elicit symptoms. When trying to better understand schizophrenia and/or identifying potential therapies it is important to consider brain development as a whole. Though brain development begins embryonically, the final maturation of cortical networks is only achieved much later in adolescence. In humans the brain reaches maturation in the early 20's and this is recapitulated in mice where interneurons continue to mature up until the end of adolescence (Spear, 2000; Crews et al., 2007). During this time the brain undergoes a period of rapid synaptic pruning and cortical thinning (Andersen et al., 2000; Crews et al., 2007; Andersen & Teicher, 2008) which coincides with a time of strong emotional states and increased stress in adolescence (Spear, 2000; Crews et al., 2007). These cortical rearrangements extend the period of interneuron development from early embryogenesis through until late adolescence and define a large time window in which environmental insults can also occur. This protracted developmental period is also likely to account for the late manifestation of symptoms observed in schizophrenia.

In this thesis, I have focused on how genetic ablation of *14-3-3ζ* results in loss Shh and its downstream transcription factors, however have not fully explored how enviormental insult can also affect the expression of these factors. Interestingly, Oskvig et al. 2012 found that prenatal exposure to LPS, replicating a bacterial infection response during pregnancy, resulted in reduced expression of downstream Shh signalling transcription factors, including *Dlx2* and *Lhx6* (Oskvig et al., 2012). Although *14-3-3ζ* is known to have genetic mutations in patients with schizophrenia, many studies have also shown that environmental factors are able to alter 14-3-3ζ expression (Zerr et al., 1998; MacKay et al., 2011; Muayqil et al., 2012). Most notably, alcohol and drugs such as cocaine have been known to change the expression levels of 14-3-3ζ (MacKay et al., 2011; Kao et al., 2011). Furthermore, these substances have been linked to the presence of psychosis (Jordaan & Emsley, 2014). Indeed, prenatal exposure to alcohol reduces the number of PV interneurons in the brain (Hamilton et al., 2017). Our data has demonstrated that 14-3-3ζ is able to regulate Shh signalling pathway hence these environmental factors affecting 14-3-3ζ may also lead to downstream effects on Shh signalling. Furthermore, Shh signalling pathway itself is also known to be altered by environmental toxins, cyclopamine and arsenic (Cooper et al., 1998; Liang Fei et al., 2010; Turner et al., 2016). The relationship between environmental factors and genetics is often complicated, this is especially true in heterogeneous disorders such as schizophrenia. Understanding this relationship better is key in effectively treating schizophrenia.

To date schizophrenia is generally treated with serendipitously discovered anti-psychotic drugs targeting the dopamine pathway. Though currently the most effective treatment option, the efficacy of anti-psychotic drugs is poor. When investigating potential therapies it is important to consider at what stage a treatment is given. Understanding interneuron development and the Shh signalling pathway has become increasingly important over the years and is not just essential for understanding interneuron deficiency, but rather has critical importance in clinical applications

such as interneuron transplantation. Interneuron transplantation was initially described by Wichterle and colleagues (1999), where interneurons derived from embryonic MGE were injected into adult mice (Wichterle et al. 1999). Remarkably, interneurons were able to migrate through the adult cortex and disperse into the appropriate layers. This technique has since been performed on several mouse models of psychosis and other neurodevelopmental disorders and represents a revolutionary treatment for schizophrenic patients (Gilani et al., 2014; Perez et al., 2013; Donegan et al., 2016; Baraban et al., 2009; Calcagnotto et al., 2010). This technique is now being developed to use stem cells (Tyson et al., 2015) which are differentiated into interneurons. Understanding the pathways driving interneurons identity and more specifically PV identity is key if this technique is to one day be used in the clinic. The identification of 14-3-3ζ as a regulator of MGE identity may aid in driving a PV subtype. Furthermore, identifying that Rac1 plays a crucial role in the non-canonical signalling pathway to control interneuron formation may also benefit in development of interneurons for transplantation as a treatment for those with schizophrenia.

Though there is a strong link between interneurons deficiencies and schizophrenia, there are few studies investigating the link between schizophrenia and Shh signalling, despite Shh signalling being well established in interneuron development. Given that major deficits in canonical Shh during early development are embryonically lethal, it is unsurprising that thus far Shh signalling has not been investigated thoroughly in schizophrenia. However, Shh signalling genes have previously been associated with schizophrenia. For example, the analysis of 623 schizophrenia trios revealed missense mutations in several Shh signalling genes known to play critical roles in interneuron development, including *Lhx6*, *Gli2* and *Gli3* (Fromer et al., 2014). Interestingly, PAK1 was found to be decreased at the protein level in patients with schizophrenia (Deo et al., 2013). These findings further highlight the link between Shh downstream targets and schizophrenia.

Currently, Shh is known to have multiple roles in interneuron development, in both the initial MGE patterning and in maintaining MGE identity. Given the dynamics of both the canonical and non-canonical pathways and their different functions in development and that defects in the canonical pathway are unlikely to be conducive to life, increased attention should be placed on investigating the non-canonical pathway and how this may help in disease treatment. This not only has importance for schizophrenia but several other neurodevelopmental disorders which are far more likely to display milder deficits in interneurons associated with defects during later stages of development (i.e. after E12.5).

There are a wealth of studies addressing the specification and subsequent expression profiles of cortical interneurons as they develop and migrate to the cortex, however, this area lacks a clear understanding of the consequences of dysfunction at early development stages and their implications in the disease process. Understanding the coordination of interneuron specification, proliferation, migration, integration and specialisation is essential to determine their role in neurodevelopmental disease and provide insight toward novel therapeutic approaches. More importantly, it is essential to understand the key regulators of these processes and how their interaction affects progression through each stage. To date, studies have used mouse models to investigate the functional relevance of transcription factors, including Lhx6, Nkx2.1 and Dlx2 (Wonders & Anderson, 2005; Butt et al., 2008; Xu et al., 2008; Flandin et al., 2011). My research therefore adds to developments in the study of the specification and migration of cortical interneurons at the signalling level and provides insights to the impact of aberrant function during early developmental processes toward neuropsychiatric outcomes. Ultimately, further research into the non-canonical Shh signalling pathway and the role of Rac1 and 14-3-3ζ within the pathway would be valuable. Identifying the exact mechanism and other molecules within the pathway would

be beneficial not only for identifying therapeutics but for a general understanding of interneuron development.

In summary, data presented here identifies a novel role of 14-3-3ζ in augmenting the non-canonical signalling pathway via Rac-1 signalling to control interneuron development. These findings highlight a crucial stage of development in interneuron formation and gives insight into possible therapeutics and tools as well as the origins of schizophrenia and related disorders.

6.2 Future Directions

A major goal of this thesis has been to decipher the cellular and molecular mechanisms controlling interneuron development, though there is still much to learn about the roles of 14-3-3ζ, Rac1 and Shh in this process. At the end of each chapter I have discussed several potential investigations to help elucidate the role of these molecules in interneuron development, though there are four areas of study that would be of the most interest to further explore; 1) identifying additional molecules within the non-canonical signalling pathway, 2) examining the electrophysiology of *14-3-3ζ* deficient mice, 3) expanding on the behavioural phenotypes of both the *14-3-3ζ KO* mice and the *Olig2-Cre; 14-3-3ζ$^{fl/fl}$* and *Dlx5/6-Cre; 14-3-3ζ$^{fl/fl}$* conditional mice, and 4) investigating whether interneuron transplantation can rescue the *14-3-3ζ* KO mouse phenotype.

Here, we identified that 14-3-3ζ and Rac1 are essential for regulating *Nkx2.1* expression, however it is unclear how Rac1 is activated upstream and the precise role that 14-3-3ζ plays in this process. In future, it would be of use to examine GEFs such as Tiam to explore whether they have a role in non-canonical Shh signalling pathway. This could be approached by performing a series of experiments where chemical inhibitors are used to block their function. Furthermore, it would be of interest to examine if increasing Rac1 activity in *14-3-3ζ* KO MGE-derived interneurons is

able to rescue the observed phenotype. This could be accomplished by introducing constitutively active Rac1 constructs to MGE explants.

Given that PV+ interneurons are essential for gamma oscillations and that my data identified a loss of PV+ interneurons in *14-3-3ζ* KO mice, it would be of interest to examine whether the *14-3-3ζ* dependent loss of cortical PV+ interneurons leads to alterations in coordinated network activity. This could be examined through the use of *in vivo* electrophysiology recordings on freely moving *14-3-3ζ* KO and *Olig2-Cre; 14-3-3ζ*$^{fl/fl}$ mice compared to controls and measure network oscillations in the gamma and theta frequencies. Based on the behavioural and cellular phenotype it would be expected that these mice would display aberrant signalling and gamma oscillations.

Since defects in attention and working memory and altered social interactions are endophenotypes of schizophrenia, and my analysis has not extensively addressed the behavioural phenotype of the *14-3-3ζ* KO mice and the *Olig2-Cre; 14-3-3ζ*$^{fl/fl}$ mice it would be of interest to examine the higher cognitive functions in these mice. This could be examined by performing several behavioural analyses including, pre-pulse inhibition, social approach and social preference, 5-choice serial reaction task (5-CSRT) and trial-unique non-matching-to-location task (TUNL). 5-CSRT is used to assess attention and response inhibition and requires mice to respond to a brief visual stimulus presented randomly in one of 5 locations. TUNL analysis is able to access spatial working memory requiring mice to remember the location of a sample phase visual stimulus when presented with multiple visual stimuli during a choice phase. Based on the findings presented in this thesis, including a loss of PV interneurons in the absence of *14-3-3ζ,* it would be expected that the *14-3-3ζ* KO mice and *Olig2-Cre; 14-3-3ζ*$^{fl/fl}$ mice would show lower accuracy at baseline or deficits in accuracy when the delay is increased.

As mentioned previously, interneuron transplantation has been used in several mouse models with neurodevelopmental disorders including schizophrenia. It would be incredibly useful to test this approach on the *14-3-3ζ* KO mice to identify if healthy interneurons or PV rich interneuron populations are able to rescue the observed phenotype.

Taken together these approaches can help elucidate the complex role 14-3-3ζ is playing in interneurons as well as understand the true effect of *14-3-3ζ* ablation.

Chapter 7: References

Agim ZS, Esendal M, Briollais L, et al. (2013) Discovery, Validation and Characterization of Erbb4 and Nrg1 Haplotypes Using Data from Three Genome-Wide Association Studies of Schizophrenia. PLoS One 8:e53042.

Aitken A (2006) 14-3-3 Proteins: A Historic Overview. Seminars in cancer biology. 16:162–72.

Alifragis P, Liapi A, Parnavelas JG (2004) Lhx6 regulates the migration of cortical interneurons from the ventral telencephalon but does not specify their GABA phenotype. J Neurosci 24:5643-5648.

Allen K, Fung S, Shannon Weickert C (2016) Cell proliferation is reduced in the hippocampus in schizophrenia. The Australian and New Zealand Journal of Psychiatry 50(5): 473–480.

Andersen P, Morris R, Amaral D, et al. (2007). The Hippocampus Book. Oxford: Oxford University Press.

Andersen SL, Teicher MH (2008) Stress, sensitive periods and maturational events in adolescent depression. Trends Neurosci 31: 183-191. 162.

Andersen SL, Thompson AT, Rutstein M, et al. (2000) Dopamine receptor pruning in prefrontal cortex during the periadolescent period in rats. Synapse 37: 167-169.

Anderson R, Lawrence A, Stottmann R, et al. (2002) Chordin and noggin promote organizing centers of forebrain development in the mouse. Development 129: 4975-4987.

Angrand P, Segura I, Völkel P, et al. (2006) Transgenic mouse proteomics identifies new 14-3-3-associated proteins involved in cytoskeletal rearrangements and cell signalling. Mol cell proteomics 5(12):2211-27.

Aoto K, Nishimura T, Eto K, et al. (2002) Mouse GLI3 regulates Fgf8 expression and apoptosis in the developing neural tube, face, and limb bud. Dev Biol 251:320–332.

Ascoli G, Alonso-Nanclares L, Anderson S, et al (2008) Petilla terminology: nomenclature of features of GABAergic interneurons of the cerebral cortex. Nat Rev Neurosci 9:557–568.

Asbreuk CH, van Schaick HS, Cox JJ, Kromkamp M, Smidt MP, Burbach JP (2002) The homeobox genes Lhx7 and Gbx1 are expressed in the basal forebrain cholinergic system. Neuroscience 109:287-298.

Backman M, Machon O, Mygland L, et al. (2005) Effects of canonical Wnt signaling on dorso-ventral specification of the mouse telencephalon. Dev Biol 279:155–168.

Balabanian K, Lagane B, Infantino S, et al. (2005) The Chemokine SDF-1/CXCL12 Binds to and Signals through the Orphan Receptor RDC1 in T Lymphocytes. J Biol Chem 280:35760–35766.

Baraban S, Southwell D, Estrada R, et al. (2009) Reduction of seizures by transplantation of cortical GABAergic interneuron precursors into Kv1.1 mutant mice. Proc Natl Acad Sci U S A 106:15472–15477.

Batista-Brito R, Rossignol E, Hjerling-Leffler J, et al. (2009) The Cell-Intrinsic Requirement of Sox6 for Cortical Interneuron Development. Neuron 63:466–481.

Baxter H, Fraser J, Liu W, et al. (2002) Specific 14-3-3 isoform detection and immunolocalization in prion diseases. Biochem Soc Trans.30:387–391.

Beasley C, Reynolds G (1997) Parvalbumin-immunoreactive neurons are reduced in the prefrontal cortex of schizophrenics. Schizophrenia Research 24:349-355.

Beasley C, Zhang Z, Patten I, Reynolds G (2002) Selective deficits in prefrontal cortical GABAergic neurons in schizophrenia defined by the presence of calcium-binding proteins. Biol Psychiatry 52(7):708-15.

Belforte JE, Zsiros V, Sklar ER, et al. (2010) Postnatal NMDA receptor ablation in corticolimbic interneurons confers schizophrenia-like phenotypes. Nat Neurosci 13: 76-83.

Belgard T, Marques A, Oliver P, et al. (2011) A Transcriptome Atlas of Mouse Neocortical Layers. Neuron 71(4): 605-616.

Bell R, Munro J, Russ C, et al. Systematic screening of the 14-3-3 eta (eta) chain gene for polymorphic variants and case-control analysis in schizophrenia. Am J Med Genet. 96(6):736-43.

Benes FM, Vincent SL, Alsterberg G, et al. (1992) Increased GABAA receptor binding in superficial layers of cingulate cortex in schizophrenics. J Neurosci 12: 924-929.

Berg D, Holzmann C, and Riess O (2003) 14-3-3 proteins in the nervous system. Nat Rev Neurosci. 4:752–762.

Boaru S, Merle U, Uerlings R, et al. (2014) Simultaneous monitoring of cerebral metal accumulation in an experiment model of Wilson's disease by laser ablation inductively coupled plasma mass spectrometry. BMC neuroscience 15:98.

Bogerts B, Häntsch J, Herzer M (1983) A morphometric study of the dopamine-containing cell groups in the mesencephalon of normals, Parkinson patients, and schizophrenics. Biol Psychiatry 18:951–69.

Boston P, Jackson P, Thompson R (1982) Human 14-3-3 protein: radioimmunoassay, tissue distribution, and cerebrospinal fluid levels in patients with neurological disorders. J. Neurochem 38:1475–1482.

Brennan D, Chen X, Cheng L, et al. (2012) Noncanonical Hedgehog signalling. Vitamins and Hormones 88:55-72.

Britto J, Tannahill D, Keynes R (2002) A critical role for sonic hedgehog signaling in the early expansion of the developing brain. Nat. Neurosci. 5:103–110.

Brodmann K (1908) Beiträge zur histologischen Lokalisation der Grosshirnrinde. VI. Mitteilung: Die Cortexgliederung des Menschen. J. Psychol. Neurol 10:231-246.

Brown M, Keynes R, Lumsden A (2001) The developing brain. Oxford University Press.

Bulfone A, Puelles L, Porteus MH, Frohman MA, Martin GR, Rubenstein JL (1993) Spatially restricted expression of Dlx-1, Dlx-2 (Tes-1), Gbx-2, and Wnt-3 in the embryonic day 12.5 mouse forebrain defines potential transverse and longitudinal segmental boundaries. J Neurosci 13:3155-3172.

Butt S, Sousa V, Fuccillo M, et al. The requirement of Nkx2-1 in the temporal specification of cortical interneuron subtypes. Neuron 59(5):722-32.

Calcagnotto M, Zipancic I, Piquer-Gil M, et al. (2010) Grafting of GABAergic precursors rescues deficits in hippocampal inhibition. Epilepsia. 51(Suppl 3):66–70

Calegari F, Haubensak W, Haffner C, Huttner W (2005) Selective lengthening of the cell cycle in the neurogenic subpopulation of neural progenitor cells during mouse brain development. J Neurosci. 25:6533–6538.

Calegari F, Huttner W (2003) An inhibition of cyclin-dependent kinases that lengthens, but does not arrest, neuroepithelial cell cycle induces premature neurogenesis. J Cell Sci. 116:4947–4955.

Cardin J, Carlén M, Meletis K, et al. (2009) Driving fast-spiking cells induces gamma rhythm and controls sensory responses. Nature 459(7247):663-7.

Carlsson A, Lindqvist M (1963) Effect of chlorpromazine or haloperidol on formation of 3methoxytyramine and normetanephrine in mouse brain. Acta Pharmacol Toxicol 20:140–410.

Cavanagh J, Mione M, Pappas I, Parnavelas J (1997) Basic fibroblast growth factor prolongs the proliferation of rat cortical progenitor cells *in vitro* without altering their cell cycle parameters. Cereb Cortex 7:293-302.

Cheah PS, Ramshaw H, Thomas P (2012) Neurodevelopmental and neuropsychiatric behaviour defects arise from 14-3-3zeta deficiency. Mol Psychiatry 17:451-66.

Chiang C, Litingtung Y, Lee E, et al. (1996) Cyclopia and defective axial patterning in mice lacking Sonic hedgehog gene function. Nature 383:407–413.

Choi S, Witek R, Yang L, et al. (2010) Activation of Rac1 promotes Hedgehog-mediated acquisition of the myofibroblastic phenotype in rat and human hepatic stellate cells. Hepatology 52(1): 278–290.

Ciemerych M, Kenney A, Sicinska A (2005) Development of mice expressing a single D-type cyclin. Genes Dev. 16;3277-3289.

Cioffi C (2013) Modulation of NMDA receptor function as a treatment for schizophrenia. Bioorg Med Chem Lett. 23(18):5034-44.

Clapcote S, Lipina T, Millar J, et al. (2007) Behavioural phenotypes of Disc1 missense mutations in mice. Neuron. 54:387–402.

Cooper M, Porter J, Young K, et al. (1998) Teratogen-mediated inhibition of target tissue response to Shh signaling. Science 280:1603–1607.

Crews F, He J, Hodge C (2007) Adolescent cortical development: a critical period of vulnerability for addiction. Pharmacol Biochem Behav 86: 189-199.

Curran C, Byrappa N, McBride A (2004) Stimulant psychosis: systematic review. The British Journal of Psychiatry 185 (3): 196–204.

DeBoer E, Anderson S (2015) Fate determination of cerebral cortical GABAergic interneurons and their derivation from stem cells. Brain Res. 1655: 277-282.

De Marco García NV, Karayannis T, Fishell G (2011) Neuronal activity is required for the development of specific cortical interneuron subtypes. Nature 72:351–355.

DeFelipe J, Jones E (1992) Santiago Ramón y Cajal and methods in neurohistology. Trends Neurosci. 15, 237–246.

DeFelipe J (1993) Neocortical neuronal diversity: chemical heterogeneity revealed by colocalization studies of classic neurotransmitters, neuropeptides, calcium-binding proteins, and cell surface molecules. Cereb Cortex 3:273-289.

DeFelipe J (1997) Types of neurons, synaptic connections and chemical characteristics of cells immunoreactive for calbindin-D28K, parvalbumin and calretinin in the neocortex. J Chem Neuroanat 14:1-19.

DeFelipe J (2002) Cortical interneurons: from Cajal to 2001. Prog Brain Res 136:215–238.

DeFelipe J, López-Cruz PL, Benavides-Piccione R, et al (2013) New insights into the classification and nomenclature of cortical GABAergic interneurons. Nat Rev Neurosci 14:202–16.

Del Arco A, Segovia G, Mora F (2008) Blockade of NMDA receptors in the prefrontal cortex increases dopamine and acetylcholine release in the nucleus accumbens and motor activity. Psychopharmacology. 201: 325-338.

Deo A, Goldszer I, Li S, et al. (2013) PAK1 Protein Expression in the Auditory Cortex of Schizophrenia Subjects. PLOSone 8(4):e59458.

Donegan J, Tyson J, Branch S, et al. (2016) Stem cell-derived interneuron transplants as a treatment for schizophrenia: preclinical validation in a rodent model. Molecular Psychiatry

Du T, Xu Q, Ocbina PJ, Anderson SA (2008) NKX2.1 specifies cortical interneuron fate by activating Lhx6. Development 135:1559-1567.

Eisenstat DD, Liu JK, Mione M, Zhong W, Yu G, Anderson SA, Ghattas I, Puelles L, Rubenstein JL (1999) DLX-1, DLX-2, and DLX-5 expression define distinct stages of basal forebrain differentiation. J Comp Neurol 414:217-237.

Ekelund J, Lichtermann D, Hovatta I, et al (2000) Genome-wide scan for schizophrenia in the Finnish population: evidence for a locus on chromosome 7q22. Hum Mol Genet 9:1049–1057.

English JA, Dicker P, Föcking M, et al. (2009) 2-D DIGE analysis implicates cytoskeletal abnormalities in psychiatric disease. Proteomics 9:3368–82.

English JA, Pennington K, Dunn M, Cotter D (2011*) The neuroproteomics of schizophrenia*. Biol Psychiatry 69:163–172.

Ericson J, Muhr J, Placzek M, et al. (1995) Sonic hedgehog induces the differentiation of ventral forebrain neurons: a common signal for ventral patterning within the neural tube. Cell 81:747–756.

Etienne O, Bery A, Roque T, et al. (2014) Assessing Cell Cycle Progression of Neural Stem and Progenitor Cells in the Mouse Developing Brain after Genotoxic Stress. J Vis Exp. (87): 51209.

Falkai P, Schneider-Axmann T, and Honer W (2000) Entorhinal cortex pre-alpha cell clusters in schizophrenia: quantitative evidence of a developmental abnormality. Biological Psychiatry. 47:937–943.

Fanselow EE, Richardson KA, Connors BW (2008) Selective, state-dependent activation of somatostatin-expressing inhibitory interneurons in mouse neocortex. J Neurophysiol 100:2640–2652.

Fantl V, Edwards P, Steel J, et al. (1999) Impaired mammary gland development in Cyl-1(-/-) mice during pregnancy and lactation is epithelial cell autonomous. Dev. Biol. 212:1-11.

Fantl V, Stamp G, Andrews A, et al. (1995) Mice lacking in cyclin D are small and show defects in eye and mammary gland development. Genes Dev. 9:2364-2372.

Farzan F, Barr MS, Levinson AJ, et al. (2010) Evidence for gamma inhibition deficits in the dorsolateral prefrontal cortex of patients with schizophrenia. Brain 133:1505–1514.

Faux C, Rakic S, Andrews W, Britto J (2012) Neurons on the move: migration and lamination of cortical interneurons. Neurosignals 20(3):168-89.

Finlay B, Darlington R (1995) Linked regularities in the development and evolution of mammalian brains. Science 268(5217):1578-84.

Fisahn A, Neddens J, Yan L, Buonanno A (2009) Neuregulin-1 modulates hippocampal gamma oscillations: implications for schizophrenia. Cereb Cortex 19:612–618.

Fishell G (1997) Regionalization in the mammalian telencephalon. Curr Opin Neurobiol. 7:62–69.

Flames N, Long JE, Garratt AN, et al. (2004) Short- and long-range attraction of cortical GABAergic interneurons by neuregulin-1. Neuron 44:251–561.

Flandin P, Zhao Y, Vogt D, et al. (2011) Lhx6 and Lhx8 Coordinately Induce Neuronal Expression of Shh that Controls the Generation of Interneuron Progenitors. Neuron 70:939–950.

Foote M, Zhou Y (2012) 14-3-3 proteins in neurological disorders. Int J Biochem Mol Biol. 3(2):152-64.

Forro T, Valenti O, Lasztoczi B, Klausberger T (2015) Temporal organization of GABAergic interneurons in the intermediate CA1 hippocampus during network oscillations. Cereb. Cortex 25:1228–1240.

Fragkouli A, van Wijk NV, Lopes R, Kessaris N, Pachnis V (2009) LIM homeodomain transcription factor-dependent specification of bipotential MGE progenitors into cholinergic and GABAergic striatal interneurons. Development 136:3841-3851.

Friocourt G, Parnavelas JG (2010) Mutations in ARX Result in Several Defects Involving GABAergic Neurons. Front Cell Neurosci 4: 4.

Fromer M, Pocklington AJ, Kavanagh DH, et al. (2014) De novo mutations in schizophrenia implicate synaptic networks. Nature 506:179–184.

Fu H, Subramanian R, and Masters S (2000) 14-3-3 Proteins: Structure, Function, and Regulation. Annual review of pharmacology and toxicology 40:617– 47.

Fuccillo M, Rallu M, McMahon AP, et al. (2004) Temporal requirement for hedgehog signaling in ventral telencephalic patterning. Development 131:5031–5040.

Fung SJ, Webster MJ, Sivagnanasundaram S, et al. (2010) Expression of interneuron markers in the dorsolateral prefrontal cortex of the developing human and in schizophrenia. Am J Psychiatry 167:1479–1488.

GaoY, Dickerson J, Guo F, et al. (2004) Rational design and characterization of a Rac GTPase-specific small molecule inhibitor. Proc Natl Acad Sci USA 101(20):7618-23.

Gardino A, Smerdon S, and Yaffe M (2006) Structural determinants of 14-3-3 binding specificities and regulation of subcellular localization of 14-3-3-ligand complexes: A comparison of the X-ray crystal structures of all human 14-3-3 isoforms. Seminars in Cancer Biology 16:173-182.

Geiger J, Lübke J, Roth A, et al. (1997) Submillisecond AMPA receptor-mediated signaling at a principal neuron-interneuron synapse. Neuron 18:1009–1023.

Geiger J, Melcher T, Koh D, et al. (1995) Relative abundance of subunit mRNAs determines gating and Ca2+ permeability of AMPA receptors in principal neurons and interneurons in rat CNS. Neuron 15:193–204.

Gilani A, Chohana M, Inan M (2014) Interneuron precursor transplants in adult hippocampus reverse psychosis-relevant features in a mouse model of hippocampal disinhibition. PNAS 111(20):7450–7455.

Glickstein S, Alexander S, Ross M (2007a) Differences in cyclin d2 and d1 protein expression distinguish forebrain progenitor subsets. Cereb Cortex 17:632–642.

Glickstein S, Monaghan J, Koeller H, et al. (2009) Cyclin D2 is critical for intermediate progenitor cell proliferation in the embryonic cortex. J Neurosci. 29:9614–9624.

Glickstein S, Moore H, Slowinska B, et al. (2007b) Selective cortical interneuron and GABA deficits in cyclin D2-null mice. Development 134:4083–4093.

Goc A, Abdalla M, Al-Azayzih A, Somanath P (2012) Rac1 activation driven by 14-3-3ζ dimerization promotes prostate cancer cell-matrix interactions, motility and transendothelial migration. PLoS One 7(7):e40594

Gonchar Y, Burkhalter A (1997) Three distinct families of GABAergic neurons in rat visual cortex. Cereb Cortex 7:347–358.

Greenberg Z, Ramshaw H, Schwarz Q (2015) Time Windows of Interneuron Development: Implications to Our Understanding of the Aetiology and Treatment of Schizophrenia. AIMS Neuroscience, 2015, 2(4): 294-321.

Guidotti A, Auta J, Davis J, et al. (2000) Decrease in reelin and glutamic acid decarboxylase67 (GAD67) expression in schizophrenia and bipolar disorder: a postmortem brain study. Arch Gen Psychiatry 57(11):1061-9.

Gulacsi A, Anderson S (2006) Shh maintains Nkx2.1 in the MGE by a Gli3-independent mechanism. Cereb Cortex 16:89–95.

Gulacsi A, Anderson S (2008) β-catenin-mediated Wnt signaling regulates neurogenesis in the ventral telencephalon. Nat Neurosci 11:1383–1391.

Gulacsi A, Lillien L (2003) Sonic hedgehog and bone morphogenetic protein regulate interneuron development from dorsal telencephalic progenitors *in vitro*. J Neurosci 23: 9862-9872.

Gutin G, Marie F, Laura P, et al. (2006) FGF signalling generates ventral telencephalic cells independently of SHH. Development 133: 2937-2946.

Hamilton G, Hernandez I, Krebs C et al. (2017) Neonatal alcohol exposure reduces number of parvalbumin-positive interneurons in the medial prefrontal cortex and impairs passive avoidance acquisition in mice deficits not rescued from exercise. Neuroscience 352(3) 52-63.

Harrison P (2004) The hippocampus in schizophrenia: a review of the neuropathological evidence and its pathophysiological implications. Psychopharmacology. 174:151–62.

Harrison P, Weinberger D (2005) Schizophrenia genes, gene expression, and neuropathology: on the matter of their convergence. Molecular Psychiatry 10:40–68.

Hashimoto T, Volk DW, Eggan SM, et al. (2003) Gene expression deficits in a subclass of GABA neurons in the prefrontal cortex of subjects with schizophrenia. J Neurosci 23:6315–6326.

Hashimoto T, Arion D, Unger T, et al. (2008a) Alterations in GABA-related transcriptome in the dorsolateral prefrontal cortex of subjects with schizophrenia. Molecular psychiatry 13:147-161.

Hashimoto T, Bazmi H, Mirnics K, et al. (2008b) Conserved regional patterns of GABA-related transcript expression in the neocortex of subjects with schizophrenia. The Am J. Psychiatry, 165, 479-489.

Heckers, S (2001) Neuroimaging studies of the hippocampus in schizophrenia. Hippocampus. 11:520–528.

Heckers S, Heinsen H, Geiger B, and Beckmann H (1991) Hippocampal neuron number in schizophrenia. A stereological study. Arch Gen Psychiatry. 48:1002–1008.

Heckers S, Konradi C (2015) GABAergic mechanisms of hippocampal hyperactivity in schizophrenia. Schizophrenia research 167(3): 4-11.

Hermeking H, Benzinger A (2006) 14-3-3 proteins in cell cycle regulation. Semin Cancer Biol. 16(3):183-92.

Hendry S, Schwark H, Jones E, et al. (1987) Numbers and proportions of GABA-immunoreactive neurons in different areas of monkey cerebral cortex. J Neurosci 7:1503–1519.

Hernández-Miranda LR, Cariboni A, Faux C, et al. (2011) Robo1 regulates semaphorin signaling to guide the migration of cortical interneurons through the ventral forebrain. J Neurosci 31:6174–6187.

Hevner RF, Daza RA, Englund C, et al. (2004) Postnatal shifts of interneuron position in the neocortex of normal and reeler mice: evidence for inward radial migration. Neuroscience 124:605–18.

Horn AS, Snyder SH (1971) Chlorpromazine and dopamine: conformational similarities that correlate with the antischizophrenic activity of phenothiazine drugs. Proc Natl Acad Sci 68:2325–810.

Hosak L (2013) New findings in the genetics of schizophrenia. World J Psychiatry 3: 57-61

Hu H, Gan J, Jonas P (2014) Interneurons. Fast-spiking, parvalbumin+ GABAergic interneurons: from cellular design to microcircuit function. Science 345:1255263.

Inan M, Petros TJ, Anderson SA (2013) Losing your inhibition: Linking cortical GABAergic interneurons to schizophrenia. Neurobiol Dis 53:36–48.

Insel TR (2010) Rethinking schizophrenia. Nature 468:187–193.

Iversen S, Iversen L (2007) Dopamine: 50 years in perspective. Trends Neurosci. 30(5):188-93.

Jakob H, and Beckmann H (1986) Prenatal developmental disturbances in the limbic allocortex in schizophrenics. Journal of Neural Transmission. 65:303–26

Jiménez D, López-Mascaraque LM, Valverde F, De Carlos JA (2002) Tangential migration in neocortical development. Dev Biol 244:155-169.

Joshi D, Catts V, Olaya J et al. (2015) Relationship between somatostatin and death receptor expression in the orbital frontal cortex in schizophrenia: a postmortem brain mRNA study. npj Schizophrenia 1(14004).

Joyce D, Bouzahzah B, Fu M, et al. (1999) Integration of Rac-dependent regulation of cyclin D1 transcription through a nuclear factor-kappaB-dependent pathway. J Biol Chem 274(36):25245-9.

Kao G, Chuang J, Cherng C, et al. (2011) Accumbal 14-3-3ζ protein downregulation is associated with cocaine-conditioned memory. Neurosignals 19(4):175-88.

Karlen SJ, Krubitzer L. (2006) The evolution of the neocortex in mammals: intrinsic and extrinsic contributions to the cortical phenotype, in Percept, Decision, Action: Bridging the Gaps (Novartis Foundation Symposia). Novartis Found Symp, West Sussex, pp:146-159.

Katayama K, Imai F, Campbell K, et al. (2013) RhoA and Cdc42 are required in pre-migratory progenitors of the medial ganglionic eminence ventricular zone for proper cortical interneuron migration. Development 140(15): 3139–3145.

Kato M, Dobyns W (2003) Lissencephaly and the molecular basis of neuronal migration. Hum Mol Genet. 1: R89-96.

Kawaguchi Y, Kubota Y (1997) GABAergic cell subtypes and their synaptic connections in rat frontal cortex. Cereb Cortex 7 :476–486.

Kawaguchi Y, Katsumaru H, Kosaka T, et al. (1987) Fast spiking cells in the rat hippocampus (CA1 region) contain the calcium-binding protein parvalbumin. Brain Res 416:369–374.

Kegeles L, Abi-Dargham A, Zea-Ponce Y, et al. (2000) Modulation of amphetamine-induced striatal dopamine release by ketamine in humans: implications for schizophrenia. Biol Psychiatry 48:627–40.

Kelsom C, Lu W (2013) Development and specification of GABAergic cortical interneurons. Cell & Bioscience 3:19.

Kenney AM, Rowitch D (2000) Sonic hedgehog Promotes G1 Cyclin Expression and Sustained Cell Cycle Progression in Mammalian Neuronal Precursors. Molecular and Cellular Biology 20(23): 9055–9067.

Kepecs A, Fishell G (2014) Interneuron cell types: Fit to form and formed to fit. Nature 505(7483):318–26.

Kimura S, Hara Y, Pineau T, et al. (1996) The T/ebp null mouse: thyroid-specific enhancer-binding protein is essential for the organogenesis of the thyroid, lung, ventral forebrain, and pituitary. Genes Dev 10 :60–69.

Komuro H, Rakic P (1992) Selective role of N-type calcium channels in neuronal migration. Science 257(5071):806-9.

Komuro H, Rakic P (1993) Modulation of neuronal migration by NMDA receptors. Science 260(5104):95-7.

Koolschijn PC, van Haren NC, Cahn W (2010) Hippocampal volume change in schizophrenia. J Clin Psychiatry 71(6):737:44.

Konradi C, Yang C, Zimmerman E, et al. (2011) Hippocampal interneurons are abnormal in schizophrenia. Schizophrenia research 131:165-173.

Lange C, Huttner W, Calegari F (2009) Cdk4/cyclinD1 overexpression in neural stem cells shortens G1, delays neurogenesis, and promotes the generation and expansion of basal progenitors. Cell Stem Cell 5:320–331.

Lavdas A, Grigoriou M, Pachnis V, Parnavelas JG (1999) The medial ganglionic eminence gives rise to a population of early neurons in the developing cerebral cortex. J. Neuroscience 19:7881–7888.

Lawrie S, Abukmeil S (1998) Brain abnormality in schizophrenia. A systematic and quantitative review of volumetric magnetic resonance imaging studies. The British Journal of Psychiatry. 172:110–20.

Lee K, Mattiske T, Kitamura K, et al. (2014) Reduced polyalanine-expanded Arx mutant protein in developing mouse subpallium alters Lmo1 transcriptional regulation. Hum Mol Genet 23 (4): 1084-1094.

Lee S, Hjerling-Leffler J, Zagha E, et al. (2010) The largest group of superficial neocortical GABAergic interneurons expresses ionotropic serotonin receptors. J Neurosci 30:16796–16808.

Lei M, Lu W, Meng W, et al. (2000) Structure of PAK1 in an autoinhibited conformation reveals a multistage activation switch. Cell 102(3):387-97.

Lei Q, Jeong Y, Misra K, et al. (2006) Wnt Signaling Inhibitors Regulate the Transcriptional Response to Morphogenetic Shh-Gli Signaling in the Neural Tube. Dev Cell 11:325–337.

Levitt P, Eagleson KL, Powell EM (2004) Regulation of neocortical interneuron development and the implications for neurodevelopmental disorders. Trends Neurosci 27:400–406.

Lewis D (2000) GABAergic local circuit neurons and prefrontal cortical dysfunction in schizophrenia. Brain Res Rev 31:270–276.

Lewis D, Levitt P (2002) Schizophrenia as a disorder of neurodevelopment. Annu Rev Neurosci 25:409–32.

Lewis D, Hashimoto T, Volk D (2005) Cortical inhibitory neurons and schizophrenia. Nature Reviews Neuroscience 6:312-324.

Li H, Chou S-J, Hamasaki T, et al. (2012) Neuregulin repellent signaling via ErbB4 restricts GABAergic interneurons to migratory paths from ganglionic eminence to cortical destinations. Neural Dev 7:10.

Liang F, Li H, Kozul C, et al. (2010) Activation of Hedgehog signaling by the environmental toxicant arsenic may contribute to the etiology of arsenic induced tumors. Cancer Res. 70(5): 1981–1988.

Libert F, Passage E, Parmentier M, et al. (1991) Chromosomal mapping of A1 and A2 adenosine receptors, VIP receptor, and a new subtype of serotonin receptor. Genomics 11:225–227.

Lieberman J, Kane J, Alvir J (1987). Provocative tests with psychostimulant drugs in schizophrenia. Psychopharmacology 91(4): 415–433.

Lim G, Albrecht T, Piske M, et al. (2015) 14-3-3ζ coordinates adipogenesis of visceral fat. Nat Commun 6:7671.

Liodis P, Denaxa M, Grigoriou M, Akufo-Addo C, Yanagawa Y, Pachnis V (2007) Lhx6 activity is required for the normal migration and specification of cortical interneuron subtypes. J Neurosci 27:3078-3089.

Lipska B, Weinberger D (2000) To model a psychiatric disorder in animals: schizophrenia as a reality test. Neuropsychopharmacology 23(3):223-39.

Liu D, Bienkowska J, Petosa C, et al. (1995) Crystal structure of the zeta isoform of the 14-3-3 protein. Nature 376(6536):191-4.

Liu JK, Ghattas I, Liu S, Chen S, Rubenstein JL (1997) Dlx genes encode DNA-binding proteins that are expressed in an overlapping and sequential pattern during basal ganglia differentiation. Dev Dyn 210:498-512.

Lodge D, Behrens M, Grace A (2009) A loss of parvalbumin-containing interneurons is associated with diminished oscillatory activity in an animal model of schizophrenia. J Neurosci 29:2344–2354.

Lu CL, Wang YC, Chen JY, et al. (2010) Support for the involvement of the ERBB4 gene in schizophrenia: A genetic association analysis. Neurosci Lett 481:120–125.

Lumb R, Wiszniak S, Kabbara S, et al. (2014) Neuropilins define distinct populations of neural crest cells. Neural Dev 9: 24.

Lysko DE, Putt M, Golden J (2011) SDF-1 regulates leading process branching and speed of migrating interneurons. J Neurosci 31:1739–1745.

Ma Y, Hang H, Berrebi S et al. (2006). Distinct subtypes of somatostatin-containing neocortical interneurons revealed in transgenic mice. J. Neurosci. 26:5069–5082.

Machold R, Hayashi S, Rutlin M, et al. (2003) Sonic hedgehog is required for progenitor cell maintenance in telencephalic stem cell niches. Neuron 39:937–950.

Machon O, van den Bout CJ, Backman M, et al. (2003) Role of beta-catenin in the developing cortical and hippocampal neuroepithelium. Neuroscience 122: 129-143.

MacKay R, Colson N, Dodd P, et al. (2011) Differential expression of 14-3-3 isoforms in human alcoholic brain. Alcohol Clin Exp Res. 35(6): 1041–1049.

Marín O (2012) Interneuron dysfunction in psychiatric disorders. Nat Rev Neurosci 107–120.

Marin O (2013) Cellular and molecular mechanisms controlling the migration of neocortical interneurons. Eur J Neurosci. 38(1):2019-29.

Marín O, Anderson SA, Rubenstein JL (2000) Origin and molecular specification of striatal interneurons. J Neurosci 20:6063-6076

Marin O, Baker J, Puelles L, et al. (2002) Patterning of the basal telencephalon and hypothalamus is essential for guidance of cortical projections. Development 129: 761-773.

Marín O, Yaron A, Bagri A, et al. (2001) Sorting of striatal and cortical interneurons regulated by semaphorin-neuropilin interactions. Science 293:872–875.

Martinez-Morales PL, Quiroga AC, Barbas JA, et al. (2010) SOX5 controls cell cycle progression in neural progenitors by interfering with the WNT-beta-catenin pathway. EMBO Rep 11:466–472.

Matsumoto H, Higa HH (1966) Studies on methylazoxymethanol, the aglycone of cycasin: methylation of nucleic acids *in vitro*. Biochem J 98:20C–22C.

Matthysse S (1973) Antipsychotic drug actions: a clue to the neuropathology of schizophrenia? Fed Proc. 32:200–205.

McKinsey GL, Lindtner S, Trzcinski B, Visel A (2011) Dlx1&2-Dependent Expression of Zfhx1b (Sip1, Zeb2) Regulates the Fate Switch between Cortical and Striatal Interneurons. Neuron 77(1):83-98.

Medina L, Abellán A (2009) Development and evolution of the pallium. Semin Cell Dev Biol 20:698-711.

Meinecke D, Peters A (1987) GABA immunoreactive neurons in rat visual cortex. J. Comp. Neurol. 261: 388-404.

Messaritou G, Grammenoudi S, Skoulakis E (2010) Dimerization is essential for 14-3-3zeta stability and function *in vivo*. J Biol Chem. 285(3):1692-700.

Mettouchi A, Klein S, Guo W, et al. (2001) Integrin-Specific Activation of Rac Controls Progression through the G1 Phase of the Cell Cycle. Molecular Cell 8:115–127.

Middleton F, Peng L, Lewis D, et al. (2005) Altered expression of 14-3-3 genes in the prefrontal cortex of subjects with schizophrenia. Neuropsychopharmacology 30:974-83.

Millar JK, Christie S, Semple CA, et al. (2000) Chromosomal Location and Genomic Structure of the Human Translin-Associated Factor X Gene (TRAX; TSNAX) Revealed by Intergenic Splicing to DISC1, a Gene Disrupted by a Translocation Segregating with Schizophrenia. Genomics 67:69–77.

Miller E (1999) Neurobiology. Straight from the top. Nature 401:650–651.

Miyamoto Y, Sakane F, Hashimoto K (2015) N-cadherin-based adherens junction regulates the maintenance, proliferation, and differentiation of neural progenitor cells during development. Cell Adh Migr. 9(3):183-92.

Miyoshi G, Butt S, Takebayashi H, Fishell G (2007) Physiologically distinct temporal cohorts of cortical interneurons arise from telencephalic Olig2-expressing precursors. J. Neurosci. 27:7786–7798.

Miyoshi G, Fishell G (2011) GABAergic interneuron lineages selectively sort into specific cortical layers during early postnatal development. Cereb Cortex 21:845–852.

Moore B, Perez V (1967) Specific acidic proteins of the nervous system. In: Carlson FD, ed. Physiological and biochemical aspects of nervous integration, Englewood Cliffs, NJ: PrenticeHall, 343-359.

Mountcastle VB (1997) The columnar organization of the neocortex. Brain 120:701-722.

Mountcastle VB (1998) Perceptual Neuroscience: The Cerebral Cortex. Harvard University Press, Harvard, pp:1-78.

Muaygil T, Gronseth G, Camicioli R (2012) Evidence-based guideline: Diagnostic accuracy of CSF 14-3-3 protein in sporadic Creutzfeldt-Jakob disease. Neurology 79(14):1499–1506.

Mukhopadhyay A, McGuire T, Peng C-Y, et al. (2009) Differential effects of BMP signaling on parvalbumin and somatostatin interneuron differentiation. Development 136:2633–2642.

Muratake T, Hayashi S, Ichikawa T, et al. (1996) Structural organization and chromosomal assignment of the human 14-3-3 eta chain gene (YWHAH). Genomics 36:63–69.

Muslin A, Xing H (2000) 14-3-3 proteins: regulation of subcellular localization by molecular interference. Cell Signal 12(11-12):703-9.

Myers AK, Meechan DW, Adney DR, et al. (2014) Cortical interneurons require Jnk1 to enter and navigate the developing cerebral cortex. J Neurosci 34:7787–801.

Nadarajah B, Alifragis P, Wong RO, et al. (2003) Neuronal Migration in the Developing Cerebral Cortex: Observations Based on Real-time Imaging. Cereb Cortex 13:607–611.

Nadarajah B, Parnavelas JG (2002) Modes of neuronal migration in the developing cerebral cortex. Nat Rev Neurosci 3:423–432.

Nakazawa K, Zsiros V, Jiang Z, et al. (2012) GABAergic interneuron origin of schizophrenia pathophysiology. Neuropharmacology 62: 1574-1583.

Nelson M, Saykin A, Flashman L, and Riordan H (1998) Hippocampal volume reduction in schizophrenia as assessed by magnetic resonance imaging: A meta- analytic study. Archives of General Psychiatry. 55:433–440.

Nery S, Fishell G, Corbin JG (2002) The caudal ganglionic eminence is a source of distinct cortical and subcortical cell populations. Nat Neurosci 5:1279–1287.

Obsilová V, Silhan J, Boura E et al. (2008) 14-3-3 Proteins: a Family of Versatile Molecular Regulators. Physiological research / Academia Scientiarum Bohemoslovaca 57:S11-21.

Ohkubo Y, Chiang C, Rubenstein JL (2002) Coordinate regulation and synergistic actions of BMP4, SHH and FGF8 in the rostral prosencephalon regulate morphogenesis of the telencephalic and optic vesicles. Neuroscience 111: 1-17.

Olincy A, Harris J, Johnson L, Pender V et al (2006) Proof-of-concept trial of an a7 nicotinic agonist in schizophrenia. Arch Gen Psychiatry 63:630–638.

Olson M, Ashworth A, Hall A (1995) An essential role for Rho, Rac, and Cdc42 GTPases in cell cycle progression through G1. Science 269:1270–1272.

Öngür D, Prescot AP, McCarthy J, et al. (2010) Elevated gamma-aminobutyric acid levels in chronic schizophrenia. Biol Psychiatry 68:667–670.

Ono K, Takebayashi H, Ikeda K, et al. (2008) Regional- and temporal-dependent changes in the differentiation of Olig2 progenitors in the forebrain, and the impact on astrocyte development in the dorsal pallium. *Dev. Biol.* 320:456–468.

Oskvig D, Elkahlounb A, Johnson K, et al. (2012) Maternal immune activation by LPS selectively alters specific gene expression profiles of interneuron migration and oxidative stress in the fetus without triggering a fetal immune response. Brian Behaviour Immunity 26(4): 623–634.

Pawson T, Scott J (1997) Signaling through scaffold, anchoring, and adaptor proteins. Science 278:2075–2080.

Penschuck S, Flagstad P, Didriksen M, et al. (2006) Decrease in parvalbumin-expressing neurons in the hippocampus and increased phencyclidine-induced locomotor activity in the rat methylazoxymethanol (MAM) model of schizophrenia. European J. Neuroscience. 23:279–284.

Perez S, Lodge D (2013) Hippocampal interneuron transplants reverse aberrant dopamine system function and behavior in a rodent model of schizophrenia. Mol Psychiatry 18(11):1193-8.

Perry T, Kish S, Buchanan J, et al. (1979) Gamma-aminobutyric-acid deficiency in brain of schizophrenic patients. Lancet 3:237–239.

Peyre E, Silva CG, Nguyen L (2015) Crosstalk between intracellular and extracellular signals regulating interneuron production, migration and integration into the cortex. Front Cell Neurosci 9: 129.

Pilaz LJ, Patti D, Marcy G (2009) Forced G1-phase reduction alters mode of division, neuron number, and laminar phenotype in the cerebral cortex. Proc Natl Acad Sci U S A 106:21924–29.

Pino D, Choe Y, Pleasure SJ (2011) Wnt5a controls neurite development in olfactory bulb interneurons. ASN Neuro 3:e00059.

Polizio A, Chinchilla P, Chen X, et al. (2011a) Heterotrimeric Gi Proteins Link Hedgehog Signaling to Activation of Rho Small GTPases to Promote Fibroblast Migration. J Biol Chem 286(22): 19589–19596.

Polizio A, Chinchilla P, Chen X, et al. (2011b) Sonic Hedgehog activates the GTPases Rac1 and RhoA in a Gli-independent manner through coupling of smoothened to Gi proteins. Sci Signal 4(200):pt7.

Polleux F, Whitford KL, Dijkhuizen PA, et al. (2002) Control of cortical interneuron migration by neurotrophins and PI3-kinase signaling. Dev 129 :3147–3160.

Preston A, Shohamy D, Tamminga C, Wagner A (2005) Hippocampal Function, Declarative Memory, and Schizophrenia: Anatomic and Functional Neuroimaging Considerations. Current Neurology and Neuroscience Reports 5:249–256.

Price M, Lemaistre M, Pischetola M, Di Lauro R, Duboule D (1991) A mouse gene related to Distal-less shows a restricted expression in the developing forebrain. Nature 351:748-751.

Puelles L, Kuwana E, Puelles E, Bulfone A, Shimamura K, Keleher J, Smiga S, Rubenstein JL (2000) Pallial and subpallial derivatives in the embryonic chick and mouse telencephalon, traced by the expression of the genes Dlx-2, Emx-1, Nkx-2.1, Pax-6, and Tbr-1. J Comp Neurol 424:409-438.

Rakic S, Yanagawa Y, Obata K, et al. (2009) Cortical Interneurons Require p35/Cdk5 for their Migration and Laminar Organization. Cerebral cortex 19(8): 1857–1869.

Ramón y Cajal S (1908). Studien ueber Nervenregeneration. Leipzig: Johann Ambrosius Barth, German trans. by J. Bresler (Spanish ed. Regeneración de los Nervios, 1907).

Ramshaw H, Xu X, Jaehne E, et al. (2013) Locomotor hyperactivity in 14-3-3ζ KO mice is associated with dopamine transporter dysfunction. Translational Psychiatry 3:e327.

Rath E, Kelly M, Bouldin D, Popko T (1995) Impaired peripheral nerve regeneration in mutant strain of mice (Enr) with Schwann cell defect. J. Neuroscience 15; 7226-37.

Reinhardt H, Yaffe M (2013) Phospho-Ser/Thr-binding domains: navigating the cell cycle and DNA damage response. Nat Rev Mol Cell Biol 14(9):563-80.

Ross M (2011) Cell Cycle Regulation & Interneuron Production. Dev Neurobiol. 71(1): 2–9.

Rubenstein J, Merzenich M (2003) Model of autism: increase ratio of excitation/inhibition in key neural systems. Genes, Brain Behav 2:255–267.

Rudy B, Fishell G, Lee S, et al. (2011) Three groups of interneurons account for nearly 100% of neocortical GABAergic neurons. Dev Neurobiol 71:45–61.

Saha S, Chant D, Welham J, McGrath J (2005) A systematic review of the prevalence of schizophrenia. PLoS Med 2(5):e141.

Samanta J, Burke GM, McGuire T, et al. (2007) BMPR1a signaling determines numbers of oligodendrocytes and calbindin-expressing interneurons in the cortex. J Neurosci 27:7397–7407.

Seeman P, Lee T (1975) Antipsychotic drugs: direct correlation between clinical potency and presynaptic action on dopamine neurons. Science 188(4194):1217-9.

Schmitt A, Steyskal C, Bernstein H, et al. (2009) Stereologic investigation of the posterior part of the hippocampus in schizophrenia. Acta neuropathologica. 117:395–407

Schwarz Q, Maden CH, Vieira JM, et al. (2009) Neuropilin 1 signaling guides neural crest cells to coordinate pathway choice with cell specification. Proc Natl Acad Sci U S A 106: 6164-6169.

Schwarz Q, Ruhrberg C (2010) Neuropilin, you gotta let me know: Should I stay or should I go? Cell Adh Migr 4.

Sheaff R, Groudine M, Gordon M, et al. (1997) Cyclin E-CDK2 is a regulator of p27 Kip1. Genes & Development 11:1464-147.

Sherr C (1993) Mammalian G1 cyclins. Cell. 73:1059–1065.

Sherr C (1995) D-type cyclins. Trends Biochem Sci. 20:187–190.

Sheth A, Bhide P (1997) Concurrent cellular output from two proliferative populations in the early embryonic mouse corpus striatum. J Comp Neurol 383:220–230.

Shi J, Levinson DF, Duan J, et al (2009) Common variants on chromosome 6p22.1 are associated with schizophrenia. Nature 460:753–757.

Shimamura K, Hartigan DJ, Martinez S, et al. (1995) Longitudinal organization of the anterior neural plate and neural tube. Development 121:3923–3933.

Silberberg G, Darvasi A, Pinkas-Kramarski R, Navon R (2006) The involvement of ErbB4 with schizophrenia: Association and expression studies. Am J Med Genet Part B Neuropsychiatr Genet 141B:142–148.

Sicinski P, Donaher J, Geng Y, et al. (1996) Cyclin D2 is an FSH-responsive gene involved in gonadal cell proliferation and oncogenesis. Nature 384:470-474.

Sicinski P, Donaher J, Parker S, et al. (1995) Cyclin D1 provides a link between development and oncogenesis in the retina and breast. Cell 82:621-630.

Sivagnanasundaram S, Crossett B, Dedova I, et al. (2007) Abnormal pathways in the genu of the corpus callosum in schizophrenia pathogenesis: a proteome study. Proteomics Clin. Appl. 1(10): 1291–1305.

Sluchanko N, Sudnitsyna M, Seit-nebi A, et al. (2011) Properties of the Monomeric Form of Human 14-3-3ζ Protein and Its Interaction with Tau and HspB6. Biochemistry 50:9797-9808.

Sohal VS, Zhang F, Yizhar O, Deisseroth K (2009) Parvalbumin neurons and gamma rhythms enhance cortical circuit performance. Nature 459(7247):698–702.

Somanath P, Byzova T (2009) 14-3-3beta-Rac1-p21 activated kinase signaling regulates Akt1-mediated cytoskeletal organization, lamellipodia formation and fibronectin matrix assembly. J Cell Physiol 218: 394–404.

Somogyi P, Tamás G, Lujan R, Buhl EH (1998) Salient features of synaptic organization in the cerebral cortex. Brain Res Brain Res Rev 26:113–135.

Spear LP (2000) The adolescent brain and age-related behavioral manifestations. Neurosci Biobehav Rev 24: 417-463.

Steinacker P, Schwarz P, Reim K, et al. (2005) Unchanged survival rates of 14-3-3gamma knockout mice after inoculation with pathological prion protein. Mol Cell Biol. 25(4):1339-46.

Steinecke A, Gampe C, Valkova C, et al. (2012) Disrupted-in-Schizophrenia 1 (DISC1) Is Necessary for the Correct Migration of Cortical Interneurons. J Neurosci 32:738–745.

Sultan KT, Brown KN, Shi S-H (2013) Production and organization of neocortical interneurons. Front Cell Neurosci 7:221.

Sussel L, Marin O, Kimura S, et al. (1999) Loss of Nkx2.1 homeobox gene function results in a ventral to dorsal molecular respecification within the basal telencephalon: evidence for a transformation of the pallidum into the striatum. Dev 126 :3359–3370.

Takada N, Pi HJ, Sousa VH, et al. (2014) A developmental cell-type switch in cortical interneurons leads to a selective defect in cortical oscillations. Nat Commun 5:5333.

Tamamaki N, Yanagawa Y, Tomioka R, et al. (2003) Green fluorescent protein expression and colocalization with calretinin, parvalbumin, and somatostatin in the GAD67-GFP knock-in mouse. J Comp Neurol 467:60–79.

Tamminga C, Stan A, Wagner A (2010) The Hippocampal Formation in Schizophrenia. Am J Psychiatry 167:1178–1193.

Toma C, Torrico B, Hervás A, et al. (2013) Exome sequencing in multiplex autism families suggests a major role for heterozygous truncating mutations. Mol Psychiatry (7):784-90.

Toresson H, Campbell K (2001) A role for Gsh1 in the developing striatum and olfactory bulb of Gsh2 mutant mice. Development 128:4769-4780.

Towbin H, Staehelin T, Gordon J (1979) Electrophoretic transfer of proteins from polyacrylamide gels to nitrocellulose sheets: procedure and some applications. Proc Natl Acad Sci U S A 76(9):4350-4.

Toyooka K, Muratake T, Tanaka T, et al. (1999) 14-3-3 protein eta chain gene (YWHAH) polymorphism and its genetic association with schizophrenia. Am J Med Genet. 88(2):164-7.

Toyo-oka K, Shionoya A, Gambello M, et al. (2003) 14-3-3epsilon is important for neuronal migration by binding to NUDEL: a molecular explanation for Miller-Dieker syndrome. Nat Genet 34:274-85.

Toyo-oka K, Wachi T, Hunt R, et al. (2014) 14-3-3ε and ζ regulate neurogenesis and differentiation of neuronal progenitor cells in the developing brain. J Neurosci. 34(36):12168-81.

Turner M, Cruz R, Mattos J, et al. (2016) Cyclopamine bioactivity by extraction method from Veratrum californicum. Bioorg Med Chem. 15;24(16):3752-7.

Tyson J, Anderson S (2014) GABAergic interneuron transplants to study development and treat disease. Trends Neurosci 37:169–177.

Tyson J, Goldberg E, Maroof A, et al. (2015) Duration of culture and Sonic Hedgehog signaling differentially specify PV versus SST cortical interneuron fates from embryonic stem cells. Development 142(7): 1267-78. 2015.

Uhlhaas P, Singer W (2010) Abnormal neural oscillations and synchrony in schizophrenia. Nature Neurosci 11(2): 100-13.

van den Berghe V, Stappers E, Vandesande B et al. (2013) Directed Migration of Cortical Interneurons Depends on the Cell-Autonomous Action of Sip1. Neuron 77:70–82.

Vidaki M, Tivodar S, Doulgeraki K, et al. (2012) Rac1-dependent cell cycle exit of MGE precursors and GABAergic interneuron migration to the cortex. Cereb Cortex 22:680–692.

Vogt D, Hunt RF, Mandal S, et al. (2014) Lhx6 directly regulates Arx and CXCR7 to determine cortical interneuron fate and laminar position. Neuron 82:350–364.

Voineskos A, Foussias G, Lerch J, et al. (2013) Neuroimaging evidence for the deficit subtype of schizophrenia. JAMA Psychiatry 70:472–480.

Volk DW, Austin MC, Pierri JN, et al. (2000) Decreased Glutamic Acid Decarboxylase 67 Messenger. Arch Gen Psychiatry 57:237–245.

Volk DW, Chitrapu A, Edelson JR, et al. (2015) Chemokine receptors and cortical interneuron dysfunction in schizophrenia. Schizophr Res;167(1-3):12-7.

Walker M, Brakefield T, Morgan A, et al. (2002) Practice with sleep makes perfect: sleep-dependent motor skill learning. Neuron 35:205–211.

Walsh T, McClellan JM, McCarthy SE, et al (2008) Rare Structural Variants Disrupt Multiple Genes in Neurodevelopmental Pathways in Schizophrenia. Sci 320:539–543.

Wang A, Lohmann K, Yang C (2011) Bipolar disorder type 1 and schizophrenia are accompanied by decreased density of parvalbumin- and somatostatin-positive interneurons in the parahippocampal region. Acta Neuropathol. 122(5):615-26.

Wang Y, Dye C, Sohal V, et al. (2010) Dlx5 and Dlx6 Regulate the Development of Parvalbumin-Expressing Cortical Interneurons. J Neurosci. 30(15): 5334–5345.

Wang Y, Li G, Stanco A, et al. (2011) CXCR4 and CXCR7 Have Distinct Functions in Regulating Interneuron Migration. Neuron 69:61–76.

Watson C, Kirkcaldie M, Paxinos G (2010) The Brain: An introduction to functional anatomy. Elservier.

Wichterle H, Garcia-Verdugo JM, Herrera DG, et al. (1999) Young neurons from medial ganglionic eminence disperse in adult and embryonic brain. Nat Neurosci 2:461–466.

Wichterle H, Turnbull D, Nery S, et al. (2001) In utero fate mapping reveals distinct migratory pathways and fates of neurons born in the mammalian basal forebrain. Development 128(19):3759-71.

Wilson S, Rubenstein J (2000) Induction and dorsoventral patterning of the telencephalon. Neuron 28(3):641-51.

Wine-Lee L, Ahn KJ, Richardson RD, et al. (2004) Signaling through BMP type 1 receptors is required for development of interneuron cell types in the dorsal spinal cord. Dev 131 :5393–5403.

Wonders CP, Welagen J, Taylor L, et al. (2008) A spatial bias for the origins of interneuron subgroups within the medial ganglionic eminence. Dev Biol 314:127–136.

Wong A, Likhodi O, Trakalo J, et al. (2005) Genetic and post-mortem mRNA analysis of the 14-3-3 genes that encode phosphoserine/threonine-binding regulatory proteins in schizophrenia and bipolar disorder. Schizophr Res 78:137-46.

Wong A, Macciardi F, Klempan T, et al. (2003) Identification of candidate genes for psychosis in rat models, and possible association between schizophrenia and the 14-3-3eta gene. Mol Psychiatry 8:156–166.

Woodcock J, Murphy J, Stomski F et al. (2003) The dimeric versus monomeric status of 14-3-3ζ is Controlled by phosphorylation of Ser58 at the dimer interface. The J. Bio Chemistry 278(38): 36323–36327.

Woodcock J, Coolen C, Goodwin K, et al. (2015) Destabilisation of dimeric 14-3-3 proteins as a novel approach to anti-cancer therapeutics. Oncotarget. 6(16):14522-36.

Woodhead GJ, Mutch CA, Olson EC, et al. (2006) Cell-autonomous beta-catenin signalling regulates cortical precursor proliferation. J Neurosci 26: 12620-12630.

Wright I, Rabe-Hesketh S, Woodruff P, David A, et al. (2000) Meta-Analysis of Regional Brain Volumes in Schizophrenia. American Journal of Psychiarty. 157:16–25.

Xu H, Jeong HY, Tremblay R, et al. (2013) Neocortical Somatostatin-Expressing GABAergic Interneurons Disinhibit the Thalamorecipient Layer 4. Neuron 77:155–167.

Xu Q, Cobos I, De La Cruz E, et al. (2004) Origins of cortical interneuron subtypes. J Neurosci 24:2612–2622.

Xu Q, Guo L, Moore H, et al. (2010) Sonic hedgehog signaling confers ventral telencephalic progenitors with distinct cortical interneuron fates. Neuron 65:328–340.

Xu Q, Wonders CP, Anderson SA (2005) Sonic hedgehog maintains the identity of cortical interneuron progenitors in the ventral telencephalon. Development 132:4987–4998.

Xu X, Jaehne E, Greenberg Z, et al. (2015) 14-3-3ζ deficient mice in the BALB/c background display behavioural and anatomical defects associated with neurodevelopmental disorders. Scientific Reports 5(12434).

Yaffe M, Elia A (2001) Phosphoserine/threonine-binding domains. Current Opinion in Cell Biology. 13:131–138.

Yaffe M, and Ya M (2002) How do 14-3-3 proteins work? Gatekeeper phosphorylation and the molecular anvil hypothesis. FEBS Letters. 513:53–57.

Yang X, Lee W, Sobott , et al. (2006) Structural basis for protein-protein interactions in the 14-3-3 protein family. Proc Natl Ac ad Sci USA 103(46):17237-42.

Yoon JH, Maddock RJ, Rokem A, et al. (2010) Gamma-Aminobutyric Acid Concentration is Reduced in Visual Cortex in Schizophrenia and Correlates with Orientation-Specific Surround Suppression. J Neurosci 30:3777–3781.

Zerr I, Bodemer M, Gefeller O, et al. (1998) Detection of 14-3-3 protein in the cerebrospinal fluid supports the diagnosis of Creutzfeldt-Jakob disease. Annals of Neurology 43(1):32-40.

Zhang S, Heming X, and Muslin A (1999) Nuclear Localization of Protein Kinase U-α Is Regulated by 14-3-3. The Journal of Biological Chemistry 274:24865-24872.

Zhang Z, Reynolds G (2002) A selective decrease in the relative density of parvalbumin-immunoreactive neurons in the hippocampus in schizophrenia. Schizophr Res. 1(55):1-10.

Zhao Y, Flandin P, Long JE, Cuesta MD, Westphal H, Rubenstein JL (2008) Distinct molecular pathways for development of telencephalic interneuron subtypes revealed through analysis of Lhx6 mutants. J Comp Neurol 510:79-99.

Zhao Y, Marín O, Hermesz E, Powell A, Flames N, Palkovits M, Rubenstein JL, Westphal H (2003) The LIM-homeobox gene Lhx8 is required for the development of many cholinergic neurons in the mouse forebrain. Proc Natl Acad Sci (USA) 100:9005-9010.

Zhao Y, Flandin P, Vogt D et al. (2014) Ldb1 is essential for development of Nkx2.1 lineage derived GABAergic and cholinergic neurons in the telencephalon. Developmental Biology 385;94-106.

Zhou CJ, Borello U, Rubenstein JL, et al. (2006) Neuronal production and precursor proliferation defects in the neocortex of mice with loss of function in the canonical Wnt signaling pathway. Neuroscience 142:1119–1131.

Zhou CJ, Zhao C, Pleasure SJ (2004) Wnt signaling mutants have decreased dentate granule cell production and radial glial scaffolding abnormalities. J Neurosci 24: 121-126.

Zimmer G, Garcez P, Rudolph J, et al. (2008) Ephrin-A5 acts as a repulsive cue for migrating cortical interneurons. Eur J Neurosci 28: 62-73.

Zimmer G, Rudolph J, Landmann J, et al. (2011) Bidirectional ephrinB3/EphA4 signaling mediates the segregation of medial ganglionic eminence- and preoptic area-derived interneurons in the deep and superficial migratory stream. J Neurosci 31: 18364-18380.

Appendix

A.1. Microarray analysis: raw data

A.1.1 Genes upregulated in *14-3-3ζ* KO mice

Transcript ID	Gene Symbol	p-value	Step up (p-value)	Fold-Change
17549080	LacZ	8.7E-05	0.344732	46.3595
17549054	LacZ	9.64E-05	0.344732	39.0391
17549096	LacZ	0.000142	0.419293	24.2687
17549150	neomycin	0.000187	0.482316	13.5768
17549062	Kanamycin/neomycin	0.000115	0.366583	10.1504
17549018	Retrotransposon vector pVLI	0.000747	0.935796	7.83653
17324110	Snord66	0.035068	0.999999	2.08415
17465636	Plxna4	0.035731	0.999999	2.0144
17548422	4932422M17Rik	0.035459	0.999999	1.86996
17310912	Laptm4b	0.023194	0.999999	1.85007
17423207	Mir3471-1	0.03496	0.999999	1.82645
17287361	Gadd45g	0.040542	0.999999	1.70417
17288309	Zfp455	0.006713	0.999999	1.69714
17352599	Gm17430	0.002912	0.999999	1.63395
17376270	Snord110	0.049146	0.999999	1.63357
17531480	3000002C10Rik	0.017735	0.999999	1.6104
17459417	Igkj3	0.02556	0.999999	1.58802
17387634	Olfr1039	0.044156	0.999999	1.58365
17375360	Spg11	0.007751	0.999999	1.58045
17321227	Kansl2	0.029118	0.999999	1.54602
17342065	Mapk8ip3	0.016392	0.999999	1.52726
17303204	Gm3667	0.043756	0.999999	1.52042
17506332	Banp	0.024598	0.999999	1.51098
17549930	Copg2as2	0.001314	0.999999	1.50486
17499736	Defa25	0.003431	0.999999	1.50417
17415076	Cntln	0.037028	0.999999	1.47724
17513871	Chmp1a	0.008262	0.999999	1.47622
17299965	Trav16d-dv11	0.049679	0.999999	1.47342
17365369	Cuedc2	0.011905	0.999999	1.47195
17356240	Sptbn2	0.012979	0.999999	1.46168
17461155	Gpr27	0.003938	0.999999	1.46157
17330684	Tagln3	0.020029	0.999999	1.45829

17328251	Parn	0.046069	0.999999	1.44202
17311272	Zfpm2	0.046378	0.999999	1.43346
17394582	Prex1	0.009823	0.999999	1.41009
17414520	Gm13775	0.041962	0.999999	1.4032
17481680	Rpl27a	0.050021	0.999999	1.40143
17487104	Psg19	0.025506	0.999999	1.40054
17312759	Cyth4	0.00767	0.999999	1.39662
17530733	Grm2	0.034688	0.999999	1.39557
17374594	Pak6	0.017745	0.999999	1.39234
17357486	Syt7	0.040881	0.999999	1.38745
17252253	Gm19967	0.032947	0.999999	1.38612
17246418	Olfr796	0.027433	0.999999	1.38137
17464404	Mrps35	0.028157	0.999999	1.38102
17484014	Acadsb	0.014841	0.999999	1.37941
17457773	Tcrb-J	0.048936	0.999999	1.37359
17411252	St6galnac5	0.016014	0.999999	1.37051
17543407	Ophn1	0.017969	0.999999	1.37014
17253505	Sdf2	0.0165	0.999999	1.36732
17351862	Smad7	0.013557	0.999999	1.35395
17477055	EU599041	0.007479	0.999999	1.35351
17229984	Darc	0.020248	0.999999	1.353
17407708	Scnm1	0.048356	0.999999	1.34608
17288160	Cdk20	0.040092	0.999999	1.34398
17306877	Adcy4	0.045445	0.999999	1.3426
17488485	Ifnl2	0.001582	0.999999	1.34147
17351232	Wdr7	0.015417	0.999999	1.33792
17475818	AF357399	0.020169	0.999999	1.3378
17476465	U2af1l4	0.03049	0.999999	1.3374
17285838	Hist1h3d	0.050059	0.999999	1.33534
17471788	Gm6590	0.000975	0.999999	1.33516
17538945	n-R5s15	0.044187	0.999999	1.3325
17245231	Lyz1	0.006122	0.999999	1.33119
17382249	Cacna1b	0.020317	0.999999	1.33053
17470764	Gm5077	0.010854	0.999999	1.32713
17231349	Ppp1r14c	0.00506	0.999999	1.32489
17506313	Jph3	0.006166	0.999999	1.32471
17234718	Gm2696	0.040643	0.999999	1.32448
17241206	Pald1	0.011513	0.999999	1.32436
17259276	Bahcc1	0.034058	0.999999	1.3243
17275234	Gm2027	0.02479	0.999999	1.32106
17517659	Man2c1	0.013503	0.999999	1.3201
17429290	Olfr1329	0.043063	0.999999	1.31872
17545327	Tro	0.008511	0.999999	1.31634

17356743	Ehd1	0.027698	0.999999	1.31406
17356994	Trpt1	0.012796	0.999999	1.31117
17404047	Zfp704	0.010305	0.999999	1.31031
17310565	Cdh18	0.039224	0.999999	1.30973
17545482	Mageh1	0.010707	0.999999	1.3073
17355386	Elac1	0.016662	0.999999	1.30682
17224730	Scg2	0.007871	0.999999	1.30673
17356070	Doc2g	0.007993	0.999999	1.30651
17405021	Sclt1	0.011102	0.999999	1.30618
17261969	Ttc1	0.033164	0.999999	1.30611
17474292	Ceacam14	0.049926	0.999999	1.30461
17548356	Gm10572	0.04781	0.999999	1.30429
17350084	Rps19-ps13	0.004413	0.999999	1.30215
17238154	Rdh9	0.042772	0.999999	1.30088
17267617	Gm15698	0.017531	0.999999	1.30054
17228293	Cacna1e	0.01606	0.999999	1.2994
17478793	Magel2	0.022112	0.999999	1.29764
17476119	Ppp1r14a	0.030626	0.999999	1.29732
17336052	Zfp563	0.033336	0.999999	1.29585
17395108	Ppp4r1l-ps	0.037012	0.999999	1.2958
17442464	Ogfod2	0.044876	0.999999	1.29576
17446060	AI506816	0.050202	0.999999	1.29474
17368646	Olfm1	0.04214	0.999999	1.29419
17465201	Ndufa5	0.03445	0.999999	1.2916
17336228	Tapbp	0.014751	0.999999	1.2906
17478942	Tm2d3	0.041652	0.999999	1.29043
17540396	Ndp	0.004112	0.999999	1.28996
17322541	Dnaja3	0.038858	0.999999	1.28962
17473765	Zfp110	0.027503	0.999999	1.2896
17454326	1700123K08Rik	0.038167	0.999999	1.28847
17277801	Spata7	0.041524	0.999999	1.28793
17383612	Dolk	0.038964	0.999999	1.28789
17529449	4922501C03Rik	0.02094	0.999999	1.28725
17487681	Zfp109	0.036403	0.999999	1.28702
17473166	Cacng6	0.02664	0.999999	1.28683
17340646	Tagap1	0.016753	0.999999	1.28553
17446981	Fndc4	0.020189	0.999999	1.28436
17376119	Chchd5	0.038555	0.999999	1.28406
17520490	Atr	0.03279	0.999999	1.28254
17434813	Sema3e	0.044325	0.999999	1.28168
17312603	Gm17271	0.039479	0.999999	1.28099
17345562	Gnmt	0.036594	0.999999	1.28074
17248263	Hba-a1	0.03337	0.999999	1.28062

17317393	Fam84b	0.023169	0.999999	1.28041
17488312	Map3k10	0.026295	0.999999	1.28036
17239360	Plagl1	0.008621	0.999999	1.27965
17427389	Cyp2j6	0.026066	0.999999	1.27959
17460099	Vax2	0.041285	0.999999	1.27907
17260261	Camk2b	0.03495	0.999999	1.27871
17357306	B3gat3	0.038377	0.999999	1.27707
17516157	Olfr899	0.003672	0.999999	1.27666
17515982	9230113P08Rik	0.021242	0.999999	1.27663
17441365	Taok3	0.019412	0.999999	1.27616
17444216	Ap5z1	0.012529	0.999999	1.2761
17369196	Fam73b	0.036059	0.999999	1.27489
17354282	Cdo1	0.049578	0.999999	1.27466
17211832	Cnnm3	0.015069	0.999999	1.27407
17537118	P2ry10	0.023584	0.999999	1.27287
17343643	Rps28	0.004792	0.999999	1.27162
17537394	Gm6604	0.003821	0.999999	1.2689
17233001	Pdss2	0.023153	0.999999	1.26863
17446440	Gm21671	0.008218	0.999999	1.26856
17323576	Ccdc74a	0.021538	0.999999	1.26569
17464201	Gm15686	0.003095	0.999999	1.26552
17215817	Olfr12	0.023616	0.999999	1.26499
17233113	Hace1	0.007943	0.999999	1.2648
17270062	Tmem101	0.043887	0.999999	1.26457
17286973	Gmpr	0.04753	0.999999	1.26425
17387565	Lrrc55	0.035324	0.999999	1.26407
17532639	mt-Ta	0.029475	0.999999	1.2639
17342403	Rhot2	0.024932	0.999999	1.26299
17501772	Sugp1	0.032338	0.999999	1.26223
17432912	Fbxo6	0.008674	0.999999	1.2621
17472884	Gm6654	0.021815	0.999999	1.26205
17359055	Exoc6	0.039862	0.999999	1.2612
17271583	Slc39a11	0.045876	0.999999	1.26052
17403701	AI115009	0.027014	0.999999	1.25993
17432790	Miip	0.042614	0.999999	1.25878
17224954	Sphkap	0.005501	0.999999	1.25825
17247635	Gm12052	0.03418	0.999999	1.25747
17357799	Olfr1440	0.049337	0.999999	1.25561
17499610	Defb5	0.009689	0.999999	1.25556
17323824	Olfr166	0.049827	0.999999	1.25554
17431955	Arhgef10l	0.007477	0.999999	1.25506
17453698	Orai2	0.022082	0.999999	1.25475
17291026	Mir1983	0.018195	0.999999	1.25366

17472192	Mgp	0.039781	0.999999	1.25339
17373484	Pex16	0.04251	0.999999	1.25192
17518138	I730028E13Rik	0.017059	0.999999	1.25098
17322355	Gpr84	0.036227	0.999999	1.25014
17235604	Zfr2	0.002506	0.999999	1.24898
17362138	Gpr137	0.007397	0.999999	1.24802
17374939	Mapkbp1	0.003106	0.999999	1.24688
17413567	Gm12678	0.011453	0.999999	1.2424
17250734	2410006H16Rik	0.004438	0.999999	1.24146
17259220	Chmp6	0.023682	0.999999	1.24018
17305012	Gprin2	0.001707	0.999999	1.24007
17299796	Trav7d-4	0.033074	0.999999	1.24001
17447045	Pisd	0.043945	0.999999	1.23942
17548336	Gm20764	0.002346	0.999999	1.23917
17547647	Gm9241	0.038782	0.999999	1.23782
17238482	Rnf41	0.048516	0.999999	1.23728
17266010	Doc2b	0.033446	0.999999	1.23722
17346281	Safb2	0.037303	0.999999	1.23713
17487664	Vmn1r167	0.048836	0.999999	1.23685
17389844	Rhov	0.007164	0.999999	1.23617
17250344	Lrrc48	0.01633	0.999999	1.23603
17446185	Fastk	0.012702	0.999999	1.23557
17429800	D830031N03Rik	0.024113	0.999999	1.23509
17460451	1600020E01Rik	0.011665	0.999999	1.23445
17325663	D930030D11Rik	0.021884	0.999999	1.23441
17430462	Iqcc	0.025045	0.999999	1.23365
17387794	Olfr1160	0.023519	0.999999	1.23279
17449516	Cox18	0.00201	0.999999	1.2326
17281927	Kcnh5	0.017896	0.999999	1.23242
17481328	Olfr659	0.00785	0.999999	1.23192
17363374	Ostf1	0.012414	0.999999	1.23187
17463454	Clec2i	0.048	0.999999	1.2318
17319596	Cenpm	0.039398	0.999999	1.23172
17506073	Mlycd	0.010985	0.999999	1.23157
17352571	Mpp7	0.017692	0.999999	1.22809
17486561	Zscan18	0.008905	0.999999	1.2276
17376541	Prnp	0.03227	0.999999	1.22754
17306983	Gzmd	0.050311	0.999999	1.22732
17424293	Rpp25l	0.002616	0.999999	1.22694
17222053	Bend6	0.011671	0.999999	1.22692
17357092	Slc22a8	0.035984	0.999999	1.22613
17291412	Prl2b1	0.004346	0.999999	1.22602
17472919	B230104C08Rik	0.027795	0.999999	1.22566

17474863	Vmn1r174	0.022349	0.999999	1.22508
17283923	Slc25a29	0.044277	0.999999	1.22307
17299582	Eddm3b	0.007242	0.999999	1.22262
17535296	n-R5s8	0.03348	0.999999	1.22135
17255759	Npepps	0.011049	0.999999	1.22081
17284435	Igh-VJ558	0.021959	0.999999	1.22057
17388728	Gm13872	0.021517	0.999999	1.21946
17468887	Vmn1r48	0.014644	0.999999	1.21828
17493632	Dgat2	0.04376	0.999999	1.21786
17509976	Slc25a42	0.018874	0.999999	1.21761
17238549	Wibg	0.021006	0.999999	1.21679
17438969	Pf4	0.033712	0.999999	1.21665
17299135	LOC101056480	0.025018	0.999999	1.21638
17417530	Mutyh	0.035021	0.999999	1.21617
17526473	Gm10684	0.043821	0.999999	1.21524
17399374	Muc1	0.033036	0.999999	1.21479
17458037	9430018G01Rik	0.048115	0.999999	1.2145
17446452	Gm10220	0.003775	0.999999	1.21438
17530027	Gm6432	0.007205	0.999999	1.21426
17524838	Tmem205	0.044241	0.999999	1.21406
17279991	Tubb2a-ps2	0.011355	0.999999	1.21405
17263516	Pemt	0.024543	0.999999	1.21404
17261942	Mir146	0.021297	0.999999	1.21355
17217383	Chit1	0.046829	0.999999	1.21346
17448815	1700025M24Rik	0.008504	0.999999	1.2134
17488105	Cyp2a22	0.020396	0.999999	1.21315
17473633	n-R5s150	0.016686	0.999999	1.21305
17451002	P2rx2	0.037622	0.999999	1.21281
17437887	Limch1	0.007839	0.999999	1.21217
17211587	Dst	0.015339	0.999999	1.21208
17241257	Col13a1	0.024073	0.999999	1.21197
17516282	Olfr967	0.012265	0.999999	1.21194
17211857	4933424G06Rik	0.015	0.999999	1.21185
17470235	Cacna1c	0.050446	0.999999	1.21143
17404122	Slc10a5	0.011728	0.999999	1.21121
17432861	Gm13054	0.01697	0.999999	1.21089
17244371	Gm15915	0.040348	0.999999	1.21076
17325410	Golgb1	0.047973	0.999999	1.20991
17344862	Olfr101	0.01859	0.999999	1.20952
17377432	Syndig1	0.016312	0.999999	1.2093
17423741	BC024582	0.041264	0.999999	1.20854
17443766	Ap4m1	0.049879	0.999999	1.20791
17433412	Zbtb48	0.029872	0.999999	1.2078

17387987	Olfr1251	0.042625	0.999999	1.20739
17300376	Il25	0.026576	0.999999	1.20679
17322128	Spryd3	2.72E-05	0.257289	1.2067
17286893	Rnf182	0.000231	0.529709	1.20656
17430253	Hmgb4	0.037995	0.999999	1.20615
17456839	n-R5s161	0.036306	0.999999	1.2054
17472443	Slco1a5	0.044817	0.999999	1.20519
17438980	Il8	0.016241	0.999999	1.20463
17418767	Csmd2	0.02043	0.999999	1.20454
17271891	Atp5h	0.001902	0.999999	1.20423
17363152	Olfr1472	0.034853	0.999999	1.20381
17476980	Vmn2r-ps54	0.020693	0.999999	1.20367
17258547	Ten1	0.042488	0.999999	1.20305
17542209	Mir224	0.030139	0.999999	1.20302
17237784	Gm4129	0.039329	0.999999	1.20264
17548016	LOC100505091	0.007732	0.999999	1.20232
17537730	Armcx4	0.038972	0.999999	1.20197
17302266	4930452G13Rik	0.044556	0.999999	1.20192
17550166	Gm12521	0.031329	0.999999	1.20126
17288350	LOC101056512	0.002002	0.999999	1.20111
17542076	Mir463	0.046864	0.999999	1.20095
17462395	Slc25a18	0.045631	0.999999	1.2004
17380549	Gm14420	0.005754	0.999999	1.20031
17414351	Palm2	0.000726	0.935796	1.1999
17373177	LOC100862024	0.03203	0.999999	1.1995

A.1.2 Genes down regulated in *14-3-3ζ* KO mice

Transcript ID	Gene Symbol	p-value	Step up (p-value)	Fold-Change
17399904	Ywhaz	0.0001	0.344732	-50.5432
17547869	Ywhaz	0.000214	0.5193	-16.4969
17316545	Ywhaz	4.48E-05	0.308427	-4.44745
17310808	Dap	0.032846	0.999999	-1.96464
17341405	Gm7072	0.010886	0.999999	-1.92307
17406527	Gm6570	0.035307	0.999999	-1.84884
17310837	Sema5a	0.012609	0.999999	-1.8452
17550590	mt-Ti	0.005722	0.999999	-1.63675
17549328	Calr	0.029598	0.999999	-1.62821
17548806	Gm9429	0.020227	0.999999	-1.59014
17365690	Gm10197	0.034054	0.999999	-1.57014

17315713	Atp5h	0.018454	0.999999	-1.55939
17548080	Gm14567	0.010143	0.999999	-1.55638
17549002	Polr2k	0.000852	0.999999	-1.54936
17319576	Nhp2l1	0.044178	0.999999	-1.50432
17414007	Hnrnpf	0.001254	0.999999	-1.49296
17403879	Ankrd13c	0.033702	0.999999	-1.46034
17542267	Xlr3a	0.038448	0.999999	-1.45616
17310827	Fam173b	0.03421	0.999999	-1.45252
17459463	Krcc1	0.027925	0.999999	-1.44533
17279833	Gm3625	0.042938	0.999999	-1.43573
17276714	Mpp5	0.015105	0.999999	-1.4337
17374848	Nusap1	0.032645	0.999999	-1.42234
17550138	Nusap1	0.032645	0.999999	-1.42234
17476609	Scgb1b3	0.001132	0.999999	-1.41434
17341390	Gm7052	0.030201	0.999999	-1.39613
17540623	Gm4297	0.027414	0.999999	-1.39581
17295362	Btf3	0.039447	0.999999	-1.39456
17548673	Hmgb2	0.050036	0.999999	-1.39422
17548873	Gm6238	0.040115	0.999999	-1.39351
17278436	Papola	0.04665	0.999999	-1.39262
17404073	Fabp5	0.030782	0.999999	-1.38524
17388037	Olfr1272	0.024026	0.999999	-1.38419
17476568	Gm4673	0.033411	0.999999	-1.381
17491501	C230091D08Rik	0.003707	0.999999	-1.3807
17428457	Cyp4a14	0.031719	0.999999	-1.36518
17315198	Mir1941	0.005174	0.999999	-1.36091
17411761	Ccne2	0.009753	0.999999	-1.35717
17217127	Nucks1	0.046467	0.999999	-1.3448
17303453	4930452B06Rik	3.11E-05	0.257289	-1.34425
17427067	Gm12597	0.016981	0.999999	-1.3281
17493024	Zfand6	0.043561	0.999999	-1.32586
17531856	4921528I07Rik	0.001717	0.999999	-1.32243
17362524	Ganab	0.022438	0.999999	-1.31611
17352229	Cyb5	0.040165	0.999999	-1.31335
17379395	Svs5	0.03292	0.999999	-1.31184
17500275	Erlin2	0.022848	0.999999	-1.30964
17334780	Metrn	0.007727	0.999999	-1.30927
17292603	Gm2848	0.050038	0.999999	-1.30642
17374612	Phgr1	0.021372	0.999999	-1.30357
17456678	Atp6v1f	0.025928	0.999999	-1.30041
17319401	Snord83b	0.006744	0.999999	-1.29992
17250341	Gm12265	6.69E-05	0.344732	-1.29871
17228066	Tsen15	0.037132	0.999999	-1.29805

17466279	Gm2663	0.02185	0.999999	-1.29641
17340427	Gm20939	0.032722	0.999999	-1.29167
17280270	Gm9292	0.007833	0.999999	-1.2908
17266520	Lgals9	0.000494	0.887343	-1.28662
17472725	Kras	0.007046	0.999999	-1.28603
17375292	Serf2	0.019236	0.999999	-1.28129
17526633	LOC100502818	0.020586	0.999999	-1.28058
17469864	Tamm41	0.037267	0.999999	-1.27975
17248249	Mpg	0.046022	0.999999	-1.2791
17395170	Slmo2	0.047126	0.999999	-1.27622
17340548	Tmem181a	0.021341	0.999999	-1.27237
17469506	Cntn3	0.019215	0.999999	-1.27083
17512755	Psmd7	0.01676	0.999999	-1.26612
17531977	Stmn1-rs1	0.036012	0.999999	-1.26267
17469089	Mrps25	0.036013	0.999999	-1.26262
17488743	Psmd8	0.041052	0.999999	-1.26207
17377418	Cst3	0.041086	0.999999	-1.25845
17225066	A530032D15Rik	0.021133	0.999999	-1.2577
17355304	4930503L19Rik	0.007996	0.999999	-1.25426
17532755	Dgkk	0.038238	0.999999	-1.25335
17533952	Gm2863	0.024772	0.999999	-1.25238
17310882	Cpq	0.009287	0.999999	-1.25221
17213515	Pard3b	0.049027	0.999999	-1.25004
17541158	Tmem255a	0.049826	0.999999	-1.24924
17526861	Dlat	0.011048	0.999999	-1.24871
17477314	Klk1b11	0.010383	0.999999	-1.24821
17473047	Gm9027	0.045962	0.999999	-1.24736
17396223	Gm16093	0.014816	0.999999	-1.24657
17281219	Nfkbia	0.007558	0.999999	-1.24629
17300086	Trav3-4	0.023397	0.999999	-1.24562
17239638	Pde7b	0.02659	0.999999	-1.24221
17515715	Zbtb44	0.040974	0.999999	-1.24138
17326567	Gbe1	0.02975	0.999999	-1.24097
17237247	Bbs10	0.011833	0.999999	-1.24003
17295125	F2rl1	0.026676	0.999999	-1.2381
17214753	Irs1	0.002663	0.999999	-1.23785
17328884	Ranbp1	0.016712	0.999999	-1.23599
17384563	Olfr351	0.022686	0.999999	-1.23551
17521014	Acad11	0.035654	0.999999	-1.23519
17316521	Pabpc1	0.027186	0.999999	-1.23507
17333833	Vmn2r107	0.042779	0.999999	-1.23364
17392828	Gm14167	0.009187	0.999999	-1.23222
17548752	Tmem202	0.014147	0.999999	-1.23195

17311428	Ebag9	0.037411	0.999999	-1.23164
17262224	9930111J21Rik1	0.048879	0.999999	-1.23007
17515819	Ets1	0.050282	0.999999	-1.23006
17238656	Olfr780	0.006584	0.999999	-1.22853
17535707	Gm14817	0.022626	0.999999	-1.22749
17408755	Fam19a3	0.047345	0.999999	-1.22687
17501748	Lpar2	0.007784	0.999999	-1.22661
17432227	Fblim1	0.028613	0.999999	-1.22569
17244545	Gm8633	0.037215	0.999999	-1.22554
17502970	Ptger1	0.03392	0.999999	-1.225
17417290	Atpaf1	0.046914	0.999999	-1.22438
17488951	Zfp146	0.042966	0.999999	-1.21905
17538171	Mid2	0.0027	0.999999	-1.21862
17291222	Hist1h3c	0.022934	0.999999	-1.21766
17435107	Lrrc17	0.000724	0.935796	-1.21724
17547813	Gm19845	0.043544	0.999999	-1.21554
17408793	Capza1	0.021861	0.999999	-1.21493
17373501	1700029I15Rik	0.019878	0.999999	-1.21195
17547923	Gm8702	0.017321	0.999999	-1.20874
17232316	Samd3	1.25E-05	0.257289	-1.20859
17480962	Anapc15	0.037849	0.999999	-1.20524
17529901	Slc25a36	0.012147	0.999999	-1.20194
17352056	Epg5	0.043406	0.999999	-1.20112
17220877	Gm10516	0.021428	0.999999	-1.20091
17342750	Nudt3	0.04062	0.999999	-1.19977
17458472	Fam221a	0.010612	0.999999	-1.19883
17427000	Dennd4c	0.015716	0.999999	-1.19626
17548281	Hmgb1	0.020559	0.999999	-1.19623
17450989	Pxmp2	0.001272	0.999999	-1.19515
17467392	Igkv19-93	7.92E-05	0.344732	-1.19382
17485553	Tmc4	0.046256	0.999999	-1.1905
17248892	Gnb2l1	0.040183	0.999999	-1.1895
17251091	Myh4	0.046208	0.999999	-1.18769
17369060	Set	0.005602	0.999999	-1.1875
17520983	Nphp3	0.034235	0.999999	-1.18656
17427563	Itgb3bp	0.038312	0.999999	-1.18639
17396228	Dnajc5b	0.04479	0.999999	-1.18576
17467191	Vmn1r24	0.046034	0.999999	-1.1857
17343026	Ppil1	0.029719	0.999999	-1.18518
17488556	Gm19897	0.034187	0.999999	-1.18451
17465942	Atp6v0a4	0.018952	0.999999	-1.18397
17545761	Gm15243	0.014964	0.999999	-1.1837
17311942	Gm20405	0.012739	0.999999	-1.18331

17536906	Gm14839	0.047939	0.999999	-1.18312
17232231	Gm15271	0.019925	0.999999	-1.1814
17542732	Gab3	0.020758	0.999999	-1.17972
17218393	Tor1aip2	0.025587	0.999999	-1.17964
17414184	4930522O17Rik	0.005792	0.999999	-1.17827
17514916	Olfr835	0.007894	0.999999	-1.17814
17445440	Steap1	0.023666	0.999999	-1.17658
17537038	Fgf16	0.008603	0.999999	-1.17619
17464238	Lyrm5	0.018979	0.999999	-1.17611
17321318	Fkbp11	0.037857	0.999999	-1.1757
17543648	Ercc6l	0.042934	0.999999	-1.17484
17506991	Nrp1	0.01846	0.999999	-1.17436
17270322	Eftud2	0.049567	0.999999	-1.17412
17377464	Cst7	0.00662	0.999999	-1.1734
17292974	H2afy	0.030846	0.999999	-1.17194
17548244	Gm19816	0.013244	0.999999	-1.17163
17371451	Klhl41	0.000165	0.455371	-1.17131
17463747	Gprc5a	0.023886	0.999999	-1.17074
17274180	Gm16497	0.041512	0.999999	-1.17051
17354356	Hdhd1a	0.01971	0.999999	-1.16983
17477454	Syt3	0.019305	0.999999	-1.16896
17320538	Arsa	0.007568	0.999999	-1.16892
17377013	Dstn	0.023061	0.999999	-1.16864
17533226	1700054O13Rik	0.032105	0.999999	-1.16848
17538350	A730046J19Rik	0.039269	0.999999	-1.16821
17276743	Plekhh1	0.041996	0.999999	-1.1681
17478476	Gas2	0.006628	0.999999	-1.16804
17544295	Astx6	0.001843	0.999999	-1.1666
17472070	8430419L09Rik	0.01621	0.999999	-1.16656
17255251	Gm11542	0.028079	0.999999	-1.16618
17467197	Vmn1r27	0.018461	0.999999	-1.16477
17305259	Gm7945	0.032209	0.999999	-1.16289
17534646	Arhgap36	0.026843	0.999999	-1.16185
17275025	Gm5434	0.02311	0.999999	-1.16125
17540584	Gm5124	0.046963	0.999999	-1.16062